The Self-assembly of Organosilane Films on Aluminium Oxide and their Application to Si-Al Composite Materials for 3D Printing

by

Ruby Alice Sims

Thesis

Submitted to Flinders University

For the degree of

Doctor of Philosophy

College of Science and Engineering

13th May 2019

Abstract

Organosilanes provide a unique opportunity to modify the physical and chemical properties of a hydroxylated surface in an environmentally friendly and cost-effective manner. The water activated self-assembly mechanism of Organosilanes in solution has been extensively studied however, the mechanism by which they interact with a surface and condense to form thin films is not well known. The original contribution to knowledge presented in this thesis is a comprehensive picture of silane-substrate interactions through both the ex-situ and in-situ monitoring organosilane films on a molecular scale. A link has been successfully made between the time dependant oscillatory surface coverage of silane films measured using X-ray Photoelectron Spectroscopy and the presence of more than one hydrolysable group on the central silicon atom. This along with the absence of such behaviour for silanes which contain just one hydrolysable group and follow a time dependant Langmuir-type growth profile indicates that the origin of this behaviour lies with the ability of silanes to oligomerise both in solution and on the surface.

Conformation of oligomerised silane islands on the surface of oscillating Propyltrimethoxysilane and Propylmethyldimethoxysilane films and the absence of these islands in Propyldimethylmethoxysilane films imaged using Auger Electron Spectroscopy, led to the proposal of a surface condensation mechanism involving the growth and desorption of oligomerised islands, the collective behaviour of which creates a measurable oscillation in surface coverage. In order to further probe the interactions of silane molecules and the substrate, the role of covalently and hydrogen bound silane species was explored. The removal of hydrogen bound species while reducing the amount of silane on the surface did not remove the oscillatory behaviour, confirming that the oscillation involves the removal of covalently bound species from the surface. This mechanism was related directly to a reversal of the equilibrium condensation reaction as a result of an increase in localised water concentrations, a product of the condensation reaction itself. The kinetics of these interactions were proposed through the creation of a theoretical 10-component mathematical model requiring competing silane-substrate and water-substrate interactions. For each oscillation to occur there must be two components present in solution, a silicon containing species and a non-silicon containing species, thought to be water.

Probing the silane-substrate interface using Sum Frequency Generation spectroscopy not only confirmed the presence of a monolayer-like coverage amongst the oligomerised islands of Propyltrimethoxysilane films, but that the order and number of defects within this film is directly related to molecular packing on the surface. The presence of an ordered, physisorbed bilayer on top of covalently bound Propyltrimethoxysilane films was also identified as a key process of the self-assembly mechanism.

This extensive investigation into the mechanism of silane film self-assembly and the knowledge accrued from it was then used to develop new application for silane films via the creation of a novel, 3D printed Al-Si composite material. The silane functionalisation of aluminium powders used as starting material for

3D-printing not only presented a new method of incorporating silicon into a 3D-printed aluminium matrix but also improved the flowability of these powders, a key property required for the Laser Metal Deposition 3D-printing process; an improvement so significant that it has allowed for the successful printing of aluminium powders previously deemed unprintable.

Declaration

I certify that this thesis does not incorporate without acknowledgment any material previously submitted for a degree or diploma in any university; and that to the best of my knowledge and belief it does not contain any material previously published or written by another person except where due reference is made in the text.

Ruby Alice Sims

December 2018

Acknowledgements

> My entire understanding of physical space has been transformed! Three-dimensional Euclidean geometry has been torn up, thrown in the air and snogged to death! My grasp of the universal constants of physical reality has been changed forever.
>
> **The 11th Doctor**

Research in this thesis was conducted at Flinders University, South Australia at the Flinders Institute for Nanoscale Science and Technology as well as the National Institute for Materials Science in Tsukuba, Japan and École Centrale de Nantes in Nantes, France.

For the duration of this research I was supported by the Flinders University Research Scholarship, as well as a yearlong International Graduate Fellowship in Japan, jointly funded by The National Institute for Materials Science and the Flinders Institute for Nanoscale Science and Technology. I was also fortunate to be awarded the Nicolas Baudin Travel Grant, jointly funded by The French Embassy in Australia, École Centrale de Nantes and Flinders University in collaboration with Naval Group.

During my candidature I attended two international conferences. Along with my research in France, the Nicolas Baudin Travel Grant allowed me to attend the International Symposium on Novel and Nano Materials, 2018 in Lisbon, Portugal. Support from the Flinders Institute for Nanoscale Science and Technology and the Australian Nanotechnology Network enabled my travel to and attendance at the International Conference on Nanoscience and Nanotechnology, 2016 in Canberra, Australia.

I am immensely grateful for each one of these funding bodies who placed their trust in me and allowed me to pursue my research goals.

To my supervisors, Professor Jamie Quinton and Associate Professor Sarah Harmer-Bassell, who each openly brought their strengths to the table and showed me great kindness and support, thank you. You have taught me to become a scientist who takes risks and asks the difficult questions of myself while always treating me as a colleague, and in your teaching led by example. To JQ, a supervisor who is full of wisdom which was strategically revealed only when I was ready and able to process it, I am now a much better teacher myself because of you. Thank you for entrusting me with a project you hold quite dear, I hope I have done the science justice and have done you proud.

During my doctoral studies approximately half of my research was conducted away from Flinders University. In October of 2016 I was fortunate to be awarded an International Graduate Fellowship by the National Institute for Materials Science in Tsukuba, Japan. This enabled me to spend a year under the mentorship of Professor Kohei Uosaki and Professor Hidenori Noguchi in the Global Research Centre for Environment and Energy based on Nanomaterials Science, Nano GREEN. Both Usoaki-sensei and Noguchi-sensei were generous with their knowledge and welcomed me into their group. During this fellowship I was also supported by Dr. Shuo Yang who showed me patience and a willingness to help whenever I asked.

物質・材料研究機構の魚崎先生を始め、野口先生、ヤンさんにお礼申し上げます。　まずは日本滞在中における研究上のご協力とそのご厚意に感謝致します。　この機会をまた将来に向けて共に活動出来ることを祈念し、再度お礼申し上げます

In the June of 2018 I was named as a Nicolas Baudin Laureate and awarded the associated Nicolas Baudin Travel Grant. This grant was jointly funded by the French Embassy in Australia, École Centrale de Nantes and Flinders University in collaboration with Naval Group and allowed me to spend three months working under the supervision of Professor Jean-Yves Hascoët at École Centrale de Nantes. I'd like to express my immense gratitude to Jean-Yves for trusting my knowledge and allowing me the freedom to pursue my ideas. Another member of the ECN team who was integral in the success of the research conducted in Nantes is Dr. Stéphane Touzé. Stéphane's expertise was invaluable and his generosity endless. He was always open to new (and sometimes unusual) ideas and gave up his time to help the project succeed.

Ma plus sincère gratitude va au professeur Jean-Yves Hascoët, Stéphane Touzé et à tous mes amis de l'École centrale de Nantes. Votre gentillesse et votre soutien ont été précieux, je n'aurais pas réussi sans vos conseils et votre patience.

It often requires a village of supporters to successfully complete a PhD. Throughout this adventure I have made many friends who I hope I can support in their endeavours as much as they have helped with mine. Dr. Raihan Rumman and Dr. Alexander Sibley, two senior members of our research group deserve a special mention for their mentorship and support, I am very grateful. Sometimes there are aspects of this journey that only a fellow PhD candidate can understand. A very special thank you to my dear friends for these conversations and the many cups of tea which have been an essential part of my routine.

To my parents and sister who have supported my intense curiosity from a young age, thank you. I applaud your ability to support me in all my endeavours, even the crazy ones you don't quite understand. I am grateful for all the lessons you have taught me; they serve to make me a better person and in turn, a better scientist.

A very wise woman once taught me that along with the family you are born into, there is also the family you choose. Often these relationships are the ones you have to work hardest at, but they have also proven to be the most rewarding. To my dearest friend Connor who has supported my growth unconditionally during the best and worst of times, and who continues to challenge me, I am indescribably grateful.

I think above all else I am grateful for the experience of the PhD, which as shown itself to be so much more than what is contained in this dissertation. Those who have embarked on a PhD have had the privilege of a truly unique and sometimes all-encompassing journey. When I made the decision to begin training as a professional researcher, I naïvely assumed that I would simply be trained in the practical skills required to conduct world class research however, the PhD has influenced every part of my life. I cannot express how this feels other than to constantly be grateful for the person I was then and the person I am now. I finally understand what it means to earn a PhD, and in many ways, it is not something you can be taught, but is something you must learn.

Idris: Are all people like this?

The Doctor: Like what?

Idris: So much bigger on the inside.

The 11th Doctor

Associated Publications

Sims RA, Harmer-Bassell SL, Quinton JS. The oscillatory adsorption of self-assembled organosilane films on aluminium oxide surfaces. *Surface and Interface Analysis.* 2018;50(8):813-818.

Sims RA, Harmer-Bassell SL, Quinton JS. The Oscillatory Adsorption of Organosilane Films on Aluminium Oxide: Film Morphology using Auger Electron Spectromicroscopy. *Applied Surface Science.* 2019;475:999-1002 DOI 10.1016/j.apsusc.2019.01.015.

Sims RA, Harmer SL, Quinton JS. The Role of Physisorption and Chemisorption in the Oscillatory Adsorption of Organosilanes on Aluminium Oxide. *Polymers.* 2019;11(3):410.

Table of Contents

List of Abbreviations and Units Used in this Thesis

3D	Three Dimensional
Å	Angstrom
AES	Auger Electron Spectroscopy
AFM	Atomic Force Microscopy
AL	Attenuation Length
APS	Aminopropyltriethoxysilane
APTS	Aminopropyltrimethoxysilane
ASF	Atomic Sensitivity Factor
CAE	Constant Analysis Energy
$CH_{3(as)}$	CH_3 asymmetrical stretching
$CH_{2(as)}$	CH_2 asymmetrical stretching
$CH_{3(s)}$	CH_3 symmetrical stretching
$CH_{2(s)}$	CH_2 symmetrical stretching
$CH_{3(FR)}$	CH_3 Fermi Resonance
CHA	Concentric Hemispherical Analyser
CMA	Cylindrical Mirror Analyser
CRR	Constant Retardation Ratio
ECN	École centrale de Nantes
eV	Electron Volt
FINST	Flinders Institute for Nanoscale Science and Technology
FOV	Field of View
IEP	Isoelectric Point
IMFP	Inelastic Mean Free Path
IR	Infra-Red

KE	Kinetic Energy
LHS-10	Leybold-Heraeus-10
LMD	Laser Metal Deposition
NIMS	the National Institute for Materials Science
nm	Nanometre
NMR	Nuclear Magnetic Resonance
OTS	Octadecyltrichlorosilane
PDMMS	Propyldimethylmethoxysilane
PMDMS	Propylmethyldimethoxysilane
PTMS	Propyltrimethoxysilane
RSF	Relative Sensitivity Factor
SAM	Scanning Auger Microscopy
SFG	Sum Frequency Generation Spectroscopy
ToF-SIMS	Time-of-Flight Secondary Ion Mass Spectrometry
vis	Visible light
WAAM	Wire Arc Additive Manufacturing
XPS	X-ray Photoelectron Spectroscopy

Definition: In this thesis, use of the term ‘substrate’ refers to bare Al_2O_3, hydroxylated quartz or sapphire substrates on which silanes can condense. The term ‘surface’ refers to the top-most layer of the surface and is used in reference to a substrate modified with silane which can consist of a complete or incomplete silane film coverage. In the case of an incomplete film, the term ‘surface’ may also include areas of the bare substrate.

1 Introduction.

1.1 The Importance of Organosilanes.

The application of organosilanes as coupling agents and adhesion promoters[1-3] is extensive throughout biological and chemical systems due to their ability to modify surface chemistry and form bonds between otherwise non-compatible materials. Silane molecules are commonly used in the form of silicone gap fillers and have been commercialised as anti-graffiti coating systems[4]. For medical applications such as dentistry a method of adhering biocompatible, durable ceramics to resin components must also poses these characteristics, silane molecules fit this brief as well as being resistant to abrasion and chemical degradation[5]. Other examples such as the adhesion of TiO_2 and cotton through 3-aminopropyltrimethoxysilane to create a new material that possesses photocatalytic and UV shielding properties[2] demonstrate the flexibility of these molecules and their broad range of applications.

Amongst these applications, the use of organosilane films for surface modification is an area of particular interest. The introduction of a silane coating enables alteration of the surface chemistry's hydrophobic or hydrophilic characteristics via an environmentally friendly method[6]. These surface alterations further lend themselves to surface protection applications, for example anti- corrosion[7] or microbial adhesion[8]. One such commercial application of silane coatings involves the application of quartz-silane based films to maintain lustre and provide protection to vehicles marketed as nano-ceramic coatings[9,10]. These coatings provide a physical barrier, protecting the metal car body from damage and thus preventing corrosion. The area of corrosion protection itself has been extensively researched, with corrosion through its degradation of infrastructure costing Australia between 3% and 5% of its annual gross domestic product in 2010[11]. Annual quantified costs include $928 million to maintain Australia's urban water industry[11] and $32 billion to maintain its bridges as estimated by The Australian Corrosion Association in 2018[12]. The most widely utilised method of corrosion protection involves the application of protective coatings creating a waterproof barrier with corrosion inhibitors on metal substrates, most containing chromate and phosphate, two highly environmentally toxic molecules[13]. An environmentally benign alternative is available in the form of hydrophobic silane molecules. The water activated self-assembly of organosilane molecules can be exploited to produce a hydrophobic barrier between metal substrates and the elements.

Silane molecules possess additional advantages over other types of protective films available today. Organosilane molecules are widely available generally at low cost and easily functionalised to produce desired characteristics[14] in addition to their ability to assemble in humid or wet environments and the stability of this chemistry at elevated temperatures greater than 100^{o}C[15]. A key point of difference between organosilane films and alternative surface coatings available is their ability to self-assemble without the need for higher temperatures or moisture during the curing process[16,17].

While the mechanism of silane hydrolysis and condensation in solution has been well studied, the mechanism by which they self-assemble on metal oxide surfaces has not been extensively investigated[18]. Optimisation of silane systems and surface coatings is typically based on empirical knowledge with the emphasis on developing new coating materials and improved performance. Given the broad interdisciplinary range of silane coating applications, understanding the mechanisms by which these molecules assemble onto a hydroxylated surface will lead to the intelligent design of experimental parameters with the aim of optimising and controlling these systems.

1.2 The Structure of Organosilanes.

Demonstrated by Propylmethyldimethoxysilane (PMDMS) below, organosilanes are a class of molecules which possess following general structure; a central silicon atom surrounded by at least one hydrolysable alkoxy (-O-CH_3) group and an organic functional group ($(CH_2)_2CH_3$). In addition to the organofunctional group, the central silicon atom may also contain one or more non-hydrolysable moieties (CH_3) in lieu of hydrolysable groups.

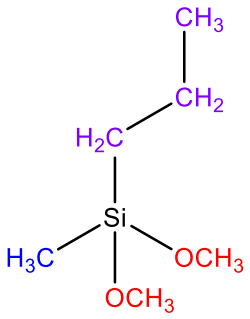

Figure 1.1: Chemical structure of the organosilane Propylmethyldimethoxysilane (PMDMS), containing an organic functional group in the form of a propyl chain (purple), a non-hydrolysable methyl group (blue) and two hydrolysable OCH_3 groups (red).

The organofunctional group represented by a propyl chain in the PMDMS molecule in Figure 1.1 can also be represented by other functional groups, which contain chemical species able to passivate the surface or couple to other chemical species. When used for surface modification, the choice of organic functional group becomes essential, as it will determine the chemical and physical properties of the newly modified surface.

1.3 The Self-assembly Mechanism of Organosilanes: Hydrolysis and Condensation

The self-assembly of organosilane molecules in solution is well known and occurs via two sequential reactions. Firstly, a water-activated hydrolysis reaction of the Si-O-CH_3 group to form a silanol (Si-OH) shown in Figure 1.2, followed by the condensation of OH groups to form siloxanes (Si-O-Si) .

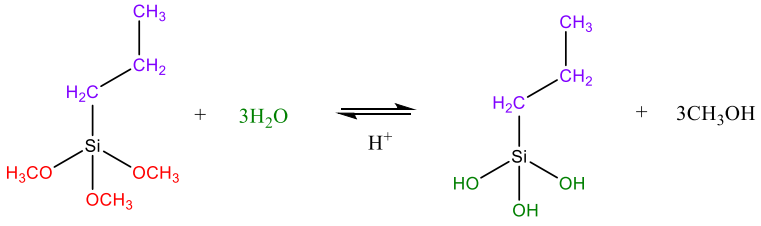

Figure 1.2: Overall reaction for the water-activated hydrolysis of Propyltrimethoxysilane (PTMS) showing the hydrolysis of all 3 methoxy OCH_3 groups (red) to the highly reactive Silanol OH groups (green).

Hydrolysis, spontaneous in the presence of water occurs when a hydroxide anion attacks the silicon atom via an S_N2 type reaction, causing the successive replacement of O-CH_3 groups with OH groups[19] as shown for the tri-functional silane Propyltrimethoxysilane (PTMS) in Figure 1.3. In the case of an acid-catalysed hydrolysis, electrophilic protonation of the O-CH_3 group enables initiation of the nucleophilic attack of water on the silicon atom and thus hydrolysis of the first methoxy group, occurring rapidly[20]. Subsequent hydrolysis of the second and third O-CH_3 groups occur stepwise following the first, the mechanism of which is shown below.

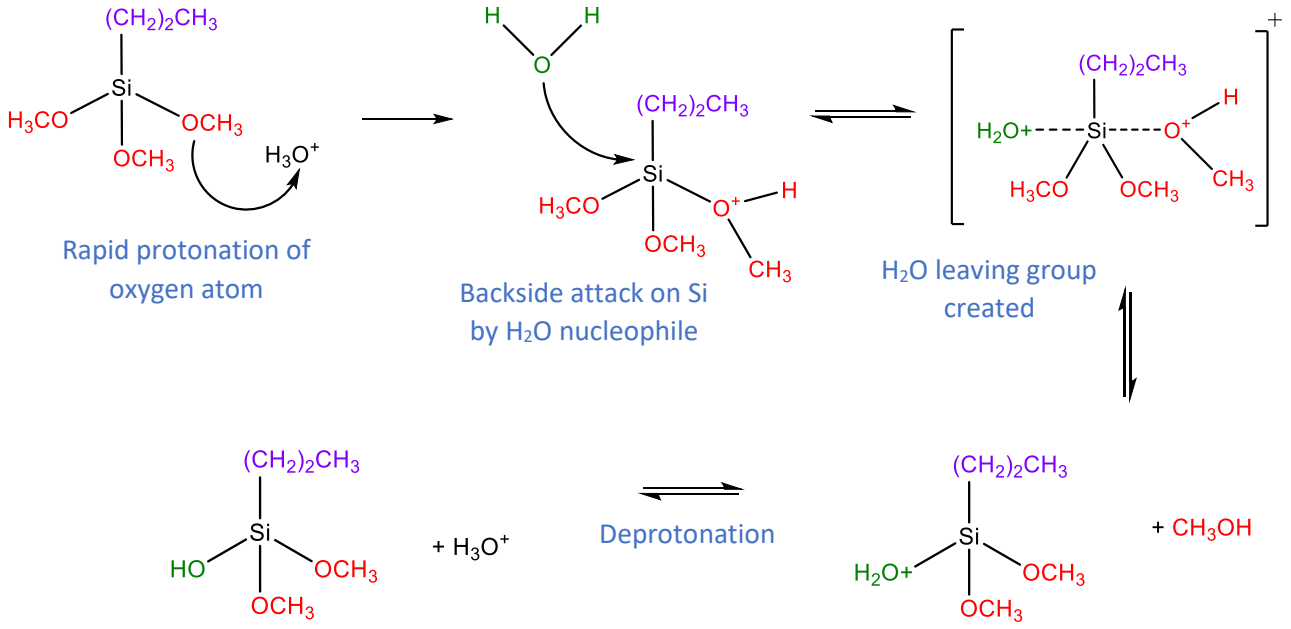

Figure 1.3: Mechanism of acid catalysed hydrolysis adapted from Lung[21] for Propyltrimethoxysilane (PTMS).

Despite alkoxy groups themselves being poor leaving groups, a protonated methoxy group is able to act as a much better leaving group. As a result of the hydrolysis reaction, highly active OH groups produced can go on to react with those of another silanols in solution via a nucleophilic silanolate ion attack causing and displacement of OH moieties[19]. In the case of a mono-functional silane such as Propyldimethylmethoxysilane shown in Figure 1.4, the condensation of two silanol molecules results in the creation of a dimer unit with no further reactions possible. The presence of multiple hydrolysable groups allows for the formation of oligomers in solution.

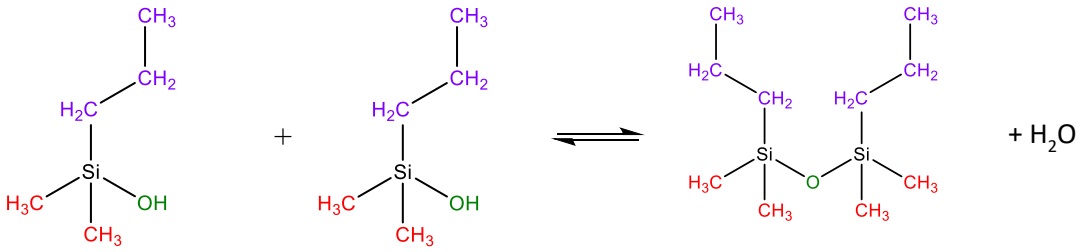

Figure 1.4: The solution-based condensation of two Propyldimethylmethoxysilane molecules each containing one hydrolysable methoxy OCH_3, group leading to the formation of a siloxane dimer.

1.4 Organosilane Film Formation

In order to create thin films of organosilane molecules on hydroxylated surface, the solution-based condensation mechanism in Figure 1.4 above can be exploited. Exposure of hydrolysed silane molecules to a hydroxylated metal surface results in a condensation reaction between OH groups of the silanol and on the hydroxylated surface, resulting in the creation of thin films. If the condensation of silanes on a hydroxylated surface follows that of silane oligomerisation in solution, the following reaction is suspected to be true;

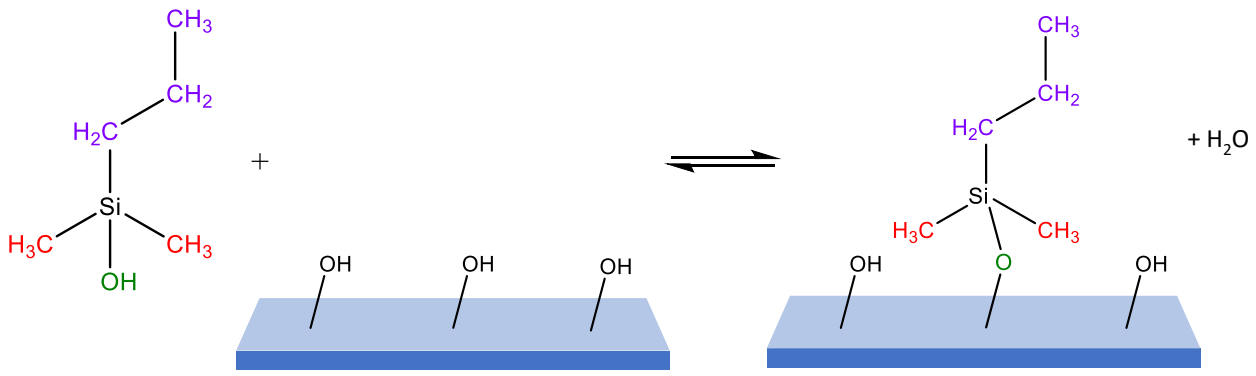

Figure 1.5: The condensation of Propyldimethylmethoxysilane, a silane containing one hydrolysable group leading to the formation of a siloxane bound to a hydroxide on the substrate.

As the number of silanol groups on the central silicon atom increases, branching and oligomerisation on the surface and in solution will result in complex oligomerised structures as shown in Figure 1.6.

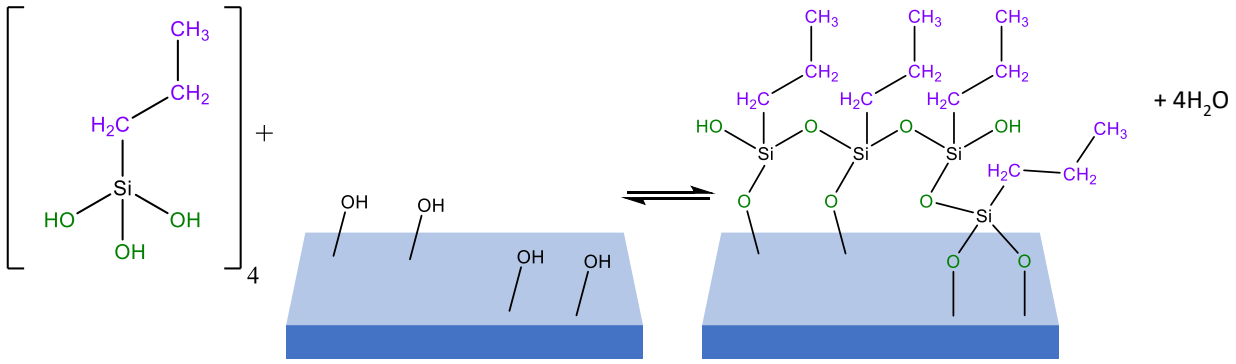

Figure 1.6: The condensation of hydrolysed Propyltrimethoxysilane molecules onto a hydroxylated surface. The increase in hydrolysed groups increases the complexity of the film, resulting in a network of branched and cross-linked siloxane oligomers.

The rate of hydrolysis and condensation is concentration dependent, with increasing concentration resulting in an increase in reaction rate. Both hydrolysis and condensation can be catalysed by acidic or basic conditions and are subsequently pH dependent. The minimum rate of hydrolysis lies at pH 7 with a change in every pH unit towards either an acidic or basic solution resulting a tenfold increase in rate[1]. For the pH

dependent condensation reaction, the rate minimum is known to lie at pH 3[1]. When determining reaction conditions it is often advantageous to increase the rate of hydrolysis, while decreasing the rate of condensation to minimise the production of oligomers in solution and maximise surface adhesion. Both of these parameters require a solution that ideally contains hydrolysed monomeric organosilane species; hence, a pH 3 solution is ideal.

In order to better understand the formation of silane films on metal oxide surfaces, it is first important to understand the general surface kinetics and thermodynamics of film formation.

1.5 Surface Kinetics:

1.5.1 Surface condensation kinetics: Langmuir adsorption

The theory of Langmuir adsorption provides a simple explanation as to the mechanism of monolayer growth on a surface with reference to the adsorption of an ideal gas onto an idealised surface as a replacement for free adsorption sites on the substrate, resulting in a monolayer on the surface[22]. This results in an exponential film growth initially increasing steeply, with the rate eventually tapering off as the vacant sites available for adsorption decrease. Langmuir adsorption can also be represented pictorially with the growth of a monolayer film occurring as the vacant adsorption sites (blue dots) are taken up by adsorbate molecules (yellow ovals) as shown below;

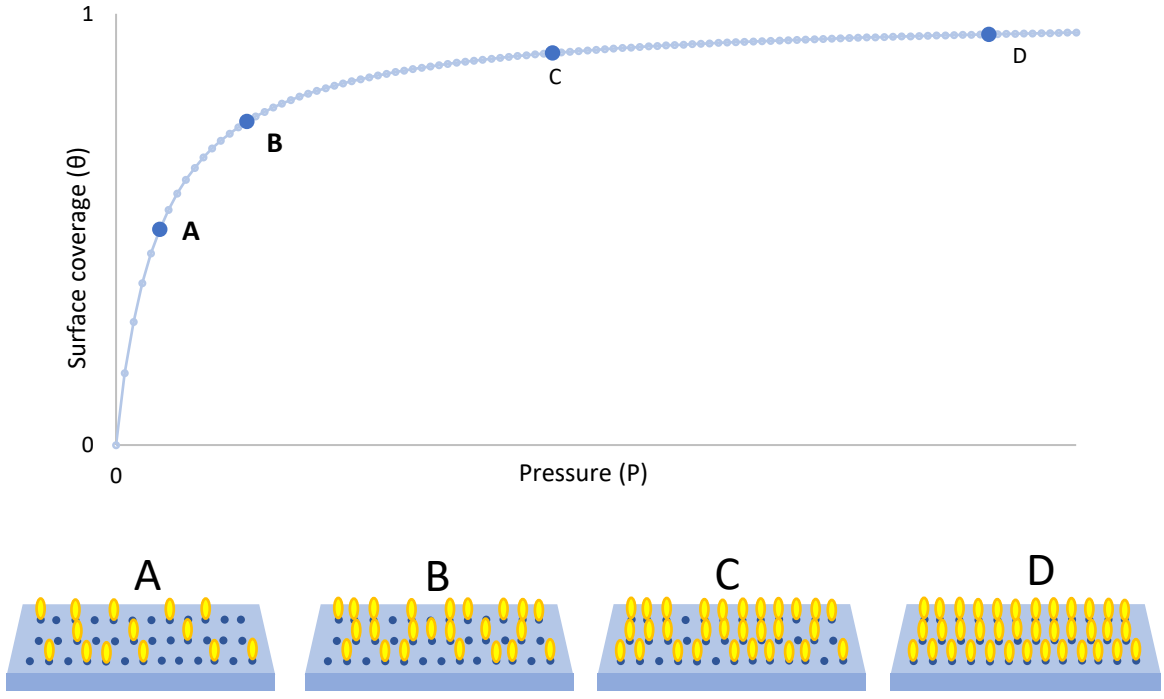

Figure 1.7: The Langmuir adsorption of an ideal gas adsorbate (yellow ovals) on an idealised surface with free adsorption sites (blue dots) detailing a value of film coverage θ as a function of pressure, P where the partial pressure P_0 is set to 1. Adapted from Masel[22].

The rate of film growth from initial adsorption (A) begins to decrease as the number of free sites decreases (B). As the number of free adsorption sites decrease even further and the pressure P exceeds the partial pressure of the adsorbate (P_0) as seen in (B) through (C), the rate of growth slows dramatically until all of the vacant substrate adsorption sites are occupied (D). The rapid decrease can partially be attributed to a rapid decease in the probability of an adsorbate finding a free adsorption site on the substrate and can be expressed by the following equation[22];

$$\theta = \frac{P}{(P + P_0)}$$

Equation 1.1

Where θ represents the overall surface coverage, P represents the partial pressure of the adsorbate and P_0 represents the pressure of the system. While expressed as a function of pressure in equation 1.1, the rate of surface coverage θ, can also be expressed as a function of time;

$$\frac{d\theta}{dt} \propto (1 - \theta)$$

Equation 1.2

Where the rate of coverage is proportional to the number of free substrate sites. In order to produce the Langmuir growth curve shown in Figure 1.7 the resulting values of θ must given by;

$$\theta = 1 - e^{-kt}$$

Equation 1.3

In order for the above film growth pattern to be true, the following thermodynamic assumptions are made[22];

- Adsorption occurs onto an immobile substrate
- All adsorption sites are equivalent
- Each adsorption site can hold only one adsorbate
- There are no interactions between adsorbate molecules
- Adsorption continues until the substrate becomes saturated

It is also important to note that formation of the monolayer shown above applies to a film which cannot act as a substrate for additional growth such as silane molecule with only 1 hydrolysable group an example of which was given in Figure 1.5. Hence this model cannot be applied to a multilayer system such as silane molecules with more than 1 hydrolysable group as shown in Figure 1.6, and provides a very general representation of chemisorption systems[22]. A further limitation of the above model is its inability to account for adsorbate-adsorbate interactions.

1.5.2 Kinetics of substrate-adsorbate interactions

Considering only the interactions between substrate and adsorbate, the condensation reaction between a silanol species and an aluminium substrate can be described via the following first order kinetic equation[23];

$$\frac{d\,[\mathrm{Si}-\mathrm{O}-\mathrm{M}]}{dt} = k[\mathrm{SiOH}][\mathrm{M}-\mathrm{OH}]$$

Equation 1.4

Where;

Si-O-M	Represents the covalent bond between silanol and metal substrate
SiOH	Hydrolysed silanols in solution
M-OH	The metal-OH bonds (free adsorption sites on the surface)

The rate of Si-O-M bond formation is proportional to the concentration of metal-OH bonds, and thus considering these interactions enable a first order kinetic equation to be used to produce a model for adsorbate-surface condensation. If adsorbate-adsorbate interactions are included the reaction becomes second order, values for θ_x can no longer be solved analytically and the model can only be solved numerically[23].

1.6 Physisorption vs chemisorption

The extent of adsorption to a substrate is often described as physisorption or chemisorption depending on the strength of the interaction between the substrate and adsorbate. Physisorption, the formation of weak interactions between the adsorbate and substrate typically range from 0.2 to 4 kJ/mol[24]. These bonds are considered the weakest of interactions and can be easily broken.

Chemisorption occurs when the adsorbate becomes chemically bound to the surface through the formation of a bond via the sharing or transfer of electrons, the most commonly known interaction of which being the formation of a covalent bond with interactions lying in the hundreds of kJ/mol. However, the strength of hydrogen bound interactions lie between that of physisorbed and covalently bound species at 12-30 kJ/mol[24]. The formation of covalent substrate-adsorbate bonds can originate from physisorbed interactions and hydrogen bound species, making the rate of condensation dependent on the rate of both physisorption and chemisorption.

1.7 Investigations into Film Formation

The majority of investigations into silane films centre around the final composition with view of determining the films' industrial applications. Examples of this include determining the composition of a double layer silane film deposited on galvanised steel using X-ray Photoelectron Spectroscopy (XPS), Auger Electron Spectroscopy (AES) and Scanning Electron Microscopy (SEM)[25]. The composition of both layers was determined and compared to that of a single layer silane film. This was done in view of determining if the silane film produced had a greater impedance and corrosion resistance than the single layer films previously produced[25].

The use of silane molecules in 'self-healing' films capable of automatically repairing themselves, repairing bulk mechanical damage and increasing the life of the substrate[16] has also become a popular area of silane film research. Silane chemistry is exploited for its ability to self-assemble in humid conditions, stability in elevated temperatures and their ability to be encapsulated within the film bulk[14,15]. Organosilane molecules are widely available generally at low cost and easily functionalised to produce desired characteristics[14]. Improvements to film performance is outcome orientated with additions of adhesion promotors and encapsulated catalysts as a solution to failures in film performance[14,16,26,27]. Current experiments centre around the optimisation of viscosity[26], healing agent[14,15,26], catalytic activity[15,26], and adhesion promotors[15] with the aim of creating a system able to heal itself at ambient temperatures without the need for external interference such as high curing temperatures or extended healing times between damage loading. The mechanism of silane self-assembly within these films is rarely investigated.

Investigations into film formation that are conducted often focus on more complex silanes such as bis-silanes, commonly used in industrial and practical applications. The surface and interface characteristics of the non-organofunctional silane, 1,2-bis(triethoxysilyl)ethane, and an organofunctional silane, g-mercaptopropyltrimethoxysilane deposited on Al, Zn and Al-43.4Zn-1.6Si (AlZn) alloy coated steel was investigated in a dissertation by Bexell in 2003[28]. A combination of Time-of-Flight Secondary Ion Mass Spectrometry (ToF-SIMS), AES and XPS were used to analyse the surface and interface characteristics of silane films and organic coatings. Results show that film composition is independent of pH during film deposition and metal substrate type[24]. This however does not mean that solution pH does not affect the rate of reaction and thus a pH of 3 is still optimum for increasing the rate of hydrolysis and while decreasing the rate of condensation. The presence of Si-O-Metal ion fragments in the ToF-SIMS spectra is also an indication that there is a chemical interaction between the silane film and metal substrate. While the results presented by Bexell[28] provide insight into the role of pH in the self-assembly of the silane molecules studied, the use of large, intricate silane molecules introduces complex intermolecular interactions to the system. In order for the fundamental mechanism of silane-substrate interactions and thus film self-assembly to be determined and successfully modelled, the effect of intermolecular interactions must be reduced as much as possible.

The formation of silane films can occur in both aqueous and anhydrous solvents. Anhydrous solvents such as benzene and toluene are commonly used to create reproducible, homogeneous silane films[29]. Silanes typically have a low solubility in water until hydrophobic hydrolysable groups are converted to hydrophilic silanol groups[28]. Cho *et al.*[15] determined that in order to control the extent of polymerisation at the silane-substrate interface and in solution, an adventitious amount of water is required in an anhydrous solution and that a low concentration of silane discourages the formation of oligomers and polymers in solution. Creating silane films at 70^{o}C was found to disrupt hydrogen bonds and reduce the number of weakly bound silane molecules[8,16]. The removal of weakly bound silane molecules via rinsing with toluene, ethanol and water was shown by Cho[14] and Cottrell[26], while curing through drying of silane films has been shown to remove water, promoting condensation of hydrogen-bound silanols to covalently bound species[13-15,19,18]. While Significant effort has been made to optimise reaction conditions in solution in order to create silane layers with structural regularities[29], the accumulative factors and fundamental mechanism of silane film self-assembly has not been determined. Constant fluctuations in film composition have been attributed to reversibly bound OTS molecules both on an oxide substrate and between OTS molecules were acknowledged during a study of the time dependent formation of OTS monolayers by Sagiv in 1980[30]. Capacitance and conductivity of the resulting OTS films revealed the presence of a true monolayer. The formation of these films in anhydrous solution, where water was only present on the surface of the substrate ensured that only OTS molecules condensed to the surface are hydrolysed; due to the long carbon chain of OTS, oligomerisation did not occur.

Studies into the film formation of the non-organofunctional silane 1,2-bis(triethoxysilyl)ethane using ToF-SIMS revealed the presence of a metal-oxygen-silicon fragment in solution after the silane was exposed to Al, Zn and an AlZn alloy. This not only indicates that there is a strong interaction between the silane and metal, but that this interaction is due to the formation of a covalent bond between the silane an the metal substrate[31], giving further weight to the proposed condensation mechanism shown in Figure 1.6. Silane films were also analysed using AES to determine the film thickness and the three-dimensional distribution of the elements via depth profiling. In 2002, the effect of solvent on the hydrolysis of the silane *y*-glycidoxypropyl trimethoxy silane was conducted using proton Nuclear Magnetic Resonance (NMR) of the hydrolysis solution in conjunction with XPS and ToF-SIMS studies of the films deposited[32]. Experiments were carried out until completion of the hydrolysis reaction and revealed that the addition of methanol to an aqueous solution prevents hydrolysis and dramatically slows the hydrolysis kinetics when added at 90% (v/v). The sole use of methanol as a solvent stops the reaction completely. When increasing the ratio of methanol to water in the solvent from 1:9 to 9:1, the hydrolysis time increased by 65.3%[32].

Alternatively the use of a water based solvent was considered for industrial applications due to the high cost as well as the ecological and health issues associated with the use of methanol and anhydrous solvents[33]. The silane Bis-1,2-(triethoxysilyl)ethane was previously used in a methanol based solvent due to its low solubility

in water. The solution stability of aqueous solvents was tested with the extent of hydrolysis and condensation reactions in a water-based silane solution questioned[29]. Si-NMR spectra was used to determine the extent of silane hydrolysis and condensation. Results revel there to be no fully hydrolysed silane monomers present in the water-based solution, however the presence of condensed species such as dimers, trimers etc was confirmed. When compared to the silane in a menthol-based solution, there was a significant increase in the presence of high molecular weight condensed species in the water-based silane solution. The ratio of oligomers to larger condensed species in the water based solution was estimated to be 40% of oligomers to 60% of larger species[33]. The results shown by Abel[32] and De Graeve[33] reveal a significant reduction in the rate of the hydrolysis reaction as the concentration of methanol in solution is increased. This may lend itself to another mechanism by which the rate of reaction is controlled in addition to concentration and pH of solution.

The effect of substrate on the morphology of silane films produced was investigated by Pan *et al*. in 2005[34]. Films of bis-(triethoxysilylpropyl)-tetrasulfide and bis-(trimethoxysilylpropyl)amine were deposited on aluminium and silicon substrates with the aim of understanding the water-silane interaction and optimising the desired properties of the resulting film. Neutron Reflectivity was used to determine the morphology and the response to water conditioning of silane films deposited on silicon wafer and aluminium coated silicon wafer. The substrate-surface interface was found to depend on both silane and substrate. As the pH of the bis-silane solution is outside of the stability region for the Al_2O_3 substrate, dissolution of the thin oxide layer occurs during film deposition, causing a water-depletion area to form at the interface region. A 10Å hydrophilic layer at the oxide-sliane interface was found on all three films produced. This layer might be due to unreacted OH groups on the substrate surface forming a hydrophilic layer that attracts water through hydrogen bonding. Differences in isoelectric point (IEP), solubility of the metal hydroxide in water as well as the density and acidity of the hydroxyl groups on the surface strongly effect the molecular structure of the film produced. The amount of unreacted OH groups and therefore the number of available OH bonding sites on the surface is highly dependent on the substrate. Shrinking and swelling of the films indicates the extent of hydrolysis and condensation. If the bis-amino silane film was fully condensed, with all methoxy groups condensed to –Si-O-Si- bonds and no condensation leading to a decrease in the films thickness occurs after it was cured at 80^{o}C. If the bis-sulfur silane film is not fully condensed, further hydrolysis and condensation of unhydrolysed ethoxy groups to siloxane bonds occurs when conditioned at 80^{o}C, evident by the shrinkage of the film instead of swelling after exposure to water at 80^{o}C. These results also confirm that 80^{o}C is sufficient to fully condense the bis-amino silane, however the bis-sulfur silane required higher curing temperatures to result in full condensation[34].

The self-assembled monolayers of 3-aminopropyltrimethoxysilane (3-APTS) on silicon surfaces and the effect on ultraviolet treatments on the assembly process were investigated by Cui *et al* in 2010[35]. XPS and Atomic Force Microscopy (AFM) results reveal the 3-APTS molecules are bound to the substrate surface in a nearly

a vertical orientation with a substantial level of disorder in molecular packing. It is suggested that the disorder is due to intermolecular interactions between the amine tails of the silane molecules. It is also stated that UV irradiation of the silicon substrates prior to the self-assembly reaction can enhance the assembly process and increase the coverage of the monolayer as UV irradiation significantly changed the surface properties of the silicon substrates used. Changes to the substrate prior to silane exposure include more carbon and less oxygen found for silane monomers coated on the UV-irradiated substrates than those coated on the as-etched substrates. Larger carbon content indicates a surface layer rich in carbon and is believed to indicate the presence of a monolayer of silane molecules formed on the substrates. AFM has also been used successfully to map the nucleation of self-assemble monolayer of long carbon chain, tri-chlorosilanes in in-situ study conducted by Iwasa *et al*[36]. Morphological behaviour revealed the growth of monolayer islands from a nucleation site on the surface with minimal surface bonds. The competitive monolayer self-assembly of chlorosilanes octyltrichlorosilane $CH_3(CH_2)_7SiCl_3$ and tridecafluoro-1,1,2,2-tetrahydrooctyl-1-trichlorosilane, CF_3-$(CF_2)_5(CH_2)_2SiCl_3$ were used to monitor the preferential deposition of the fluorinated compound on fused silica using Sum Frequency Generation Spectroscopy (SFG)[37]. Evidence of the co-adsorption of fluorinated and non-fluorinated molecules in mixed monolayers was found and reveals that unlike similar Langmuir-Blodgett films, the different silanes do not segregate into different phases.

Studies into film formation give an insight into the effects of altering conditions, and an indication of the techniques used to analyse silane films, their capabilities and complimentary nature. However as detailed above, the adsorbate-adsorbate interactions in solution and on the surface play a significant role in the mechanism of film growth. By investigating the mechanism of film growth using large, complex silane molecules the mechanism of film growth with respect to only the adsorbate-substrate interactions cannot be accurately investigated.

Simplification of silane molecules used to determine the mechanism of film growth were investigated by Quinton *et al*.[23,38-41] In order to minimise intermolecular interactions between silane molecules, Propyltrimethoxysilane (PTMS) was used. This silane was chosen as it is one of the simplest molecular structures of silane commercially available[39]. The propyl chain reduces interactions while allowing the silane to remain stable in solution. An oscillation in the growth of silane films as a function of both time and concentration was observed by using X-ray Photoelectron Spectroscopy to analyse the films produced when exposed to metal oxide substrates[23,38-43]. Initially the oscillatory behaviour appeared to be present upon exposure to aluminium but not iron[39,43]. Later experiments and subsequent publications reveal this oscillation is present for many metal oxide substrates including chromium, zinc, aluminium and iron[42]. This behaviour is not unique to trialkoxysilanes and has also been observed by Houssiau & Bertrand[44], who demonstrated the existence of oscillatory adsorption behaviour in alkyltrichlorosilane adsorption on evaporated aluminium surfaces from bicyclohexyl $(C_6H_{11})_2$ solution. Their result independently verified the existence of the oscillatory adsorption behaviour and showed that this oscillatory behaviour is not due to the choices of silane

or experimental coating technique used, but rather is a very real phenomenon that appears to occur in general for silane solutions, regardless of whether the solvent is aqueous or organic in nature. The existence of active species on the non-hydrolysable organofunctional group further complicates the adsorption process. Quinton & Dastoor[45] demonstrated that the existence of an active functional species such as an NH_2 can adsorb to the substrate through hydrogen bonding. Furthermore, for the conditions in their study the aminotrialkoxysilane molecules were shown, on average to reorient themselves as part of the self-assembly process.

The IEP is also shown to have a dramatic effect on the rate of oscillation. The closer the IEP is to the pH of solution, the quicker the initial adsorption rate of silane on the surface[42]. The slightly more complex silane *y*-aminopropyltriethoxysilane (APS) was also studied in order to determine if the oscillatory nature is present for more complex molecules[45]. Using XPS to determine the extent of film coverage and ToF-SIMS to analyse the time dependence of the known bonding moieties of the APS molecule it was seen that the molecular orientation of the adsorbate changes as a function of time[45]. In order to explain the single oscillation observed, a mathematical model was produced By Quinton & Dastoor[23,41] to fit the experimental data collected. In order to understand the mechanism of growth and the model proposed, it is necessary to understand the simpler model for a 2-component system a Langmuir adsorption.

1.8 Modelling Langmuir adsorption

In order to understand the role of individual components in the overall Langmuir adsorption profile shown in Figure 1.7, the mechanism of adsorbate-substrate adsorption can be modelled. In the case of Langmuir adsorption, a 2-component model is sufficient to describe substrate-adsorbate interactions. To understand this, we must note that the condensation reactions shown in Figure 1.4 and Figure 1.5 tend towards equilibrium and not completion. The presence of this dynamic equilibrium allows the molecules to become reversibly bound to the substrate.

Hence, if we consider that the first component, θ_1 approaches the substrate but remains reversibly bound, while a second component, θ_2 approaches but can only become irreversibly bound to the substrate upon the displacement of θ_1, the sum of θ_1 and θ_2 shown in Figure 1.8 will result in the Langmuir adsorption curve described by Masel[22,38,41]. It is important to note that while the representation of 2 single components results in the overall Langmuir growth profile from a mathematical standpoint, in reality these components do not represent individual molecules. Components in fact represent the collective behaviour of molecules in solution, initiated upon the introduction of the substrate.

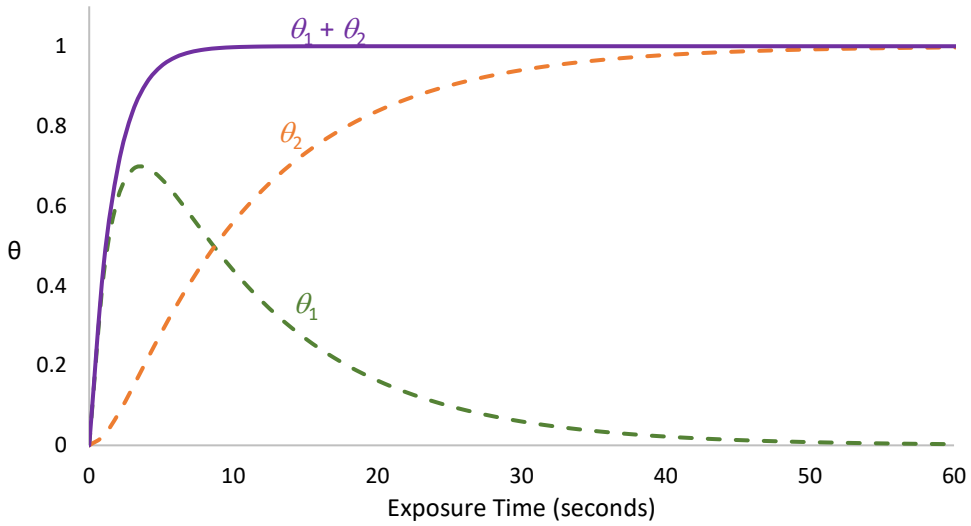

Figure 1.8 The two component model used to describe the Langmuir mechanism of film growth. The sum of θ_1 and its displacement by θ_2 results in the exponential growth curve typical of Langmuir adsorption adapted from Quinton[38].

The initial adsorption of θ_1 can be described via the following first order kinetic equation;[41]

$$\frac{d\theta_1}{dt} = k_1(1-\theta) - k_2\theta_1$$

Equation 1.5

Where the rate of θ_1 adsorption depends on the number of free substrate adsorption sites and the displacement by θ_2. Subsequently the rate of θ_2 depends on the number of θ_1 species present via;[41]

$$\frac{d\theta_2}{dt} = k_2\theta_1$$

Equation 1.6

In reality θ_1 and θ_2 can represent the same molecule, with displacement of θ_1 by θ_2 describing the conversion of a hydrogen adsorbate-substrate bond to a covalent bond. Hence the decrease in θ_2 does not necessarily represent the removal of a molecule from the surface, but rather a reduction in the specific hydrogen bound adsorbate-substrate interactions.

1.9 Modelling the oscillatory nature of adsorption and desorption

As reported previously by Quinton *et al*,[23,38-41] the overall adsorption of the organosilane PTMS to a metal oxide surface does not behave as predicted by the basic adsorption theory described by Langmuir, but rather undergoes an oscillation in film coverage as a function of both time and concentration. In order to explain the oscillatory nature observed, the following kinetic model was produced.

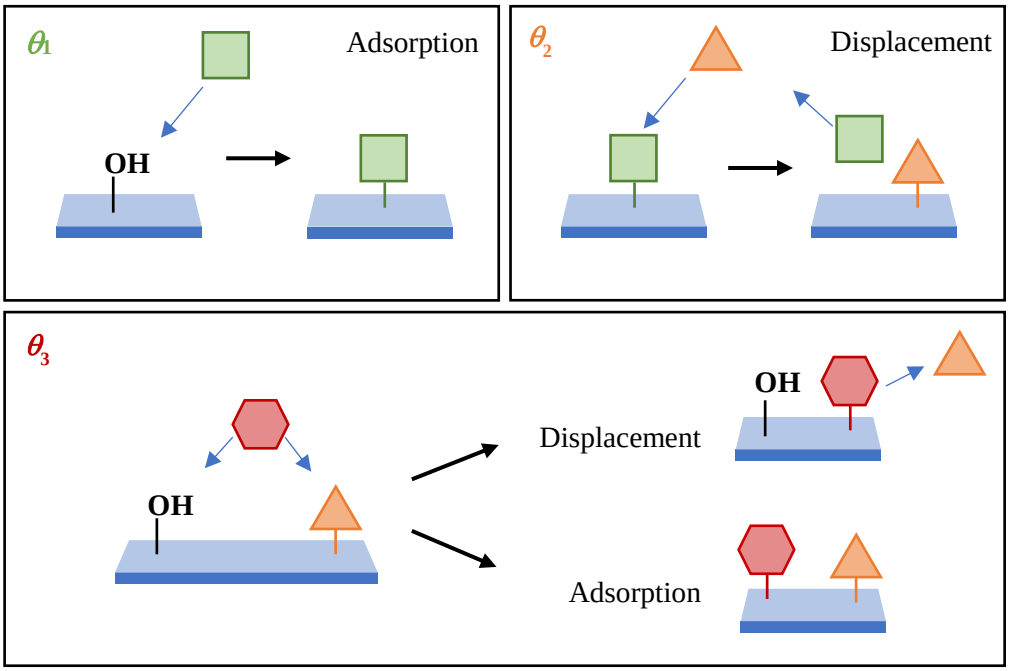

Figure 1.9 The three component model to describe the oscillatory nature of PTMS adsorption on metal oxide surfaces, adapted from Quinton[38]. Silicon containing species are represented by squares and hexagons, while the non-silicon containing species (H_2O) is represented by a triangle.

Originally approached from a purely mathematical stand point, it was proposed that in order for an oscillation to occur, the system must contain at least three separate components represented by squares, triangles and hexagons in Figure 1.9. Initially the model was produced by assuming that each individual species (of varying chain length and overall oligomer size) adsorbed according to Langmuir kinetics. This was done in order to obey the first order kinetic reaction described for the condensation reaction shown in Equation 1.2. The overall rate of which can be described by the following equation[38,41];

$$\frac{d[S_L]}{dt} = k_H[H^+][S'][S_H]$$

Equation 1.7

Where;

$[S_L]$ Is the concentration of Si-O-(Surface) bonds

$[S_H]$ The concentration of Free OH adsorption sites

$[S']$ The concentration of silanols in solution

k_H Rate constant.

The incorporation of all three components as silicon containing species and thus the sum of θ_1, θ_2 and θ_3 shown in

Figure 1.10 produces surface coverage as a function of time as predicted by Langmuir kinetics. In order to produce an oscillation, the sum of θ_1 and θ_3 were used, leading to the conclusion that θ_2 in the model shown in Figure 1.9 must represent a non-silicon containing species. Upon further examination of the condensation reaction shown in Figure 1.4 through Figure 1.6, it was proposed by Quinton & Dastoor[23,38-41] that the non-silicon containing species, θ_2 represented by triangles in Figure 1.9 is in fact water produced by the condensation of bonds localised to those becoming displaced. While this is highly possible the role of the hydrophilic hydroxylated surface cannot be ignored as shown by Pan *et al*[34], who proposed that an aqueous layer at the silane-substrate interface was due to the hydrogen bonding of water molecules to available -OH substrate adsorption sites.

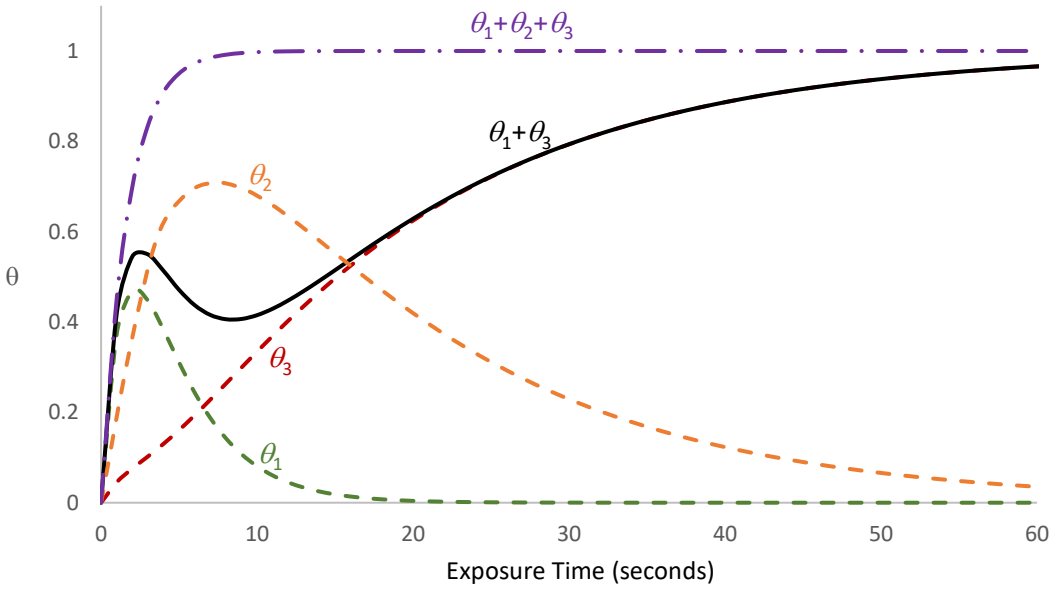

Figure 1.10 Surface coverage predicted as a function of time for the three component model proposed adapted from Quinton[38,41]. In order to produce an oscillation only θ_1 and θ_3 are considered to be silicon containing species.

Furthermore, in order to account for the initial adsorption, desorption and subsequent re-adsorption seen in the experimental data produced, a unique rate constant is required for each process (known as k_1, k_2 *and* k_3)[38,41]. The general process shown in Figure 1.11, reveals how the presence of three components each with their own adsorption or desorption process and unique rate constant, produce a mathematical function to fit the oscillatory behaviour seen experimentally.

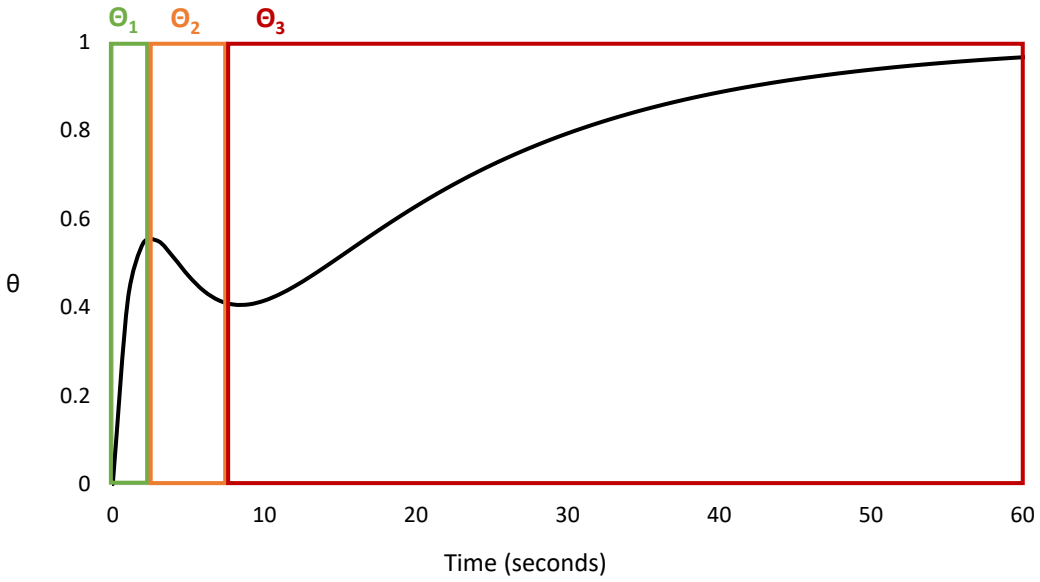

Figure 1.11 General process of PTMS adsorption onto metal oxide surfaces as modelled by Quinton detailing the mathematical account of initial adsorption (I), desorption (II) and subsequent re-adsorption (III) seen in the experimental data[38].

Initially the rate of θ_1 follows the adsorption as seen in the 2 component model above, where the rate of adsorption depends on the number of free substrate adsorption sites[41].

$$\frac{d\theta_1}{dt} = k_1(1-\theta) - k_2\theta_1$$

Equation 1.8

Where $k_2\theta_1$ takes in to account the rate decrease as θ_1 is displaced by θ_2. The rate of displacement further depends on the presence of θ_1[41].

$$\frac{d\theta_2}{dt} = k_2\theta_1 - k_3\theta_2$$

Equation 1.9

Leading to the rate of re-adsorption being dependent on both the number of free substrate adsorption sites and the presence of θ_2.

$$\frac{d\theta_3}{dt} = k_3(1-\theta) + k_3\theta_2$$

Equation 1.10

As for relative rates it was noted by Quinton[38] that k_1 and k_2 appear to be very similar in magnitude, while k_3 is considerably smaller. Indicating that the initial adsorption and desorption processes occur quickly with the rate of k_2 largely dependent on k_1, while the overall adsorption process of k_3 is much slower by comparison[38] as at equilibrium the rate of adsorption must equal the rate of desorption if the rate of desorption is presumed to follow a first order rate law[22]. It is also important to note that the rate of silanol condensation is predicted to be much more rapid towards a surface than in solution[1,38].

1.9.1 Surface reaction mechanisms

The mechanism by which organosilanes adsorb to a metal oxide substrate using a surface catalyst requires a chemical reaction. The kinetic control of this adsorption can be explained by 3 generic mechanisms[22].

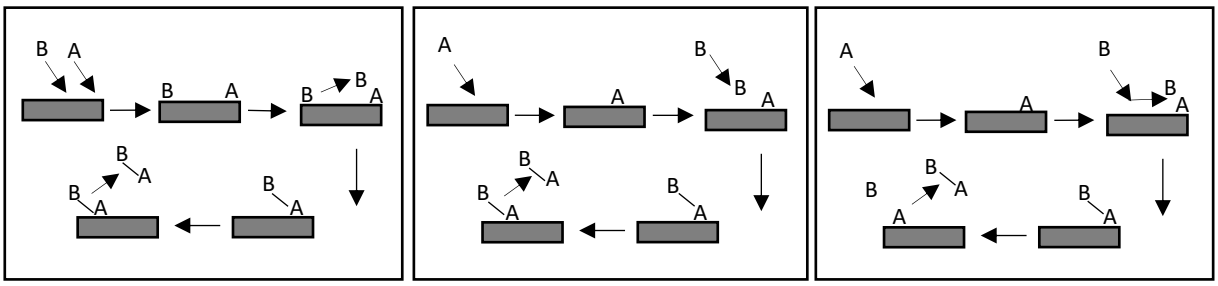

Figure 1.12: Schematic of 3 generic mechanisms used to explain kinetics of silane adsorption. Langmuir-Hinshelwood (left), Rideal-Eley (centre) and Precursor (right) mechanism for the reaction of silanes A and B in A + B --> A-B. Adapted from Masel[22].

Langmuir-Hinshelwood: B diffuses across the surface to join with A

Rideal-Eley: B joins directly to A (without binding to surface)

Precursor: B initially joins to the surface and diffuses towards A where is desorbs and joins to A (combination of first 2 mechanisms)

The thermodynamically and kinetically controlled mechanisms described above assume that adsorption increases in a particular order, despite the majority of adsorption being thought to occur through the Langmuir-Hinshelwood mechanism[22], it has been shown by presence of an oscillation, that organosilane film growth does not necessarily behave in this way[38].

1.9.2 Desorption: Le Chatelier's Principle

According to Le Chatelier's principle a system in a dynamic equilibrium will shift the position of its equilibrium to adjust to changes such as an increase in concentration, pressure or temperature[46]. As the condensation reaction detailed above tends towards equilibrium via the formation of a hydrogen bond between adsorbate

and substrate, hydrogen bound adsorbate species can be removed by an increase in the local water concentration of the system. This increase can be attributed to the products of the condensation reactions resulting in the formation of an Si-O-Si bond between two silanol species shown in Figure 1.4, the condensation of silane species to a hydroxylated substrate shown in Figure 1.5 and the hydrophilic nature of hydroxylated surfaces. In response to a localised increase in water present, the equilibrium shifts to the left and the hydrogen bonds between adsorbate and substrate may be broken, causing the removal of film from the substrate. With reference to the model shown in Figure 1.9 water molecules represented by a triangle displace the initial silanol adsorbed to the surface (represented by a square) creating another free OH site on the surface to which the third component, a silicon containing species (represented by a hexagon) can adsorb.

1.10 Surface condensation thermodynamics and energy barriers

Although the formation of a covalent adsorbate-substrate bond is thermodynamically favourable, such a bond is only possible via the formation of a hydrogen bond as described by the 2-component model. The formation of covalently bound Si-O-Si or Si-O-Substrate bonds via a hydrogen bound intermediate has also been proposed by Arkles[47].

If the displacement of the hydrogen bound θ_1 species by θ_2 described in the 3-component model occurs prior to conversion to a covalently bonded species, the displacement through the shift in dynamic equilibrium prevails over the thermodynamically favourable product. In order to take into account the role of thermodynamics in the system, it is helpful to think of the formation of hydrogen and covalent bonds and the energy required for these reactions as potential wells[48].

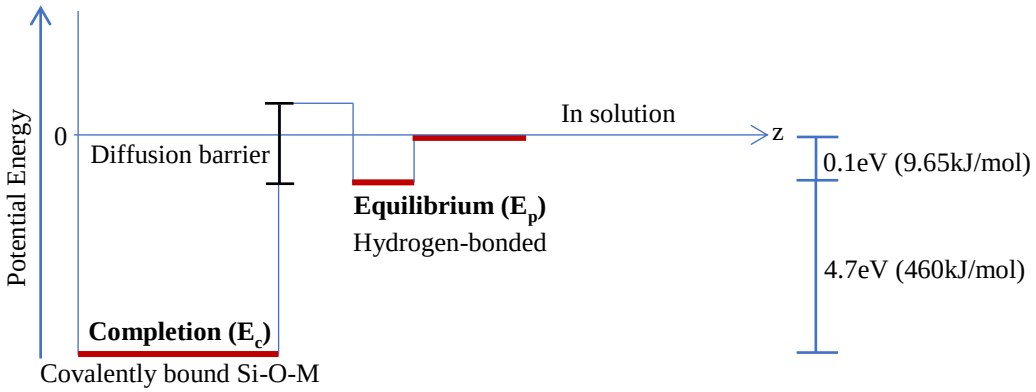

Figure 1.13 Potential energy diagram for chemisorption on a planar surface to show the conversion of hydrogen to covalently bound silane adsorption adapted from Prutton[49] . Bond energies specific to the formation of Si-O and hydrogen bonds taken from Cottrell[24].

Once the adsorbate is in the hydrogen bonded equilibrium potential well, it can become covalently bound by crossing the diffusion barrier towards the thermodynamically favourable product or become displaced by a

localised increase in water concentration. A pictorial representation of the formation of a covalently bound film via the formation of two hydrogen bounds with a PMDMS dimer is shown below;

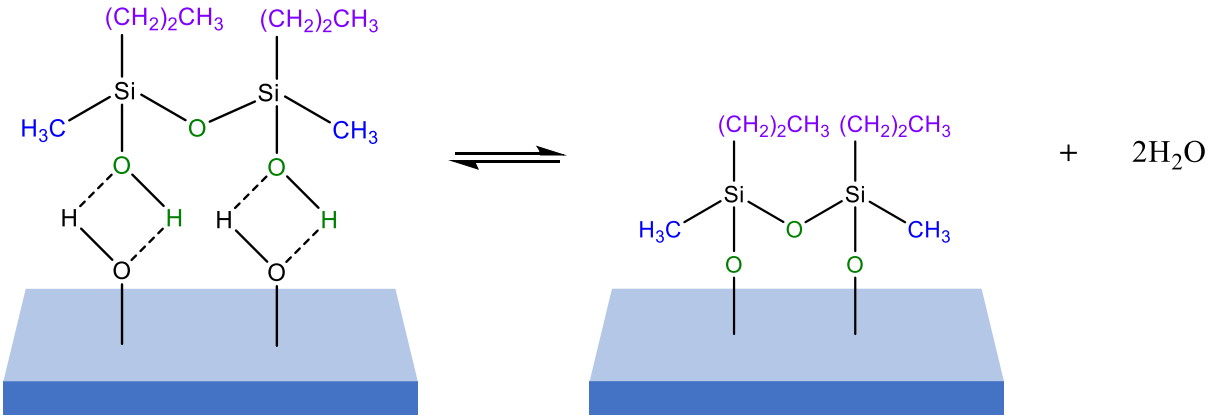

Figure 1.14: The formation of a covalently surface bound dimer of PMDMS via the formation of 2 hydrogen bonds between silane and surface OH groups. The conversion of hydrogen to covalently bound species was first described by Arkles[47].

1.11 Three-dimensional printing of aluminium powders

Polymers are still the most widely known three-dimensional (3D) printing material with thermoplastic 3D printers first commercialised in the 1980s. The marketplace is now flooded with affordable thermoplastic printers and is predicted to reach in excess $1billion by 2025 despite the decreasing cost of starting materials[50]. 3D printing allows users to cost effectively design and build intricate, custom structures layer-by-layer that would previously be impossible in a domestic and commercial setting[51]. Naturally, this has led to research into 3D printing of materials other than thermoplastics such as Additive Manufacturing and the 3D printing of metals.

The ability to 3D print materials has provided a new and improved way of building structures and expands upon the capabilities of additive manufacturing by merging the 3D printing technologies currently available and the knowledge of metal manufacturing commonly utilised for casting, forging and machining. 3D printing of metal materials is an emerging field of manufacturing research as it provides an opportunity to decrease processing time, create intricate custom structures and reduce the presence of joint failures over traditional methods of metal manufacturing such as welding, forging, rolling or casting[52]. Referred to as Additive Manufacturing as the process involves the layer upon layer joining of materials to make objects from 3D model data, as opposed to subtractive manufacturing methods. Additive Manufacturing has significant implications commercially as it reduces costs related to quality as a single computer program can be used indefinitely to create reproducible, high quality structures while also reducing manufacturing time of parts in terms of speed and work force required when compared to traditional forging or casting processes[53].

Current applications include research in the automotive, aerospace, medical and defence space and have now expanded from the confines of a laboratory to become available commercially[54,55]. There are currently two main methods of metal 3D printing available commercially, Wire Arc Additive Manufacturing (WAAM) and Laser Metal Deposition (LMD). Both methods are currently undergoing intense research, development and optimisation and have been derived from the original method of polymer 3D printing. Both methods involve the construction of single layers fused together, gradually built over time to create a 3-dimensional structure.

Wire Arc Additive Manufacturing, known as WAAM begins with the material to be printed in the form of a wire. A traditional arc welding mechanism is attached to a robotic arm and layers built via the welding of the wire. As each layer is comprised of single wire exploited as the consumable electrode, welded to the layer above and below, the layer thickness, commonly referred to as wall height remains fixed, typically ranging between 1-2mm high and up to 17mm wide[56] and is heavily dependent on the radius of the original wire[57]. While increasing the wall height significantly increases the speed of manufacturing and the size of products printable, it decreases the level of intricacy possible in the final printed structure and requires additional machining to complete the part[57]. It is because of this that WAAM is more commonly used in the manufacturing of larger, less intricate parts.

The second means of metal 3D printing and the method utilised in this thesis is Laser Metal Deposition (LMD). The process has since evolved, but the concept of creating a thermal field induced by a moving laser was first patented by Brown *et al*. in 1982[58]. LMD requires starting materials in the form of powders ranging from 20-90 µm with common granulometries ranging from 40-90 µm. Small particle sizes are preferred as they possess a higher surface area for laser interaction, requiring less energy for improved melting[59,60] and increase the density of printed products[61]. Powdered metals are deposited by a stream of argon and sintered in layers simultaneously melting small quantities of material using a laser to form a clad after solidification, with wall heights typically ranging between 0.1 and 2mm and a typical width of approximately 1mm[52]. Although the construction of larger structures is possible using LMD, significantly smaller wall heights than that of WAAM and ability to vary composition of the printed material in-situ, has led to LMD becoming the preferred method of metal 3D printing for repair, remanufacturing and complex surfaces[57].

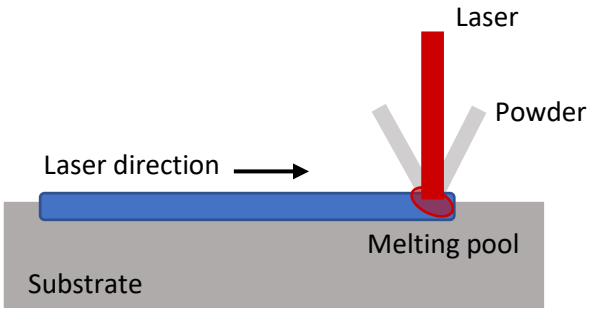

Figure 1.15: Laser Metal Deposition process adapted from Cheikh[52].

Parameters such as wall height, powder flow rate and true path of the laser are all programable[52,58]. The presence of multiple feeders and reservoirs for starting materials allow for the programming of different feed rates and control over composition at any time during the manufacturing process. This overcomes a common challenge of composite materials using a powder metallurgy process where the sintering temperature must be carefully controlled as to only partially melt the metal of lowest melting point, binding the materials together[58]. The rapid solidification process of LMD also allows for the production of non-equilibrium phases and in-situ composite formation[62-64]. This has enabled the creation of novel composite materials not possible with conventional metal manufacturing processes. Aside from the creation of new parts, LMD processing is commonly used in the repair of metal components[65,66].

Efforts to understand and optimise the production of LMD printed materials and determine the effects of processing parameters have followed with the properties of the printed material found to be dependent on both the sintering mechanism as well as the microstructure of the printed material[67]. Kelly and Kampe[54] demonstrated the importance of microstructural evolution and characterisation in multilayer builds through the observation of Ti-6Al-4V grain boundaries and a difference in macroscopic morphology of the laser deposited material and layer bands between them. These differences were found to be a result of the complex thermal reactions occurring during the build process and not as a result of segregation or oxidation of layers in between layer depositions. This is crucial as it allows for the LMD process to be conducted under atmospheric conditions. Mahamood *et al*.[68] determined that as the flow rate of powder is increased, the wear resistance of the Ti_6Al_4V/TiC printed composite decreased however, increasing laser powder increased wear resistance. While Hong *et al*.[69] investigated the changing microstructure of TiC/Inconel 718 composites through varying laser power and Lalas *et al*. investigated the effect of varying process speed, powder feed rate and surface tension between added material and substrate to estimate cladding geometry[70]. In order to understand the process of composite material manufacturing using LMD, modelling and system controls were also explored[71-74]. Oliveira *et al*. created a theoretical model which was then tested experimentally to understand the relationship between laser cladding parameters and geometrical characteristics of individual laser tracks[75]. This research continues to contribute to the intelligent design of reaction parameters and choice of starting materials however, it must be said that while it gives a general indication of the impact of chosen parameters, the introduction of a new material requires the re-optimisation of manufacturing conditions to obtain the desired properties within the printed product.

Powders used as the starting material for the LMD process are produced using gas atomisation and commonly involve alloys such as Al-12Si. Aluminium is chosen due to its low melting temperature, low density (2.7 g/cm^3), high strength to weight ratio and good corrosion resistance when compared to other metals. The additive manufacturing of Al 4047 and Al 7050 alloys using LMD was investigated throughout the PhD of Singh in 2017[76]. Once again, the effect of deposition parameters on the morphology and mechanical

properties of the printed structures were investigated using scanning electron microscopy, tensile strength and Energy Dispersive X-ray Spectroscopy (EDS).

Silicon is commonly found as an impurity in aluminium alloys however, it is often added intentionally when casting to improve both the fluidity, castability and wear resistance[76]. The Al-Si phase diagram was initially studied by Fraenkel in 1908[77] and revealed the insolubility of silicon in aluminium and aluminium in silicon at room temperature. It describes the relationship between composition and phase occurrence as a function of temperature. It also shows the correlation between the solidification sequence and melting/solidification temperatures, as well as equilibrium phases that can form and solubility limits for alloy or impurity additions along with dissolution temperatures for secondary phases, resulting in a decrease in the melting temperature and the contraction during solidification. The introduction of silicon also decreases the weight of the overall product due to the low density of silicon. Cast alloys can contain anywhere from 5 to 22% silicon as at 12.5%wt Si a eutectic composition is reached[78-80]. The melting points of pure silicon are 1414^{o}C and aluminium, 660^{o}C but when combined at 577^{o}C liquid transforms into two different solid phases on cooling and the reverse on heating. This is important as typically the solubility of Si in Al is low and can result in the formation of silicon particles and aluminium rich solid solution phases[81]. Al-Si-Cu and Al-Mg-Si cast alloys are very popular commercially. Increasing the solidification rate creates much finer grain structures and eutectic dispersions resulting in an increase in strength and ductility and the addition of silicon in concentrations greater than the eutectic composition, known as hypereutectic alloys then contain silicon particles that provide improved wear resistance[81]. Much work has been done to test the physical and mechanical properties of aluminium-silicon eutectic alloys including composition and morphology[79,82], effects of growth velocity and temperature[83], the effect of environmental conditions such as humidity on the wear of these alloys[80], wear resistance and degradation mechanisms[84].

Until recently very few alloys could be printed reliably as the solidification dynamics lead to the formation of irregular microstructures grains and cracks in the printed materials. In 2017 Martin *et al.*[85] presented a method of overcoming this by introducing nm sized hydrogen stabilised zirconium nucleants to control solidification and promote the nucleation of new grains.

Current methods of printing include the use of Al-Si alloy powders as a starting material or exploitation of multiple feeders possible in LMD, where Si and Al are mixed at the point of laser contact. However, as the flowability of silicon powders is very low, freely flowing silicon carbide powders are commonly used[86] (the impact of powder flowability will be investigated in more detail in Chapter 8). For the LMD printing of hypereutectic Al-11.28Si alloy, the primary silicon particles at 5-10 µm were found to be significantly smaller than those obtained in conventional modified hypereutectic alloys where the primary silicon phases average 40 µm[86]. This is crucial as the size of eutectic Si particles contributes significantly to microhardness, with smaller particles resulting in increased hardness. The maximum microhardness of the LMD printed structure was determined to be 2.5 times that of the raw eutectic alloy. Comparisons between microstructure and

fatigue[87], deposition parameters and density[88], the effect of laser pulsing[61] and the effect of atmosphere on structural properties[59] have all been investigated for various compositions of Al-Si alloys. Computer simulation and modelling of Al-Si deposition have been used to investigate both the mechanism, kinetics of deposition[60] and the effect of altering deposition parameters. Phase field modelling of LMD printed Al-Si-10Mg alloys were created by Nandy *et al.*[67]. Simulation parameters included temperature gradient, laser power and scan speed with Increasing temperature gradients resulting in increased dendritic growth while dendrites joining and creating grain growth at increasing deposition times.

1.11.1 The flowability of Al powders in LMD 3D printing

When using LMD to manufacture metal products the physical and mechanical properties of the final product are commonly considered and thoroughly investigated however, physical properties of the powdered starting materials must also be considered. One such property essential for successful 3D printing is the flowability or 'liquid like' nature of the powder, with a continuous flow of powder through the system required for the LMD process. Typical granulometries used for LMD sit in the range of 40-90 µm, making the use of aluminium powders challenging. Flowability of microscale structures is directly related to the weight, surface energy and surface roughness of the particles with fine aluminium particles agglomerating naturally due to weak van der Waals forces[89-91]. Particles at extreme ends of the surface roughness scale ie. a large surface roughness or extremely flat surfaces experience large adhesion forces due to contact areas[92]. However, altering the surface roughness on a nanoscale[93] and surface energy[92,94] of Al powder particles can increase flowability significantly.

Common methods to improve the flowability of Al powders include the addition of guest molecules onto the surface to increase the surface roughness[93] and the modification of the surface chemistry of the powder using organic and inorganic molecules, reducing surface energy[92,94]. A recent application of silane films involves the functionalisation of aluminium powders in order to alter the physical properties of particles commonly used as a starting material for a variety of applications such as metal powder painting[95] and improving the compatibility of aluminium powders in different solvents[96]. Silane functionalised aluminium powders have been used previously for casting in an Al-epoxy composite[97]. Tensile modulus, strength, fracture toughness and wear resistance were improved with SEM imaging revealing that this was due to an improved dispersion and bonding of aluminium particles in the epoxy, due to the silanisation of aluminium powders.

It is commonly reported that the functionalisation of metal oxides alters the surface energy of metal oxide surfaces. Jallo *et al*.[92] successfully compared the effect of increasing surface roughness with inorganic host molecules against surface modification using methylchlorosilane, revealing that while the use of guest molecules on the surface increased the flowability, results were significantly improved following silane functionalisation. Chen *et al*.[94] also investigated the modification of aluminium powders through

functionalisation with methyltrichlorosilane, reporting an increase in the flowability of the aluminium powder upon that of unmodified powder. A process of functionalising Al powders with methyltrichlorosliane in anhydrous solvent has been patented by Johnston *et al*.[92], with reports that this treatment increased both the fluidity and packing density of the powders. The effects of silane modification on the flowability and dispersibility of aluminium powders was also investigated by Stevens *et al*.[98] by modifying the surface hydrophobicity of the 4 μm Al powder particles using both n-octadecyltrimethoxysilane and tridecafluoro-1,1,2,2-tetrahydrooctyl-1-triethoxysilane. The flowability of Al powders was tested at increasing humidity levels and compared to bare Al particles with a native oxide layer. Flowability of silane functionalised powders at increasing humidity was made possible by preventing the formation of water bridges and reducing the van der Waals interactions between particles.

The improved flowability of Al powders through functionalisation with silane molecules will be exploited and applied to LMD 3D printing for the creation of a novel, Si-Al composite material in this thesis. The accumulation of knowledge throughout the investigation of the mechanism of silane self-assembly will assist in the design of a cost efficient and environmentally friendly method of silane-powder functionalisation and increase the ease of LMD printing with aluminium powders. The printed material will be of a composition not previously created using this method.

1.12 Aim and scope of this research

Up to this point, the applications, importance and advantages of silane films along with the common methods used to characterise these films have been shown. While the solution-based mechanism of silane self-assembly has been well established in the literature, it is necessary for the fundamental interactions between silane molecules and the substrates to which they condense to be understood. This knowledge has allowed the intelligent design of molecules and experimental conditions for desired outcomes.

This dissertation endeavours to bridge this gap in knowledge through the systematic investigation of silane condensation behaviour on aluminium-based substrates and investigate a new, novel application for this knowledge by;

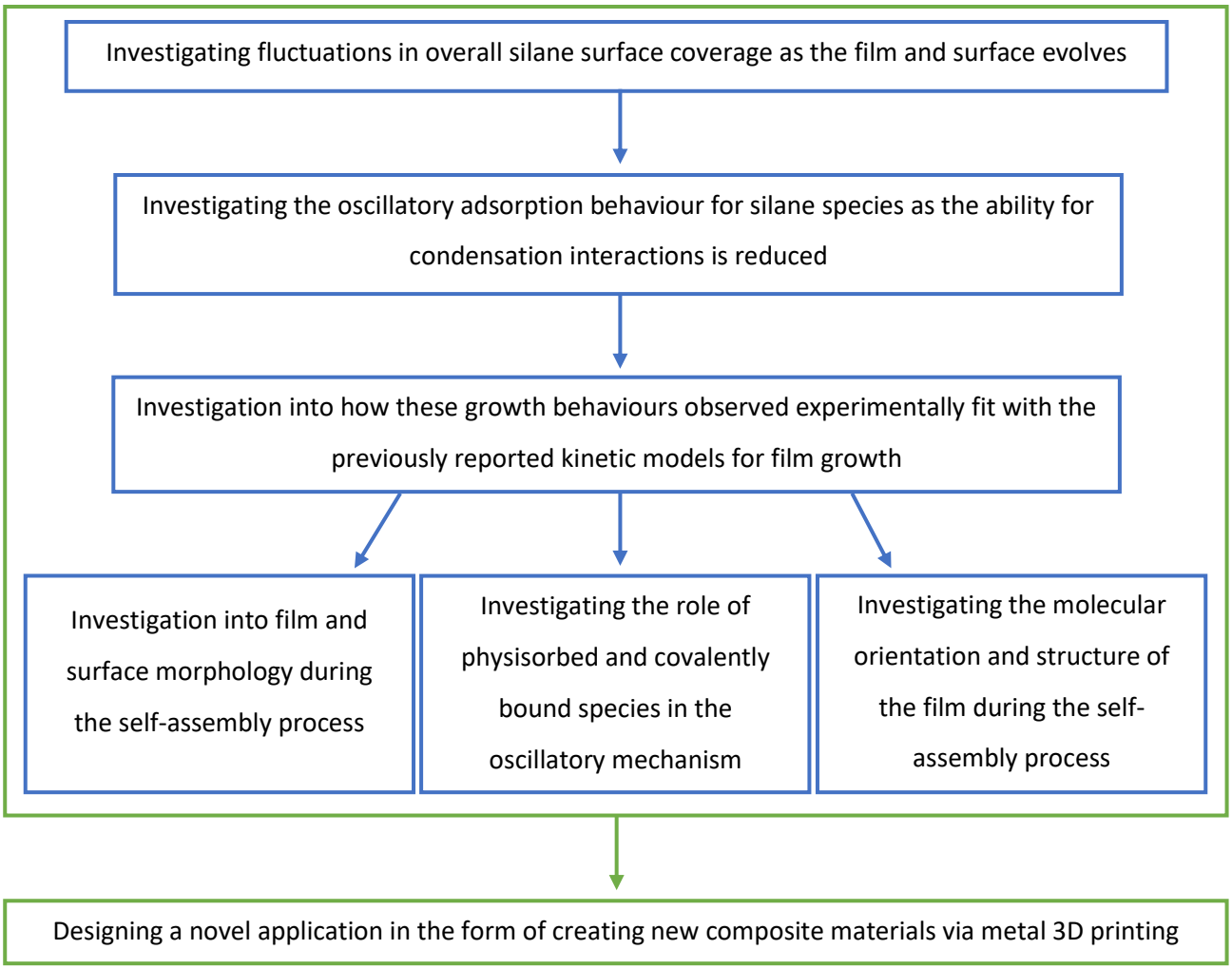

Investigating the mechanism of silane-substrate interactions has shed a light on the self-assembly mechanism on a molecular scale. Through both the ex-situ and in-situ monitoring of organosilane film formation, the origins of the oscillatory adsorption behaviour of silane films during self-assembly are explained. Film morphology including the orientation and order of silane molecules within the film during the growth of

silane films are investigated and give an insight in to the methods of controlling these features through choice of silane structure and experimental conditions. A comprehensive understanding of these interactions has also led to a new application for these molecules in the 3D printing field through the design of a novel Si-Al composite material.

2 Experimental Methods.

The preparation conditions of silane films, the substrate used and post self-assembly processing all have a significant impact on the morphology of the resulting film. Surface analysis techniques currently used to analyse thin films and powder particles in this thesis include X-ray Photoelectron Spectroscopy (XPS), Scanning Electron Microscopy (SEM), Electron Dispersive X-ray Spectroscopy (EDS), Sum Frequency Generation Spectroscopy (SFG) and Auger Electron Spectroscopy (AES). These techniques are used in different modes to obtain information on the near-surface composition when used in conjunction with methods of removing surface layers such as argon sputtering enable the determination of film composition of the material as a function of depth from the original surface[99]. While XPS, SEM-EDS and AES collect measurements from the surface of the film, SFG probes the interface between film and substrate or film and the atmosphere above it. Each analysis technique, while giving a unique information and insight into the films produced, require unique sample preparation methods. Hence, the experimental conditions for film preparation and post assembly processing are described below followed by the technique used to analyse the surface.

2.1 Organosilane species

The three silane species Propyltrimethoxysilane (PTMS), Propylmethyldimethoxysilane (PMDMS) and Propyldimethylmethoxysilane (PDMMS) used in this thesis were chosen after taking into consideration the simplicity of molecules, necessary to reduce the number of intermolecular interactions occurring on the surface and the ease of commercial availability while remaining a true representation of the larger, more complex molecules used commercially. Steric hinderance due to bulkiness of alkoxy groups affects the rate of hydrolysis with large alkoxy groups increasing the steric repulsion of water moving towards the silicon atom[100,101]. The inert propyl chain and rapidly hydrolysable methoxy groups present in PTMS, PMDMS and PDMMS helped limit interactions between silane molecules to hydrolysable groups while stabilising the molecules in solution[18]. This is essential as a limitation of the Langmuir adsorption mechanism shown in Figure 1.7 is that it does not take into account adsorbate-adsorbate interactions and must do so in order to remain a first order equation solvable numerically. The structural consistency of the three silanes chosen also ensures that the steric hindrance and inductive effects created by the propyl chain are equivalent for all silanes. Despite best efforts, interaction between molecules in solution and on the surface are unavoidable and is identified as a limitation of this work.

The environmental impact of reaction conditions and bi-products was also taken into consideration with molecules (and thus leaving groups) comprised of carbon and oxygen, the bi-products of condensation are limited to methanol and water. PTMS of 97% was purchased from Sigma Aldrich, Australia. PMDMS and PDMMS of 97% purity were purchased from Silar laboratories, USA.

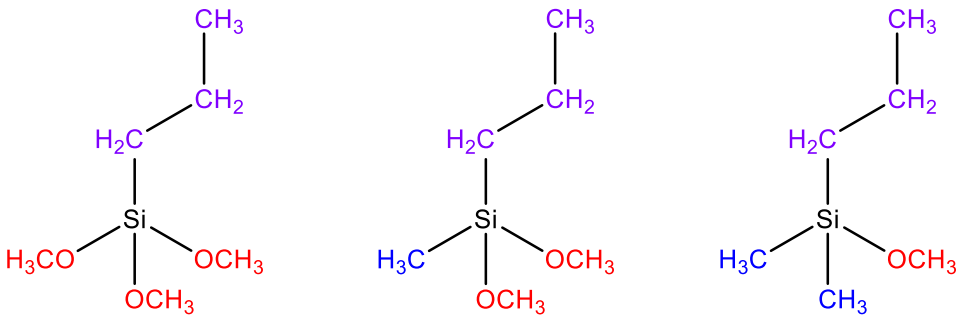

Figure 2.1: Pictorial representations of the three silanes Propyltrimethoxysilane, PTMS (left), Propylmethyldimethoxysilane, PMDMS (middle) and Propyldimethylmethoxysilane, PDMMS (right) used to investigate the mechanism of organosilane film self-assembly in this dissertation.

2.2 Determining the growth of silane films as a function of exposure time

2.2.1 Preparation of silane films for XPS, AES and SEM analysis

99.99% pure aluminium foil was purchased from Sigma Aldrich, Australia and cut into 10x10mm substrates. Due to its high purity it can be assumed that there is little variation across the substrate surface, important when creating a homogenous oxide layer[38]. Aluminium foil substrates were pre-treated with either P1200 grade wet/dry sandpaper with an average particle size of 15 µm or 1 µm diamond paste polish purchased from Struers, Australia. (details of surface abrasion are given for each data set). Samples were rinsed with Milli-Q water and placed in a 1:1 EtOH:H_2O solvent reduced to pH 3 with glacial acetic acid and placed in a ultrasonic bath for one hour. This pre-treatment process was designed to remove the oxide layer (Al_2O_3) present naturally on the surface of Al foil and enable the creation of a fresh oxide layer resulting in optimum, reproducible substrate conditions for silane condensation. This procedure also enabled the recycling of substrates as it removed any previously deposited silane films from the surface.

A 1:1 EtOH:H_2O solvent made to pH 3 with acetic acid referred to from here on out as *aqueous solvent* was used to create all silane films unless specified otherwise. The solution was prepared and gently stirred using a magnetic stirring bar, monitored for pH stability and agitated before each use. Ethanol in acidic solvent may result in the transesterification of methoxysilanes, resulting in the production of ethoxysilanes. The transesterification of a PTMS molecule by ethanol may result in the formation of $CH_3(CH_2)_2Si(OCH_3)_{3-n}(OCH_2CH_3)_n$ following the replacement of a methyl group of an -OCH_3 on the central silicon atom, by CH_3CH_2 in ethanol. By the same mechanism, a PMDMS molecule may be transformed into a $CH_3(CH_2)_2SiCH_3(OCH_3)_{2-n}(OCH_2CH_3)_n$ molecule and PDMMS into $CH_3(CH_2)_2Si(CH_3)_2OCH_2CH_3$. In this case, the resulting silanes are all hydrolysable with the fully hydrolysed products being equivalent to the hydrolysed products of PTMS, PMDMS and PDMMS shown in Figure 1.2. As the proposed model of silane film formation is only concerned with silane-substrate interaction and does not take into account intermolecular interactions, this will not further complicate the model.

Two film preparation methods were then employed. The first resembled conditions commonly used to create silane films in water-based solvents and required the addition of silane to the aqueous solvent create a 1%v/v concentration of silane. The time between silane exposure to the aqueous solvent and exposure to substrates is referred to hydrolysis time and the length of time substrates were exposed to the silane solution is for here on referred to as *exposure time*. It has previously been reported that silanes are considered fully hydrolysed when the solution becomes homogeneously colourless – the point of dissolution. Prior to this, silanes do not form stable monomeric hydrolysed silanols, rather, they condense to one another in solution. Silane molecules generally have a low solubility in aqueous solutions, and thus form a separate layer in solution. The solution was then allowed to hydrolyse for one minute in the case of PDMMS and one hour for PTMS and PMDMS before substrates were exposed to the solution successively for the desired exposure time.

The second film preparation method required the exposure of substrates to a silane solution which had not undergone hydrolysis prior to substrate exposure (and referred to as *no hydrolysis time*). This method was created to examine the effect of silane oligomerisation on film morphology and required the simultaneous exposure of substrates and initiation of the hydrolysis reaction. To achieve this, upon removal form the pre-treatment solution, samples were once again rinsed with Milli-Q Water before being submerged in the aqueous solvent. It was only once all substrates were submersed in the solvent and the solution was stirring that silane was added to create a 1% v/v solution with substrates removed from solution at increasing exposure times ranging from 5 to 200 seconds. The timer was started upon addition of silane to the solvent, hence substrate exposure times quoted include the exposure to unhydrolysed silane. Upon removal from solution all samples regardless of sample preparation method were dried with N_2 and cured at 80^{o}C for 1 hour in order to remove all remaining water from the surface and force the condensation reaction to completion. The majority of films produced in this thesis were simply dried and cured once removed from solution however, a select subset of films underwent a rinsing procedure which required samples to be rinsed with a gentle stream of Milli-Q water from a safety wash bottle for 10 seconds prior to being dried with N_2 and cured.

The extent of silane surface coverage was then determined using X-ray Photoelectron Spectroscopy (XPS) for all films. This process was repeated 3 times for both the *hydrolysed* and *no hydrolysis* data sets of each silane and the average of each exposure time across the three data sets taken. Film morphology was determined using Scanning Electron Spectroscopy (SEM) and Auger Electron Spectroscopy (AES) with Scanning Electron Microscopy (SEM).

2.2.2 X-ray Photoelectron Spectroscopy (XPS)

Electron spectroscopy techniques, X-ray Photoelectron Spectroscopy (XPS) along with Auger Electron Spectroscopy (AES, to be described in section 2.2.4 below) are based on the analysis of energy of secondary electrons emitted as a result of excitation by photons, electrons, ions or neutrons[99]. The depth of surface analysed is dependent of the inelastic mean free path (IMFP), or the distance an ejected electron can travel through the sample bulk and reach the detector without the loss of energy. XPS and AES both require ultra-high vacuum analysis chambers and an electron gun (AES) or an X-ray source (XPS). The reason for ultra-high vacuum is twofold; firstly to avoid electron scattering on gas molecules in the path from sample to analyser and secondly, to avoid attenuation and distortion of the spectra by surface contamination[99]. In order to satisfy both conditions a pressure lower than 10^{-9} Torr is used.

XPS is a highly sensitive analysis technique used to obtain the elemental composition of a given surface[102]. Based on the photoelectric effect presented by Albert Einstein in 1905[103], XPS was created by Kai Siegbahn, who consequently received the Nobel Prize in 1981 for his work[104]. Siegbahn exploited the knowledge that the incidence of soft X-rays on a surface excites a core shell electron and may give it enough energy to escape

the shell to be ejected as a photoelectron[99]. If this occurs, the atom now in its excited state relaxes by transitioning an $L_{(1)}$ electron. The energy liberated from the relaxation is ejected as an X-ray via X-ray fluorescence also known as the Auger effect. The kinetic energy of the expelled photoelectron is a result of the initial energy of the incident X-ray (*hv*) minus the binding energy of the expelled electron to the core shell of the specific atom (E_b) minus the work function of the spectrometer (Ø) and can be derived from the following equation[99,102];

$$E_K = hv - E_B - \emptyset$$

Equation 2.1

As the initial energy of the incident X-ray is known for a particular source, for example the XPS instrument at Flinders University uses either an Al or Mg Kα soft X-rays from a SPECS XR-50 source initially installed in 2008 and replaced in 2017 with an energy of 1486.6 and 1253.6 eV[105] respectively, the initial binding energy of the electron can be determined and subsequently used to identify the elemental source. The work function (Ø), a value used to account for the work function of the material and the analyser is also known. The spectrum produced shows peaks at specific binding energies (eV) relative to the origin of the photoelectron. Automatic subtraction of the photoelectron energy from the incident X-ray energy is performed by the software program, X-Sect[106] used as the spectrum is produced. These calculations assume that the photoemission process is elastic and therefore does not undergo an energy loss between photoemission and detection[102], giving rise to photoelectrons that have a kinetic energy which reflect the discrete binding energy levels of the atom from which they came. However, the presence of inelastic (loss of energy) mechanisms is unavoidable. Secondary electrons resulting from inelastic emission dominate the background at lower kinetic energies (relating to higher binding energies) causing a gradient in the background of an XPS survey scan over the scanning range used (1000eV to 0 eV). Along with peaks representing the binding energy of core photoelectrons, peaks due to the photoemission of valence electrons and Auger emission can also be seen[106]. An advantage of a dual X-ray source system is the ability to separate and deconvolute Auger peaks from XPS peaks by switching the excitation energy. As discussed in detail below in section 2.2.4, the binding energy and therefore Auger peak position is dependent on the excitation energy. Changing the energy of the incoming X-rays by switching the source will shift the energy of the resulting Auger peak, while the binding energy of an XPS peak does not change with a change in excitation energy.

While relative intensities of the resulting peaks relate to the percentage of the atom present in the sample, they must also be adjusted to account for the probability a core electron will become excited and emitted from the atom, a value specific to each individual element. These values known as Atomic Sensitivity Factors (ASF) are well known and representative of a differential cross section. Once the peaks of a spectrum have been identified and the intensity calculated, the percentage of each element within the sampled area can be determined[106].

Ejected photoelectrons are analysed using a concentric hemispherical analyser (CHA) electron spectrometer. Photoelectrons are focused through a lense and a negative voltage applied to hemispheres $\mathbf{V_2}$ while hemisphere $\mathbf{V_1}$ remains grounded, creating a potential as shown in Figure 2.2. The potential along the median radius surface is given by the following equation[102];

$$V_0 = \frac{V_1 R_1 + V_2 R_2}{2R_0}$$

Equation 2.2

Where,

- $\mathbf{R_1}$ Is the inner radius and
- $\mathbf{R_2}$ The outer radius
- $\mathbf{V_1}$ The smaller hemisphere potential
- $\mathbf{V_2}$ the large hemisphere potential

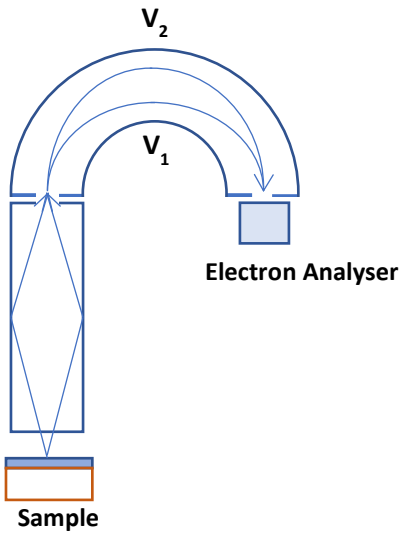

Figure 2.2: Schematic of a hemispherical electron analyser detailing the direction of photoelectrons from the sample towards the electron analyser and the application of voltages 1 and 2 (V_1 and V_2), adapted from Kibel[107] and Briggs & Seah[102].

Electrons that are traveling too fast will collide with the top hemisphere, while electrons travelling too slowly will be attracted to the lower hemisphere, therefore only electrons with a specific energy (known as the pass energy) will reach the detector. The pass energy is scanned by ramping the voltage applied to V_2 as the spectrum is collected[107]. The larger the hemisphere the smaller the potential required to curve the electrons towards the detector. Electrons are focused towards the entrance slit by a lens system, which also retards their velocity so that the kinetic energy of the electrons now matches the pass energy of the hemisphere.

The relationship between the energy of the electron and the potential of the hemisphere can be described by the following equation[102];

$$e\Delta V = E\left(\frac{R_2}{R_1} - \frac{R_1}{R_2}\right)$$

Equation 2.3

For the LH-10 XPS used at Flinders University, there are 2 different modes available to analyse the incoming photoelectrons, each with their own advantages detailed below.

To create a survey scan of the surface the energies of electrons emitted over a wide range of kinetic and therefore binding energies need to be scanned and the voltages applied to the lens system varied. The efficiency at which these electrons reach the detector is heavily dependent on the lens system[108]. The electrons are slowed down by the initial retardation point and the pass energy (potential between the hemispheres) is set. The retard ratio or the factor by which the electrons are slowed is fixed. For example, if the retard ratio is set to 10 and 1000 eV electrons are to be detected they will be slowed down to 100 eV, resulting in a constant resolving energy and constant (although increased) signal to noise ratio across the spectra produced, referred to as Constant Retardation Ratio (CRR) mode. Contrary to survey scans, high resolution scans typically occur over a short energy range of up to 20 eV, the pass energy remains fixed and it is only the lens that retards the velocity of the electrons entering the hemisphere to a range acceptable for the analyser[108], known as Constant Analysis Energy (CAE) mode. For example, if the pass energy is set to 50 eV then electrons of 1000 eV will need to be slowed by 950 eV to reach the detector. Resulting in a constant energy resolution and better signal resolution at lower kinetic energies. The signal to noise ratio does vary across the energy range measured, however it is not deemed significant as the energy range measured is so short.

X-rays can penetrate deep in to the bulk of the sample, sometimes as far as 1 µm[106], but it is the IMFP (λ), the depth at which electrons can escape through the surface with their characteristic kinetic energy that limits the depth of a surface that can be analysed. The sampling depth can be determined directly from the IMFP and the analysis geometry[109]. For electrons in the range of 100-1000 eV, the IMFP typically lies between 1-3 nm with the minimum IMFP seen for energies around 100 eV, increasing as the binding energy of the electron increases[109]. It is this that makes XPS ideal for analysing monolayers on a surface with a film and substrate of differing elemental composition[102]. As the name inherently implies, values calculated for the IMFP assume photoelectrons follow a linear path to the analyser and therefore do not take into account elastic scattering. Attenuation length however, eliminates majority of the errors associated with elastic scattering, leading to a more conservative estimate of film thickness and analysis depth, and can be calculated from the following equation[110];

$$\lambda_{(AL)} = 0.316a^{3/2}\left(\frac{E}{Z^{0.45}\left[ln\left(\frac{E}{27}\right)+3\right]}+4\right)$$

Equation 2.4

Where,

Z The atomic number of the element

E The electron kinetic energy (eV)

a The lattice parameter.

For which the attenuation length of an electron with kinetic energy of 1000 eV can be calculated to a standard deviation of 9%[110]. In order to take into account the effects of elastic scattering, Attenuation Lengths are used in lieu of the IMFP in sampling depth and film thickness calculations.

Table 2.2.1: Attenuation length of pure elements of specific kinetic energies. Attenuation lengths are calculated from Equation 2.4 and kinetic energies determined by the energy of a Mg K_α X-ray source and the Binding energy of the core electrons to the element in question. Table adapted from Moulder[105].

Element	Attenuation Length (nm)	KE (eV)
Al	2.37	1180.6
Si	2.48	1154.6
C	2.4	969.6

When X-rays are incident on a surface and photoelectrons are ejected, a positive charge is created on the surface, causing peaks to become distorted and shift to higher binding energies. This charging is due to a potential created on the surface, which electrons must overcome in addition to the energy by which they are bound to the nucleus (binding energy). This energy can be calculated by multiplying the binding energy (eV) by the potential created (in volts) and is subsequently also the magnitude at which peaks are shifted due to charging. In order for a sample to be suitable for XPS analysis, there must be a way to overcome charging, this is generally accomplished through the analysis of conductive samples. It is also possible to overcome charging through the use of an electron flood gun to replenish the electrons ejected from the surface. The LH-10 XPS system has a low energy electron flood gun incorporated, focusing a low energy electron beam at the surface to neutralise the surface. It is also possible to ease the need for charge compensation by placing conductive copper or aluminium tape in close proximity to the sampled area. Samples must also be able to

withstand ultra-high vacuum conditions in the range of 10^{-10}Torr, free from excess solvent and secured to the sample mount.

Aluminium oxide photoelectrons ejected from Al_2O_3 experience less electron repulsion and greater attraction to the nucleus due to their higher oxidation state[111] giving the Al electrons of the Al_2O_3 molecules a higher binding energy than metallic aluminium. As the aluminium substrate was conductive, no charge compensation was necessary during data acquisition.

Silane surface coverage was measured using a Leybold-Heraeus LHS-10 X-ray Electron Spectrometer. Mg K_α soft X-rays with an energy of 1253.6 eV [105] generated with a SPECS XR-50 Dual-Anode X-ray source. A base pressure of 2.0 x 10^{-9} Torr, take-off angle of 90^o and pass energy of 20 eV were used in the analysis of all silane films reported in this thesis.

2.2.2.1 Peak Fitting and the Deconvolution of High-Resolution Spectra.

Data was collected with the LabView based program X-Spect, written by Dr Anders Barlow[112]. CASA XPS version 2.3.15dev87 ©2009, a licenced peak fitting software designed specifically for the analysis of XPS data was employed for all curve fitting using a mixture of Gaussian and Lorentzian peak shapes, while the background subtraction was conducted using a Shirley function[113]. Multiple components can be observed within the high resolution XPS peaks produced due to the unique binding energies of the main element in question to another element. An example of a primary peak with well known, clearly defined components is the C *1s* peak. Each of the C *1s* components are a result of the discretely different binding energies seen for the carbon-oxygen, carbon-carbon, carbon-hydrogen and carbon-silicon bonds. Although the differences in binding energies are not large enough to cause an entirely separate peak, each individual component must be accounted for when fitting high resolution spectra correctly. Spectra are conventionally calibrated to the main C-C C *1s* peak at 285 eV[5,105,111,114]. Spectra in this report were calibrated to the main C-C C *1s* peak at 285 eV and Si *2p* peaks then fit with a single component at 103 eV[115]. This is higher than the binding energy of 99 eV[105] typically associated with Si *2p* peaks due to the presence of Si-O bonds associated with silanes. Due to the resolution of the XPS available, no further deconvolution was possible. The Al 2p peaks were fit with 3 components, first a single component at 76 eV representing the aluminium oxide on Al foil and 2 components, Al $2p_{1/2}$ and Al $2p_{3/2}$ at 73 eV, representing the Al metal bonds. Aluminium metal doesn't experience complete splitting of these orbitals, but rather asymmetry in the peak. Al oxide photoelectrons experience less electron repulsion and greater nuclei attraction due to their higher oxidation state[111] giving the Al oxide electrons a higher binding energy than metallic aluminium. A comprehensive table of peak components used in the analysis of silane film on aluminium substrates can be seen in Table 2.2.2 and an example of peak fitting given in Figure 2.3.

Table 2.2.2: Binding energies (eV) of the high resolution XPS peak components used to analyse XPS peaks resulting from the adhesion of silane molecules to aluminium oxide surfaces. All peaks are to be normalised to the main C-C contribution of the C 1s peak.

	Peak Component	**Binding Energy (eV)**
Carbon (C 1s)	C-C	285 [5,105,111,114]
	C-O	+1.6 [5,111,114]
	C=O	+3 [5,111]
	C-Si	-1.5 [5,116,117]
Aluminium (Al 2p)	Al_2O_3	74.6 [111]
	Al (metal)	72.9 [105,117]
	Al-Si	72.5 [111]
Silicon (Si 2p)	Si 2p	103 [115]

The application of XPS in the characterisation of silane thin films is enabled by the presence of an elemental marker in the film (silicon) and substrate (aluminium). Si *2p* and Al *2p* peaks were fit according to the peak fitting specifications above and used comparatively to determine a value of surface coverage. In order to produce a value representing the extent of adsorbate coverage, a ratio of the peak intensities for Si *2p* and Al *2p* is taken as Si:(Si+Al). The resulting value gives an indication as to the extent of film coverage at low surface coverages[38].

An example of fits for the Si 2p and Al2p peaks is shown in Figure 2.7 below, the sum of all components was used to calculate a Si:(Si+Al) value of 0.61.

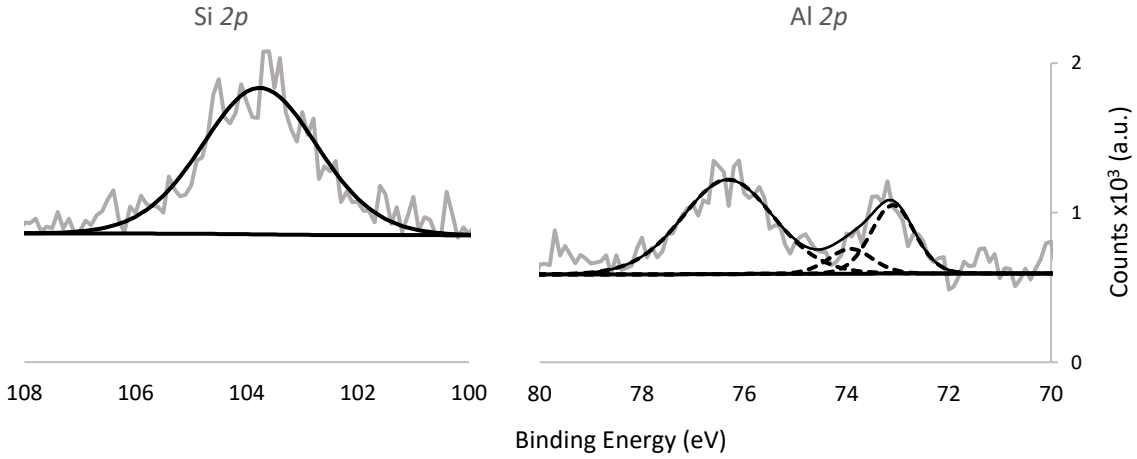

Figure 2.3: The fit and deconvolution of high-resolution Si 2p (left) and Al 2p (right) XPS spectra of 1% PTMS in aqueous solvent exposed to aluminium oxide for 5 seconds, obtained in CAE mode using an Mg Kα X-ray source.

Each data point presented in the time dependent adsorption profiles of PTMS, PMDMS and PDMMS represents the average of 3 individual samples with the error given as the standard deviation.

2.2.3 Scanning Electron Microscopy (SEM)

Scanning Electron Microscopy (SEM) is an imaging technique able to analyse bulk specimens[118]. Images are created when electrons are accelerated through a voltage difference between cathode and anode[119]. Electrons interact with the surface in a variety of ways; they may elastically scatter off atoms and be collected by the analyser as backscattered electrons. Elastically scattering may also result in the ejection of an electron from atoms within the surface, detected as secondary electrons. Both backscattered and secondary electrons can be used to gain topographical information. Inelastic scattering can also result in the production of X-rays, detected by a fluorescent X-ray detector and used to gain information regarding the elemental composition of the surface, commonly known as SEM-EDS. Samples with large variations in depth can be sharply imaged at lower magnifications[119]. SEM is used extensively in characterising and imaging thin films. Examples include the size and distribution of the phase-separated silane droplets imaged using SEM[14]. However, Scanning Electron Microscopy is relevant to this study as the Auger Electron Spectromicroscope available at Flinders University utilises SEM in imaging samples for elemental mapping capabilities. Surface features of interest are identified using SEM imaging of the surface and subsequently analysed using AES.

2.2.4 Auger Electron Spectroscopy (AES)

Auger Electron Spectroscopy (AES) is another highly sensitive surface analysis technique used to determine the elemental composition of thin films. AES is named after Pierre Auger[120] following his publication *Sur l'effet photoélectrique compose*[121] in 1925 and based in part on the processes presented by Lise Meitner just a few years earlier[122] and like XPS is based on the photoelectric effect described by Einstein[103]. The PHI-710 AES instrument at Flinders University was utilised in all AES analysis for this thesis, was purchased from PHI Electronics in Minnesota, USA and installed in 2015.

Samples analysed via AES are irradiated with focused beam of primary electrons at high energy (1-20K eV)[99], with samples analysed in this study at an incident electron beam of to 10kV, 10nA, a time per step of 10ms and base pressure of 10^{-10}Torr. These electrons penetrate the surface of the sample, exciting electrons with the energy released either as in the case of XPS, ejected as a photoelectron[99] or following core level ionisation the atom will relax to a lower energy state with the excess energy emitted from the shell as an Auger electron[123]. As with XPS analysis, Auger electrons reaching the detector without inelastic scattering are characteristic of the element they originated, with Auger electrons having a kinetic energy characteristic of

the parent ion. Simply, the kinetic energy of the Auger electron can be estimated as the difference in the energy levels for the atom as the energy is equal to the energy difference between the singly ionized initial state and the doubly ionized final state, represented by the following equation[123];

$$KE = (E_A - E_B) - E_C - \emptyset$$

Equation 2.5

Where E_A-E_B represents the energy gained by the core-hole annihilation and E_C represents the energy needed to overcome the binding energy of the Auger electron.

More exact calculations of Auger electron energies should take into account the coulomb repulsion energy between the two holes in the final state and the relaxation energies and can be given by the following equation[123];

$$\mathrm{KE} = \mathrm{E_A} - \mathrm{E_B} - \mathrm{E_C} - \mathrm{H} + \mathrm{R_{in}} + \mathrm{R_{ex}}$$

Equation 2.6

Where H is the hole-hole interaction energy of the two-hole final state, and R_{in} and R_{ex} are the intra-atomic and extra-atomic relaxation energies, respectfully.

As with XPS, all elements with the exception of hydrogen and helium emit Auger electrons and an element is identified by its Auger spectrum[124]. Elements are identified by the position of the Auger peaks, while the concentration is related to peak intensity[123]. Analysis depth due to the attenuation length (includes elastic and inelastic scattering) is typically between 0.3 and 5 nm for electrons between 50 and 2500 eV[99,123] making AES more surface sensitive than XPS.

Notation of core level electrons differs to that of XPS, elements are identified and labelled corresponding to the energy levels involved in the transitions occurring in the creation of the auger electron. The first label corresponds to the energy level of the initial core hole, the energy level of which is often an indicator of the transition types to follow. The second and third labels refer to the initial energy levels of the two electrons involved in the Auger transition[123]; for example in a $KL_1L_{2,3}$ transition, K represents the core level hole, L_1 represents the relaxing electron's initial state while $L_{2,3}$ represents the emitted electron's initial energy state.

The most commonly used Auger electron energy analyser is the Cylindrical Mirror Analyser (CMA). Similar to the XPS analyser (shown in Figure 2.2), the path of electrons is curved by applying a voltage bias. However, the location of the analyser relative to the sample differs in AES to that of XPS. The AES analyser is located directly above the sample to eliminate shadowing produced when the analyser is at a 45-degree angle to the sample. This is particularly important when producing SEM images of the surface.

2.2.4.1 *Interpretation of Spectra*

The resulting AES spectra consists of inelasticity scattered primary electrons and secondary electrons with the number of electrons detected as a function of electron kinetic energy. AES spectra are commonly converted to a differentiated spectrum with a five point Savitzky-Golay filter[123,125] in order to remove the steep background observed and increase the intensity of the spectra peaks above the noise[123], effectively optimising the signal to noise ratio. An example of the raw and differentiated spectra is shown in Figure 2.4;

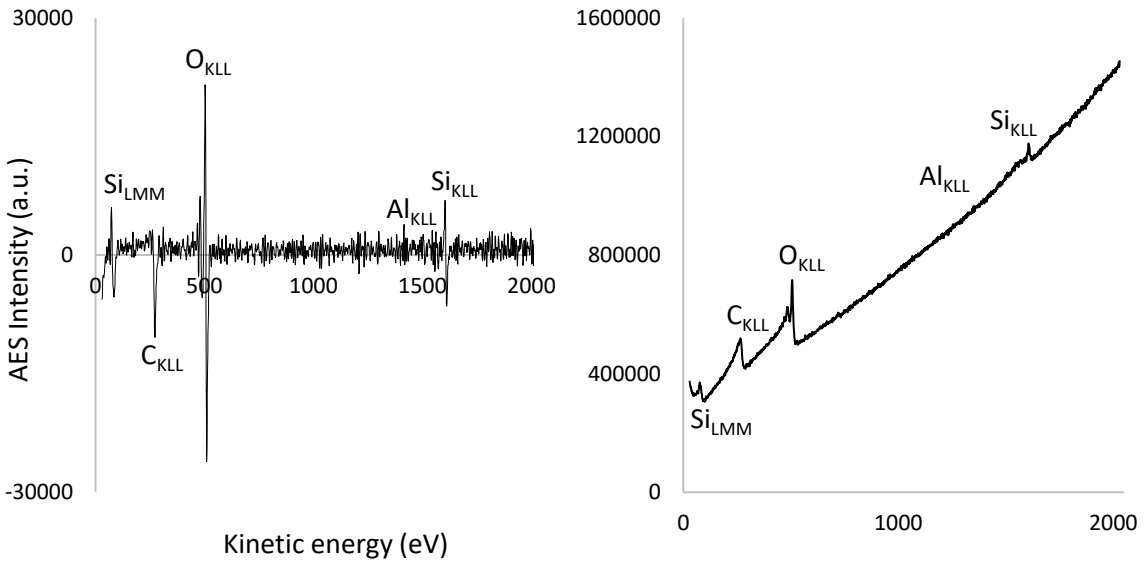

Figure 2.4: AES spectra for a film created when a 1 µm diamond paste polished aluminium foil substrate was exposed to 1%v/v PMDMS in aqueous solution for 80 seconds. The differentiated spectra (left) and raw spectra (right) of the sample are used to identify peaks representing elements present on the surface.

For the identification of silane films, much like XPS, the presence of a Si_{KLL} peak was taken to represent the presence of a silane film while Al_{KLL} was used to indicate the aluminium foil substrate.

High resolution spectra of Al_{KLL} at 1396 eV, Si_{KLL} at 1621 eV, C_{KLL} at 275 eV and O_{KLL} at 510 eV peaks were then obtained. It is often beneficial to obtain these high-resolution peaks to confirm the presence of elements in the case where survey spectra peaks are small or noisy. An example of this can be seen through the absence of a clear Al_{KLL} peak at 1396 eV in the survey spectra shown in Figure 2.4 and the presence of this peak in the high resolution spectra shown in Figure 2.5.

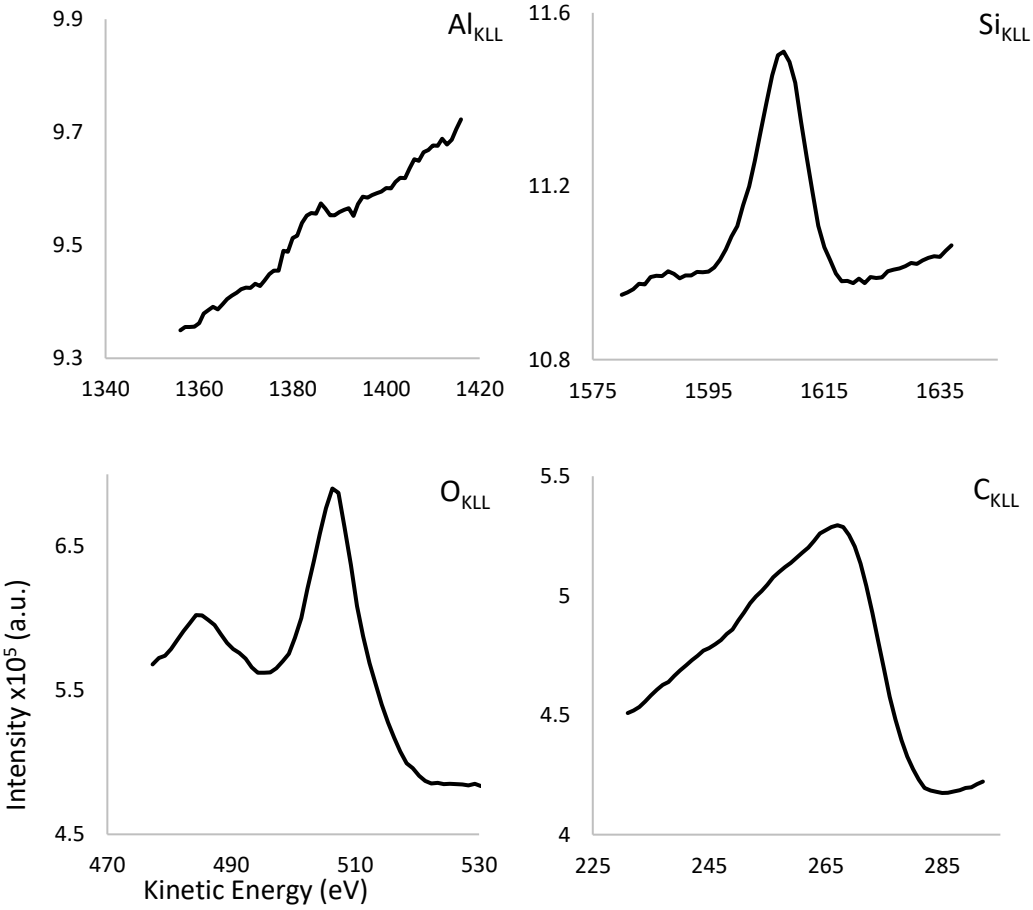

Figure 2.5: AES high resolution Al_{KLL}, Si_{KLL}, O_{KLL} and C_{KLL} spectra for a film created when a 1 µm diamond paste polished aluminium foil substrate was exposed to 1%v/v PMDMS in aqueous solution for 80 seconds.

A significant advantage of the PHI-710 AES instrument available at Flinders University is that it comes equip with SEM capabilities, allowing SEM and AES analysis to be performed in situ. This allowed for the identification of areas of interest and direct alignment of SEM images with the associated elemental maps and depth profiles without intermittent exposure to atmospheric conditions during the transfer of samples between instruments. When combined with the necessary scanning electronics such as SEM, AES can be used to map the distribution of elements on the surface with very high spatial resolution[123]. The value of surface coverage, Si:(Si+Al) used to determine film growth from XPS spectra can be obtained using the peak-to-peak height of AES peaks. However, in this case AES in combination with SEM was utilised to investigate the morphology of films produced. Peak area analysis in XPS is generally more accurate than peak-to-peak height analysis in AES[99].

The creation of elemental maps with an overlap of SEM imagery is a powerful tool in surface analysis. The identification of areas of interest on the surface and the subsequent elemental mapping of those areas creates a 2-dimensional image of silane films on the surface. The resolution and accuracy of the maps produced depends both on the number of pixels in the map and the way in which the peaks themselves are analysed. As a spectrum is collected for each pixel within the map, the accuracy of the data within that

spectrum is dependent on the number of points within that spectrum used to determine the intensity of that element within the pixel. A 2-point collection takes the selected maxima (peak) and minima (background) rage and converts this into an intensity value. The calculated intensity values are weighted against the intensity of the signal in other points within the map, with the final map representing the relative intensity of the element in the surface analysed, all processed with PHI's Multipack software[123]. Maps are commonly shown in thermal mode, where pixels of highest relative intensity represented in white/bright yellow, and those with the lowest relative intensity shown in black. For the analysis of films in this thesis, a balance between resolution and processing time was struck with 2-point maps of 256x256 pixels acquired.

2.2.4.2 Depth profiling

Depth profiling is another important application of AES, creating compositional depth profiles by combining AES with ion beam sputter etching[123] and when combined with the elemental mapping of silane films create a 3-dimensional picture of silane films on the surface. The sample is eroded by bombardment with ions, also known as sputtering. The newly revealed sample layer is profiled after each sputtering cycle. The surface composition and morphology of the sample can be determined as a function of both depth and sputter time[126]. Surface morphological and chemical analysis by cross-sectional scanning electron microscopy and AES analysis was used to analyse silicon thin films created using chemical vapour deposition by Sveen and Shi in 2011[127]. A distinct layer of film was detected from the SEM images obtained while AES depth profiling revealed how deposition time affected the thickness of film produced[127]. However, in this case the SEM and AES measurements were acquired separately. As mentioned above, the PHI-710 instrument used to analyse films in this thesis eliminates the need to transfer samples by combining AES and SEM in the same instrument. The choice of sputter rate and duration between the collection of each spectra can create a comprehensive profile of the films' morphology. For thin films lower sputter intensity and duration will result in a delicate, detailed analysis of the surface while thicker films may require longer, more intense sputtering in order to effectively profile the surface. The changing intensity of elements during the sputtering process can reveal compositional changes throughout the structure of films, not possible when using purely surface or film-substrate interface sensitive techniques. One such example of this is the discovery of a double layer silane film deposited on galvanized steel[25], with the inner composition of the film found to differ from surface composition. The thickness and non-uniformity of silane films on aluminium surfaces can also be determined using depth profiling through the alternative sputtering and spectra collection of thin films[128]. In this thesis, the intensity of C_{KLL}, O_{KLL} and Si_{KLL} peaks in the silane layer are used to indicate the presence of the silane films and oxide layer on the surface. After sputtering the intensity of C_{KLL}, O_{KLL} and Si_{KLL} reduce to a minimum, while the Al_{KLL} signal intensity increases to a maximum indicating the film-substrate interface and eventual sputtering of the bare Al substrate. The intensity and duration of sputtering was optimised for each sample based on an accumulative understanding of the films' composition following multiple sputtering

experiments. In order to determine the thickness of silane films, the intensity of high-resolution peaks is monitored in-between sputtering of the surface using an argon electron gun. Sputtering time and power of the electron beam can be altered so that the desired amount of the surface is removed between each spectra collection. An example of the parameters chosen to remove 1.03 nm of the surface between each acquisition with a total profile depth of 58.6 nm over 57 cycles can be seen in Table 2.2.3;

Table 2.2.3: Argon electron beam parameters used to remove 1.03 nm of surface in-between spectra acquisition for a film created when a 1 µm diamond paste polished aluminium foil substrate was exposed to 1%v/v PMDMS in aqueous solution for 80 seconds.

Time (min)	Depth (Å)	Interval	Cycles	Sputter	Rate (Å/min)
20	586	0.35	57	1kV 2x2mm	29.3

Where time indicates the total sputtering time, depth indicates the total sputtering depth, interval details the number of times per minute of sputtering data acquisition occurs, followed by the number of cycles, beam power and size (sputter) and the sputtering rate. If this profiling depth is deemed to be insufficient once the depth profile is complete, the same (or altered) parameters can be reapplied to continue the depth profiling process.

While determining these parameters, the range of energies used to measure each high-resolution peak must also be determined. This is achieved by selecting a point on the surface and determining the appropriate region for each peak of interest. The following regions were chosen in conjunction with the beam parameters shown in Table 2.2.3.

Table 2.2.4: Peak ranges chosen based on high resolution spectra shown in Figure 2.5 for the depth profiling for a film created when a 1 µm diamond paste polished aluminium foil substrate was exposed to 1%v/v PMDMS in aqueous solution for 80 seconds.

Peak	Sweeps	Range (eV)
C_{KLL}	20	234.2-305.1
O_{KLL}	20	477.3-532
Si_{KLL}	25	1580-1635.9
Al_{KLL}	15	1356-1416

Sweeps indicates the number of times the region is repeated scanned or 'swept' for each acquisition. Increasing the number of sweeps increases the total integrated count time of the spectrum and thus the signal to noise ratio improves. Following each sputter, high resolution spectra is acquired for each peak based

on the range parameters shown in Table 2.2.4. As each layer of a surface comprised of a silane film on an aluminium oxide substrate is removed, the Si_{KLL}, O_{KLL} and C_{KLL} peaks reduce in intensity, and the Al_{KLL} signal of the substrate increases. An example of this can be seen in Figure 2.6;

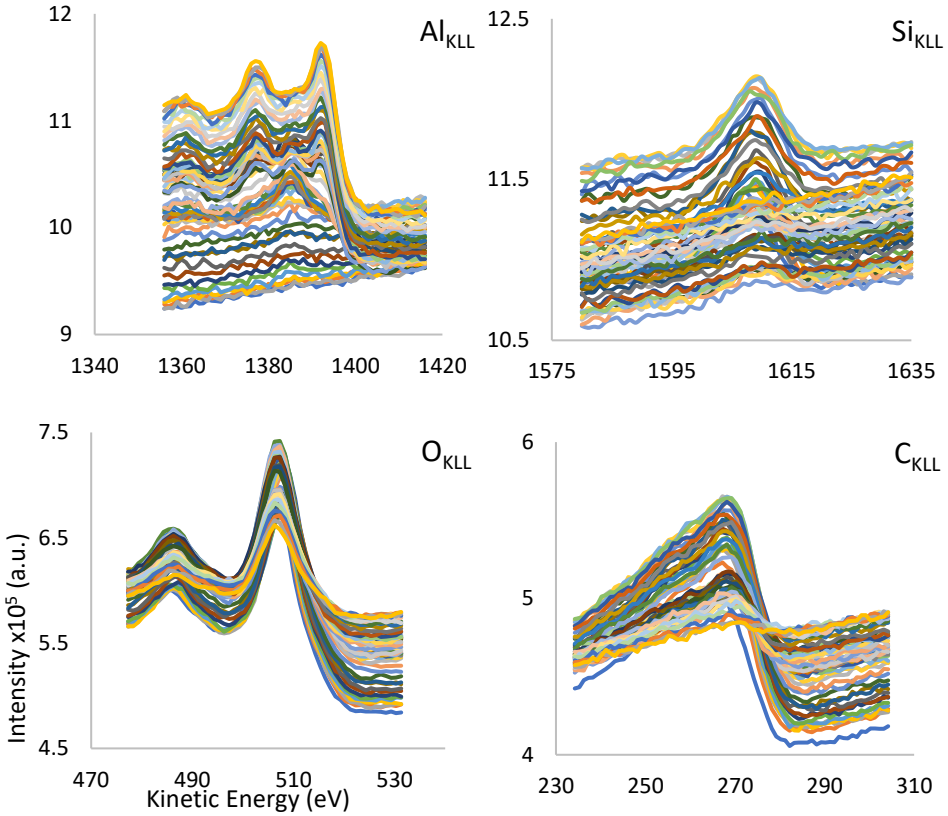

Figure 2.6: AES high resolution Al_{KLL}, Si_{KLL}, O_{KLL} and C_{KLL} spectra acquired between each removal of 1 nm from the surface of a film created when a 1 µm diamond paste polished aluminium foil substrate was exposed to 1%v/v PMDMS in aqueous solution for 80 seconds.

The peak intensity from each individual spectrum collected are compiled and plot as a function of sputter depth, creating a profile of film throughout each of the layer sputtered. Surface oxide, silane film, aluminium oxide layer and the aluminium substrate can be identified within the film and the thickness of these layers identified.

2.3 Determining the orientation and order of Molecules within silane films

In order to determine the behaviour of silane molecules within the film both in- and ex-situ, a technique named Sum Frequency Generation Spectroscopy (SFG) was employed. SFG can be exploited as a surface and interface specific method of vibrational spectroscopy that reveals both structural and conformational information for molecules on a surface[129] and has been used previously to study the dependence of pH on the structure of water molecules on fused quartz modified by a monolayer of octadecyltrichlorosilane, (OTS)[130] as well as the density and conformation of OH groups at the water-sapphire interface[131]. The results of these studies demonstrated the ability of a measurable SFG signal to be produced for a long hydrocarbon-chained silane coupling agent film.

2.3.1 Sum Frequency Generation Spectroscopy (SFG)

Developed in 1987 and first published by Shen *et al*. in Nature[129], Sum Frequency Generation Spectroscopy (SFG) is an Infra-Red (IR) Spectroscopy based technique allowing the determination of molecular orientation and extent of order at a desired interface. Unlike XPS and AES where samples must be analysed at ultra-high vacuum, SFG analysis can be conducted under ambient conditions[132]. This allows for in-situ measurements of film formation by probing the substrate-film interface during film formation or diffusion[133]. Another advantage SFG offers in the analysis of thin films is its sensitivity to breaks in inversion symmetry, allowing it to be interface sensitive and sensitive to the conformation of alkyl chains[132]. A sophisticated method of vibrational spectroscopy, a scanning IR signal excites and causes vibration of molecules at an interface, while a visible light (vis) source pulses. Interfaces can include any combination of solid/liquid/air interfaces where a break in symmetry is present. When the incident visible and IR beams overlap the IR pulse is tuned through a resonance band of the adsorbate[134]. Interaction of the IR and vis light, in space and time creates an Ultra Violet (UV) SFG signal, equivalent to the sum of the two input frequencies by;

$$\omega_{\mathrm{SFG}} = \omega_{\mathrm{vis}} + \omega_{\mathrm{IR}}$$

Equation 2.7

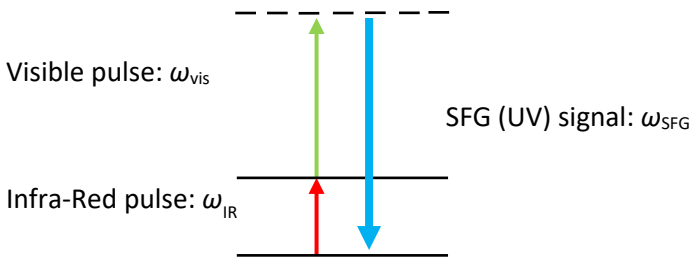

Figure 2.7: The overlap of IR and visible light in space and time resulting in the creation of an UV SFG signal equivalent to the sum of the two input frequencies, described by Equation 2.7.

Excitation by IR provides a vibrational response, which is then upconverted by the visible beam through a Raman process. That is, the vibration induced by IR and excitation by vis results in the emission of a UV SFG signal. Thus, it is also a requirement that the vibrational modes probed must be both IR and Raman active. IR frequencies resonate with vibrational transition frequencies of a surface molecule resulting in the enhancement of the SFG signal. The vibrational spectrum of the adsorbate is detected as the IR frequency is scanned across the resonance of molecules at the interface.

In order to be surface and interface specific, SFG must be a second order process sensitive to anisotropy, the input must have a tuneable IR frequency to excite vibrational transitions, and the output should be in near-IR or visible so it can be detected by a photomultiplier[129]. The combination of tuneable IR and vis light to produce a UV SFG signal fits these parameters thus, SFG is more suitable for analysis of substrate-film interfaces than other surface sensitive or IR techniques such as Second Harmonic Generation (SHG) as it has the surface sensitivity in addition to molecular detection through characteristic vibrational transitions. The resulting signal contains both resonate (via IR) and non-resonant (light interactions that are not a result of molecular vibrations) contributions.

When the external electric field becomes equal to or exceeds the local intramolecular electric field of the molecules probed, the surface electrons will start to polarise. This effect is not linear, as the field becomes stronger the polarisation of electrons does not increase linearly. As there are two incoming waves, vis (1) and IR (2) we can explain them both in terms of their own electric field E by;

$$E_{\mathrm{vis}} = E_0 \sin(\mathrm{k}_1 x - \omega_1 t + \phi)$$

Equation 2.8

$$E_{\mathrm{IR}} = E_0 \sin(\mathrm{k}_2 x - \omega_2 t + \phi)$$

Equation 2.9

Where k takes into account space, ω frequency, t time and ϕ denotes the starting position along the wave.

As SFG is a nonlinear optical process, the polarisation of the two incoming frequencies may not be the same as the outgoing SFG signal. The polarisation (*P*) of the SFG signal produced depends on the electric field of the incoming IR and vis light as well as $\chi^{(2)}$, which in a centrosymmetric medium produces no SFG signal;

$$P^{(2)}(\omega_3) = \chi^{(2)} : E_{vis}(\omega_1)\, E_{IR}(\omega_2)$$

Equation 2.10

The tensor $\chi^{(2)}$ takes into account the possible interactions of light depending on the polarisation of light. Polarisation dependence can be exploited when determining the orientation of molecules at the surface. The polarisation of incident IR and vis light will affect the strength of the SFG signal produced as shown in Equation 2.10. Electromagnetic radiation is polarised in a direction perpendicular to its direction of propagation. For the reflection of a laser from a surface, the electric field of the incident laser pulse is *p* polarised if the electronic field vector is in the same plane as the incident pulse and its reflection. If the electric field vector is perpendicular to its plane of reflection the electric field vector is *s* polarised[134]. Conventionally, the polarisation of each beam is listed in decreasing frequency. In the SFG system used for this thesis an IR light at 1064 nm and visible light at 53 2nm resulted in an SFG signal of approximately 450 nm. Therefore, if an *s-s-p* polarisation was set this translates to the following polarisation combination SFG(*s*), vis(*s*) and IR(*p*). The substrate lies in the x-y plane, with the z-axis perpendicular to the surface. *P* polarised incident light will induce polarisation in the z-axis, *s* polarised incident light will induce polarisation in the x- and y-axis. *s-s-p* polarisation has been found to produce a strong SFG output when probing the methyl groups of long carbon chain surface bound silanes[37,133,135,136] and is commonly used for the production of a strong SFG signal for the symmetric and asymmetric stretching of the C-H stretching mode of methyl groups.

As the technique is nonlinear, the number of possible interactions for a single combination of incident polarisations is greater than one. *s-s-p* polarisation can result in the following combinations; X_{xxy} X_{xyz} X_{yxz} X_{yyz}[134], where each index represents different beam of light, with its corresponding polarisation listed from short wavelength to long wavelength. Depending on the symmetry of the functional group being probed some of these combinations may be 0. For a combination to be zero, it must be symmetrical in all directions. When one plane of symmetry has been broken, for example at an interface, there are combinations present that are not 0. $\chi^{(2)}$ takes into account the possible combinations in Equation 2.10 and is what gives SFG its interfacial selectivity. Different combinations within $\chi^{(2)}$ can be measured by changing the polarisation of the incoming light to manipulate the possible combinations. With this in mind, the orientation of molecules will have a significant effect on the SFG signal produced. For *s-s-p* mode where the signal is most sensitive to molecules orientated perpendicular to the surface, branched, disordered oligomers will not produce an SFG signal[137].

As described in Equation 2.10 above, the SFG signal produced at an interface depends on broken inversion symmetry, but the intensity of the outgoing SFG signal is dependent on the incoming light and the probability of reflection and transmission which can be described by a Fresnel factor. The Fresnel factor describes the fraction of light that is transmitted, and the fraction reflected. This value depends on the angle of incidence and the refractive index of the media at the interface[138] and becomes important when changing properties of the interface or the environment that surrounds it.

A major advantage of SFG over other surface analysis techniques such as IR and RAMAN is the inability of many substrates to produce an SFG signal from the bulk, eliminated due to the centrosymmetric nature of many substrates. Centrosymmetry cancels out the effects of dipole moments within the bulk and this renders it SFG inactive. In this case all possible combinations of x,y and z are zero, that is all directions and symmetries are equal. This allows for the detection of weak signals produced by very low surface coverages to be measured at the interface, perfect for the analysis of thin or patchy films on a substrate. The surface sensitivity of SFG can be demonstrated practically by the formation of an OTS monolayer on fused silica in liquid hexadecane and CCl_4[129]. Bare quartz exposed to hexadecane reveals the absence of peaks in the characteristic CH_2 and CH_3 region, despite liquid hexadecane having a strong IR adsorption band in this region due to its high number of C-H stretches. Upon the formation of an OTS monolayer on the silica surface in hexadecane clear CH_3 peaks become visible due to the terminal methyl group of the OTS chain. Similarly, the formation of and OTS monolayer in CCl_4 reveals a nearly identical spectra to that produced in hexadecane, demonstrating the signal is being produced exclusively by the terminal methyl group of the film, with no solvent or substrate contribution[129]. A variety of substrates have been used to monitor silane films with the conformation of silanes on polymer surfaces examined by Loch *et al*.[139] and Chen *et al*.[140] and metal substrates by Ito *et al*.[141].

Unlike XPS and AES where Si and Al are used to monitor silane film growth, in order to exploit the interface and orientation specificity of SFG in the analysis of organosilane films the propyl chain of PTMS, PMDMS and PDMMS becomes the focus. The terminal CH_3 group is known to produce two characteristic SFG peaks at 2870 cm^{-1} for the symmetric stretching vibrational mode and 2945 cm^{-1} for the asymmetric stretching vibrational mode[130]. The CH_2 group contained within a long carbon chain has also been shown to produce 2 characteristic peaks for the symmetric and asymmetric stretching at approximately 2845 cm^{-1} and 2915 cm^{-1}. This allows for determination of molecular ordering of the film as the presence of an SFG signal representing a CH_2 group indicates the presence of *gauche* defects within the film[142].

As mentioned above, SFG can be conducted under ambient conditions and this allows for the opportunity to conduct in-situ experiments. A specific wavelength representing a peak of interest can be selected and the intensity of the SFG signal at that wavelength measured repetitively over a selected period of time. For example, monitoring characteristic wavelengths representing the CH_3 peak and CH_2 peak as a function of silane exposure time can discern the extent of ordering and how this changes with film diffusion[133]. Loch *et*

al.[136,139] have conducted studies into the conformations of silane molecules at polymer/silane interfaces using SFG. Results show that the conformation is dictated by both the functional groups present on the polymer surface and the chemical composition of the silane.

2.3.1.1 Preparation of silane films for SFG analysis

Due to the versatility of SFG and the ability to collect film-substrate interface information from samples both in- and ex-situ, the sample preparation methods differ slightly for each process. Experimental conditions including solvent, type of silane and concentration in solution were kept consistent (unless stated otherwise) with those used to create films for XPS and AES analysis above to allow the direct comparison of film behaviour across the three techniques. Al foil substrates were deemed inappropriate for SFG analysis due to their rough surface, therefore IR grade sapphire and quartz semi-cylindrical prisms were purchased from Crystal base, Japan. The flat face of each semi-cylindrical substrate was cleaned and pre-treated using a 0.5 µm aluminium polishing suspension on a polishing wheel, rinsed with Milli-Q water before submersion in piranha solution created by adding 10 mL of H_2O_2 to 30 mL of concentrated H_2SO_4. Samples were exposed to the piranha solution for 10 minutes while the solution was stirred. Sulfur residue was removed from the surface following piranha treatment by 2 repetitions of boiling the substrates in Milli-Q water for 5 minutes. Clean samples were stored in Milli-Q water until used. As with the pre-treatment process employed for Al foil substrates, this procedure was implemented to remove contaminants form the surface and create consistently reproducible substrates for silane condensation. This pre-treatment process also allowed for the reuse of substrates as it removed previously adsorbed silane from the surface.

It is well known that water reacts with Al_2O_3 to produce aluminium hydroxylates, $Al(OH)_3$ and aluminium-oxyhydroxylates, AlO_2H. The surface hydroxylation of sapphire substrates by submersion in aqueous solution has previously been reported[143,144]. While other methods of sapphire and quartz hydroxylation include water plasma[145] and water vapour deposition[146] a pre-treatment with piranha and storage in water was deemed sufficient in this case.

Silane films were created by securing the semi-cylindrical sapphire or quartz prism substrates into a flow cell which holds the prism in place while a solution is introduced from below. The IR and vis beams are focused through the prism onto the interface between the flat surface of the prism and the solvent. Large volumes of solvent can be introduced through bubbling argon gas into the solvent bottle and letting the increase in pressure of the closed system force the solvent through, while small volumes of solvent (less than 3 mL) can be introduced to the system through a syringe. A cross-sectional schematic of the in-situ cell detaining the direction of solvent and argon flow, the position of incoming IR and visible light, outgoing SFG signal and the substrate/cell interface can be seen along with a top down photo of the cell can be seen in Figure 2.8;

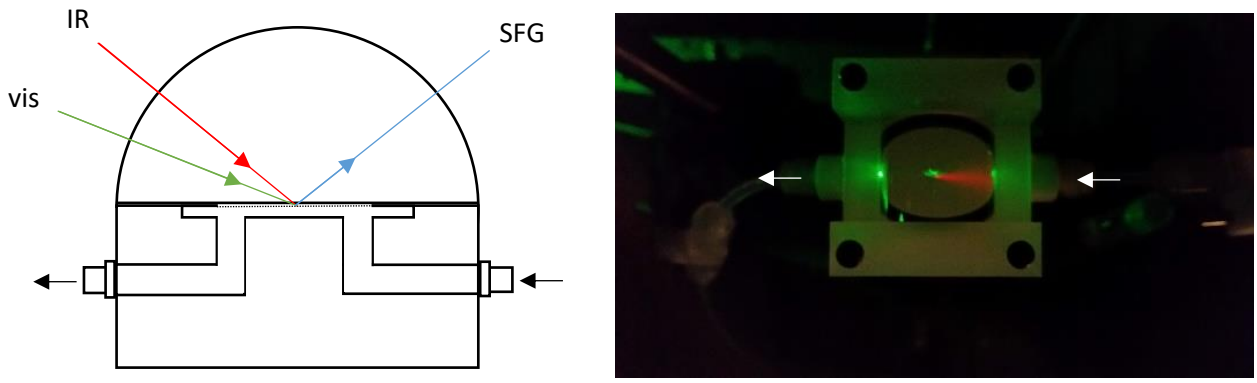

Figure 2.8: Flow cell used to measure the SFG signal created upon interaction of silane and the quartz substrate. Arrows show the flow of solvent, water and argon gas through the system and the direction of IR, visible and SFG light are shown in the cross-section schematic (left) and top down photo (right).

As IR light is not visible to the naked eye, a red guide laser is used to position the IR laser beam as shown in Figure 2.8. Where the SFG spectra were directly compared to the time dependent adsorption profiles on aluminium oxide measured using XPS sapphire prism substrates were used. For samples where the SFG spectra were not directly compared to these adsorption profiles, quartz substrates were used. While it is known that the difference in IEP between silane and substrate effect the rate of silane self-assembly[42], the effect of changing substrate was investigated for this system in Chapter 7.

The cell was filled with aqueous solvent in order to optimise the SFG signal. A 1%v/v silane in aqueous solvent solution was created and immediately pushed through the cell using a syringe. The solution was allowed to sit in the cell, in contact with the substrate for the prescribed exposure time before being flushed from the cell with argon. Once dried with argon, the SFG C-H stretching region was measured from 2800-3000 cm^{-1} to determine the molecular conformation within the film. To create rinsed samples, the in-situ cell was flushed with 10 mL of Milli-Q water to remove silane containing solvent and remove physisorbed species from the surface, prior to flushing the system with argon.

Film stability tests were also carried out by monitoring the conformation of the film following repeated exposure to water. Films were created as detailed above, dried with argon and the SFG C-H stretching region measured from 2800-3000 cm^{-1} to determine the initial conformation of the film. Water was then reintroduced to the cell for increasing amounts of time, flushed with argon and the C-H stretching region remeasured.

2.3.1.2 In-situ SFG measurement procedure

The procedure for in-situ measurement of silane films used in this thesis was based on the work done by Zhang *et al*[137] who successfully probed the CH_3 symmetrical stretching peak at 2870 cm^{-1} of sodium stearate

solution and compared the CH_3 and CH_2 symmetrical stretching regions revealing the adsorption behaviour of these molecules at the fused quartz/solution interface. Zhang's study revealed two integral mechanisms of sodium stearate/quartz interactions and demonstrated the power of SFG in revealing this behaviour. Firstly, in-situ probing of the CH_3 symmetrical stretching peak at 2870 cm^{-1} revealed the presence of a signal indicating the presence of ordered molecules at the interface, as the concentration of stearate in solution was increased. At the point where concentration was increased to the point of agglomeration, an SFG signal was no longer produced. Secondly, the presence on a bilayer was examined through exploitation of SFG selection criteria and the formation of a monolayer.

A clean, pre-treated quartz substrate was secured in the flow cell, and filled with aqueous solvent. Once the signal was optimised, repeated monitoring of the SFG signal at 2870 cm^{-1} began to gain a baseline. A 1% v/v PTMS silane solution in aqueous solvent was introduced to the cell and the SFG signal for the $CH_{3(s)}$ peak at 2870 cm^{-1} measured every 2 seconds. The cell was then flushed with water and argon to remove the silane solution and end the film growth process.

2.3.1.3 Specifics of the SFG system

The SFG system used in this thesis is located at the National Institute for Materials Science in Tsukuba, Japan. The specifics of this system are as follows; EKSPLA PL2250 Series Laser; Nd:YAG, 1064 nm laser, 30 ps pulse duration, 50 mJ pulse energy (at 1064 nm), 8 mm beam diameter (at 1064 nm), 20 Hz repetition rate. All SFG spectra were collected in SSP (SFG, vis, IR) polarisation. This polarisation is only sensitive to vibrational modes normal to the surface of the substrate. Experiments were conducted in a climate-controlled laboratory kept at 22 $\pm$ 2 °C in order to prevent a change in Fresnel factor due to fluctuations in temperature. The IR beam was focused with a CaF_2 Lens and a beam diameter of approximately 0.5 mm at the surface. The visible beam was unfocused and about 2 mm in diameter. The IR beam is tuned automatically within the range measured (2800-38000 cm^{-1}) and step width between measurements was set to 2 cm^{-1}. As with adsorption profiles analysed using XPS, each sample was created in triplicate and the average calculated. Errors quoted represent the standard deviation.

2.3.1.4 Optimisation of the SFG signal

The spectral resolution of the IR beam was calibrated by measuring IR spectra of a polystyrene reference sample and adjusting the wavenumber measured to match the known values for each peak in the spectra. For the SFG system used in this thesis, the IR resolution was adjusted by 1cm^{-1} Wavenumbers.

In order to initially optimise the SFG signal, a bare quartz substrate was used to manually optimise the SFG signal through the adjustment of sample stage height and IR laser position while monitoring the signal at 3250 cm^{-1}. Quartz was chosen for initial optimisation as the quartz-air interface produces a strong SFG signal

due to breaks in symmetry at interface; once this was achieved, the signal was considered optimised and the SFG system calibrated. Alternative substrates could then be studied.

Initially, the SFG signal is measured at all stages of optimisation without the application of polarisation filters. Polarisation of the IR, visible (vis) and SFG light can not only alter the intensity of the SFG signal but also alter the selectivity of the light to specific molecular orientations at the interface. Once the SFG signal was optimised for bare quartz, the SFG signal for the C-H stretching region was optimised. A reference sample of bare quartz modified with a monolayer of OTS was used to measure the SFG signal for the CH_3 terminal groups on the octadecyl chain. Exploiting the selectivity rules detailed in section 2.3.1, the octadecyl chain of the highly ordered monolayer produces a strong SFG signal at 2870 cm^{-1} due to symmetric stretching of the CH_3 group. This same signal is produced for terminal CH_3 groups of ordered carbon chains of any length, along with asymmetrical CH_3 stretching at 2950 cm^{-1}. Symmetric stretching requires less energy to cause vibration and thus the $CH_{3(s)}$ peak is lower in wavenumber than an asymmetrical stretching. For carbon chains containing *gauche* defects, CH_2 a symmetric stretching signal occurs at 2850 cm^{-1} and asymmetric at 2920cm^{-1} [142]. The prominence of $CH_{3(s)}$ peaks is directly related the order of the film as an ordered (trans conformation) propyl chain would produce a prominent CH_3 peak from the terminal methyl group and no CH_2 symmetric or asymmetric peaks. An example of a quartz sample modified with OTS containing *gauche* defects indicated by the presence of CH_2 peaks at 2850 and 2920 cm^{-1} was reported by Ye *et. al.* in 2001[142] and closely resembles many of the SFG spectra for PTMS, PMDMS and PDMMS films in this thesis. The SFG spectra of the OTS reference sample used to optimise the SFG signal measured using *s-s-p* polarisation can be seen in Figure 2.9. The absence of CH_2 peaks reveals the quartz OTS reference sample to be that of a highly ordered, compact film and very closely resembles the spectra reported for highly ordered, compact OTS films[130,142,147].

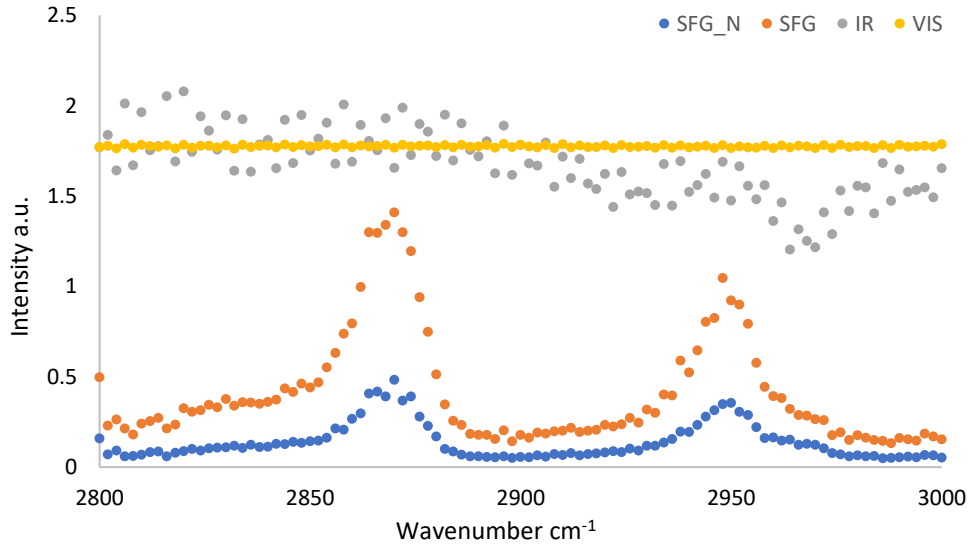

Figure 2.9: CH stretching region SFG signal of fused quartz modified with OTS, measured in air. SFG_N (Blue) is the SFG (orange) signal normalised to the IR (grey) signal measured using s-s-p polarisation. The Visible light signal is shown in yellow.

The raw SFG signal along with a spectrum normalised to the IR signal are shown in Figure 2.9, the decision of which spectra to use is at the discretion of the analyst based on the stability of the IR laser intensity. If the IR laser intensity remains stable across the spectra measured, it is acceptable to use the raw SFG signal data. Due the instability of the IR signal observed at 2970 cm^{-1} in Figure 2.9 the decision was made to use spectra normalised to the IR signal intensity in all further analysis.

Each time the substrate is changed, whether in composition, shape or simply from one sample to the next, the system must be re-optimised to ensure the IR and visible light overlap and the SFG signal produced is focused towards the analyser, the process is methodical and stringent. The substrate, solvent and polarisation are changed methodically while continuing to optimise the stage height and position of the incoming IR and visible light as substrates, solvents or samples are changes. This procedure is essential as the signal for the sapphire-air interface is significantly weaker than that of the quartz-air interface and would not be measurable if the system is not stringently optimised for each individual sample.

As mentioned above, this process began with optimisation for a flat quartz substrate. Once this was achieved, the signal was optimised for the semi-hemispherical prism used in the in-situ flow cell. The Quartz prism was secured in the cell and exposed to Milli-Q water while the SFG signal was optimised by adjusting the sample height and IR laser position while monitoring the SFG signal produced at 3250 cm^{-1}. The water/quartz and water/sapphire interface is strongest when using *p*-*p*-*p* polarisation. Upright molecules are more in line with the plane of incidence and will be more sensitive to *p*-polarisation, molecules lying down parallel to the substrate (perpendicular to the plane of incidence) are more sensitive to *s*-polarisation (*s*-*p*-*s*). *p*-*p*-*p* polarisation probes all possible combinations and while containing the most information, it is difficult to determine directional specific behaviour. The SFG signal was first optimised for pp polarisation (IR and vis) with no polariser lens on the SFG signal. The *p* polarising lens was then added to the SFG signal path and the optimisation parameters adjusted. As mentioned above, *s*-*s*-*p* polarisation has been found to produce a strong SFG output when probing the methyl groups of long carbon chain surface bound silanes[37,133,135,136] and the selective sensitivity of the *s*-*s*-*p* polarisation to the vibrational mode normal to the surface of an isotropic media can also be exploited[142]. This polarisation is best suited to molecules standing upright, perpendicular to the substrate. It is because of this that *s*-*s*-*p* polarisation was used to analyse the silane films produced in this thesis.

As detailed above, Fresnel factors will change the intensity of the SFG signal produced. While experiments were conducted in a climate-controlled lab to reduce changes in Fresnel factors during the collection of spectra, the impact of changing the environment on the SFG signal intensity is shown in Figure 2.10;

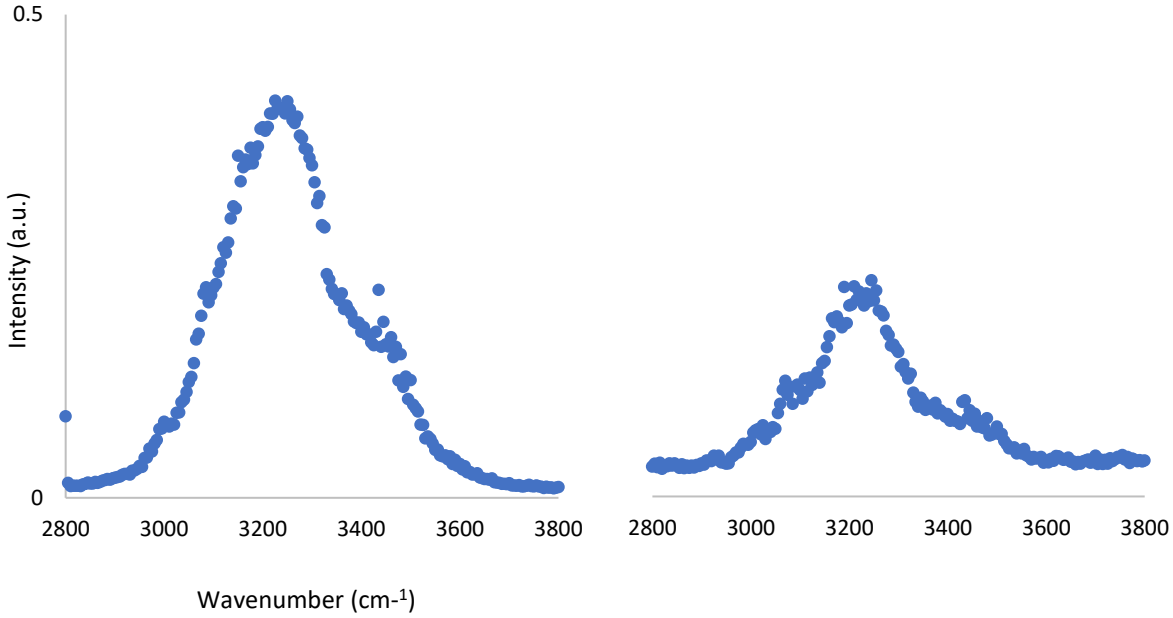

Figure 2.10: The normalised SFG O-H stretching region of the water/quartz (left) and aqueous solvent/quartz (right) interface. Signal at 3250 cm^{-1} wavenumbers was used to optimise the SFG signal in s-s-p polarisation mode.

The optimised SFG signals of the water/quartz and aqueous solvent/quartz interface were measured in the O-H stretching region ranging from 3000 to 3600 wavenumbers (cm^{-1}) in *s-s-p* polarisation. The intensity of the SFG signal is reduced upon the addition of solvent, this can be attributed to the decrease in water and increase in ethanol interacting with the substrate and a change in optical constants. Despite a reduction in SFG signal intensity, the two main O-H stretching peaks at approximately 3200 cm^{-1} representing perfect hexagonal conformation referred to as *ice like conformation*[148] and random asymmetric OH stretching referred to as *liquid like conformation* at 3450 cm^{-1} [148] are prominent in both spectra. Measuring the full O-H stretching region shown in Figure 2.10 also served to demonstrate how residual water on the surface may interfere with the spectra obtained for the C-H stretching region. The C-H stretching region used to determine the intensity of CH_3 and CH_3 peaks shown overlaps with the beginning of the O-H stretching region at approximately 2980 cm^{-1}. To determine the practical impact of this overlap, a PTMS film was created in aqueous solvent, the cell flushed with argon and the SFG spectra collected. Water was then introduced into the cell and the SFG spectra collected once more. A comparison of these two spectra is shown in Figure 2.11;

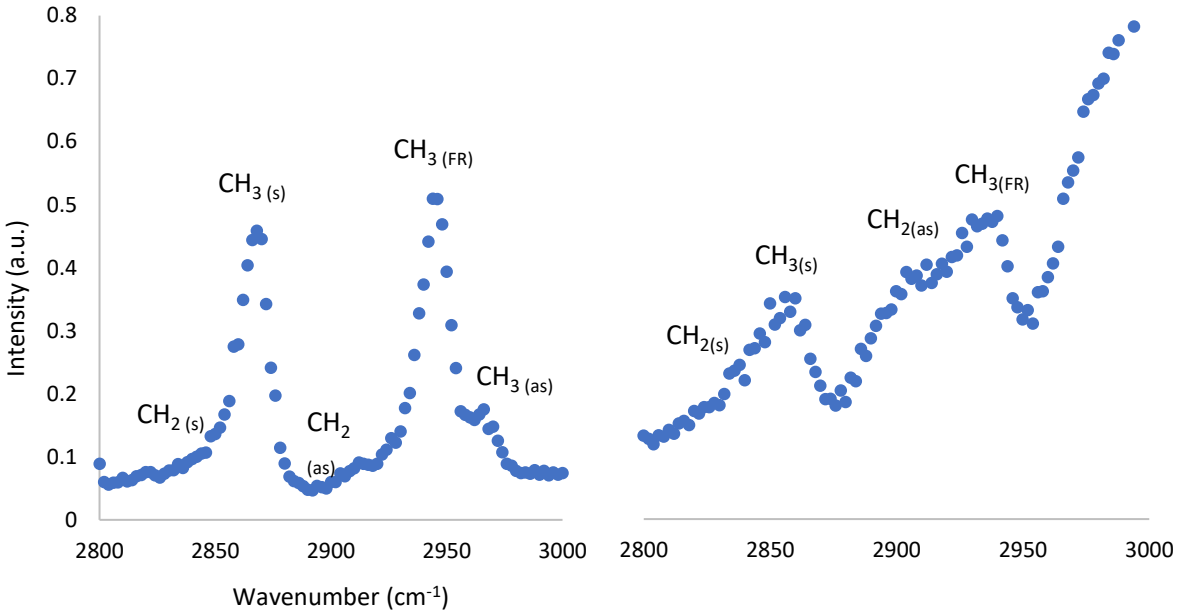

Figure 2.11: Normalised SFG C-H stretching region of a PTMS film after 5 seconds of exposure under argon (left) and while exposed to Milli-Q water (right), collected in s-s-p mode for the determination of water O-H stretching interference on the C-H stretching region. (as) denotes asymmetric stretching while (a) denotes symmetric stretching and (FR) Fermi resonance.

This comparison served two purposes, firstly, while the water and solvent-quartz O-H region appears to overlap the C-H region, the SFG spectra produced for a PTMS film under argon does not show any such interference, confirming the successful removal of water from the interface. This is compounded by the significant impact the presence of water on the substrate has on the same film in an aqueous environment, increasing the gradient of the background significantly. Secondly, it gives an insight into effect of water on the presence of defects in the film. As can be seen in Figure 2.11, the symmetric and asymmetric stretching of CH_2 increases when compared to the symmetric and asymmetric CH_3 stretching signals. This may be due to hydrophobicity of the propyl chain causing an increase of the number of *gauche* defects in the film. This theory will be investigated further in Chapter 7.

2.3.1.5 Peak Fitting and Deconvolution of SFG spectra

The SFG spectra obtained in the C-H stretching region of 2800-3000 cm^{-1} were fit to Equation 2.11[129,149].

$$I_{SFG}(\omega) \propto \left| X^{\leftrightarrow(2)}_{eff,NR} + \sum_n \frac{A^{\leftrightarrow}_{eff,n}}{\omega_{IR} - \omega_n + i\Gamma_n} \exp(i\varphi) \right|^2$$

Equation 2.11

Where $X_{eff,NR}^{\leftrightarrow(2)}$ is the nonresonant contribution for the surface nonlinear susceptibility (surface molecules), a characteristic coefficient of the medium; ω_{IR} is the IR angular frequency; A_n is amplitude of vibration with resonant angular frequency ω_n; Γ_n is the damping factor and φ is the phase difference in radians between the resonant and non-resonant terms of the n^{th} vibrational mode.

The contribution of each functional group was determined through deconvolution of this fit. As shown in Table 2.3.1, there is a large distribution in the reported values for C-H stretching peak assignments. This is related to the energy shift when using different alkyl chain molecules and substrates. As the SFG spectra of PTMS, PMDMS and PDMMS on quartz and sapphire have not be reported before, the peak assignments differ slightly from some values in Table 2.3.1, but remain within the range previously reported for alkyl chain molecules.

Table 2.3.1: Peak assignments adopted for interpretation of organosilane SFG spectra, along with associated references to studies that have established these as standards for peak assignments in the C-H stretching region of 2800-3000 cm^{-1}.

Peak assignment	Peak Maximum (Wavenumber, cm^{-1})	PTMS, PMDMS and PDMMS peak assignments Wavenumber (cm^{-1})
CH_2(s)	2840[133,150] 2845[151] 2850[139,140,150,152] 2851, 2855[132] 2855[142,153] 2859[142]	2845
CH_3(s)	2865[150] 2870[139,140,151] 2875[153] 2878[152] 2879[142] 2880 [132]	2870
CH_2(as)	2895[150] 2916 [132] 2917[142,152] 2919[132] 2930[139,140]	2912-2914
CH_3(FR)	2940[132] 2945[152] 2940[142]	2942-2945
CH_3(as)	2945[133,139,150] 2954 (out-of-plane) [132] 2955[151] 2956 [132] 2960[140] 2962[152] 2965[153] 2868 (in-plane) [132]	2960-2966

An example of the film created upon the exposure of 1%v/v PDMMS to a sapphire substrate for 160 seconds and the deconvolution of its fit to Equation 2.11 using values shown in Table 2.3.1 can be seen in Figure 2.12

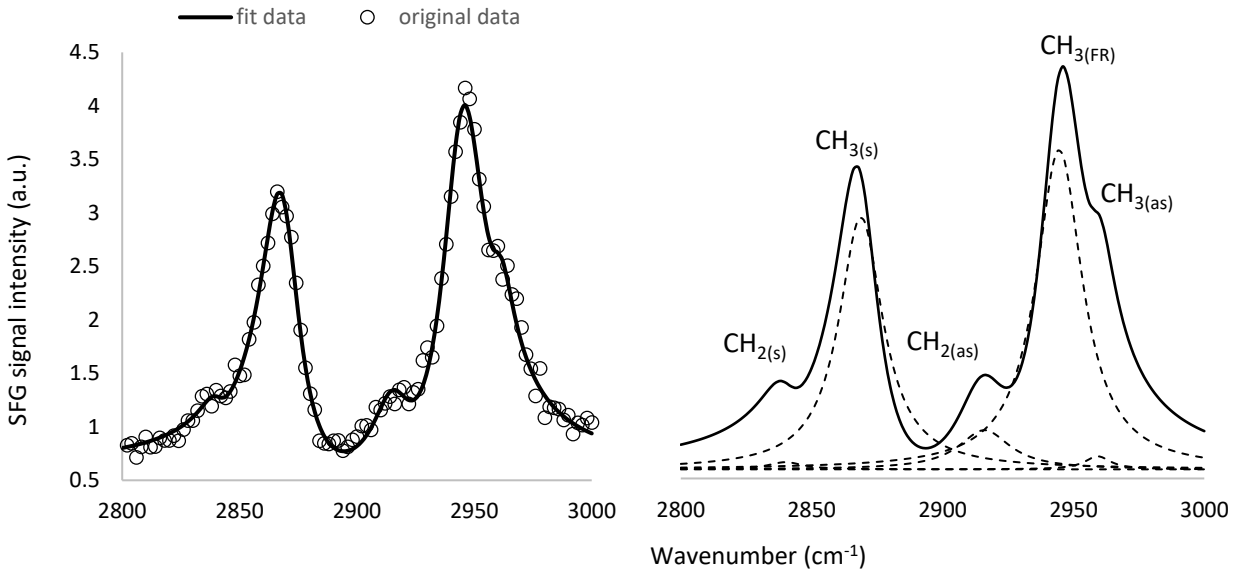

Figure 2.12: Normalised SFG spectrum of the film produced when 1% v/v PDMMS was exposed to a sapphire substrate for 160 seconds, fit to Equation 2.11 (left). Deconvolution of the data fit detailing the contribution of each functional group in the spectrum (right). (as) denotes asymmetric stretching while (s) denotes symmetric stretching and (FR) Fermi Resonance.

The presence of an SFG signal from CH_3 indicates molecules within the film are orientated with their propyl chains perpendicular to the substrate. The presence of methylene groups due to symmetric and asymmetric stretching, at 2842 cm^{-1} and 2920 cm^{-1} respectively strongly resemble spectra previously reported for a fused quartz surface modified with an OTS monolayer containing *gauche* defects[142]. As mentioned above, peaks at 2870 cm^{-1} and 2965 cm^{-1} represent the symmetric and asymmetric stretching of the terminal methyl group, while the peak at 2945 cm^{-1} is assigned to the Fermi resonance of the symmetric CH_3 group and an overtone of the C-H bending modes[154]. The absence of a $CH_{2(s)}$ contribution would indicate molecules within the film are in a *trans* conformation[150] where CH_2 groups have centrosymmetry and are therefore SFG inactive[142]. In this conformation, only the terminal centrosymmetric and able to contribute to the SFG spectrum[152]. Therefore, the ratio of $CH_{3(s)}$:$CH_{2(s)}$ peak amplitude can be used as a measure of order in the propyl chain of molecules within the film[155]. For each deformation in the carbon chain there is an unpaired CH_2 group created, the intensity of the CH_2 peak in the spectrum is due to the accumulation of *trans-gauche* deformations and the average orientation of those groups along the chain.

Monitoring the ratio of $CH_{3(s)}$:$CH_{2(s)}$ peak amplitude during the self-assembly of organosilane films will reveal the order and orientation of silane molecules at the substrate-film interface as the film assembles.

2.4 Silane Functionalised Al powders for 3D printing

As detailed in section 1.11 methods used to functionalise aluminium powders with silane often require the use of anhydrous or pH altered aqueous solvents. These methods also require long processing times and the use of specialised instrumentation to cure and further process the powders. To reduce cost, processing time and impact on the environment an altered method of powder silane functionalisation was created. This process allowed for the complete functionalisation, cure and refinement of powders with a start to print time of just a few hours. By using water as the sole solvent complexity of the process and environmental impact were significantly reduced and allowed this process to be performed with minimal wet chemistry facilities.

2.4.1 Preparation of PTMS functionalised Al powders

Three unique Al powders were chosen for PTMS functionalisation based on their potential for LMD 3D-printing. All powders were produced using a gas atomisation process containing at least 94% aluminium with granulometries ranging from 23-100 µm. Each powder was given a reference number for this thesis, powder 1 was purchased from Aeromet International, England while powders 2 and 3 were supplied by Naval Group, the details of which can be found below;

Table 2.4.1:Elemental composition and granulometries of powders used for PTMS functionalisation and LMD 3D printing.

Powder Number	Composition	Particle size (µm)
1	$Al_{(94\%)}$ $Cu_{(5\%)}$ $Mg_{(0.33\%)}$	20-63
2	$Al_{(95\%)}$ $Cu_{(5\%)}$	63-80
3	$Al_{(95\%)}$ $Cu_{(5\%)}$	80-100

Chemical analysis reveals the presence of Si, Fe, B, Ti and Ag trace elements within the powders, each less than 0.08% and unlikely to affect the condensation of PTMS on the surface.

In order to simplify the functionalisation process and move into a more cost efficient and greener production, acetic acid and ethanol were omitted from the solvent with the reaction occurring solely in distilled water. As the rate of reaction and film growth is not directly compared to other films produced in this thesis, alterations to solvent composition and experimental procedure in order to optimise the process for this application is of no consequence. All 3 powders underwent the same processing procedure, with the creation of an aluminium slurry facilitating PTMS functionalisation. 250 g of powder was added to 300 mL of distilled water and stirred using a magnetic stirring bar. 53 mL of PTMS was added to the solution to create a 15%v/v

silane in water solution. An increase in concentration upon the 1% used to coat Al foil substrates in this thesis was deemed necessary due to the significant increase in the surface area to volume ratio of the Al powder vs foil. Once again, as the mechanism of condensation is not being directly compared to other films in this thesis, the increase in concentration is of no consequence. The solution was stirred continuously for 1 hour before filtering. A small volume (approx. 50 mL) of water was used to rinse and remove any residual Al powder from the reaction container. The filtered powder was then cured at 100^{o}C for 2 hours. Following curing, an ultrasonic filtering system was used to separate any agglomerated powder particles. The powder was passed through 2 sieves, firstly a 160 µm mesh followed by a 100 µm mesh. As the original particles ranged from 23 µm to 100 µm in size, removal of all particles larger than 100 µm was sufficient to remove the majority of agglomerated particles in the matrix of all 3 powders. The morphology and distribution of these powders was imaged using SEM. The presence of silane on the Al powders was confirmed using Electron Dispersive X-ray spectroscopy (EDS) and the impact of these films on the flowability of the powders measured using a standardised flowability test.

2.4.2 Measuring powder flowability

Flowability tests were conducted on both PTMS modified and unmodified powders using a LPW PowderFlow standard flowability test kit. The flowability of powders was determined by measuring the length of time taken for 150g of powder to pass through an aperture. Once filled, the vessel is opened, and the powder allowed to flow through the aperture. In order to initiate the flow of powder, a single tap on the side of the vessel is standard. Two aperture sizes are commonly utilised firstly, a Carney flow tunnel with a 5mm aperture and if successful a second test with a smaller 3mm Hall flow tunnel. While rudimentary, this system was successfully used to directly compare the flowability of powders pre- and post-silane functionalisation with the flow time rounded to the nearest 0.1 second, the average of three replicates taken and the improved flowability given as a percentage.

2.5 3D-printing Laser Metal Deposition (LMD)

In order to 3D print metal powders using LMD, a substrate is required as a contact point for the first layer to be sintered to. A 2 mm thick Al 2025 rolled plate was used to as the substrate, sandblasted prior to printing. PTMS functionalised powder was loaded into the reservoir of an IREPA MultiClad Machine located at École Centrale de Nantes, France. carried by argon gas and transported coaxially to the IPG 2 kW continuous fibre laser, with a wavelength of 1070 nm beam through a coaxial nozzle. A 670 w laser power with laser spot diameter of 0.6 mm and mass flow rate of 1.5$\pm$0.2 gm/min was used at a speed of 2000 mm/min to build a 10x10x10 mm cube of printed Al. The true path strategy, or the programmed path of the laser was set to an alternate zig zag pattern. That is, each layer was printed in lines perpendicular to the direction of the previous

layer with 1x1 cm cubes printed. Multiple cubes were printed for each powder, labelled A through F with vertical and horizontal wall height optimised for each sample the details of which can be found in Table 2.5.1 below;

Table 2.5.1: List of 3D-printed silane functionalised aluminium samples, their corresponding starting materials and printing wall height parameters.

Printed Sample	Powder	Programmed layer height (mm)
A	1	0.3
B	1	0.2
C	2	0.2
D	2	0.2
E	3	0.2
F	3	0.16

Once printed, samples were cut to create a cross section using a water cooled, diamond bladed drop saw for microscopic analysis. Samples were then hot mounted in a mixture of Bakelite and a conductive Diallyl phthalate Cu filled polymer using a Struers Hot Mounting Press. The use of a conductive polymer was essential as it allowed for the easy spectroscopic analysis of the surface using AES. Samples were ground and finely polished using a Struers Tegramin 25 automated polisher and DiaPro diamond suspension polishing solutions ranging in size from 9-1 µm. Samples were then etched in Keller's reagent, a mixture of 5 mL nitric, 3 mL hydrochloric and 2 mL hydrofluoric acid in 190 mL of water for 30 seconds to reveal grain boundaries and other microstructure characteristics. Samples were stored under desiccant until analysed using AES-SEM.

3 The Adsorption Profiles of Organosilane Films.

The following chapter is based in part on the paper;

Sims RA, Harmer-Bassell SL, Quinton JS. The oscillatory adsorption of self-assembled organosilane films on aluminium oxide surfaces. *Surface and Interface Analysis.* 2018; 50(8): 813-818 DOI 10.1016/j.apsusc.2019.01.015.

While the oscillatory adsorption behaviour of PTMS has been established, the adsorption profiles of other silane species as a function of exposure time have been used to gain a greater insight into the mechanism of silane film-self-assembly. By reducing the number of hydrolysable -OCH_3 groups on the central silicon atom, along with hydrolysis time as a method of reducing oligomerisation, the mechanism of organosilane film self-assembly has been explored.

The characterisation of silane film adsorption was achieved by monitoring silane surface coverage on an aluminium oxide substrate as a function of exposure time using X-ray Photoelectron Spectroscopy (XPS). As discussed in Section 2.2.2 the surface sensitivity of XPS is directly related to the Inelastic Mean Free Path of photoelectrons ejected from the surface upon excitation of photons from an X-ray source. With the attenuation length of Si*2p* photoelectrons calculated to be 2.4 nm, XPS becomes an ideal technique for determining the average elemental composition of thin films. By exploiting the presence of silicon as an elemental marker in the film and aluminium in the substrate, the extent of silane surface coverage on the aluminium substrate can be determined. To achieve this and make adsorption values more sensitive to the lower surface coverages observed, a ratio of Si:(Si+Al) was used to represent silane surface coverage.

3.1.1 The XPS characterisation of silane films

For every sample analysed using XPS, both a survey and high-resolution spectra of the C *1s*, O *1s*, Si *2p* and Al *2p* regions were collected using the LHS-10 XPS instrument at Flinders University, as detailed in section 2.2.2 (a detailed explanation of high resolution XPS peak fitting procedures used in this thesis can also be found in section 2.3.1.5). Survey spectra of the entire binding energy spectrum from 1000-0 eV, an example of which can be seen in Figure 3.1, were collected in CRR mode and due to its increased signal to noise ratio, used for qualitative analysis of the surface. Collecting information from a wide range of binding energies allows for the efficient identification of contaminants as well as the presence of silane films on the surface. An example of a bare Al substrate exposed to the pre-treatment process outlined in section 2.2.1 (shown in blue) used as a control and the spectrum of a film created following a 5 second exposure to 1% PTMS in aqueous solvent (orange) is shown in Figure 3.1 below;

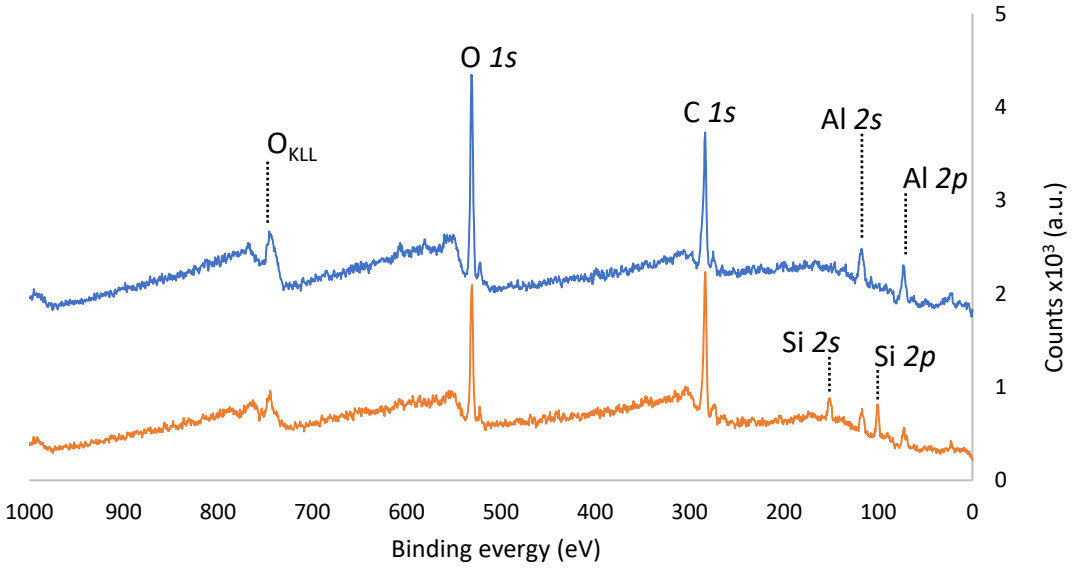

Figure 3.1: XPS survey spectra of 1% PTMS in aqueous solvent exposed to an aluminium oxide substrate for 5 seconds (orange) along with the offset survey spectra of bare aluminium foil (blue) obtained in CRR mode using an Mg K_α X-ray source.

The absence of peaks representing Si *2s* and Si *2p* on the bare Al_2O_3 substrate, along with the presence of such peaks in a sample exposed to a 1% PTMS solution for 5 seconds confirms the use of Silicon as an elemental marker in the film and Aluminium as an elemental marker in the substrate as well as the absence of contaminants on the bare Al control. The absence of silicon on the control substrate (shown in blue) also confirmed the effectiveness of the re-polishing and cleaning procedures outlined in section 2.2.1 and the ability to reuse substrates.

As shown in Figure 3.1, not all peaks in the XPS spectra are due to XPS peaks. An oxygen Auger peak can be seen at 743 eV caused by the decay of a more energetic electron (from the L shell), dropping down to fill the hole created when the O *1s* photoelectron is ejected (K shell). The excess energy released during this transition (from the L shell) is collected by the analyser and a peak created in the spectrum (labelled O_{KLL}).

Control samples exposed to pre-treatment and silane-free solvent are reported as t=0 in subsequent time dependent adsorption profiles. The initial processes involved in condensation and adsorption are of most interest as they will ultimately determine the nature of film growth to follow and subsequent composition of the film. The adsorption profiles of PTMS, PMDMS and PDMMS were each monitored from 0 to 200 seconds in order to capture the initial adsorption behaviour of each species.

3.2 The Adsorption Profile of Propyltrimethoxysilane Films

The oscillatory adsorption behaviour of PTMS, which when completely hydrolysed contains an inactive propyl chain and three active silanol Si-OH groups was initially revealed by Quinton *et al.*[23,38-43]. The presence of a single oscillation reaching an initial maximum coverage at 30 seconds, followed by a Langmuir Type film growth for a concentration of 0.75% v/v exposed to aluminium substrates in a pH 3 aqueous solution was reported[23,38-40]. In an effort to recreate the oscillatory behaviour previously reported and determine the effect of increasing PTMS concentration on both the rate of reaction and the oscillation itself, the concentration of PTMS in solution was increased to 1%v/v. Films were initially created following a wet/dry sandpaper polish and a 1-hour hydrolysis time and as detailed in section 2.2.1 silane surface coverage measured and plot as a function of time[48].

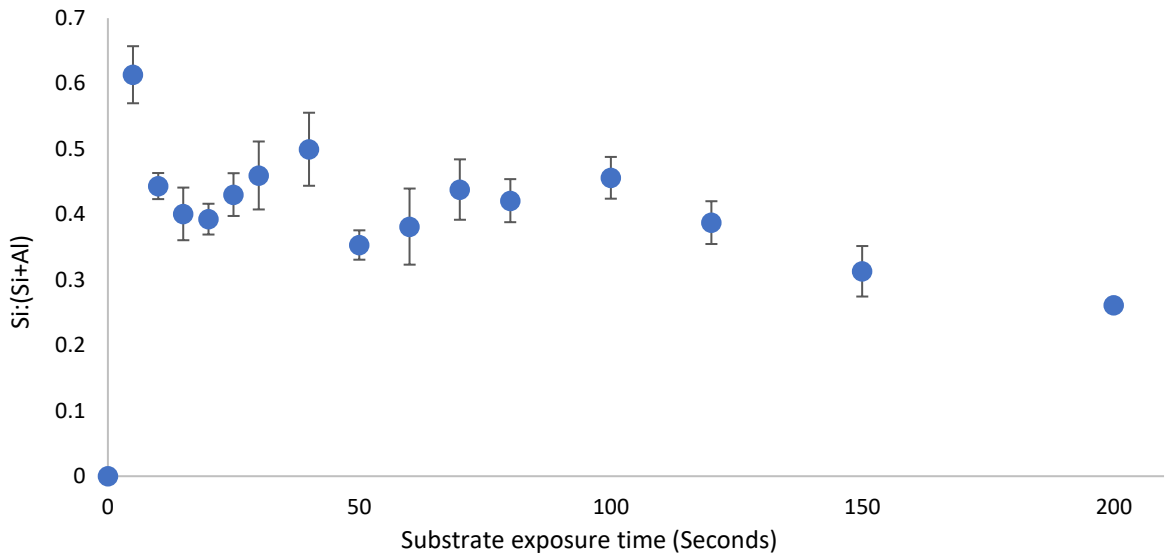

Figure 3.2: The time dependent adsorption profile of 1% v/v PTMS in aqueous solvent on sandpaper polished aluminium foil substrates after the solution was allowed to hydrolyse for 1 hour Each data point represents the average of three replicates with the error quoted as the standard deviation[48].

As predicted based on reaction kinetics described in section 1.5.2 increasing the concentration of PTMS in solution to 1% v/v increased the reaction rate such that the initial oscillation is shifted from 30 seconds to 5 seconds of film growth. However, the adsorption profile shown in Figure 3.2 also reveals the presence of multiple oscillations in addition to those previously reported. In order to understand the presence of multiple oscillations, the behaviour of molecules both in solution and on the surface must be considered. Through the deliberate choice of solution pH condensation becomes the rate determining step over hydrolysis[18] however, further examination of this reaction reveals more than one rate of condensation; formation of an Si-O-Si siloxane bond between silane molecules and the formation of Si-O-Surface bonds. In order to account for the presence of an oscillation such as the one observed in Figure 3.2, the condensation between silanol molecules must occur at a faster rate than that of Si-O-Substrate bonds. It is the collective behaviour of these molecules, initiated upon the introduction of an aluminium oxide substrate which produces a measurable oscillation. The presence of a measurable oscillatory behaviour can also be attributed to the ability of PTMS to form a myriad of possible oligomer configurations in solution and on the substrate. It is true that a completely hydrolysed PTMS molecule can bind to the hydroxylated substrate via all three OH functional groups, however if this does not occur, the remaining OH groups remain highly reactive. This can result in the condensation to other silane molecules and the growth of large dendritic, tree-like structures branching out from the substrate surface as shown in Figure 3.3. The desorption of these larger silane species is thought to contribute greatly to the measurable coverage oscillation as the desorption of a large oligomer will have a considerably larger effect on the surface silicon measured compared to the desorption of a single PTMS monomer.

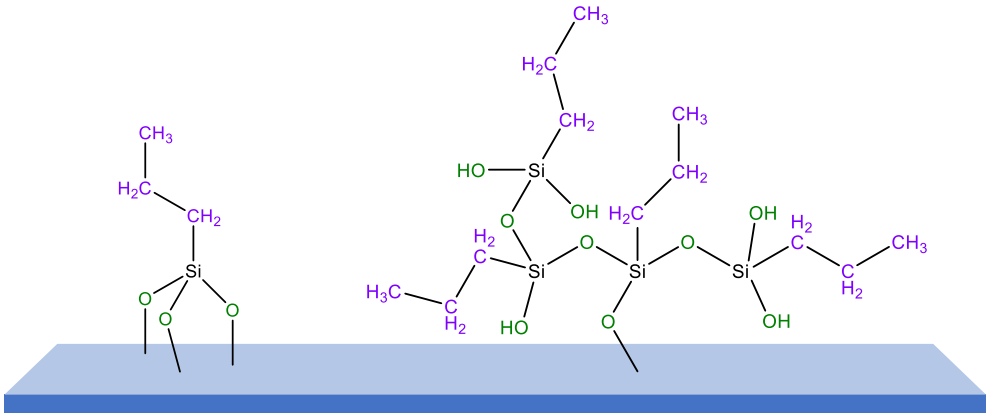

Figure 3.3: Examples of possible condensation products on a hydroxylated surface for the tri-functional silane PTMS.

One limitation of the data presented above is that exposure times represent a specific time point and are a representation of the average elemental composition within the sampled area. It is possible that these oscillations occur at a greater rate than can be accurately measured with current capabilities. If this is the case, the oscillation reported here is aliasing a much faster process.

Si:(Si+Al) values were calculated from the average of 3 samples, with all samples all exposed to the X-ray beam for an equivalent length of time. However, to definitively determine if beam damage contributes to the measured oscillatory behaviour, prolonged exposure tests were conducted. High resolution Si *2p* and Al *2p* spectra of the silane film were initially collected, and subsequently measured two more times following one hour and two hours of direct exposure to the X-ray beam. Both peak intensity and position were monitored to ensure any X-ray induced damage did not have a significant impact on the surface coverage measured.

Table 3.2.1: Peak intensities of a 1%v/v PTMS in aqueous solvent at initial analysis, after 1 hour and 2 hours of exposure to the MgKα X-ray beam.

	Fit Peak intensities (%)			**Variation (eV)**
	Initial analysis	**+1hr**	**+2hr**	
Si *2p*	40.9	41.5	41.6	0.7
Al *2p* (Al_2O_3)	59.1	58.5	58.3	0.8
Si:(Si+Al)	0.41	0.42	0.42	0.01

Table 3.2.2: Peak positions of a 1%v/v PTMS in aqueous solvent at initial analysis, after 1 hour and 2 hours of exposure to the MgKα X-ray beam

	Peak positions – Binding Energy (eV)			**Variation (eV)**
	Initial analysis	**+1hr**	**+2hr**	
Si *2p*	104.1	104.3	104.9	0.8
Al *2p* (Al_2O_3)	76.1	76.2	76.2	0.1
Al $2p^{1/2}$	73.2	72.8	73.4	0.6
Al $2p^{3/2}$	74.0	73.6	74.2	0.6

The variation in both peak intensity and position were determined with no discernible damage measured. From this it is assumed that beam damage does not have a significant impact on the values of Si:(Si+Al) measured and therefore does not contribute to the oscillatory adsorption observed.

3.2.1 The effect of substrate surface roughness

Surface roughness can have a significant effect on the way in which molecules interact with a surface. The edge of an abrasion will possess a different surface energy to that of a flat surface, potentially resulting in an increase or decrease in both the rate of condensation and the amount of silane adsorbed. In order to determine if the level of abrasion results in preferential adhesion of silane molecules and thus has an influence on the oscillatory behaviour, the adsorption of silane molecules on aluminium foil substrates polished down to a 1 µm surface roughness were examined. The oscillatory adsorption profile shown in Figure 3.2 was created by abrasion of the surface with P1200 wet/dry sandpaper resulting in a minimum surface roughness of 15 µm, a protocol implemented in an effort to represent industrial conditions. In order to reduce the surface roughness of the substrate, a fresh batch of Al foil was polished using 1 µm diamond paste. All other sample preparation methods remained constant as detailed in section 2.2.1. Diamond paste polished substrates were exposed to silane for exposure times representing key points along the oscillatory curve and compared to those abraded with sandpaper. The Si:(Si+Al) values were plotted in Figure 3.4 along with the oscillatory curve produced for sandpaper polished substrates.

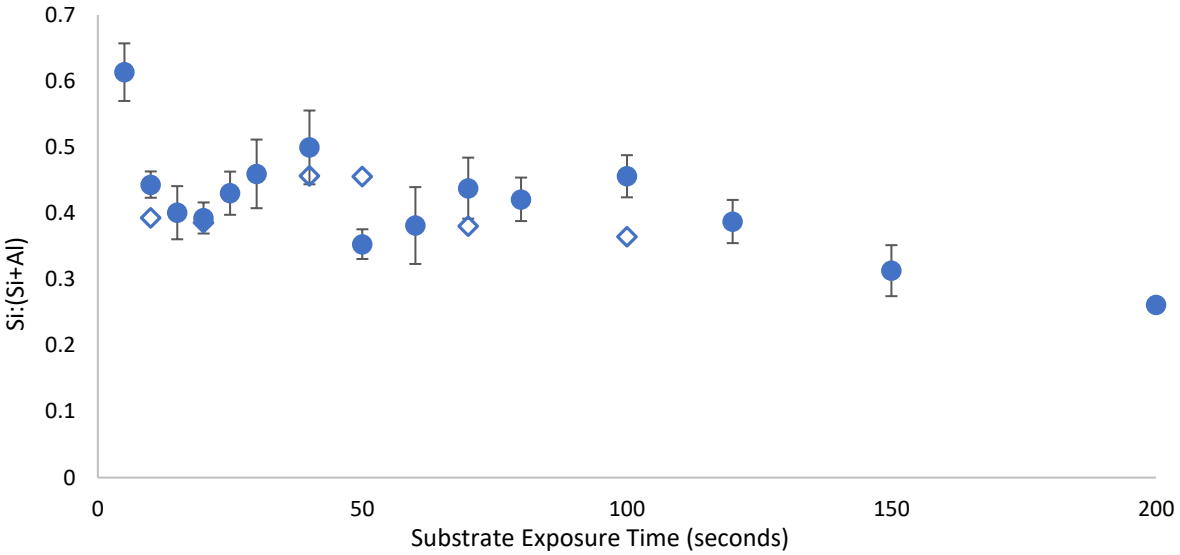

Figure 3.4: The time dependent adsorption profile of 1% v/v PTMS in aqueous solvent on sandpaper abraded aluminium foil substrate (filled circles) and 1 µm diamond paste polished substrates (open diamonds) after solution was 'hydrolysed' for 1 hour. Each data point represents the average of three replicates and the error quoted as the standard deviation.

Upon the direct comparison of individual diamond paste polished substrate exposure times to those polished with sandpaper, surface roughness appears to have no significant influence on surface coverage, indicating that the amount of silane on the surface is irrespective of any potential difference in surface energy and does not result in an increase or decrease in PTMS growth on the surface roughness scale measured.

As the impact of surface roughness on the adsorption profile measured using XPS was deemed insignificant, PTMS samples in all subsequent investigations were polished using 1 µm diamond paste. This decision was made as samples were to be subsequently imaged using SEM and the elemental composition of the surface mapped using AES. Flatter substrates would result in the improved visibility of silane film islands and interesting surface characteristics directly related to silane film formation and not substrate surface roughness. As described in section 2.2.1, 1 µm diamond paste was used to remove potential contaminants on the surface, enable the formation of a new oxide layer and create reproducible surfaces for silane condensation. The height of these oxide layers is profiled in Chapter 6 and found to be consistent and reproducible.

3.2.2 The effect of PTMS hydrolysis time

As mentioned in Section 1.4, the deliberate choice of pH 3 in aqueous solvent creates an environment where condensation is the rate limiting step[18]. Despite this, Si-OH groups formed as a result of the hydrolysis reaction are highly reactive with one another, and condensation can occur before the all Si-OCH_3 groups have been hydrolysed to Si-OH groups. It is for this reason that the choice of hydrolysis time must be deliberate and based on the specific experimental conditions used. Despite Industrial procedures commonly allowing

for hydrolysis times ranging from 1 to 48 hours, the point of dissolution for 1%v/v PTMS aqueous solvent was observed to be less than one minute. Reducing the amount of time between initiation of the hydrolysis reaction and the exposure of substrates to solution allows for a determination of hydrolysis and condensation reaction rates as well as the effect of oligomerisation on the oscillatory growth. As shown earlier in Figure 3.3, the number of condensation products both on a hydroxylated surface and in solution is extensive. To investigate the proposed surface mechanism, the effect of oligomerisation in solution prior to substrate exposure was examined. This was achieved by submerging all substrates in aqueous solvent following pre-treatment. While stirring, silane was introduced to the solvent containing substrates and substrates removed sequentially following the desired exposure time, resulting in exposure times which include exposure of substrates to unhydrolysed silane. The initiation of hydrolysis upon exposure to Al substrates, referred to *no hydrolysis time* allowed for the determination of reaction rate relating to film formation and gave an insight into the role of oligomerisation on the oscillatory growth mechanism.

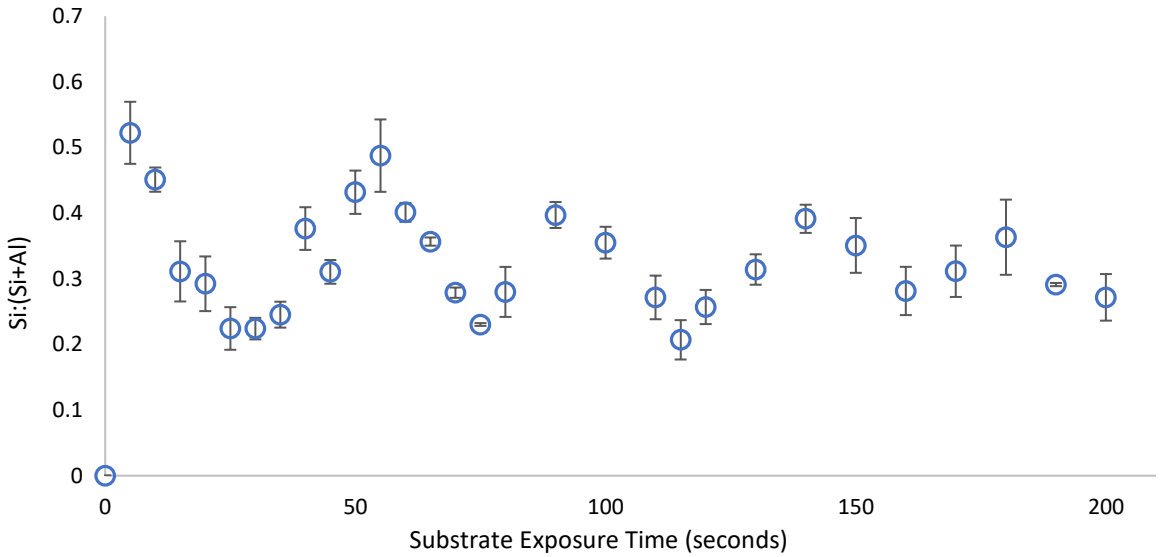

Figure 3.5: The time dependent adsorption profile of 1% v/v PTMS in aqueous solvent when exposed to 1 µm diamond paste polished aluminium foil substrates following the simultaneous initiation of the hydrolysis reaction and substrate exposure (no hydrolysis time). Each data point represents the average of three replicates with the error quoted as the standard deviation.

The presence of silane on the substrate after just 5 seconds of PTMS exposure to the aqueous solvent and aluminium substrates reveals the rate of reaction in this case to be extremely fast. The time taken for PTMS molecules to disperse throughout the aqueous solvent, hydrolyse and condense on the substrate falls between 0 and 5 seconds. While under optimum conditions hydrolysis can occur quickly[18] with hydrolysis of PTMS shown to occur in less than 20 seconds at 0.75%v/v in pH 3 aqueous solvent[23,43,45,156], this short hydrolysis time is in direct contrast to the methods of silane film formation commonly used in the commercial manufacturing of silane films where hydrolysis times can be as long as 48 hours.

The initial oscillation for both 1-hour and no hydrolysis time PTMS solution derived films follow the same path with an initial peak at 5 seconds and trough at approximately 20 seconds. However, a decrease in hydrolysis time and thus a decrease in the extent of oligomerisation in solution prior to substrate exposure increases the rate of oscillatory behaviour overall. A direct comparison of adsorption profiles for 1-hour and no hydrolysis data sets reveal an increase in the number of oscillations present over the 200 seconds measured. During the early stages of hydrolysis and condensation, prominent formations of silane molecules in solution include monomer, dimer and trimer units. The presence of this oscillatory behaviour during the early stages of film growth suggests the desorption of silanol species and involves both small and large oligomerised PTMS species, while the presence of smaller silane molecules increases the rate of oscillation. This increase in oscillatory rate may be the direct result of an increased mobility of smaller molecules both in solution and on the surface. Limiting the extent of oligomerisation through a reduction in hydrolysis time also affects the amount of silane on the surface resulting in a 15% decrease in the observed coverage of the initial adsorption peak, presumably due to the reduction initial concentration of hydrolysed silane at the moment of sample insertion into the solution, but the rate of formation stable.

3.3 The Adsorption Profile of Propylmethyldimethoxysilane Films

In the case of PTMS films shown above, oligomerisation was limited by reducing hydrolysis time however, oligomerisation can also be reduced by limiting the number of condensation reactions possible and thus the complexity of oligomerised products. To further probe the nature of fundamental interactions involved in the oscillatory adsorption behaviour, the number of hydrolysable methoxy groups was reduced from the three present in PTMS, to two in Propylmethyldimethoxysilane (PMDMS)[48].

Although the exploitation of mono-functional silanes to produce monolayer films and the use of tri-functional silanes to produce multilayer films[157-159], along with a connection between an increase in steric hindrance due to the bulkiness of alkoxy groups shown to increase steric repulsion of water and decrease the rate of hydrolysis[100] has been established in the literature, the effect of reducing the number of hydrolysable groups on the oscillatory adsorption profile of organosilanes has not been investigated previously.

As with PTMS film preparation, the adsorption profile of PMDMS was initially created under conditions geared towards industrial relevance with substrates sandpaper abraded and a 1-hour hydrolysis time given prior to substrate exposure. If the mechanism of oscillatory growth is directly tied to the ability of silane molecules to oligomerise as predicted from the adsorption profiles of PTMS, the time dependent adsorption profile of PMDMS should also contain this oscillatory behaviour, while increasing the rate of oscillation and reducing the amount of silane on the surface.

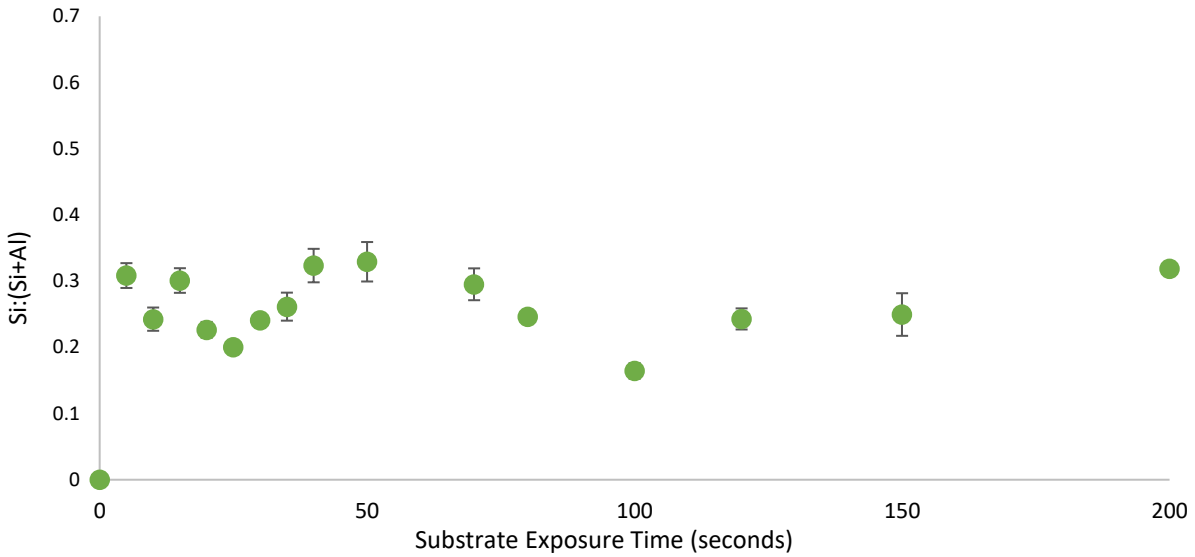

Figure 3.6: The time dependent adsorption profile of 1% v/v PMDMS in aqueous solvent on sandpaper polished aluminium foil substrates following a 1-hour hydrolysis time. Each data point represents the average of three replicates and with error quoted as the standard deviation[48].

As predicted, the time dependent adsorption profile of PMDMS contains multiple oscillations similar to those observed for PTMS in Figure 3.2. As PMDMS molecules are able to condense to one another both in solution and on the substrate, water molecules can become trapped underneath the film, forcing the dynamic equilibrium of the condensation reaction to the right and the subsequent desorption of PMDMS molecules from the surface. A direct comparison of PTMS and PMDMS adsorption profiles produced under the same experimental conditions reveal that the rate of oscillation during the first 200 seconds of film self-assembly are drastically different.

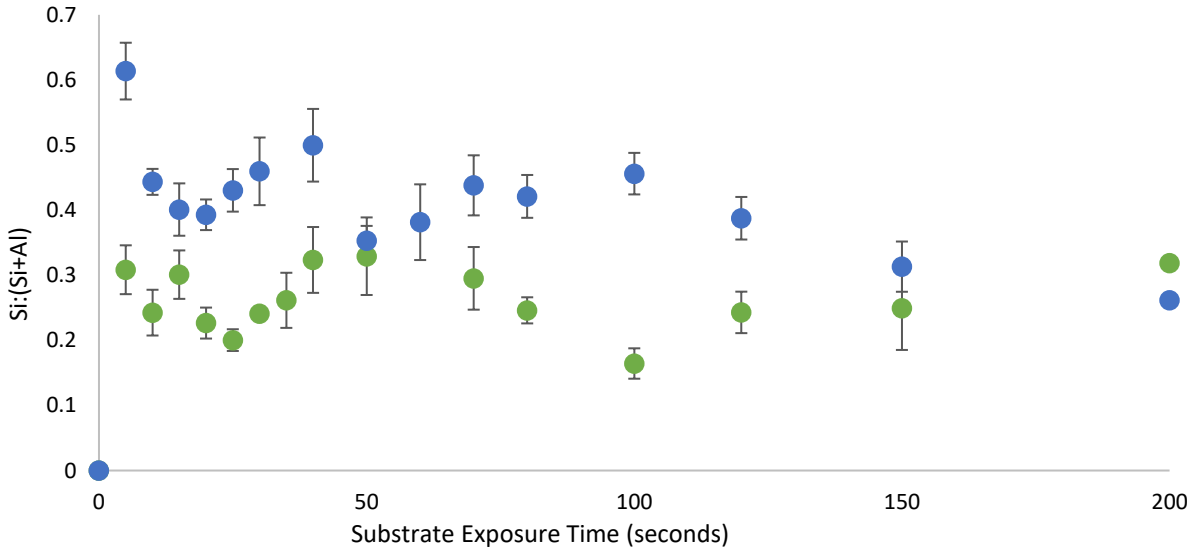

Figure 3.7: Direct comparison of 1%v/v PTMS (blue) and 1%v/v PMDMS (green) adsorption profiles on sandpaper polished Al foil substrates following a 1-hour hydrolysis in aqueous solvent. Each data point represents the average of three replicated and the error quoted as the standard deviation.

The initial adsorption peak of both PTMS and PMDMS sit at 5 seconds however, the two oscillations quickly become out of phase with one another. This combined with consistently lower Si:(Si+Al) values for PMDMS surface coverage compared to those of PTMS indicates an increased rate of PTMS oligomerisation. The amount of silane on the surface differs between PTMS and PMDMS adsorption profiles with the maxima of PTMS adsorption at a Si:(Si+Al) value of 0.61 and minima of 0.35 while the maxima and minima of PMDMS adsorption lies at 0.33 and 0.16 respectively. As shown in Figure 3.3, the presence of a single, large oligomer will have a significantly greater impact on the measured silane surface coverage when compared to that of a single monomer unit. This is consistent with the reduction in surface coverage observed for PTMS films upon the reduction in hydrolysis time and is most likely due to the accessibility of hydrolysed groups on oligomerised molecules to other hydrolysed silane molecules and the hydroxylated substrate, not only reducing the complexity of products possible but also the probability of successful condensation.

Much like reducing oligomerisation through reducing hydrolysis time, a reduction in the number of hydrolysable groups both increases the rate of oscillation indicating an increased mobility of smaller molecules on the surface and decreases the amount of silane on the surface as the complexity of condensation products is reduced.

3.3.1 The effect of PMDMS hydrolysis time

Thus far, oligomerisation has been limited by reducing both hydrolysis time and the number of hydrolysable species within the silane molecule. While reducing the rate of PTMS oligomerisation did not impact the rate at which silane molecules first appear on the surface following exposure to the hydroxylated substrate, in order to determine if reducing oligomerisation further by reducing both the number of hydrolysable groups and hydrolysis time, reduces the rate of reaction such that the rate of hydrolysis and thus initial condensation is impacted, the hydrolysis time of PMDMS was reduced, the results of which are shown in Figure 3.8 below.

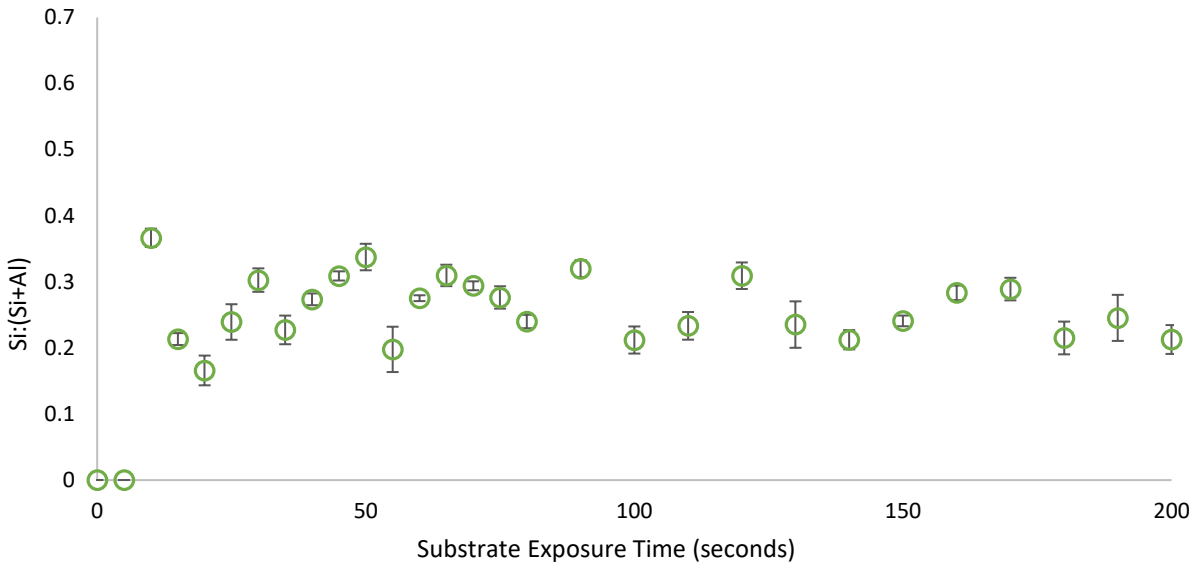

Figure 3.8: The time dependent adsorption profile of 1%v/v PMDMS in aqueous solvent when exposed to 1 µm diamond paste polished aluminium foil substrates following the simultaneous initiation of the hydrolysis reaction and substrate exposure (no hydrolysis time). Each data point represents the average of three replicates with the error quoted as the standard deviation.

While the presence of an oscillation during all stages of PMDMS film self-assembly indicates once again that this behaviour is due to both smaller (monomer, dimer, trimer...) silane molecules during the initial stages of growth as well as larger oligomers during the later stages, the rate of self-assembly has been reduced such that the first adsorption peak occurs at 10 seconds (Figure 3.8). The time required for PMDMS molecules to disperse throughout the aqueous solvent, become hydrolysed and successfully condense onto the aluminium substrate is increased up on that of PTMS. While it has been established by Chambers *et.al*[100] that an increase in alkyl group bulkiness decreases the rate of hydrolysis due to increased water repulsion, an -OCH_3 group in PTMS is replaced with a CH_3 group in PMDMS, and thus the bulkiness of alkyl groups in the molecule overall does not increase.

If this increase in initial self-assembly time were simply a result of the step-wise hydrolysis of silane molecules, the rate of PTMS adsorption and oscillation would be slower than that of PMDMS as it takes longer to hydrolyse 3 methoxy groups compared to just two. As this not the case, it is likely that this decrease is a result of a reduction in the number of possible interactions and thus a reduction in the rate of successful condensation reactions in the surface. A similar conclusion was drawn by Waddell *et al.*[160] who determined that the solvolysis rate is reflective of an increase in the number of covalent bonds to the surface and to neighbouring silane molecules. In the case of a PMDMS film created following a 1-hour hydrolysis time shown in Figure 3.6, PMDMS molecules have already become hydrolysed and condensed to one another in solution, and thus are immediately available for condensation to the surface resulting in an initial adsorption peak at 5 seconds. This decrease in rate may be due to the decrease in the number of sites able to undergo condensation. Once the condensation reaction begins and silane appears on the surface, the rate of

oscillation is faster than that of PTMS, with both PTMS and PMDMS contain 4 oscillations after the initial peak in surface coverage within the first 200 seconds of film self-assembly. However, as PMDMS appears on the surface later than PTMS, it can be said that the rate of oscillation is faster. This once again points towards an increased mobility of smaller molecules both in solution and on the surface, resulting in an increased rate of collective adsorption and desorption. The amount of PMDMS on the surface following a reduction in the hydrolysis time is slightly lower than that of PMDMS films produced following a 1-hour hydrolysis time, following the trend observed for PTMS and remains consistent with a decrease in the potential of PMDMS to condense to the substrate and restricted growth through oligomerisation to other PMDMS molecules.

The oscillation in adsorption of PMDMS appears more irregular and erratic than PTMS films prepared under the same conditions. It may be that the oscillatory rate is increased such that it cannot be as clearly defined at 5 second sampling intervals. Unfortunately, increasing sampling rate significantly decreases the accuracy of the individual time points, increasing the error of the x-axis unreasonably. This has been identified as a current limitation of this sampling method. However, an oscillatory behaviour is still present within 1 standard deviation of three replicates (y-axis error) and thus an oscillation is still reported here.

3.4 The Adsorption Profile of Propyldimethylmethoxysilane Films

While a reduction in the number of hydrolysable groups has increased the rate of oscillation and decreased the amount of silane observed on the surface, oscillations have been observed for both PTMS and PMDMS, both molecules which possess the ability to oligomerise. Further reduction in the number of hydrolysable groups to just 1 in Propyldimethylmethoxysilane (PDMMS), not only decreases the probability of successful oligomerisation, but more importantly eliminates the ability to oligomerise. The number of possible condensation products is decreased to just two; condensation to the surface via a single Si-O-Metal bond or the condensation of two PDMMS molecules in solution creating dimers, rendering the molecule inert as shown in Figure 3.9[48].

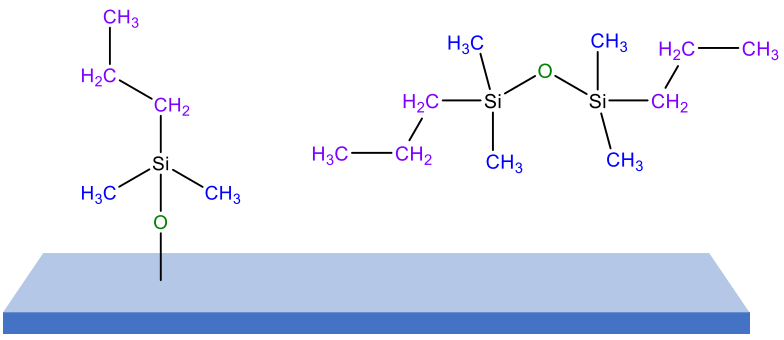

Figure 3.9: The two possible condensation products for the mono-functional silane PDMMS. First, the adsorption to a hydroxylated surface (left) and the second, formation of dimers in solution (right).

To confirm the role of silane oligomerisation in the oscillatory behaviour of Organosilanes, the time dependent adsorption profile of PDMMS was measured. If the oscillatory mechanism of silane-substrate condensation is dependent on the ability of silane molecules to oligomerise as indicated by both PTMS and PMDMS, the time dependent adsorption profile of PDMMS should not contain an oscillatory behaviour. In order to remain consistent with films produced for PTMS and PMDMS designed to mimic industrial methods of film formation, PDMMS was initially allowed to hydrolyse in aqueous solvent for 1-hour. However, when exposed to an aluminium oxide substrate, no silane was recorded on the surface. It was determined that all PDMMS molecules had condensed to one another in solution, forming inert dimers which were unable to condense onto the substrate. As PDMMS molecules cannot oligomerise to the point where the molecular weight becomes large enough to cause insolubility, the assumption of complete condensation was made solely on the absence of condensed silane on the substrate. The point of dissolution for a 1% v/v PDMMS in aqueous solvent was observed to be less than a minute, from this it was determined that in order to create a solution in which the PDMMS molecules have not completely dimerised, the solution was allowed to hydrolyse for just one minute before exposure to the Al_2O_3 substrate.

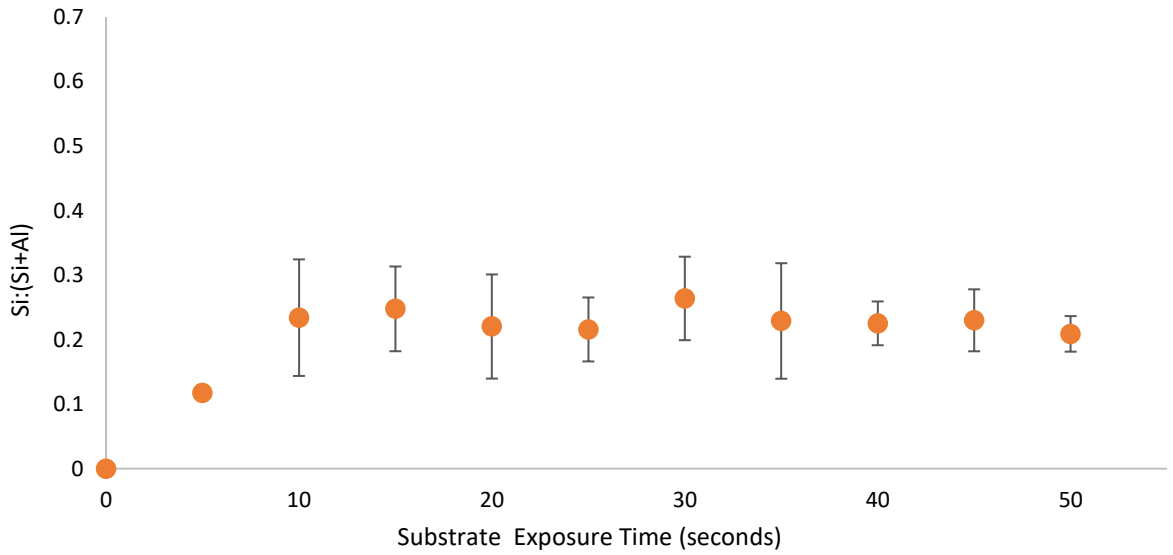

Figure 3.10: The time dependent adsorption profile of 1% v/v PDMMS in aqueous solvent on sandpaper polished aluminium foil substrates following a one minute hydrolysis time. Each data point represents the average of three replicates and with error quoted as the standard deviation[48].

Similar to the initial adsorption of PTMS and PMDMS shown in Figure 3.2 and Figure 3.6 respectively, the presence of silane on the surface occurs after just 5 seconds of film growth, confirming the one minute hydrolysis time is sufficient in creating a solution whereby PDMMS monomers have become hydrolysed but have not yet completely dimerised[48].

While an absence of an oscillatory behaviour in the adsorption profile of PDMMS confirms the oscillatory behaviour observed for PTMS and PMDMS is dependent upon their ability to oligomerise, in the absence of

this ability the adsorption profile resembles that of a Langmuir-type growth mechanism. That is, silane molecules descend and condense onto the surface independent of one another until all available surface sights are occupied, creating a steep increase in the amount of silane on the surface followed by a plateau.

The condensation of PDMMS molecules sit in the same dynamic equilibrium as PTMS and PMDMS, and like PTMS and PMDMS, PDMMS can be affected by a shift in this equilibrium. For PDMMS a reversal of the dimerisation or silane-metal bond process will result in either two hydrolysed monomers that can then compete for adsorption once again or the creation of a PDMMS monomer unit and a free surface adsorption site. These PDMMS molecules and free adsorption sites remain equivalent to those present before condensation and are thus free to undergo the same reaction repeatedly. It is possible, however unlikely that this will occur as an increase in the local water concentration is difficult to obtain in a dynamic system and is only thought to occur in PTMS and PMDMS systems due to the entrapment of water beneath oligomerised islands of film, not probable in the condensation of PDMMS[48].

As PDMMS molecules can also form inert dimers in solution, the rate of dimer formation may also have an impact on the amount of silane on the surface. If the formation of dimers in solution is faster than the formation of Si-O-Metal bonds this may result in available surface sights remaining open.

3.4.1 The effect of PDMMS hydrolysis time

When comparing the silane surface-condensation rate of PMDMS to PTMS a reduction was observed, and it was suggested that this may be a result of a reduction in the number of possible interactions and thus a reduction in the rate of successful condensation on the surface. In order to determine if the time required for PDMMS molecules to disperse throughout the solvent solution, become hydrolysed and successfully condense onto the aluminium substrate is increased up on that of PMDMS, conforming to the trend observed when comparing PTMS to PMDMS above, the adsorption profile of PDMMS with no hydrolysis time was measured and is shown in Figure 3.11.

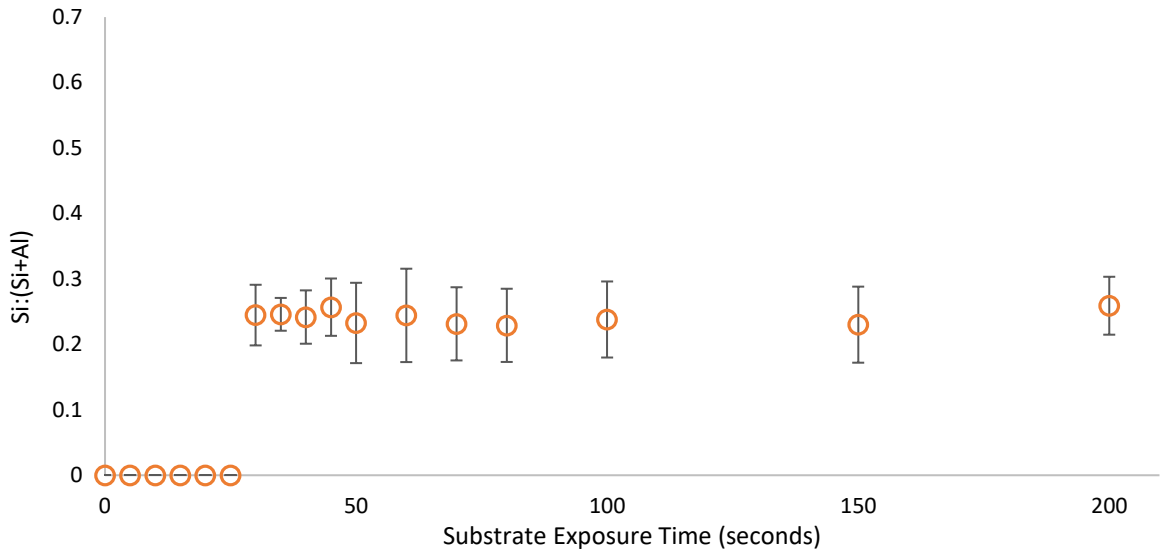

Figure 3.11: The time dependent adsorption profile of 1% PDMMS in aqueous solvent when exposed to 1 µm diamond paste polished aluminium foil substrates following the simultaneous initiation of the hydrolysis reaction and substrate exposure (no hydrolysis time). Each data point represents the average of three replicates with the error quoted as the standard deviation.

The time required between exposure of PDMMS to aqueous solvent and the first appearance of silane condensed onto a substrate is increased once again upon a reduction in the number of hydrolysable groups. This is a logical progression of a trend established between PTMS and PMDMS as the presence of just one hydrolysable group significantly decreases the probability of a successful condensation reaction occurring. While this appears to contradict the idea presented above that smaller molecules possess an increased mobility in solution and on the surface, the speed of initial condensation appears to be dominated by the potential to have a successful interaction with a free adsorption site. As it is impossible for oligomers of PDMMS to form, it cannot be confirmed whether the rate of reaction would slow with increasing silane size. However, this trend has been observed for both PTMS and PMDMS with the initial rate of condensation dominated by the potential for successful interactions and the subsequent rate of oscillation dominated by the continued growth of these molecules.

As expected, the surface coverage of PDMMS is slightly lower than PMDMS and significantly lower than PTMS at a Si:(Si+Al) value of just 0.25 on average. This remains consistent with the reduction in surface coverage as a result of a reduction in oligomerisation observed above. If we assume the amount of PDMMS on the surface following exposure to a solution containing no PDMMS dimers sits at approximately 0.25 as shown in Figure 3.11, it can be said that the surface coverage of both PMDMS and PTMS which reach well above this value is due to the formation of a multilayer system enabled by oligomerisation. The rate of PDMMS dimer formation, which prevented the condensation of silane on the surface following a 1-hour hydrolysis time was thought to have an impact on the maximum surface coverage value obtainable for PDMMS. However, the comparison of Si:(Si+Al) maxima of one minute hydrolysis in Figure 3.10 and no hydrolysis in Figure 3.11 does

not change, indicating that dimerisation of PDMMS does not have an impact on the maximum surface coverage obtainable for PDMMS on the scale measured. Factors influencing the maximum surface coverage of PDMMS possible and its predicted value for an idealised system is discussed further in Chapter 4.

A link has been successfully made between the time dependant oscillatory surface coverage of silane films and the presence of more than one hydrolysable group on the central silicon atom. This along with the absence of such behaviour for silanes which contain just one hydrolysable group and follow a time dependant Langmuir-type growth profile indicate that the origin of this behaviour lies with the ability of silanes to oligomerise both in solution and on the surface.

4 Modelling Organosilane Adsorption Profiles

While the presence of multiple oscillations for both PTMS and PMDMS have been shown experimentally in Chapter 3, in order to determine the influence of individual components in the film, their associated rate constants and to predict future oscillatory behaviour the following mathematical model is proposed.

This chapter details the fit of experimental data shown in Chapter 3 to a 2-component for Langmuir growth and the creation of a multi-component mathematical model which extends upon the 3-component model originally proposed by Quinton[23,38,41] and requires the addition of a further 2 unique components per oscillation observed.

In chapter 3, the rate of silane film self-assembly was attributed to three different factors. Firstly, the initial rate of condensation was linked to the rate of hydrolysis and the probability of successful condensation interactions. Secondly, the rate of oscillation itself was linked to the ability of silane oligomers to continue to grow both in solution and on the surface and lastly, a difference in the rate of Si-O-Si (oligomerisation) and Si-O-Metal (film) bonds was established. However, in order to create an oscillation an increase in the concentration of water molecules is required to shift the dynamic equilibrium and cause desorption. Therefore, the rate at which water molecules cause this desorption will greatly impact both the rate of oscillation and the maximum surface coverage of silane films attainable. The concept of modelling this oscillatory behaviour was first introduced by Quinton *et al.*[23,38,41] and began with the concept of a 2-component model based on Langmuir kinetics and extended to a 3-component model in order to create a single oscillation in surface coverage and enable the determination of rate constants for the PTMS oscillation observed experimentally. Components considered in these models were limited to silane and water molecules and did not take into account the rate of initial condensation or intermolecular interactions as this would result in a second order equation, which could not be solved numerically. In order to determine the rate constants for the both the adsorption profiles shown experimentally in chapter 3, PDMMS data was first fit to the 2-component model.

4.1 The Langmuir adsorption of PDMMS – Fit to a 2-component model

A 2-component model was created to fit the 1st order kinetic model of Langmuir film growth, explained in detail in section 1.8, necessary as a starting point in order to explain the non-equilibrium adsorption for the time dependant oscillation of PTMS. Langmuir growth, the simplest adsorption mechanism involves the initial descent of hydrolysed silane molecules (Si-OH) onto the surface until all the free surface sites are occupied[22] in order to create a monolayer on the surface[161]. This 2-component Langmuir model proposed by Quinton[23,38,41] differs from the original Langmuir adsorption isotherm derived under equilibrium conditions as the condition of equilibrium has been removed, a necessary step to describe the kinetic behaviour of adsorbate behaviour. In the 2-component model, this initial adsorption of molecules onto the hydroxylated substrate (M-OH) occurs via a hydrogen bond, and the resulting species labelled as θ_1. Hydrogen bound species are then converted to covalently bound Si-O-Metal species and labelled as θ_2. Therefore, components 1 and 2 can represent the same silane molecule, with the distinction solely on the method of bonding however, mathematically they are defined as unique components. This simple representation of adsorption where substrate-adsorbate interactions are dependent on the concentration of metal-OH bonds enables the following first order kinetic equation to be used[41];

$$\frac{d\,[\mathrm{Si-O-M}]}{dt} = k[\mathrm{Si-OH}][\mathrm{M-OH}]$$

Equation 4.1

Where the rate of silane-metal (Si-O-M) bond formation is dependent on the number of hydrolysed silane molecules, (Si-OH) and free substrate adsorption sites (Metal-OH). A pictorial representation focused on θ_1 to θ_2 conversion of PDMMS shown below;

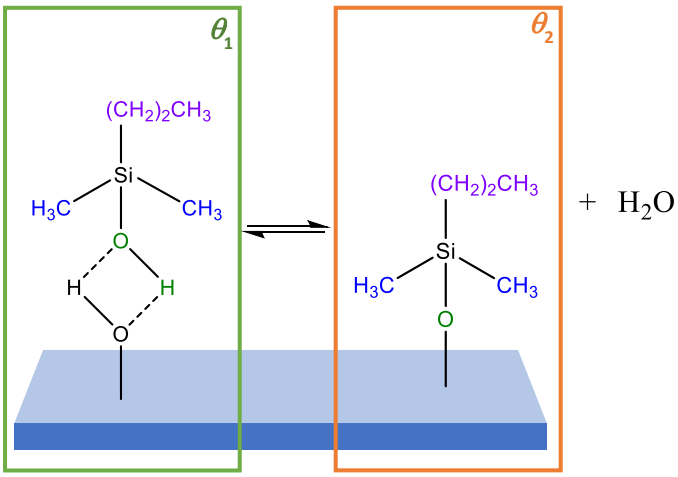

Figure 4.1: The conversion of hydrogen bound θ_1 represented by a PDMMS monomer (green) to θ_2, a covalently bound PDMMS monomer (orange) in the 2-component model.

In the case of the hydrogen bound θ_1 and the covalently bound θ_2, both species contain silane, and therefore the sum of the two result in a Langmuir adsorption curve.

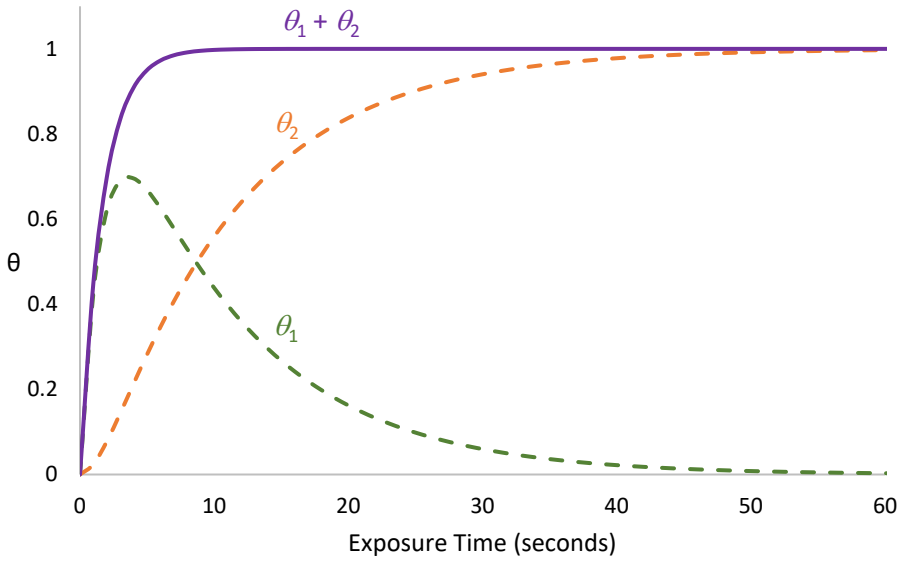

Figure 4.2: The conversion of physisorbed θ_1 (green) to covalently bound θ_2 (orange) in the 2-component model as a function of time, with the sum of θ_1 and θ_2 resulting in a Langmuir adsorption curve (purple). Adapted from Quinton[23,38,41].

The kinetics of species θ_1 have been described as being dependant on both the number of free surface adsorption sites (1-θ) and the subsequent displacement of θ_1 by species, θ_2 via the following equation[38];

$$\frac{d\theta_1}{dt} = k_1(1-\theta) - k_2\theta_1$$

Equation 4.2

Consequently, the formation of species θ_2 is dependent on the number of θ_1 species available to displace and can be described by[38];

$$\frac{d\theta_2}{dt} = k_2\theta_1$$

Equation 4.3

In order to solve θ_2 and θ_2 and the rate constants, k_1 and k_2 must be placed into the following matrix and solved[38];

$$\begin{bmatrix}\theta_1\\ \theta_2\end{bmatrix} = \begin{bmatrix}-k_1-k_2 & -k_1\\ k_2 & 0\end{bmatrix}\begin{bmatrix}\theta_1\\ \theta_2\end{bmatrix} + \begin{bmatrix}k_1\\ 0\end{bmatrix}$$

Equation 4.4

This matrix shown above was used to solve the two first order differential equations analytically (which were subsequently simplified) and an equation given for species the time dependence of θ_1 and θ_2;

$$\theta_1 = \frac{1}{2\sqrt{{k_1}^2 - 6k_1k_2 + {k_2}^2}} e^{-\frac{1}{2}\left(k_1-k_2+\sqrt{k_1-6k1k_1+{k_2}^2}\right)t}$$

$$\left(\left(\left(-1+e^{\sqrt{{k_1}^2-6k_1k_2+{k_2}^2}t}\right)k_2 + \left(1+e^{\sqrt{{k_1}^2-6k1k_2+{k_2}^2}t}\right)\sqrt{{k_1}^2-6k_1k_2+{k_2}^2}\right)A - \left(-1+e^{\sqrt{{k_1}^2-6k_1k_2+{k_2}^2}t}\right)k_1(A+2B)\right)$$

Equation 4.5

$$\theta_2 = \frac{1}{2\sqrt{{k_1}^2-6k_1k_2+{k_2}^2}} e^{-\frac{1}{2}\left(-k_1+k_2+\sqrt{{k_1}^2-6k_1k_2+{k_2}^2}\right)t}\left(2e^{\frac{1}{2}\left(-k_1+k_2+\sqrt{{k_1}^2-6k_1k_2+{k_2}^2}\right)t}\sqrt{{k_1}^2-6k_1k_2+{k_2}^2}\right.$$
$$+ e^{\left(-k_1+k_2+\sqrt{{k_1}^2-6k1k_2+{k_2}^2}\right)t}\left(k_2(2A-B)+\left(k_1+\sqrt{{k_1}^2-6k_1k_2+{k_2}^2}\right)B\right)$$
$$\left.+ e^{(-k_1+k_2)t}\left(\left(-k_1+\sqrt{{k_1}^2-6k_1k_2+{k_2}^2}\right)B + k_2(-2A+B)\right)\right)$$

Equation 4.6

Solving for A and B results in two simultaneous equations;

$$A = \frac{1}{\left(\frac{k_1}{k_2} - 1\right)}$$

Equation 4.7

And

$$B = \frac{k_1}{k_2}\left(\frac{1}{\left(\frac{k_1}{k_2} - 1\right)}\right)$$

Equation 4.8

Previously, once solved, arbitrary values of k_1 and k_2 were chosen and the system plotted. However, as shown in Figure 3.10 and Figure 3.11 the adsorption of PDMMS follows a Langmuir-type adsorption profile. This generalised 2-component model can be applied to the mechanism of film growth for the mono-methoxy, PDMMS as the number of interactions are limited to a single silane-surface condensation or a single silane-silane condensation. Upon silane exposure, the water activated hydrolysis reaction is initiated and Si-O-R groups converted to Si-OH silanol species[1]. The presence of OH species in both the silanol molecule and the hydroxylated surface promote the formation of hydrogen bonds, creating θ_1. The conversion of hydrogen bound θ_1 to covalently bound θ_2 occurs via a condensation reaction. While θ_1 can be displaced by a water molecule in solution via the same mechanism proposed for PTMS and PMDMS displacement in Chapter 3 it can only be replaced by an equivalent PDMMS molecule classified mathematically as the same component.

In order to determine the rate constants, k_1 and k_2 for formation of PDMMS film self-assembly, the 2-component model was fit to the adsorption profile of PDMMS. An obvious issue when fitting the 2-component model is that the equilibrium coverage predicted by the model to be 1 however, the average value obtained experimentally is just 0.25. The intensity ratio of Si:(Si+Al) represents surface coverage, not physical coverage and as such, it is unreasonable to expect the value of surface coverage obtained experimentally to reach 1 as this is the value predicted by the ideal system of Langmuir adsorption detailed in section 1.5.1, where an ideal gas adsorbs onto an idealised surface. In reality, neither the substrate or PDMMS molecules adhere to this idealised standard. The Al_2O_3 surface is not atomically flat, nor does it contain a complete layer of evenly dispersed -OH adsorption sites, while PDMMS intermolecular interactions and inability to obey ideal gas laws, preclude it from this definition. Even in an idealised system, it is impossible for the maximum value of surface coverage for PDMMS to reach 1 due to the way in which surface coverage is measured. While the absence of an aluminium peak would in fact result in a Si:(Si+Al) value of 1, the attenuation length of aluminium is 2.37 nm[105], significantly larger than that of a silane molecule. Thus, even in the event of a complete monolayer PDMMS film, a Si:(Si+Al) value of 1 is unattainable.

As both θ_1 and θ_2 contain silane and are involved in the calculation of Si:(Si+Al) and θ_2 does not reach 1, the values obtained experimentally for PDMMS adsorption can be normalised to 1 without the need for scaling factors. Rate constants of 0.99 and 0.1 were determined for k_1 and k_2 respectively by completing a nonlinear regression on the experimental data previously normalised to 1 and shown in Figure 4.3.

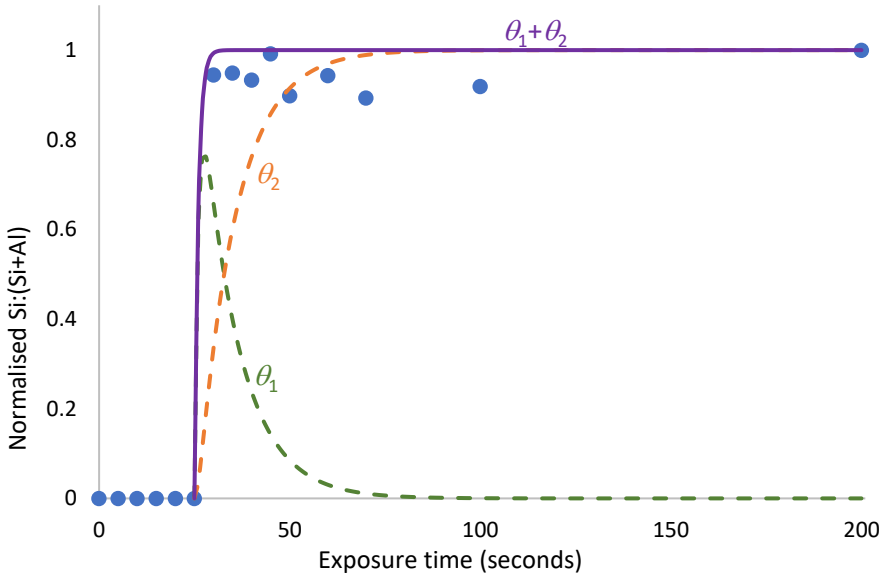

Figure 4.3: The Langmuir-type adsorption profile for the self-assembly of PDMMS as a function of exposure time fit to a 2-component model with rate constants of 0.99 for k_1 and 0.1 for k_2.

With respect to the formation of θ_1 on the surface, the rate of formation is defined as being directly related to the number of available surface adsorption sites and the displacement of θ_1 by θ_2 (Equation 4.2). It assumes that condensation occurs immediately upon the exposure of water to the system and does not take into account the time required for the formation of hydrolysed θ_1 species in solution. However, the adsorption profile of PDMMS revealed the dispersion, hydrolysis and initial condensation takes between 25 and 30 seconds. It is because of this that once the rate of θ_1 band θ_2 formation was fit to the experimental data, it must be offset to account for the initiation of θ_1 condensation

As the adsorption and desorption of silane species occurs continuously in a dynamic equilibrium, it is important to note that spontaneous desorption has been ignored in this model. Rate constants quoted represent the total adsorption rate of each silane species. The assumption of a collective adsorption behaviour initiated by the introduction of an aluminium oxide substrate to the silane solution, gives the kinetic rates context and validity.

4.2 The multiple oscillations of PTMS – Requirements of a 10-component model

The formation of a monolayer such as PDMMS requires a molecule which cannot act as a substrate for additional growth and as such the model used to explain PDMMS cannot be applied to PTMS or PMDMS and gives a very general description of chemisorption systems[22].

The ability of PTMS molecules to oligomerise in solution creates an ever-changing morphology of species in solution and on the surface. Much like the 2-component model used to describe the Langmuir growth of PDMMS mathematically, each oscillation requires a new set of species even if it is possible different components could represent the same molecule in solution. Following the creation of the 2-component model, it was used successfully as a platform for the addition of a third component based on displacement kinetics to describe a single oscillation in surface coverage[23,38,41].

A detailed description of the 3-component model has been given in section 1.8, and is represented by Figure 4.4;

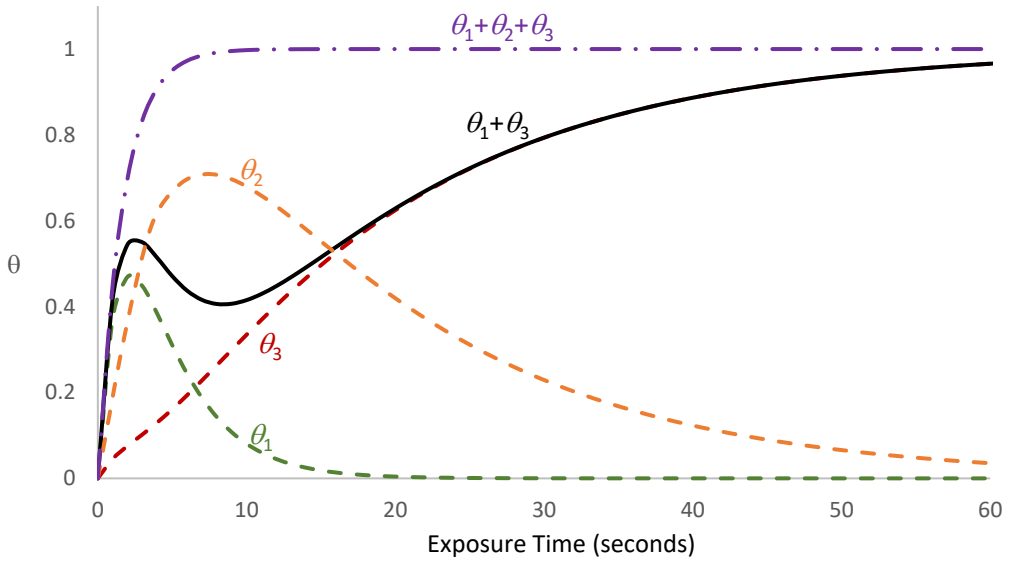

Figure 4.4: Silane surface coverage as a function of time for the 3-component model detaining the contribution of each component and the sum of silane containing components θ_1 and θ_3, resulting in a single oscillation in surface coverage. Adapted from Quinton[23,38,41].

Where the rapid adsorption of silane species onto the substrate (θ_1) results in the initial increase in surface coverage observed. As the silane condensation reaction sits in a dynamic equilibrium, it is then proposed that an increase in water molecules causes a shift in the equilibrium causing desorption of silane molecules (θ_2). As the equilibrium attempts to rebalance, the adsorption of silane species on the surface occurs once again (θ_3). In the 3-component model, adsorption of (θ_3) resembles a Langmuir-type growth curve. Each of these mechanisms were given a unique rate constant, k_1, k_2 and k_3 respectfully. If it is assumed that all three species

in solution contain silane, the sum of θ_1, θ_2 and θ_3 results in an adsorption profile resembling Langmuir-type growth as shown by the purple line in Figure 4.4. If it is assumed that θ_2 does not contain silane and the sum of θ_1 and θ_3 are plot as a function of time, a single oscillation in surface coverage is observed as shown by the black line. Hence, the rate constants k_1 and k_3 represent the formation of Si-O-metal bonds, while k_2 is associated with the rate of Si-O-metal bond breakage[41].

However, the adsorption profile of 1%v/v PTMS in aqueous solvent originally presented in Figure 3.5 and reproduced below for ease of reference contains many more oscillations than the one described by the 3-component model. A logical extension of the 3-component model is required in order to account for the additional oscillations observed.

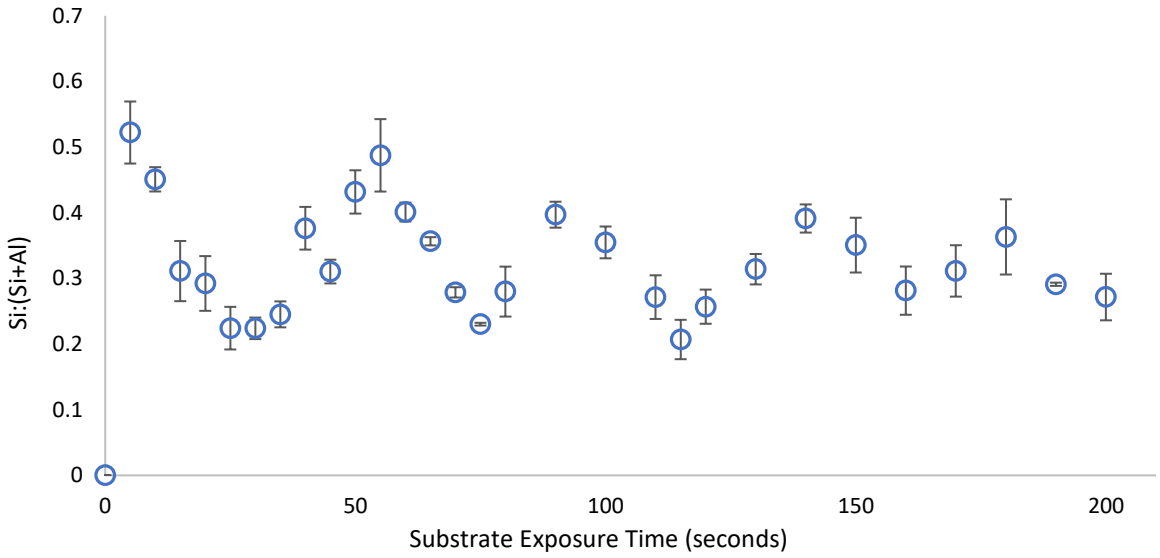

Figure 4.5: The time dependent adsorption profile of 1% v/v PTMS in aqueous solvent when exposed to 1 µm diamond paste polished aluminium foil substrates following the simultaneous initiation of the hydrolysis reaction and substrate exposure (no hydrolysis time). Each data point represents the average of three replicates with the error quoted as the standard deviation.

To extend upon and apply the current 3-component model to subsequent oscillations, additional components each with their own unique rate constants are required. For as long as the oscillatory behaviour continues, additional components can be added to the model to account for the adsorption and desorption of adsorbates. Displacement kinetics and the 3-component model were used in order to determine that ten unique components are required in order to fit the five oscillations observed for PTMS films in Figure 4.5. This resulted in the creation of the 10-component model given in Figure 4.6.

It is important to note that while it has been speculated θ_2 represents a water molecule in the 3-component model and is thus reasonable to extrapolate to the representation of water by all evenly numbered components in the system, with respect to the mathematical model all components are considered unique with the assignment of silicon or non-silicon containing species made possible only once the model has been

established and fit to the experimental data. This prevents biasing of the model and a forced fit to the experimental data.

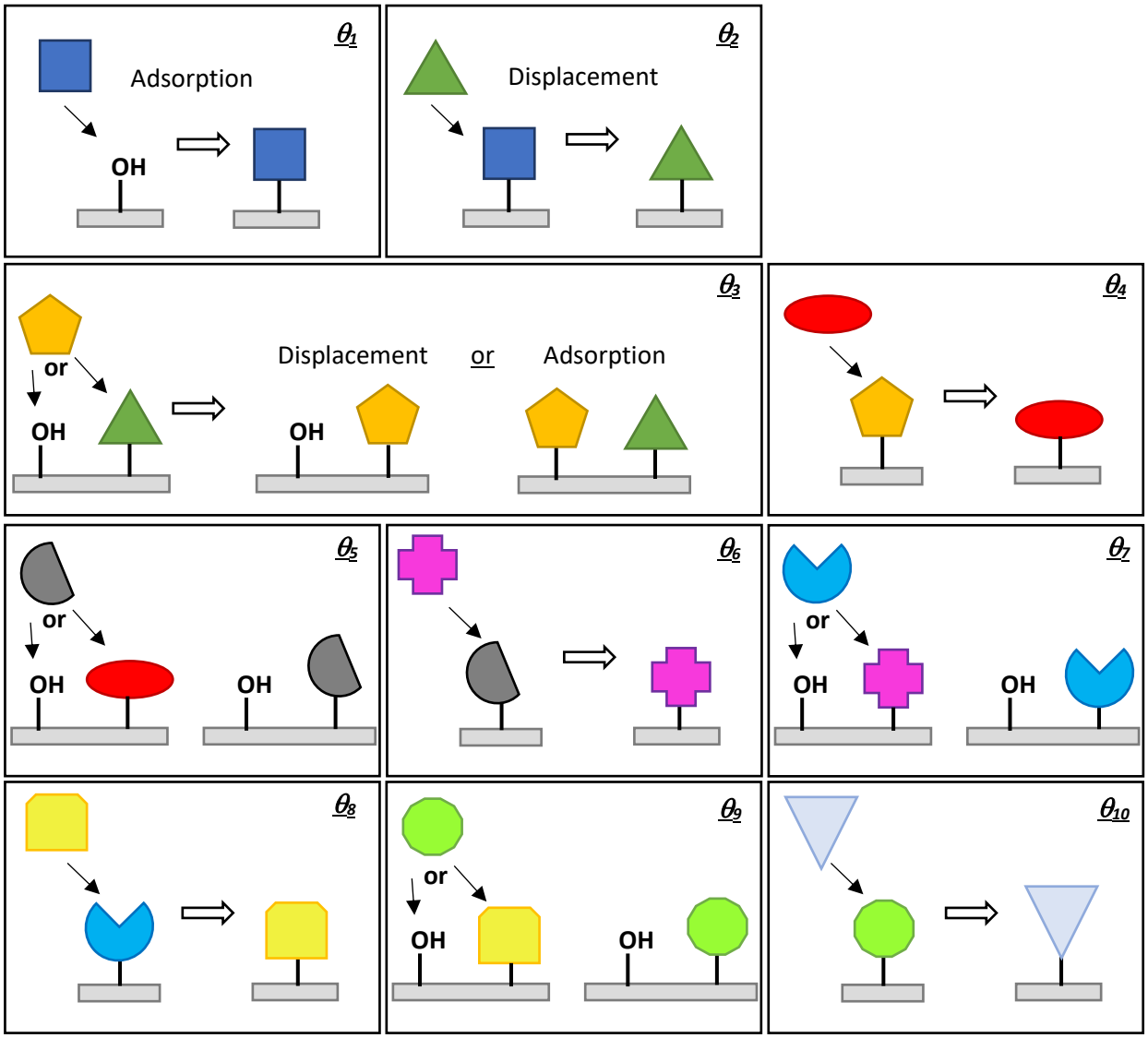

Figure 4.6: The 10-component model used to represent multiple oscillations in surface coverage observed for PTMS adsorption on metal oxide surfaces. In this model all components are considered equal.

The 10-component model proposed in Figure 4.6 describes the initial adsorption of an adsorbate, described as θ_1 onto a free surface adsorption site (-OH). This is followed by the displacement of the adsorbed species θ_1 by θ_2. The displacement of adsorbed species continues however, upon the descent of θ_3 towards the surface it has the option to either displace θ_2 or take a free adsorption site (OH).

Adsorption to an original free OH surface site or displacement of an OH surface site which has previously displaced a silane species is possible by any silane species in solution. As in practice these OH surface sites are equivalent, for simplification and ease of understanding, the model proposed in Figure 4.6 above demonstrates an example of displacement and adsorption to a free surface site in the products of θ_3 and then shows the product of displacement in every scenario that follows. It is also important to understand

that in reality the 10-component model is an oversimplification of the true interactions happening on the surface. The model does not take into account silane-silane interactions, nor does it account for spontaneous desorption as this would result in a second order equation, which cannot be solved numerically. Given the 10-component model an equation for the rate of adsorption for each component on the surface can be determined.

As with the 3-component model, the initial adsorption of θ_1 is dependent upon the number of free adsorption sites, which can be noted as (1- θ) where θ represents the species present in the system at that point in the oscillatory process such as θ_1+ θ_2+ θ_3+ θ_4… and so on. The rate of θ_1 is also dependent on the rate at which θ_1 is displaced by θ_2 and can be represented with the following equation[41];

$$\frac{d\theta_1}{dt} = k_1(1-\theta) - k_2\theta_1$$

Equation 4.9

With this in mind, based on displacement kinetics described in detail in Section 1.5.2 the rate of θ_2 is dependent on the number of θ_1 species in which it can displace and the rate at which it itself is displaced by θ_3 and given by[41];

$$\frac{d\theta_2}{dt} = k_2\theta_1 - k_3\theta_2$$

Equation 4.10

In the original 3-component model, the adsorption of θ_3 is dependent on the number of free adsorption sites and the number of θ_2 species present which it can displace. The rate of this adsorption is given by Equation 4.11[41] and results in the Langmuir-type adsorption curve for θ_3 observed in Figure 4.4.

$$\frac{d\theta_3}{dt} = k_3(1-\theta) + k_3\theta_2$$

Equation 4.11

As mentioned above, in order to account for continued oscillations and develop a model to fit the adsorption profile of PTMS observed in Figure 4.5 at least ten components are required and therefore Equation 4.11 must be reconsidered to account for the desorption of θ_3 by θ_4. As in Equation 4.11, the rate of θ_3 adsorption is dependent on the number of free adsorption sites and θ_2 species it can displace (which is subsequently dependent on the number of θ_1 species available for displacement hence the representation by (1-θ)), but is now also dependent on the rate at which it is displaced by θ_4 via;

$$\frac{d\theta_3}{dt} = k_3(1-\theta) - k_4\theta_3$$

Equation 4.12

The addition of a fourth component to the model comes in the form of θ_4 which is dependent on the number of θ_3 present for it to displace and the rate at which it is then displaced by θ_5 by;

$$\frac{d\theta_4}{dt} = k_4\theta_3 - k_5\theta_4$$

Equation 4.13

A pattern begins to emerge with the rate of evenly numbered species dependent on the number of species present in which it can displace and the rate at which it itself is displaced by subsequent species. Odd numbered species are dependent on the number of free adsorption sites (which includes sites previously displaced by evenly numbered species) and the rate at which they themselves are displaced by subsequent species. Given this, the rate of θ_5 formation is represented by;

$$\frac{d\theta_5}{dt} = k_5(1-\theta) - k_6\theta_5$$

Equation 4.14

This is followed by θ_6 whose rate of formation is given by;

$$\frac{d\theta_6}{dt} = k_6\theta_5 - k_7\theta_6$$

Equation 4.15

The rate of θ_7 is given by;

$$\frac{d\theta_7}{dt} = k_7(1-\theta) - k_8\theta_7$$

Equation 4.16

The rate of θ_8 by;

$$\frac{d\theta_8}{dt} = k_8\theta_7 - k_9\theta_8$$

Equation 4.17

Then the rate of θ_9 is given by;

$$\frac{d\theta_9}{dt} = k_9(1-\theta) - k_{10}\theta_9$$

Equation 4.18

And finally θ_{10} by;

$$\frac{d\theta_{10}}{dt} = k_{10}\theta_9 - k_{11}\theta_{10}$$

Equation 4.19

If this oscillatory behaviour were to continue, additional components would be required (2n for n oscillations), with corresponding individual rate constants. To fit the proposed 10-component model shown in Figure 4.6 to the experimental data and solve each of the corresponding rate constants, the series of rate equations above (Equation 4.9 to Equation 4.19) must be placed in the following matrix;

$$\begin{bmatrix} \theta1 \\ \theta2 \\ \theta3 \\ \theta4 \\ \theta5 \\ \theta6 \\ \theta7 \\ \theta8 \\ \theta9 \\ \theta10 \end{bmatrix} = \begin{bmatrix} -(k1+k2) & -k1 & -k1 & 0 & 0 & 0 & 0 & 0 & 0 & 0 \\ k2 & -k3 & 0 & 0 & 0 & 0 & 0 & 0 & 0 & 0 \\ -k3 & -k3 & -(k3+k4) & 0 & 0 & 0 & 0 & 0 & 0 & 0 \\ 0 & 0 & k4 & -k5 & 0 & 0 & 0 & 0 & 0 & 0 \\ -k5 & -k5 & -k5 & -k5 & -(k5+k6) & 0 & 0 & 0 & 0 & 0 \\ 0 & 0 & 0 & 0 & k6 & -k7 & 0 & 0 & 0 & 0 \\ -k7 & -k7 & -k7 & -k7 & -k7 & -k7 & -(k7+k8) & 0 & 0 & 0 \\ 0 & 0 & 0 & 0 & 0 & 0 & k8 & -k9 & 0 & 0 \\ -k9 & -k9 & -k9 & -k9 & -k9 & -k9 & -k9 & -k9 & -(k9+k10) & 0 \\ 0 & 0 & 0 & 0 & 0 & 0 & 0 & 0 & k10 & -k11 \end{bmatrix} \begin{bmatrix} \vartheta1 \\ \vartheta2 \\ \vartheta3 \\ \vartheta4 \\ \vartheta5 \\ \vartheta6 \\ \vartheta7 \\ \vartheta8 \\ \vartheta9 \\ \vartheta10 \end{bmatrix} + \begin{bmatrix} k1 \\ 0 \\ k3 \\ 0 \\ k5 \\ 0 \\ k7 \\ 0 \\ k9 \\ 0 \end{bmatrix}$$

Equation 4.20

This matrix can then be used to solve a series of first order differential equations, solved analytically and an equation given for species θ_1 through θ_{10}.

Once again spontaneous desorption of silane species is neglected, and the collective behaviour of silane species represented by each component to allow direct comparison of rate constants with experimentally observed oscillations (representing the net adsorption of each component). Solutions to the ten coupled differential equations shown in Equation 4.20 will result in the production of ten equations which can be solved linearly representing the general solution for the formation of θ_1 through θ_{10}. However, this is not simple, θ_1 is a combination of two exponential functions, θ_2 a combination 3 exponents and so on. The relationship between the coefficients and the rate constants would become apparent, enabling the simultaneous equations to be solved and by substituting the coefficients back into the adsorbate functions, the expression each rate co-efficient in terms of their rate constants will be achieved. With the help of scaling factors, these components can then be fit to the experimental data and the rate constants for each component determined. Unfortunately, this is beyond the computing power currently available. The intention is to secure access to this type of computing power in the near future and complete these calculations. However, all is not lost; based on the patterns observed in the 3-component model and the knowledge of desorption kinetics, a 10-component model can be predicted a plot as a function of time with arbitrary rate constants used.

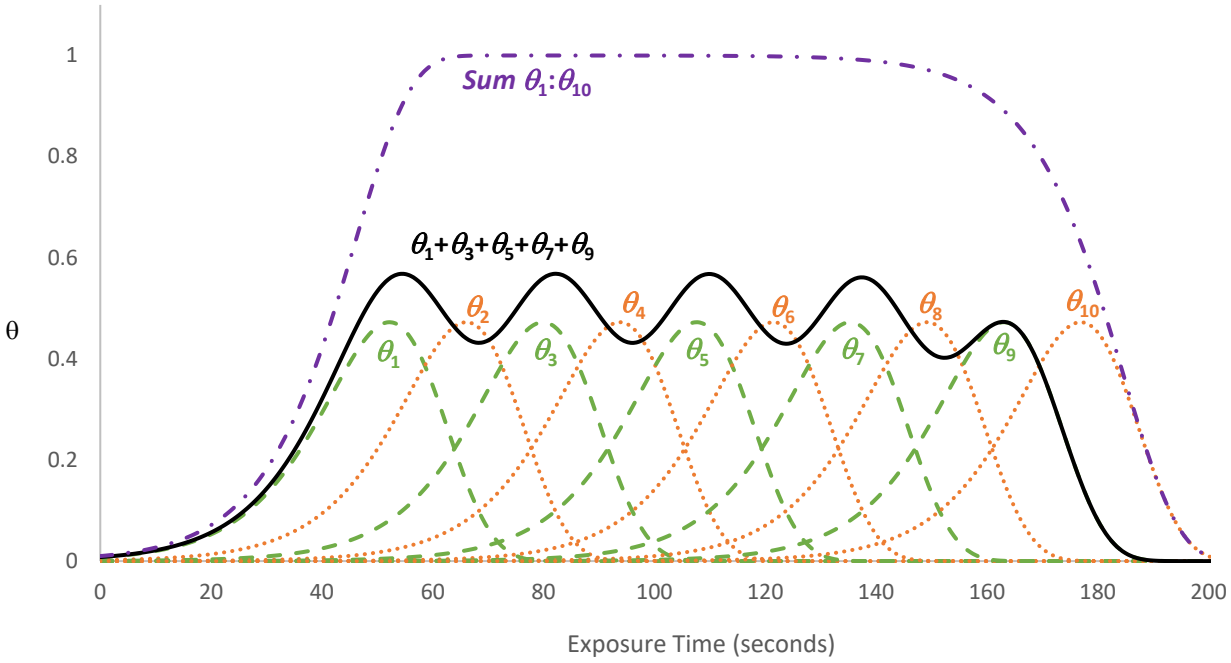

Figure 4.7: The 10-component model used to represent for multiple oscillations in surface coverage. The green lines represent odd numbered components and orange lines represent evenly numbered components, while the sum of odd numbered components is represented in black. The sum of all components is represented in purple.

Much like the 3-component model, the sum of all components (shown in purple) results in the Langmuir-type film growth observed for the 2-component model, indicating that not all species in the model contain silane. The sum of odd numbered components (shown in green) results in multiple oscillation similar to what is observed experimentally for the self-assembly of PTMS films in Figure 4.5. Not unlike the 3-component model, odd numbered components contain silane while evenly numbered components do not. Based on the condensation equilibrium reaction, it is logical to assign these components to water.

While in the 10-component model the sum of all components does follow the Langmuir-trend initially it decreases as the oscillations stop. This is simply a result of terminating the model at ten components, if these oscillations were to continue, the sum of all components would remain at 1. The surface coverage for silane containing components also decreases as the last component, θ_{10} is a non-silicon containing species. As described above, terminating the above model at ten components, results in the last species in the oscillation representing desorption by a non-silicon containing species, predicted to be water. When plot as a function of time as shown in Figure 4.7, the model indicates the complete removal of silane from the surface. This is easily remedied by the addition of an eleventh component however, due to the absence of experimental data to support either trend, the model the model was terminated at ten components.

In fact, the presentation of θ_{10} in the model above is not stickily representative of the experimental data presented. While there is evidence to support the adsorption of θ_{10}, there is no evidence to support its desorption. Once again, the decision was made to present the complete adsorption and desorption of θ_{10} as

it is likely that if the exposure timeline is extended the oscillation would continue requiring the further addition of components to the model.

Given the assignment of silane and water species based on the 10-component adsorption plot shown in Figure 4.7, the 10-component model has been reproduced to reflect this and clearly demonstrates the desorption of silane species (green, odd number components) by water molecules (orange, evenly number components) resulting in the creation of free OH adsorption sites available for silane re-adsorption.

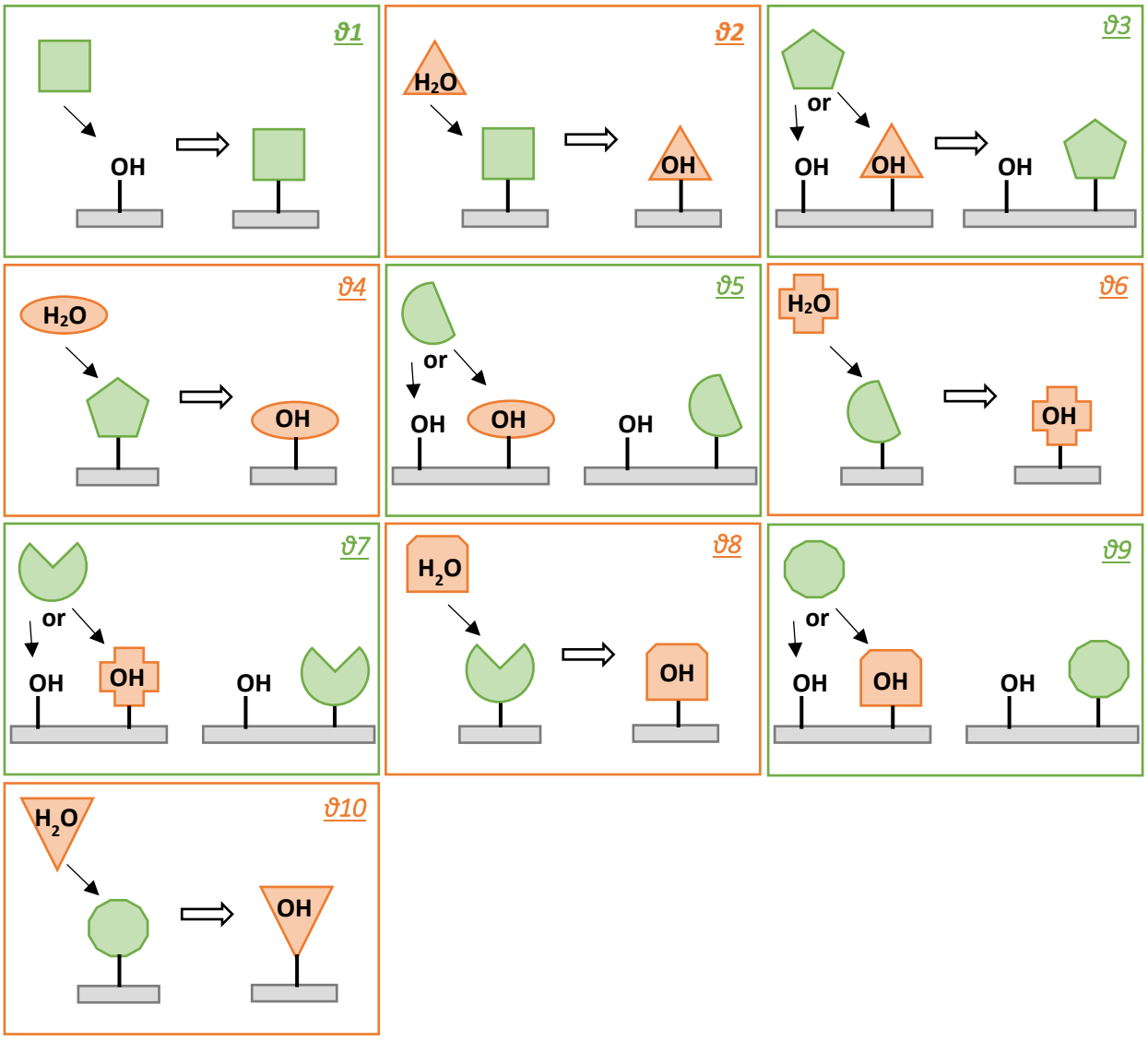

Figure 4.8: The 10-component model used to represent multiple oscillations in surface coverage observed for PTMS adsorption on metal oxide surfaces. For the sum of silane containing components to create an oscillation in surface coverage odd numbered species (green) represent silane molecules, while evenly number species (orange) represent water.

It is also important to acknowledge that in reality, there are many more than ten unique components present in solution, but it is the collective behaviour of silane species initiated by the introduction of an aluminium oxide substrate and silane to the water-based solvent that results in a measurable oscillation. Although it is thought that a collective behaviour of silane and water molecules on the surface create a measurable oscillation as seen in Chapter 3 once silane and water molecules have been displaced from the surface, they are free to re-adsorb onto the surface once more. For example, θ_1 and θ_5 may represent the same silane molecule in solution, adsorbed initially, displaced by a water molecule such as θ_2 and re-adsorbed onto the substrate at a later time, with the system becoming infinitely more complex as self-assembly proceeds.

Great consideration has been given to the kinetics required for multiple silane components in solution above however, the thermodynamics of this system must also be taken into consideration. Thermodynamically, covalent adsorbate-substrate formation is favourable over hydrogen bound adsorbate-substrate adsorption, although such a bond is only possible via the formation of a hydrogen bond first, as described by the 2-component model[38]. In the 3-component model, the displacement of θ_1 by θ_2 during the conversion of θ_1 to a covalently bound species can occur. In this case, the shift in dynamic equilibrium prevails over the thermodynamically favourable θ_1 covalent bond formation and a decrease in silane surface coverage is observed. In the instance of a 10-component model, the mechanism of film formation remains the same. The formation of covalently surface-bound silane species occurs via the formation of a hydrogen bond and can be displaced by a water molecule during this process. Upon a shift in the dynamic equilibrium the displacement of a silane species from the surface prevails over the thermodynamically favourable covalent bond formation and silane surface coverage decreases.

While the 10-component model has not yet been successfully fit to the multiple oscillations observed experimentally for PTMS on aluminium oxide, it has been shown to produce multiple oscillation in silane surface coverage given the assignment of silane and water species. The displacement of silane species by water molecules is consistent with the 3-component model and remains a valid explanation of silane adsorption kinetics.

5 The Role of Physisorbed and Covalently Bound Species in Organosilane Film Self-Assembly

The following chapter is based in part on the paper;

Sims RA, Harmer SL, Quinton JS. The Role of Physisorption and Chemisorption in the Oscillatory Adsorption of Organosilanes on Aluminium Oxide. *Polymers.* 2019;11(3):410

As the formation of a covalently bound silane film is shown to occur through the formation of a hydrogen bond[47], determining the role of physisorbed and covalently bound species in the oscillatory adsorption mechanism of silane self-assembly will give a greater insight into the fundamental mechanism of silane film growth on a molecular scale.

This chapter details the role of physisorbed and covalently bound species in the oscillatory mechanism of film self-assembly. The impact of weakly bound species on the surface condensation kinetics of both the Langmuir-type film growth of PDMMS and oscillatory growth of PTMS and PMDMS was determined by removing these species form the surface while monitoring the silane adsorption as a function of exposure time using XPS[162].

Throughout this thesis, the mechanism behind the oscillatory behaviour of PTMS and PMDMS has been linked to a shift in the dynamic condensation reaction. However, the formation of a covalently bound film is facilitated by hydrogen bond formation and thus the question must be asked, is this oscillatory behaviour a result of the displacement of weakly bound silane species or does it also include the removal of covalently bound species from the surface as a shift in the condensation equilibrium suggests? And similarly, how does the removal of physisorbed species from PDMMS films affect the Langmuir-type adsorption profile?

In order to separate physisorbed species from covalently bound species on the surface, a rinsing procedure was implemented. Details of the rinsing procedure can be found in section 2.2.1 and involve gently rinsing samples with Milli-Q water prior to drying with N_2 and curing. A limitation of this method is that it does not discriminate between the types of physisorbed species on the surface. Physisorbed species is a broad term that includes all Van Der Waals interactions and, in some instances, entanglement (A detailed description of physisorbed and covalently bound species can be found section 1.6.). While the mechanism clearly defines the formation of a hydrogen bound species, any combination of these physisorbed interactions may be present on the surface, the difference between which cannot be determined by rinsing the film. This does not prevent the role of these species from being determined as it is not the rinsed solution which is examined, rather the film which remains on the surface. Post rinse it is assumed that silane species which remain on the surface are covalently bound. In films which are not rinsed, removal of all remaining water from the surface by curing forces the condensation reaction to completion, effectively converting hydrogen bound to covalently bound silane species. While rinsed films are also cured, physisorbed species have already been removed from the surface[162].

5.1 Role of physisorbed and covalently bound species in the adsorption profile of Propyldimethylmethoxysilane

The mechanism of Langmuir film growth involves the initial descent of silane molecules onto the surface until all the free surface sites are occupied[22] creating the surface species θ_1 in the 2-component model proposed by Quinton[41]. The species assigned as θ_1 is then replaced by θ_2 through the conversion of the hydrogen bond to a covalent bond as described in Figure 5.1;

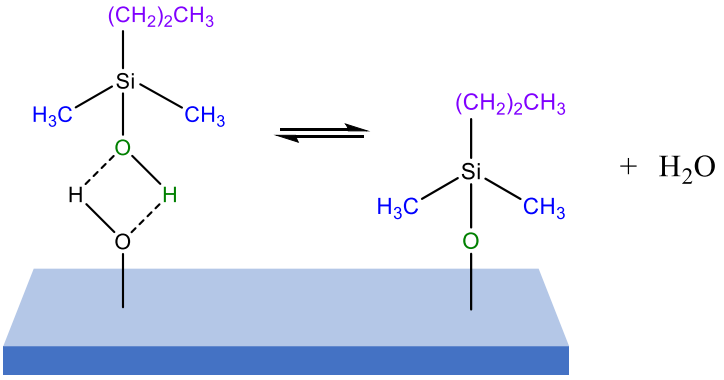

Figure 5.1: The formation of a covalently surface bound PDMMS molecule (right) via the formation of a hydrogen bond (left).

The Langmuir-type adsorption profile of PDMMS was first revealed in section 3.4 and subsequently fit to a 2-component model[41] in section 4.1. The impact of weakly bound species on the surface condensation kinetics of the Langmuir-type film growth of PDMMS can be investigated by removing physisorbed species from the surface, effectively separating these 2-components in the film. As θ_1 and θ_2 can represent the same silane molecule where the difference is simply whether it is hydrogen or covalently bound to the surface, θ_1 can be removed by rinsing the film prior to its conversion to θ_2. If the original θ_1 and final θ_2 are not a result of a conversion of the same molecule from hydrogen bound to covalently bound film and rather the result of a displacement of θ_1 by another PDMMS molecule creating a new θ_1 which is then effectively converted to θ_2, the same logic can be applied. The ability to separate these species can also give an insight into the rate of θ_1 (hydrogen bound) to θ_2 (covalently bound) conversion on the surface. The time dependent adsorption profile of rinsed PDMMS films created following a one minute hydrolysis was directly compared to the adsorption profile of non-rinsed films first revealed in Chapter 3, Figure 3.10 and shown in Figure 5.2 below.

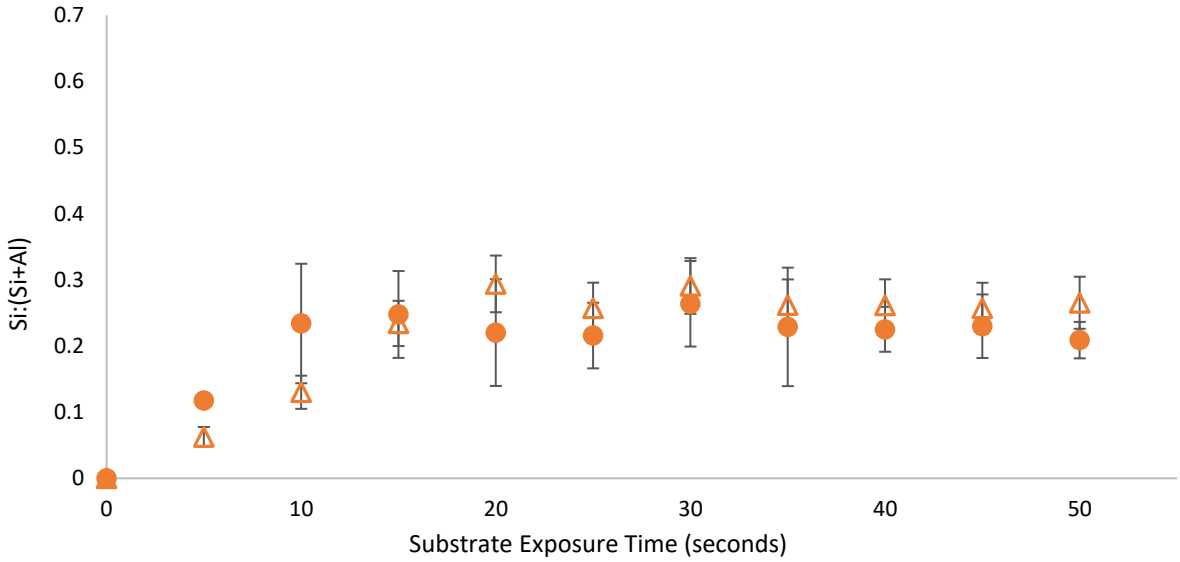

Figure 5.2: Langmuir-type adsorption of 1% PDMMS in aqueous solvent on sandpaper polished aluminium foil substrates measured using XPS following a one minute hydrolysis time. Upon removal from solution, samples were either dried with N_2 (filled circles) or rinsed with Milli-Q water (open triangles) prior to drying and curing. Each point represents the average of 3 replicates with the error quoted as the standard deviation[162].

The effect of removing physisorbed silane species from the surface of PDMMS films was shown to reduce the amount of silane on the surface during the initial stages of film growth. The direct comparison of both adsorption profiles indicates a removal of physisorbed species from the surface shifts the plateau in surface coverage (the point where film growth is complete) from 10 seconds to 15 seconds; before this point the PDMMS film on the surface contains a mixture of θ_1 and θ_2 on the surface. Despite the removal of physisorbed species from the film during the first 15 seconds of film growth, the amount of physisorbed species on the surface is shown to be minimal, demonstrating the speed at which θ_1 is converted to θ_2 on the surface. Multiple surface coverage values of rinsed samples are reported to have a slightly higher surface coverage than non-rinsed samples. This is due to the values reported being the average of 3 replicates however, rinsed and non-rinsed surface coverage values samples fall within the 1-standard deviation error[162].

The thermodynamics of θ_1 to θ_2 conversion was also considered. While the formation of a covalently bound θ_2 is thermodynamically favourable, it can only occur once the adsorbate is in the hydrogen bound potential well as θ_1 where it can then cross the diffusion barrier to become θ_2. A diagram of potential well along with a detailed description can be found in section 1.10. Desorption of silane molecules is thought to occur due to an increase in localised water concentration and reversal of the dynamic equilibrium condensation reaction. As the amount of silane adsorbed on the surface was not

found to decrease after 15 seconds of PDMMS self-assembly (Figure 5.2), it can be said that the rinsing procedure does not contribute to this mechanism by removing covalently bound silanes.

5.2 The Role of physisorbed and covalently bound species in the adsorption profiles of Propyltrimethoxysilane and Propylmethyldimethoxysilane

While the kinetics of a multilayer system with multiple oscillations in surface coverage becomes increasingly complex and a 2-component model can no longer be used to represent the kinetics of self-assembly, the thermodynamics requiring the conversion of hydrogen bound to covalently bound species remain the same. In order for silane molecules to condense to one another or a hydroxylated substrate, they must fall into the hydrogen bound potential well and cross the diffusion barrier to become covalently bound. Once the adsorbate is in the hydrogen bound equilibrium potential well, it can become covalently bound by crossing the diffusion barrier towards the thermodynamically favourable product or become displaced by a water molecule in solution[162].

While the role of physisorbed and covalently bound species on the surface of PDMMS films was established in Section 5.1, the role of these species in the oscillatory growth mechanism is unknown. A shift in the dynamic condensation equilibrium would imply the removal of both physisorbed and cogently bound species from the surface however, this remains untested.

If the oscillation in surface coverage observed for PTMS and PMDMS films is a direct result of physisorbed species on the surface, rinsed films should follow that of a Langmuir-type curve, similar to that of PDMMS. However, if oscillations in surface coverage are due to the removal of both physisorbed and covalently bound species from the surface, an oscillatory behaviour would persist following the removal of physisorbed species.

In order to determine the role of physisorbed and covalently bound species in the oscillatory mechanism of film formation, both PDMMS and PTMS films were rinsed prior to curing and the adsorption profiles directly compared to those of their non-rinsed counterparts.

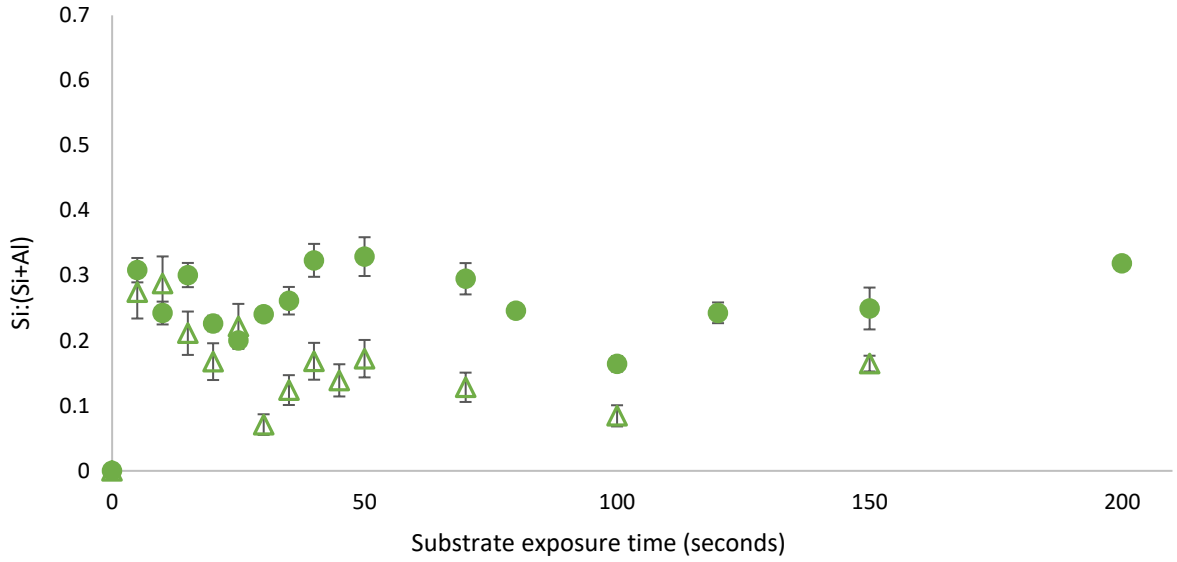

Figure 5.3: Oscillatory adsorption of 1% PMDMS in aqueous solvent on sandpaper polished aluminium foil substrates measured using XPS following a 1-hour hydrolysis time. Upon removal from solution, samples were either dried with N_2 (filled circles) or rinsed with Milli-Q water (open triangles) prior to drying and curing. Each point represents the average of 3 replicates with the error quoted as the standard deviation[162].

Despite the removal of physisorbed species from the surface, an oscillation in surface coverage is present for covalently bound species during the self-assembly of PMDMS, with the oscillation following that of films containing both physisorbed and covalent bound species prior to curing. The presence of physisorbed species does not appear to affect the rate of oscillation, but simply increases the amount of silane present on the surface. As a reversal in the dynamic equilibrium and the mechanism of film self-assembly presented in this thesis suggests, reversal of the condensation reaction is occurring on species which are both physisorbed and covalently bound to the surface and this oscillatory behaviour is not solely due to the oscillation of physisorbed species on the surface. Oscillations of covalently bound species would suggest that water trapped under the film is creating an increase in the localised water concentration, shifting the dynamic equilibrium and a reversal of the condensation reaction[162]. To help confirm the results and conclusions of PDMMS, the adsorption profile of rinsed PTMS films were also investigated.

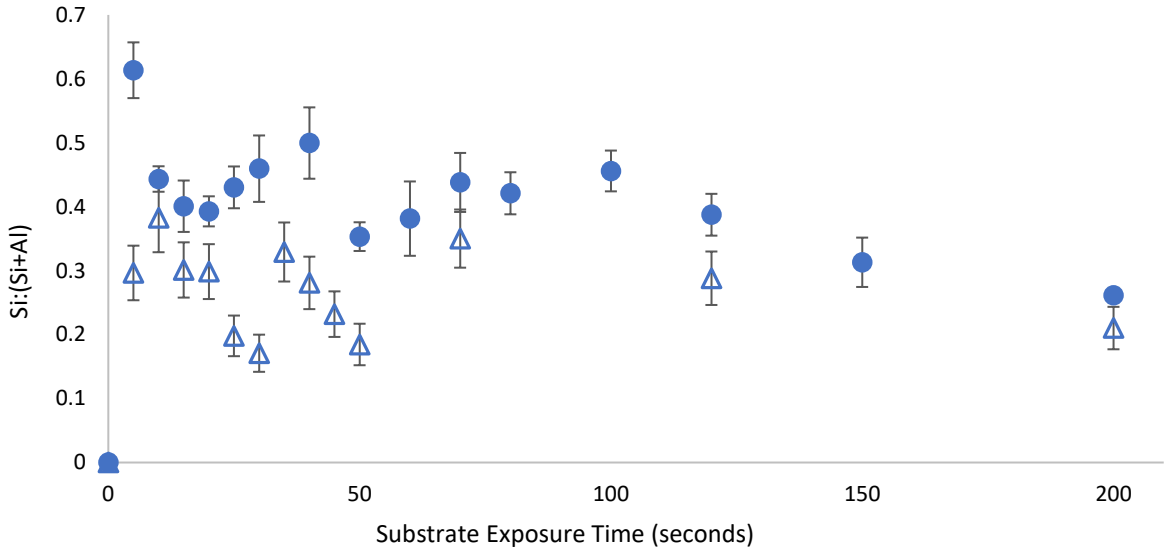

Figure 5.4: Oscillatory adsorption of 1% PTMS in aqueous solvent on sandpaper polished aluminium foil substrates measured using XPS following a 1-hour hydrolysis time. Upon removal from solution, samples were either dried with N_2 (filled circles) or rinsed with Milli-Q water (open triangles) prior to drying and curing. Each point represents the average of 3 replicates with the error quoted as the standard deviation[162].

As with PMDMS, the oscillation of PTMS silane coverage persists despite the removal of physisorbed species from the surface. Contrary to PMDMS, the removal of physisorbed species from the surface significantly reduced the amount of silane on the surface after 5 seconds of film growth. This reduction in the initial surface coverage may indicate that the majority of PTMS molecules are initially physisorbed to the surface[162].

While rinsing samples it also became evident that the effectiveness of the curing process in removing water from the film, forcing the condensation reaction to completion must be confirmed. This also presented an opportunity to test the stability of these films post cure. PTMS which had already been through the initial curing and XPS analysis processes were taken from a set of films used to determine the original adsorption profile, rinsed in Milli-Q water and reanalysed.

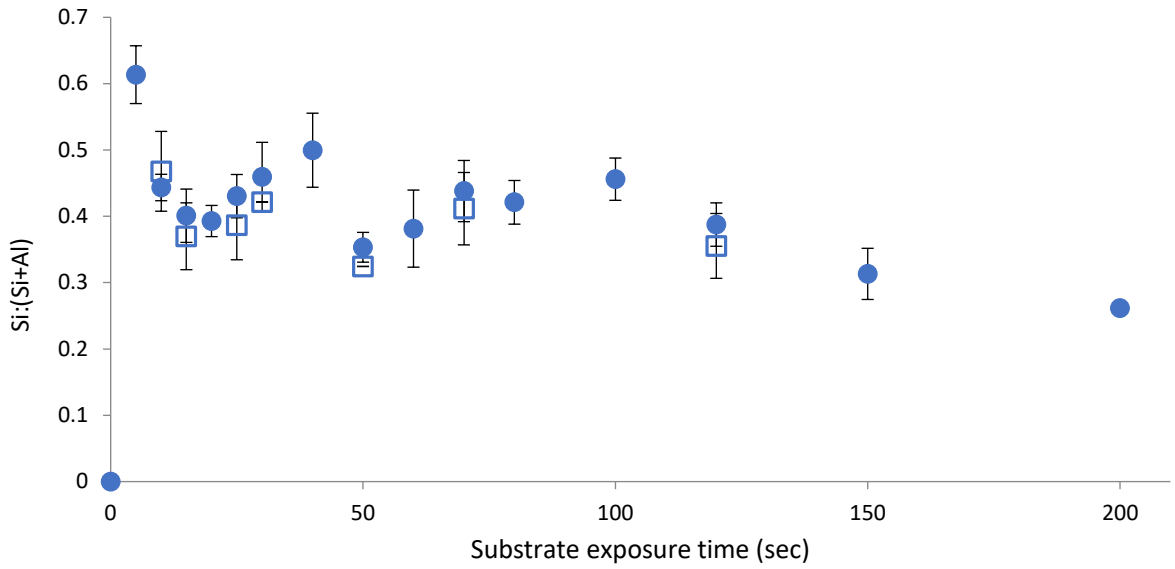

Figure 5.5: Oscillatory adsorption of 1% PTMS in aqueous solvent on sandpaper polished aluminium foil substrates measured using XPS following a 1-hour hydrolysis time. Upon removal from solution, films were cured (filled circles), measured using XPS, rinsed with Milli-Q water (open squares) and remeasured. Each point represents the average of 3 replicates with the error quoted as the standard deviation.

Once films were cured the PTMS film appeared to become stable and was not removed by rinsing confirming that the curing process forced the condensation reaction to completion and no physisorbed species were present on the surface. While all species on the surface are covalently bound, the difference between films rinsed pre-cure in Figure 5.4 and post cure in Figure 5.5 is the potential for water to become trapped under the film during the self-assembly process, reversing the equilibrium reaction.

Through removal of physisorbed species on the surface of PDMMS films the rate of conversion from hydrogen bound to covalently bound species was inferred as well as confirming the rinse's effectiveness in removing only those species which are physisorbed species from the surface. The removal of physisorbed species from the surface of PMDMS and PTMS films confirmed the role of both species in the oscillatory growth process and conformation to the mechanism of oscillation proposed by a shift in the dynamic condensation mechanism.

6 Film Morphology During the Self-Assembly of Organosilane Films.

The following chapter is based in part on the paper;

Sims RA, Harmer-Bassell SL, Quinton JS. The Oscillatory Adsorption of Organosilane Films on Aluminium Oxide: Film Morphology using Auger Electron Spectromicroscopy. *Applied Surface Science.* 2019;475:999-1002.

Published sections have been appropiately referenced in the text.

Thus far the mechanism of organosilane film self-assembly has been investigated by monitoring the amount of silane on the surface of aluminium oxide substrates using XPS. While the solution-based condensation mechanism of silane molecules with more than one hydrolysable group detailed in section 1.3 suggests that the presence of more than one hydrolysable group would allow for oligomerisation of silanes condensed onto a hydroxylated surface, the presence of these oligomers has not been confirmed and their relationship to the oscillatory adsorption is unclear.

This chapter revels the development of film morphology during the self-assembly mechanism of Organosilanes PTMS, PMDMS and PDMMS through acquiring Auger Electron Spectroscopy (AES) elemental maps and Scanning Electron Microscopy (SEM) images of the surface. The Langmuir-type growth mechanism, the oligomerisation of silanes with more than one hydrolysable group and the effect of silane oligomerisation time on film morphology eluded to in Chapter 3 is explored further by mapping silane films at increasing exposure times.

6.1 The Exploration of film morphology using Auger Electron Spectroscopy

As the tri-methoxy silane, PTMS contains 3 hydrolysable groups in the form of $–OCH_3$ extensive oligomerisation via the condensation of silanol molecules both in solution and on a hydroxylated substrate, is expected to become prevalent as film growth progresses. While the nucleation of self-assembled silane monomers was successfully mapped by Iwasa *et al*[36] using in-situ AFM, the morphology of multilayer systems such as those proposed for PTMS and PMDMS as they relate to the oscillatory behaviour have not been investigated.

In Chapter 3, the oscillatory behaviour of PTMS and PMDMS along with the Langmuir-type adsorption mechanism was investigated through the determination of bulk elemental composition and thus the extent of silane surface coverage on aluminium oxide using XPS[48]. It is true that XPS reveals an oscillation in the overall surface coverage for PTMS and PMDMS films as a function of exposure time however, AES allows for a more comprehensive study of the films morphology and gives an insight into the size, shape and thickness of the film through the use of elemental mapping and depth profiling.

To further investigate the mechanism of silane film self-assembly, the morphology of PTMS, PMDMS and PDMMS films was determined using Auger Electron Spectroscopy (AES), a technique combining both Scanning Auger Microscopy (SAM) and Scanning Electron Microscopy (SEM). AES allows for SEM images of the surface to be captured, together with SAM elemental mapping of the desired field of view. The resulting image gives a 2-dimensional map of elemental composition and can reveal grain boundaries, preferential growth and film morphology characteristics previously unattainable using conventional XPS. In addition, the ability to sputter the surface using an argon gun between spectra collection allows for depth profiling and the determination of not only silane film coverage in the x-y plane, but the thickness of these films in the z- plane.

6.1.1 The characterisation of silane films using AES

All silane films analysed in this chapter were taken from samples used to create the adsorption curves shown in Chapter 3 and thus were prepared using the methods detailed in section 2.2.1.

Following XPS analysis detailed in section 2.2.2, AES measurements were performed with a Scanning Auger Nanoprobe, model PHI-710 from Physical Electronics, Minnesota, USA. Details of the AES technique used in this analysis can be found in section 2.2.4 with the following settings used. The incident electron beam was set at 10kV, 10nA and time per step of 10ms. In the same way XPS was

used to analyse silane films, elemental markers of silicon at a kinetic energy of 1619 eV and aluminium at 1396 eV[123] were exploited as representatives of the film and substrate respectively. Initial survey spectra for both large, generalised areas and smaller areas of interest identified using SEM on the surface were collected from 1100 to 30 eV and used to confirm the presence of silane on the surface along the presence of any contamination. High resolution spectra of Al_{KLL} at 1396 eV, Si_{KLL} at 1621 eV, C_{KLL} at 275 eV and O_{KLL} at 510 eV peaks were then obtained, an example of which is given in section 2.2.4. Upon conformation of the presence of silane on the surface, an SEM image was captured and the distribution of elements on the surface mapped. In order to create an elemental map of the surface, a spectrum is collected for each pixel within the map with the intensity of colours chosen representing the relative intensity of the element in the surface analysed. Thermal colours were applied with black representing a low relative intensity through to yellow, representing high relative intensity, all processed using PHI's Multipack[123] software. Once a map of the surface and corresponding high-resolution spectra had been acquired, the surface was depth profiled. Combining elemental maps and their corresponding SEM images with depth profiling data gives information about the film in both the x-y and z plane. 2-point acquisition, 256x256 pixel maps were created for key samples along the growth curve of each silane. These elemental maps were then directly compared to the SEM images of the area mapped and depth profiles acquired.

6.2 The morphology of Propyldimethylmethoxysilane films

In contrast to the oscillatory film growth of PTMS and PMDMS, PDMMS has been shown to follow a Langmuir-type growth mechanism[48]. Determining the morphology of the Langmuir-type PDMMS films during the self-assembly mechanism will give an insight into the appearance of AES elemental maps of known Si:(Si+Al) values for monolayer coverages. This will also allow for a direct comparison to the morphology of PTMS and PMDMS films with the ability to oligomerise. The adsorption curve for PDMMS as a function of time is shown again in Figure 6.1 for ease of comparison, with the samples selected for AES elemental mapping colour coded. The elemental maps of these samples along with their accompanying SEM images is then shown in Figure 6.2.

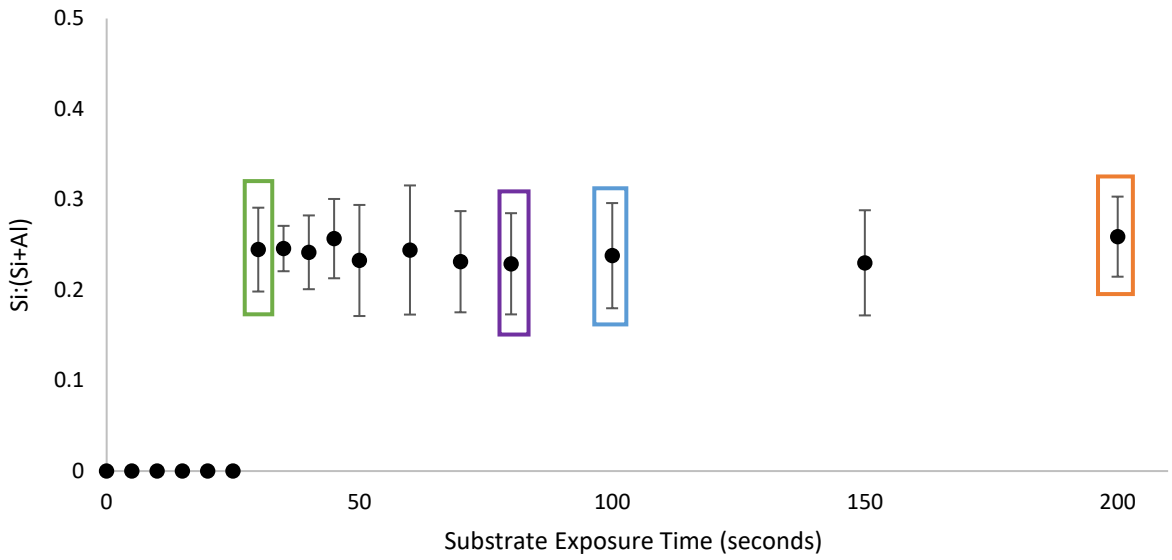

Figure 6.1: The time dependent adsorption profile of 1%v/v PDMMS in aqueous solvent when exposed to 1 µm diamond paste polished aluminium foil substrates following the simultaneous initiation of the hydrolysis reaction and substrate exposure (no hydrolysis time). Coloured squares detail areas mapped using AES shown in Figure 6.2.

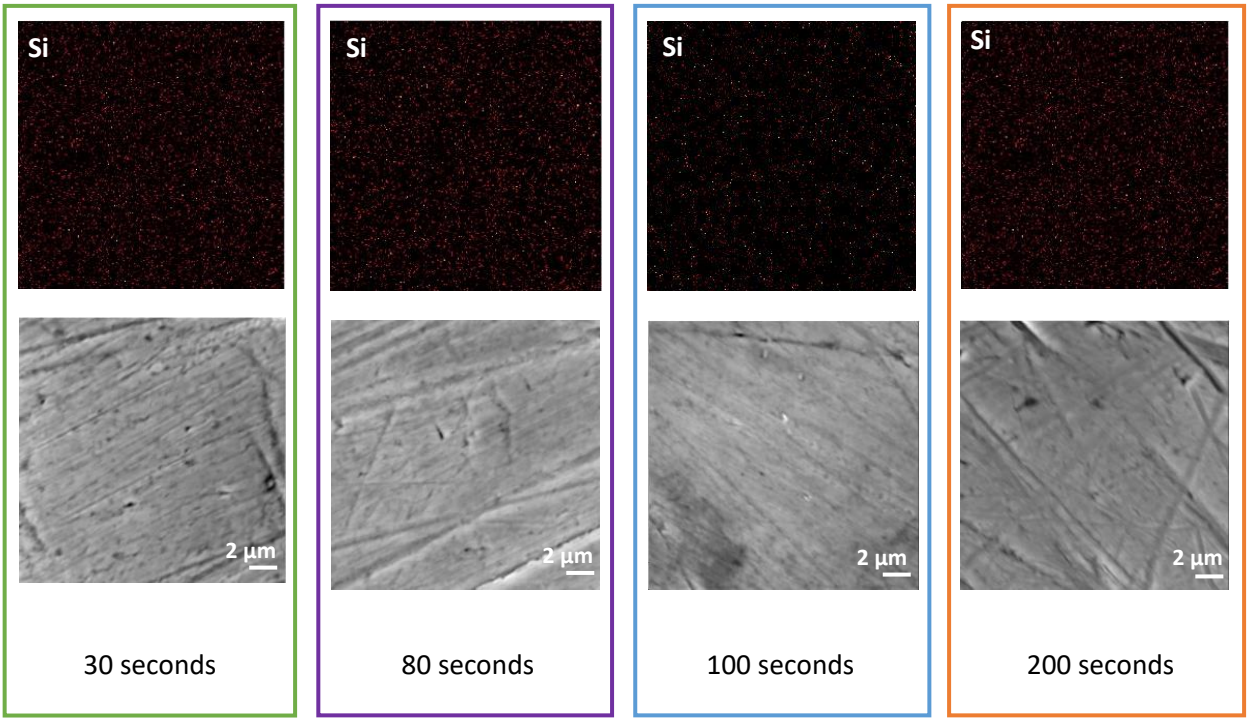

Figure 6.2: AES Si_{KLL} maps for selected exposure times along the time dependent adsorption profile of 1%v/v PDMMS in aqueous solvent when exposed to 1 µm diamond paste polished aluminium foil substrates. Maps are shown in thermal mode where yellow indicates a high relative intensity of silicon, black indicates a low relative intensity.

AES elemental maps of PDMMS films appear to have a uniform coverage from the onset of silane condensation and do not appear to change in morphology at increasing exposure times. This remains consistent with the mechanism of Langmuir film growth detailed in section 1.5.1, where silane molecules collectively descend and condense on to the surface until all available -OH surface sites are occupied. This is expected as the PDMMS molecule has only 1 hydrolysable group, and thus can only bind to one other silane in solution and become inert or bind to the substrate via one bond. The morphology of the resulting film resembles that of an incomplete monolayer.

Depth profiling of PDMMS films was also performed and revealed the thickness of the silane layer to be approximately 5 nm for each film. It comes as no surprise based on the silicon elemental maps shown in Figure 6.2 and the mechanism of Langmuir film growth that all the depth profiles obtained for PDMMS films resemble one another. An example depth profile of a PDMMS film produced following 100 seconds of growth, mapped in Figure 6.2 is shown below.

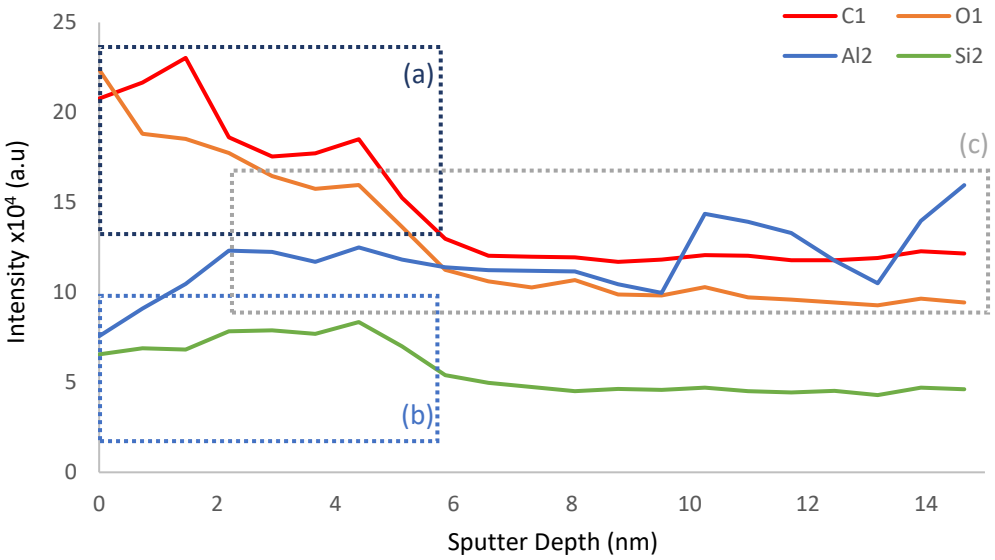

Figure 6.3: AES depth profile for a film produced following exposure of 1%v/v PDMMS to a 1 µm diamond paste polished aluminium foil substrate in aqueous solvent for 100 seconds, mapped in Figure 6.2. Features of the profile are also identified as surface oxygen (a), silane layer (b) and Al substrate (c).

Features of the profile can be identified as representing known layers of the surface. While there is a clear decrease in the Si_{KLL} signal intensity at between 5 nm and 6 nm, it is important to remember that aluminium substrates were polished with 1 µm diamond paste, subsequently corresponding to the maximum surface roughness of the sample. When depth profiling the film, the surface is sputtered away evenly and thus surface roughness must be taken into consideration when quoting film thickness, noted as a limitation of this method. Despite this, the identification of surface features within the profile is still significant and trends can be identified. The decreasing carbon and oxygen signal intensities correspond with one another and are most likely due to adventitious species as a

result of the atmospheric sample storage conditions prior to analysis. The imcomplete nature of PDMMS surface coverage and the short attenuation length of Auger electrons (described in section 2.2.4), results in the presence of an intense aluminium signal despite the presence of an intense silicon signal. It is also interesting to note that there is no distinct definition between adventitious oxygen and the oxide layer in PDMMS samples. This is also likely to be due to the incomplete nature of PDMMS surface coverage and the attenuation length of oxygen auger electrons. For films with a thicker and more complete silane coverage, it is expected that clear definition between surface oxygen and the oxide layer between the aluminium substrate and silane film will be visible, as well as the absence of an aluminium peak revealed only once sufficient layers of the silane film have been removed.

6.3 The morphology of Propylmethyldimethoxysilane films

Unlike PDMMS, PMDMS molecules containing two hydrolysable groups can oligomerise in solution and as the proposed mechanism of oscillatory adoption suggests, on a hydroxylated substrate. Monitoring PMDMS film morphology during the self-assembly process may confirm the presence of oligomerised island of film. This would provide further evidence towards the proposed mechanism of film self-assembly whereby water molecules become trapped underneath islands of film, increasing the localised water concentration and shifting the dynamic condensation equilibrium.

As with PDMMS, samples used to create the oscillatory adsorption curves of PMDMS shown in Chapter 3 were analysed using AES and elemental maps produced for key points along the oscillatory curve. The time dependent adsorption curve of PMDMS is shown again in Figure 6.4 for ease of comparison, with the samples selected for AES elemental mapping colour coded. The elemental maps of these samples along with their accompanying SEM images can be seen in Figure 6.5;

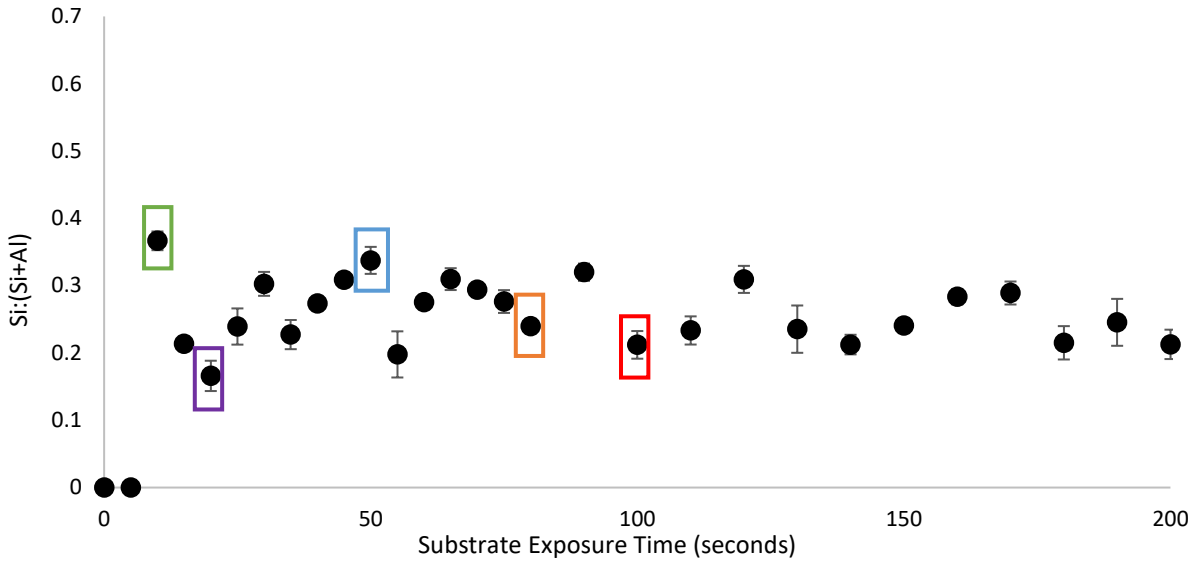

Figure 6.4: The time dependent adsorption profile of 1%v/v PMDMS in aqueous solvent when exposed to 1 µm diamond paste polished aluminium foil substrate following the simultaneous initiation of the hydrolysis reaction and substrate exposure (no hydrolysis time). Coloured squares detail areas mapped using AES shown in Figure 6.5.

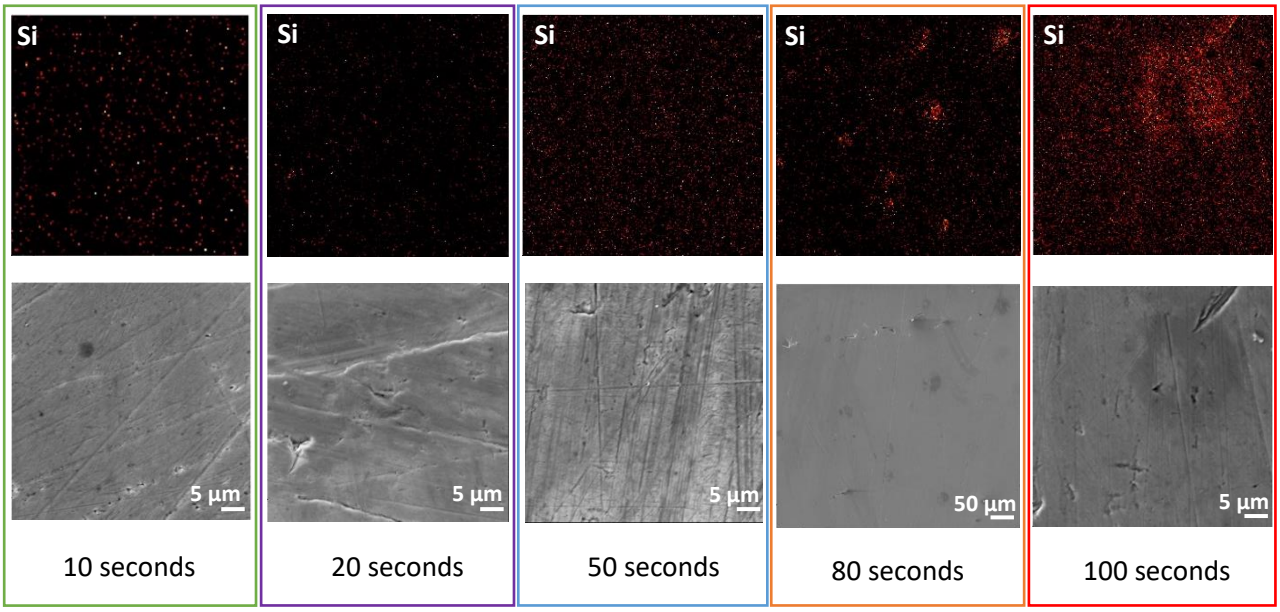

Figure 6.5: AES Si_{KLL} maps for selected exposure times along the time dependent adsorption profile of 1%v/v PMDMS in aqueous solvent when exposed to 1 µm diamond paste polished aluminium foil substrates. Maps are shown in thermal mode where yellow indicates a high relative intensity of silicon, black indicates a low relative intensity. FOV 50 µm (10s, 20s, 50s and 100s) and FOV 500 µm (80s).

Following 10 seconds of PMDMS film growth, the AES elemental map shown in

Figure 6.6 closely resembles those of PDMMS monolayer-type films absent visible oligomerisation. Unexpectedly, this Langmuir-type film morphology is also present after 20 and 50 seconds of film

growth. Multiple areas of the 10 second film were mapped with no oligomerisation observed, another example of which is shown in Figure 6.6 below. In order to measure the thickness of the film and determine if this corresponded to the thickness of PDMMS monolayer films, area 1 and 2 shown on the SEM image were both depth profiled.

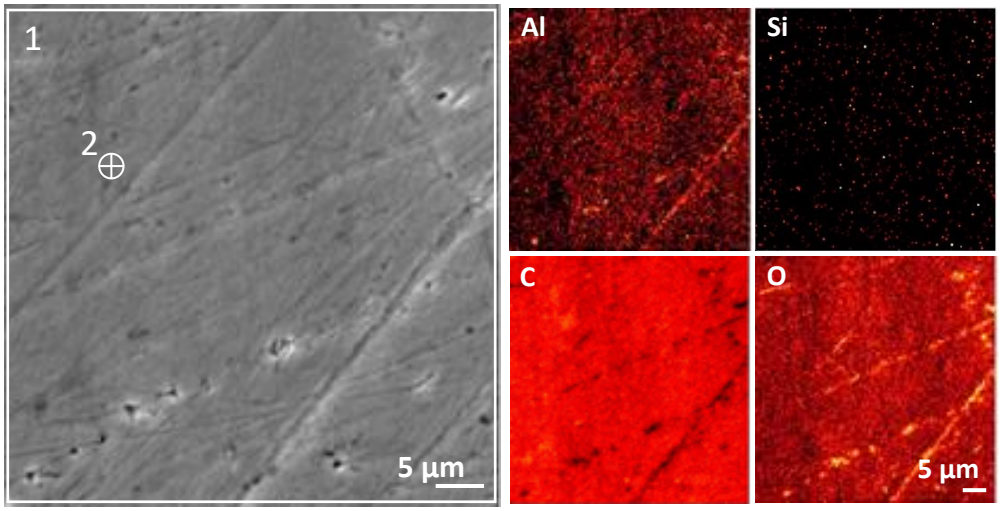

Figure 6.6: Al_{KLL}, Si_{KLL}, C_{KLL} and O_{KLL} AES maps and corresponding SEM image of the film created following the 10 seconds exposure of 1% v/v in aqueous solvent exposed to a 1 µm diamond paste polished aluminium foil substrate. Maps are shown in thermal mode where yellow indicates a high relative intensity of silicon and black indicates a low relative intensity. Areas 1&2 denote the areas measured during depth profiling (shown in Figure 6.7).

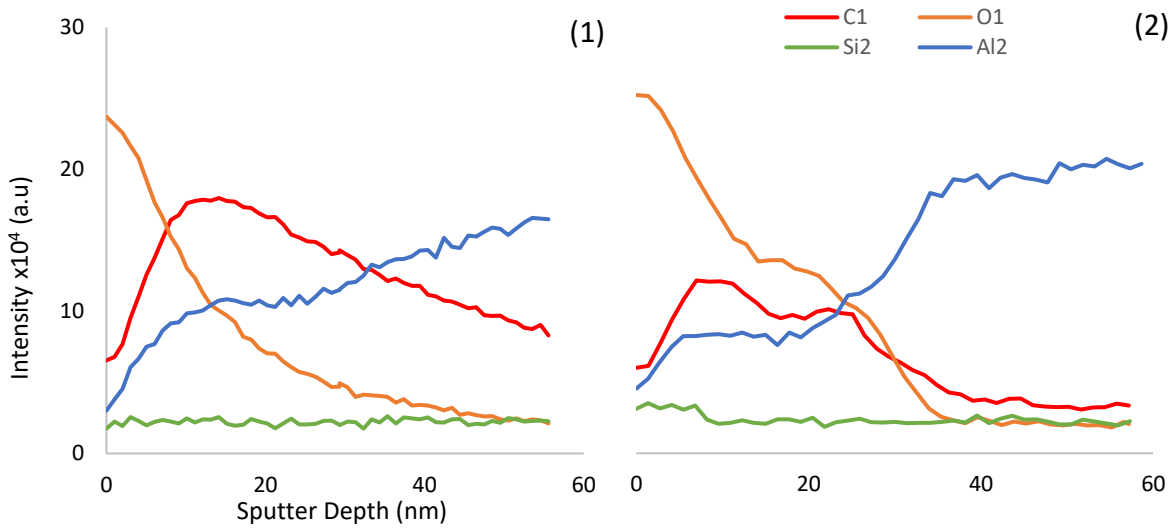

Figure 6.7: AES depth profiles of Al_{KLL}, Si_{KLL}, C_{KLL} and O_{KLL} AES peak intensities for area 1 and 2 for the 10 second exposure of 1%v/v PMDMS to a 1 µm diamond paste polished aluminium foil substrate in aqueous solvent mapped in Figure 6.6. Area 1 represents the entire FOV, while area 2 represents a selected of the surface.

A striking difference in the level of detail is shown when comparing area 1, which represents the average signal intensity of the entire field of view (FOV) and area 2, a single point on the surface. While both profiles follow a similar trend, area 2 contains well defined features and clear boundaries between the silane film, oxide layer and aluminium substrate. The depth profile of area 2 revealed a clear decrease in the Si_{KLL} signal at 8 nm, similar to the 5 nm measured for PDMMS films where only monomers can condense onto the substrate indicating that PMDMS molecules on the surface is also comprised of small silane molecules.

While the first 50 seconds of PDMMS film self-assembly appear to result in the formation of a monolayer-like film, as the proposed mechanism suggests, islands of PMDMS oligomers begin to appear on the surface between 50 and 80 seconds. An SEM image with a much larger 500 µm FOV is shown in Figure 6.8 for the 80 second sample in order to show the size and distribution of islands on the surface. Multiple islands appear across the entire surface observed and range between 20 µm and 40 µm in diameter. AES Si_{KLL} maps of PMDMS islands not only confirms the presence oligomerisation and island growth on the surface but enables entrapment of water molecules underneath islands of film, increasing the localised water concentration and shifting the dynamic condensation reaction resulting in desorption of the film.

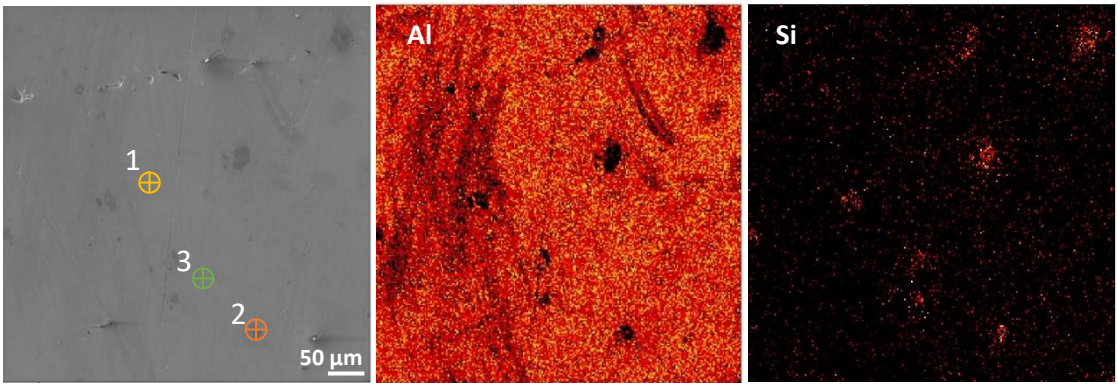

Figure 6.8: Al_{KLL} and Si_{KLL} AES maps and corresponding SEM image of the film produced following the exposure of 1 µm diamond paste polished aluminium foil substrate to 1% v/v PMDMS in aqueous solvent for 80 seconds. Maps are shown in thermal mode where yellow indicates a high relative intensity of silicon and black indicates a low relative intensity. Areas 1, 2 and 3 represent areas of the surface measured during depth profiling.

The islands present after 80 seconds of PMDMS self-assembly also depth profiled to determine the magnitude of oligomerisation within these islands of PMDMS films. Three areas of the surface marked on the SEM image in Figure 6.8 including two islands and an area of the surface which appears to denote a layer similar to the film present at 50 seconds were profiled.

As part of the profiling process, high resolution spectra of areas 1, 2 and 3 were taken prior to the first round of sputtering.

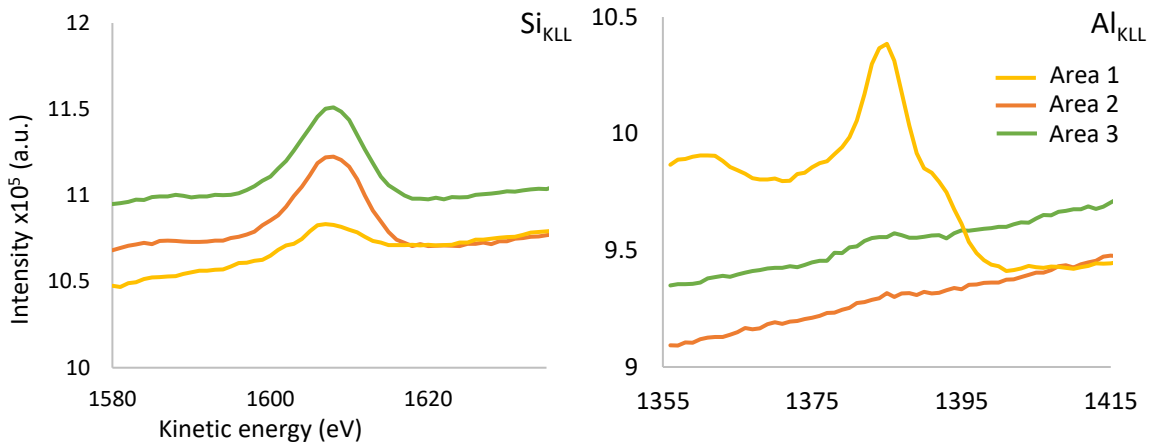

Figure 6.9: AES high resolution Al_{KLL} and Si_{KLL} spectra for areas 1 through 3 shown in Figure 6.8 of the film produced following the exposure of 1µm diamond paste polished aluminium foil substrate to PMDMS in aqueous solvent to for 80 seconds.

High resolution spectra of areas 1 through 3 in Figure 6.9 reveal that all 3 areas contain silane however, the Si_{KLL} signal for area 1 is considerably lower than that of the silane islands in areas 2 and 3. This gives an indication of the amount of silane on the surface in each of these areas and the extent of oligomerisation within the island observed. An inverse relationship can be seen for the Al_{KLL} peaks and can once again be attributed to the height of the silane films and the attenuation length of aluminium Auger electrons. It is expected that as layers of the film are sputtered away, the silicon signal intensity will decrease while the aluminium signal intensities increase.

As with the depth profile of PDMMS show in Figure 6.3, the intensity of Al_{KLL}, Si_{KLL}, C_{KLL} and O_{KLL} AES signal intensities were collected between each sputtering cycle and plot as a function of sputter depth.

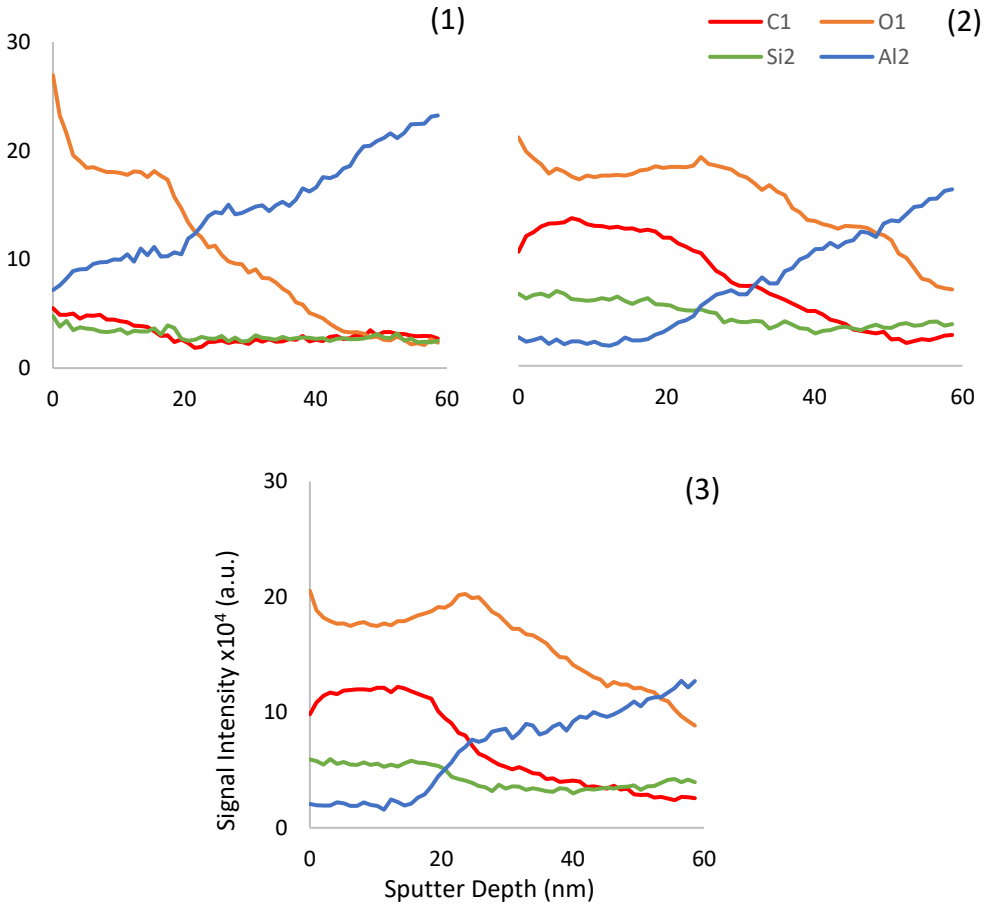

Figure 6.10: AES depth profiles of areas 1, 2 and 3 created from the high resolution Al_{KLL}, Si_{KLL}, C_{KLL} and O_{KLL} AES spectra for a film produced following the exposure of 1µm diamond paste polished aluminium foil substrate to 1%v/v PMDMS in aqueous solvent for 80 seconds.

The presence of a 10 nm thick oxide layer between the aluminium substrate and silane film, 35 nm and 25 nm thick silane islands covered in a further oxide layer just a few nanometres thick were identified in the depth profile of areas 2 and 3 respectively. Similar features were identified in area 1 with the silane film measured at approximately 10 nm thick. Features in area 1 more closely resemble the depth profile of PDMMS films shown in Figure 6.3 and while it can't be definitively said that this film is composed of a monolayer as PDMMS does have the ability to oligomerise, the depth profile of area 1 indicates the presence of a film containing monomer or small silane oligomers in the form of dimers and even trimer molecules. These regions are determined by not only comparing the signal of the aluminium substrate to the silicon in the silane film, but by also taking into consideration the presence of adventitious carbon on the surface and within the silane film as well as the presence of

oxygen, both on top of the film and as an oxide layer between the silane film and aluminium substrate. Depth profiles in Figure 6.10 were then converted in to a table comparing the height of surface features determined.

Table 6.3.1: Compilation and definition of AES surface profile regions for areas 1 through 3 determined from the depth profiles seen in Figure 6.10 for the film produced following the exposure of 1µm diamond paste polished aluminium foil substrate to PMDMS in aqueous solvent to for 80 seconds.

Surface layers	Spot 1 (~nm)	Spot 2 (~nm)	Spot 3 (~nm)
Surface Oxide	8	4	4
Silane Film	10	35	25
Substrate Oxide layer	30	10	10
Al Substrate	Substrate		

In order to simplify the information obtained in these depth profiles and directly relate it to the silicon AES map of the surface, a cross section schematic of the surface was created from the regions identified in Table 6.3.1;

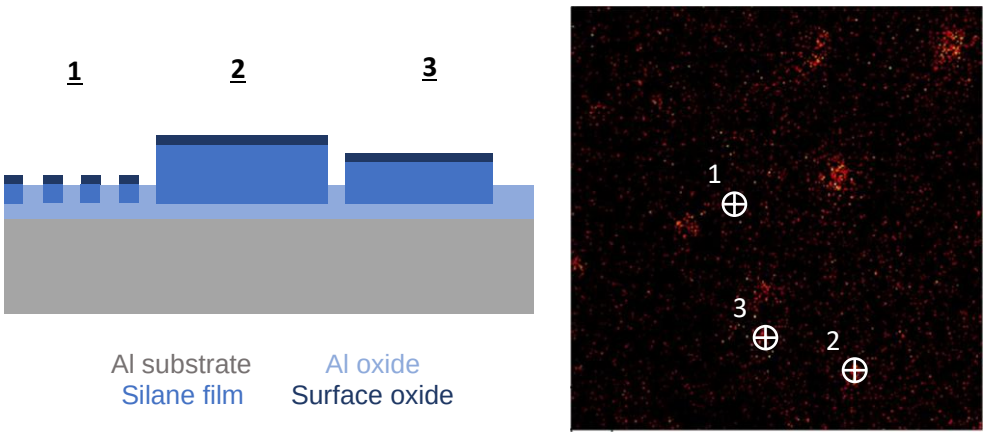

Figure 6.11: Cross section schematic of AES surface profile regions for areas 1 through 3 determined from the depth profiles seen in Figure 6.10 for the film created when an aluminium substrate was exposed to 1%v/v PMDMS solution for 80 seconds (left). The accompanying AES Si_{KLL} map and areas measured are shown for reference on the right.

It is important to note that these boundaries are not as clean and uniform as shown in the cross section image created, evident as the depth profiles contain increasing and decreasing gradients not horizontal plateaus and vertical drops thus, profiling depths are only approximate and Figure 6.11 an oversimplification of the complex morphology of the film. However, it is a useful tool in visualising the

high volume of information contained in these profiles. Depth profiles of all 3 areas reveal the height of silane islands varies amongst the areas profiled (z-axis), corresponding with the variation in island width (x) and length (y) observed in Figure 6.8. Island 2 appears the largest with an x-y diameter of approximately 20x20 μm and has the highest height (z) of 35 nm. Island 3 appears smaller at approximately 10x10 μm and is thinner at approximately 25 nm. Both islands are significantly larger in the x-y direction than the z direction indicating that oligomerisation is more likely to occur parallel to the substrate as opposed to growing perpendicularly. In Area 1, the film thickness is just 10 nm, similar to the thickness of the PMDMS film observed after 10 seconds of silane exposure in Figure 6.5 and the Langmuir-type films of PDMMS in Figure 6.2.

All areas of the sample measured have an outermost layer of oxide between 4 nm and 8 nm thick, this may be in part contributed to by the presence of unhydrolysed Si-O-CH_3 or uncondensed Si-OH on the outermost layer of the silane island but is most likely due to an oxide layer incurred during film curing and transfer to the analysis chamber. By simply measuring the O_{KLL} peak intensity, it is impossible to differentiate between the oxide layer on the outermost surface and the oxide layer between silane film and the substrate. However, when the O_{KLL} profile is compared to the Si_{KLL} peak intensity profile, the two oxide layers can be clearly differentiated. The incomplete nature of the silane film in area 1 is demonstrated by the presence of an intense Al_{KLL} peak in Figure 6.9 despite the silane film in this area shown to be approximately 10 nm thick and the maximum penetration depth of AES 5 nm as detailed in section 2.2.4. After silane has condensed onto the surface any areas of Al substrate not covered in a dense layer of silane continue to oxidise as shown in Figure 6.11. While at different peak intensities carbon and silicon depth profiles follow similar trends, although the intensity of the carbon peak is consistently larger than the silicon peak. This is most likely due to adventitious carbon on the surface but could also be due to the propyl chain present on all PMDMS molecules.

At least one area of the surface representing an island and one area representing the overall thin film for each exposure time shown in Figure 6.5 was depth profiled and the results collated into Table 6.3.2.

Table 6.3.2: Compilation of approximate film and island heights taken from AES surface profile regions of films created along the time dependent adsorption profile of 1%v/v PMDMS in aqueous solvent.

Exposure time (Seconds)	Film height (~nm)	Island height (~nm)
10	8	-
20	10	-
50	8	-
80	9	20-35
100	10	30

Depth profiles of 10, 20, 50, 80 and 100 second films when combined with AES mapping reveal that in the early stages of film growth, when monomer and small oligomer units are present in solution, film morphology reflects this with the presence of a thin film approximately 8 nm thick after 10 seconds of substrate exposure to the silane solution, similar to the film morphology for PDMMS seen in Figure 6.2. The surface coverage continues to oscillate as shown in Figure 6.4, however despite the amount of silane on the surface changing, the morphology of the film remains similar to the monolayer until silane islands become present on the surface between 50 and 80 seconds of exposure to the Al_2O_3 substrate. The presence of an oscillation in silane surface coverage prior to the formation of islands on the surface indicates that in the early stages of film formation, reversal of the condensation reaction in due to a collective behaviour involving small monomer, dimer and even trimer silane units as predicted in section 3.2.2. After 100 seconds of silane self-assembly, the presence of silane islands on the surface is well established, demonstrating the difference in rate for the oligomerisation of silane molecules in solution vs on the surface with the latter being faster. It is because of this that it is useful to think of the surface containing 2 different types of film in terms of an incomplete, evenly dispersed monolayer-like film and large, branched oligomerised islands.

6.4 The morphology of Propyltrimethoxysilane films

The direct comparison of PTMS and PMDMS time dependent adsorption profiles in Chapter 3 showed an increase in both the amount of silane on the surface and the rate of initial condensation. This along with a decrease in the rate of oscillation, predicted to be a result of the reduced mobility of large silane oligomers, indicated that the rate of island formation on the surface of PTMS films was faster than that of PMDMS films. Once again, the time dependent adsorption curve of PTMS is reproduced in

Figure 6.12 for ease of comparison, with the samples selected for AES elemental mapping colour coded. The Si_{KLL} maps of these samples along with their accompanying SEM images can be seen in Figure 6.13;

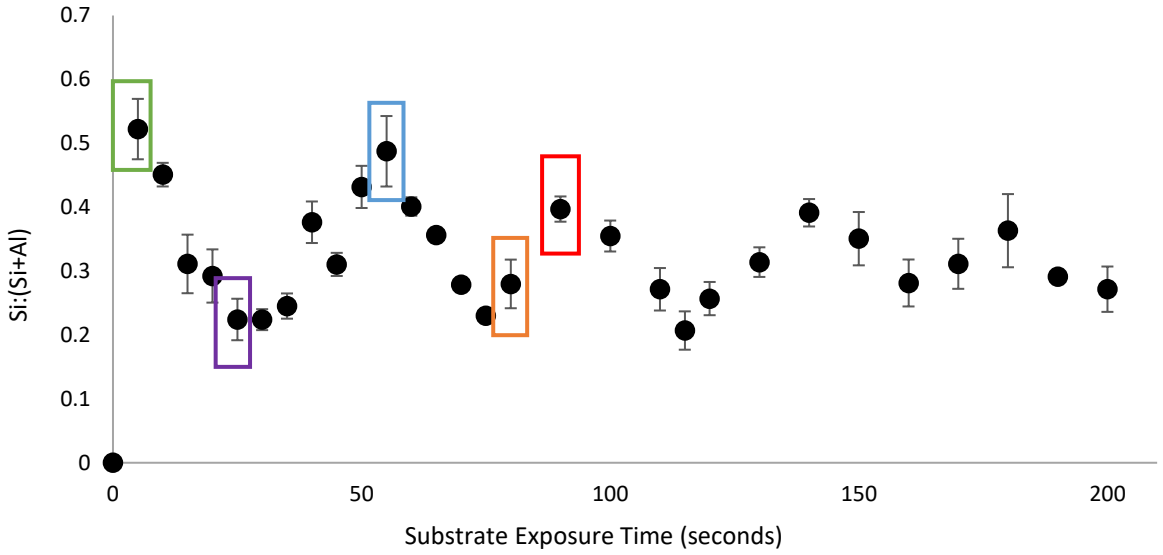

Figure 6.12: The time dependent adsorption profile of 1%v/v PTMS in aqueous solvent when exposed to 1µm diamond paste polished aluminium foil substrates following the simultaneous initiation of the hydrolysis reaction and substrate exposure (no hydrolysis time). Coloured squares detail areas mapped using AES shown in Figure 6.13[163].

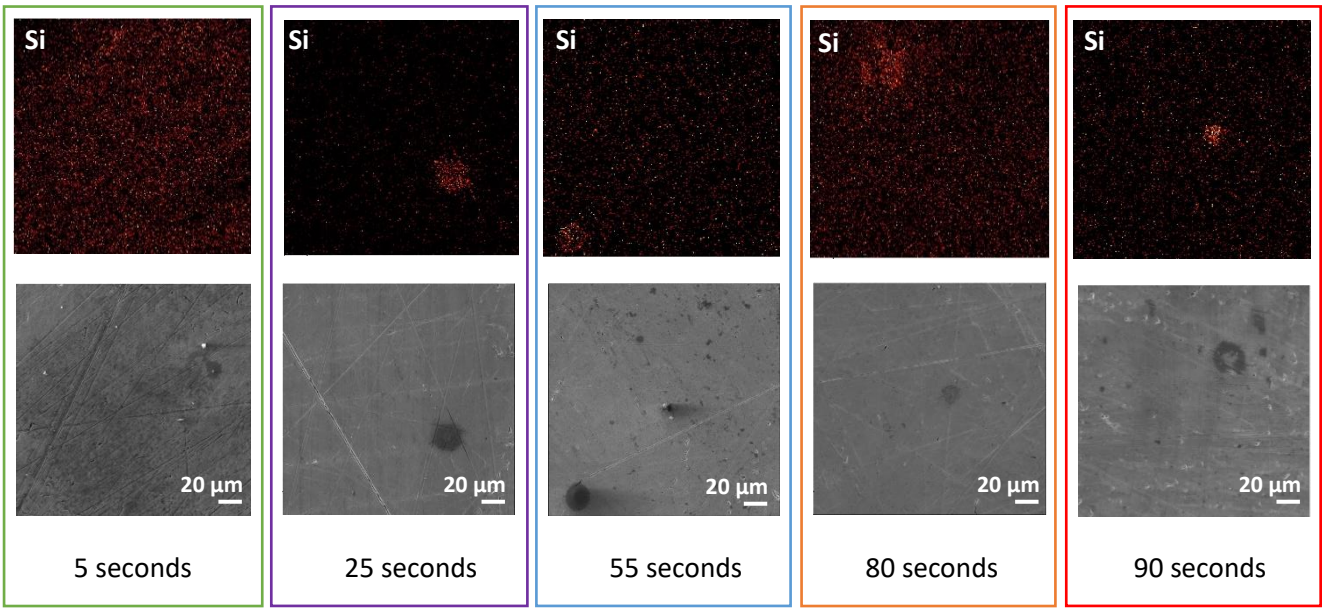

Figure 6.13: AES Si_{KLL} maps for selected exposure times along the time dependent adsorption profile of 1%v/v PTMS in aqueous solvent when exposed to 1 µm diamond paste polished aluminium foil substrates. Maps shown in thermal mode where yellow indicates a high relative intensity of silicon, black indicates a low relative intensity[163].

PTMS film morphology in the first 5 seconds of film growth appears to resemble that of PDMMS monolayer films and the early stages of PMDMS film growth. Both the intensity of the AES Si_{KLL} map in Figure 6.13 and the Si:(Si+Al) value of 5.2 for surface coverage in Figure 6.12 indicate that this film contains the highest concentration of silane on the surface of all silane films produced in this thesis. To determine if the film does in fact resemble that of a monolayer or contains oligomerised molecules, the surface was depth profiled and the silane film determined to be approximately 10 nm thick. In section 6.2, the height of PDMMS monolayer films was determined the approximately 5 nm. The presence of a 10 nm thick film however does not simply indicate that the film on the surface contains 2 layers of PTMS. As mentioned above, the surface was polished using a 1 µm diamond paste and therefore a minimum surface roughness of 1 µm can be expected. While SEM images of the surface in Figure 6.13 give the appearance of a flat surface it is not nanometre flat and thus, variations in the surface roughness will cause variations in the height of silane films measured. With this in mind, it can be said that the surface of a PTMS film following 5 seconds of self-assembly on aluminium oxide contains small silane units such as monomers, dimers and trimers similar to the early stages of PMDMS film growth and much like PMDMS, these small silane units are involved in the oscillatory mechanism during the early stages of film growth[163].

Contrary to PMDMS film growth, PTMS oligomers begin to appear on the surface between 5 and 25 seconds of self-assembly. This gives an insight into the rate of condensation on the surface and in solution. In the case of PMDMS, small (monomer/dimer/trimer) silane molecules are desorbing and reabsorbing onto the substrate but are not condensing to one another in solution at the same rate as PTMS molecules. PMDMS molecules form a monolayer-type film until between 50 and 80 seconds of exposure before oligomerised silanes appear on the surface. As with PMDMS, at least one island and one area appearing to represent a thin PTMS film were profiled for each exposure time mapped, a detailed table of these film heights can be seen in Table 6.4.1;

Table 6.4.1: Compilation of approximate film and island heights taken from AES surface profile regions of films created along the time dependent adsorption profile of 1%v/v PTMS in aqueous solvent.

Exposure time (Seconds)	Film height (~nm)	Island height (~nm)
5	10	-
25	8	24
55	10	28
80	8	38
90	9	42

PTMS islands on the surface of 5, 55 and 80 seconds of film growth appear comparable in size, shape and distribution to PMDMS at 80 and 100 seconds of self-assembly. PTMS islands then appear to increase considerably in both the x-y and z direction. While this could be due to the random discovery and mapping of a larger PTMS film at 100 seconds, multiple areas of the surface were explored in an effort to eliminate this possibility. An increase in the extent of PTMS oligomerisation and subsequently, larger PTMS islands above that of PMDMS islands is expected as the presence of three hydrolysable groups increases the probability of successful condensation reactions and creates an increased opportunity for oligomerisation. While PMDMS molecules also oligomerise on the surface and form islands, this appears to occur at a much slower rate than PTMS. This increased rate of oligomerisation indicated by the rate of island formation on the surface of PTMS supports the increase in both the amount of silane on the surface and a decrease in oscillation due to reduced mobility of larger molecules predicted Chapter 3.

Comparison of PTMS film features in Table 6.4.1 at increasing exposure times revealed that the height of the thin PTMS film surrounding oligomerised islands remains stable during the oscillatory process. If the thin film present was to continue to oscillate, silane molecules would oligomerise further in solution before re-adsorbing onto the substrate. This would result the film becoming sparse and potentially increasing the number of islands in solution and on the surface. The presence of this thin film after 90 seconds of exposure refutes this claim and in fact points to the stabilisation of this thin film on the surface. However, the height of the silane islands measured increases slowly as exposure time increases, indicating that it is the number and size of these islands undergoing a collective adsorption-desorption mechanism contributing to the oscillation in the later stages of self-assembly. The increase in condensed silanol molecules on the surface increases the complexity of the film, resulting in a network of branched and cross-linked siloxane oligomer islands as detailed previously in section 1.4.

The presence of two different types of film in terms of an incomplete, evenly dispersed monolayer-like film and large, branched oligomerised islands appeared in the Si_{KLL} maps and depth profiles of both PMDMS and PTMS films. In order to investigate the presence of a stable, thin PTMS film during the oscillatory growth process, the silane surface coverage indicated by Si:(Si+Al) in Chapter 3 were directly compared for PTMS and PDMMS films.

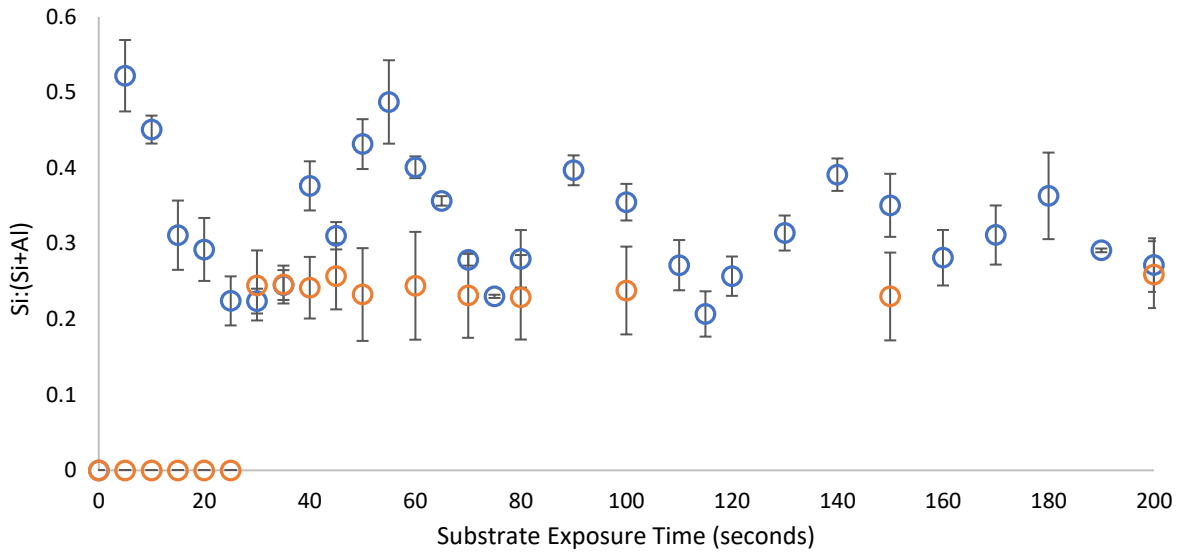

Figure 6.14: The time dependent adsorption profile of 1%v/v PDMMS (orange) and 1%v/v PTMS (blue) in aqueous solvent when exposed to 1 µm diamond paste polished aluminium foil substrates following the simultaneous initiation of the hydrolysis reaction and substrate exposure (no hydrolysis time). Each data point represents the average of three replicates with the error quoted as the standard deviation.

The minimum surface coverage of PTMS films corresponds to the maximum surface coverage obtained for PDMMS monolayer films, indicating when the desorption of PTMS films occurs, the amount of silane left on the surface is approximately equivalent to that of a monolayer of PDMMS. When combined with AES maps of the surface, it can be said that after 30 seconds of film growth the majority of the oscillation in PTMS films due to the repeated adsorption and desorption of PTMS oligomers while the thin, monolayer-like PTMS film becomes stable on the surface.

Hydrolysis time of the silane solution has been shown to have little effect on the rate of initial PTMS condensation with the appearance of silane on the surface after just 5 seconds of film self-assembly in both cases measured using XPS in section 3.2. However, PTMS films created following a 1-hour hydrolysis time have been allowed to condense to one another in solution prior to the exposure of an aluminium oxide substrate. The amount of PTMS on the surface measured using XPS is also slightly higher for samples created following a 1-hour hydrolysis time. It is because of this that despite a PTMS film being present in the surface after 5 seconds of film self-assembly regardless of hydrolysis time, it is reasonable to expect that the morphology of these films is vastly different[163].

The surface of a PTMS film created following a 1-hour hydrolysis of the silane solution was mapped and directly compared to that of a film created without a solution hydrolysis time (both exposed to silane solution for 5 seconds). Depth profiles of both films were subsequently obtained and directly compared.

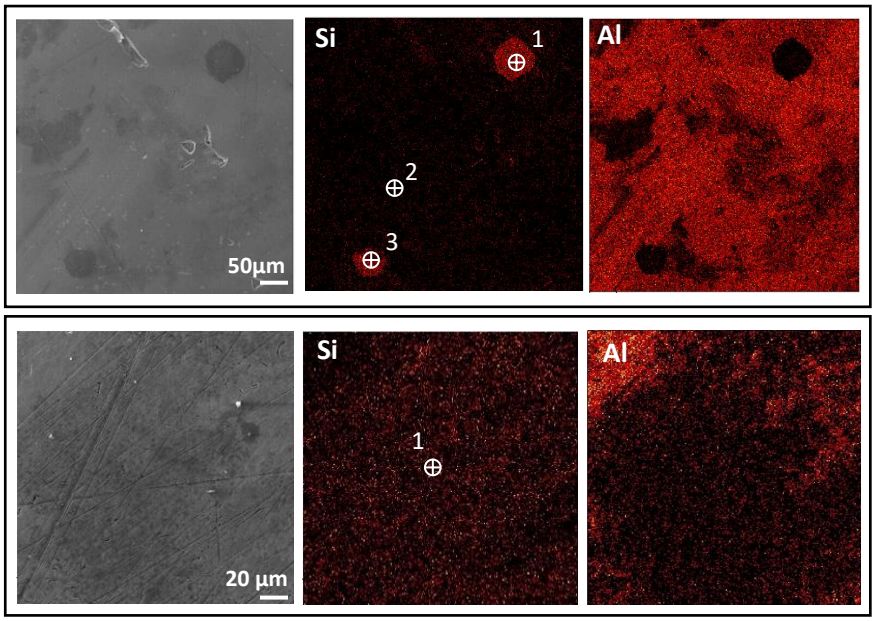

Figure 6.15: Comparison of AES Si_{KLL} and Al_{KLL} maps created upon the exposure of 1%v/v PTMS in aqueous solvent to 1 µm diamond paste polished aluminium foil substrates for 5 seconds following either a 1-hour hydrolysis time (top) or no solution hydrolysis time(bottom). Maps are shown in thermal mode where yellow indicates a high relative intensity of silicon and black indicates a low relative intensity[163].

Table 6.4.2: Compilation of approximate film and island heights taken from AES surface profile regions of films created upon the exposure of 1 µm diamond paste polished aluminium foil substrate to 1%v/v PTMS in aqueous solvent to for 5 seconds following a 1-hour solution hydrolysis or no solution hydrolysis time.

Surface Layers	**1-hour hydrolysis**			**No hydrolysis**
	Spot 1 (~nm)	**Spot 2 (~nm)**	**Spot 3 (~nm)**	**Spot 1 (~nm)**
Surface Oxide	4	5	5	6
Silane Film	125	5	100	10
Substrate Oxide layer	15	15	20	25
Al Substrate	substrate			

A hydrolysis time of 1-hour prior to a 5 second exposure appears to result in a surface coverage consisting of large, uniform islands similar to, but slightly larger than those seen in the later stages of film growth for a PTMS solution with no hydrolysis time. However, depth profiles reveal these islands to be much larger than first assumed with thicknesses of approximately 100 nm and 125 nm recorded. It appears that when allowed to oligomerise in solution first, larger (while still disk shaped) silane

molecules form, and as the aluminium substrate is exposed to the oligomerised PTMS solution these large silane oligomers descend on to the surface. When an aluminium substrate is exposed to an unhydrolysed PTMS solution, a monolayer like film appears at first with island growth in the x-y direction is favoured and disc like silane island appearing much thinner and later in the self-assembly process. While this may seem intuitive, the stark contrast between the morphology of film created upon exposing a bare Al substrate to an extensively oligomerised solution and a solution containing small silane molecules is key as it demonstrates the difference between the rate of silane-metal (substrate) condensation and silane-silane condensation, necessary to produce oscillations in silane adsorption as opposed to monotonic growth; while also demonstrating the extent of oligomerisation of PTMS molecules possible when left in aqueous solvent for an extended period of time[163].

Surprisingly, the depth profile of spot 2 for the 1-hour hydrolysis solution in Figure 6.15 revealed that despite silane molecules being exposed to aqueous solvent and the extensive oligomerisation of many silane molecules, small silane units are still present in solution and able to condense onto the substrate.

Monitoring film morphology as a function of exposure time and comparison to the oscillatory surface coverage has given an insight into the rate of condensation with regards to oligomerisation on the surface and in solution and demonstrates the effect of increasing the number of hydrolysable groups within a system that already had the ability to oligomerise. A direct correlation between silane oligomerisation and oscillation can now be made.

7 The Orientation and Order of Organosilane Molecules During Film Self-Assembly.

Research in this chapter was made possible through the award of an International Cooperative Graduate School Fellowship at the National Institute for Materials Science (NIMS), Japan. under the supervision of Professor Kohei Uosaki and Associate Professor Hidenori Noguchi along with the help of Dr. Shuo Yang.

Sum Frequency Generation Spectroscopy (SFG) enables the detection of an ordered air/solvent/film/substrate interface irrespective of the disordered environment surrounding it. In this chapter the silane-substrate interface was monitored during film formation, to determine the conformation of molecules within the film. Moreover, the ability to measure film order allows for the monitoring of changes within the growing film on a molecular scale and their behaviour as oscillations in the adsorption occur.

As detailed in section 2.3**,** an advantage of SFG in the analysis of thin films is its sensitivity to breaks in inversion symmetry, resulting in an interface sensitive technique able to monitor the conformation of alkyl chains within a silane film[132]. When in a *trans* conformation, molecules in the film are orientated such that the terminal CH_3 groups are perpendicular to the substrate and only peaks representing the CH_3 asymmetric and symmetric stretching are present. The presence of peaks representing CH_2 asymmetric and symmetric stretching indicate the presence of *gauche* defects in the film. Therefore, SFG can be used to probe the adsorption and desorption of molecules from a surface as well as the conformation of adsorbed molecules. While the SFG signals of CH_3 and CH_2 have previously been used to investigate the extent of molecular ordering of long carbon chain silanes such as octadecyltrichlorosilane (OTS)[129,142], octyltrichlorosilane[37] and, *N*-(2-aminoethyl)-3-aminopropyltrimethoxysilane[133] it was also thought that the resonance of the Si-O bond of the silane could be exploited. This would allow a direct investigation into the adsorption and desorption of the short carbon chained molecules investigated in this thesis. However, the resonance of the Si-O bond is too low down the IR frequency range to be detected using the current SFG system available at NIMS. It is also unlikely that a measurable SFG signal will be produced for this bond as it is buried in the film, and not at the interface. Thus, the behaviour of the silane films produced were investigated through the behaviour of the propyl chain.

It is important to distinguish between the terminology of *disorder* and *defects* used in this thesis. *Disorder* is related to the presence of an SFG signal, an SFG signal will not be produced by a completely disordered film or a film which contains centrosymmetry. The term *defects* relates to the presence of a CH_2 signal indicating *gauche* defects within the film. This is quantified by calculating the CH_3:CH_2 SFG signal intensity for the silanes used in this thesis.

7.1 The orientation and order of organosilane molecules within completed films

Ex-situ measurements of the silane film/air interface as a function of exposure time can give an insight into the behaviour of individual molecules at each stage of film growth within completed films (films where the self-assembly process has been terminated by removal from the silane containing solution). Comparison of the $CH_{3(s)}$:$CH_{2(s)}$ reveals how the order of silane molecules within the film changes along adsorption curve, giving insight into the impact of oligomerisation and molecular level mechanisms involved on the oscillatory behaviour of PTMS and the Langmuir-type adsorption of PDMMS.

In order to determine the behaviour of molecules within the film and allow them to be directly compared with the adsorption profiles obtained using XPS and AES already discussed in Chapters 3, 5 and 6, silane films were produced at increasing exposure times on flat sapphire substrates. Hitherto films in this dissertation have been created on the native oxide of 99.99% pure Al foil substrates. However, the rough surfaces of these samples do not allow for the creation of a sufficient SFG signal. In order to create films that were comparable to the adsorption curves measured using XPS, taking in to account the IEP and composition of the substrate, sapphire substrates were used. All films directly compared to the adsorption profiles measured with XPS and film morphology images using SEM/AES were created on a semi-cylindrical sapphire prism.

It is ideal to measure the film in a closed system in order to eliminate exposure of the film to atmosphere, thought to be the cause of a significant attenuation in the SFG signal by altering the ordering of molecules within the film and give a more accurate depiction of the film during its growth. It is for these reasons that silane films were created in an in-situ cell allowing complete control of the environment films were exposed to during silane exposure, during the drying process and during analysis.

Technically, as the film is measured after silane and solvent are removed from the cell and the film is exposed to an argon atmosphere, these measurements cannot be considered in-situ. However, they allow for analysis of film conformation immediately after its creation. As the curing process used to force silane films to completion on aluminium oxide, it was necessary to determine if the curing process itself impacts the amount of silane adsorbed into the substrate. A series of samples created according to methods outlined in section 2.2.1 were prepared without the curing process and compared to the coverage of the same exposure times for cured substrates using XPS. No discernible difference in the Si:(Si+Al) ratio was measured in either case. Confirming that while potentially having an effect on the order of molecules within the film, curing does not have an effect on the amount of silane on the surface and thus films created in the in-situ cell can be directly compared to the silane adsorption profiles produced in Chapter 3.

To determine the order of molecules within the film along the oscillatory adsorption curve, the SFG signal was measured for increasing exposure times. Each spectrum was fit to Equation 2.11 and the contribution of each functional group determined through deconvolution of this fit, an example of which was given in Figure 2.12.

7.1.1 The order of Propyldimethylmethoxysilane molecules during Langmuir-type adsorption

It was first proposed in Chapter 3 that the presence of a Langmuir-type adsorption profile for PDMMS was directly linked to its inability to oligomerise, the time dependent adsorption profile fit to a 2-component model based on Langmuir kinetics in Chapter 4, the presence of a stable, covalently bound film confirmed in Chapter 5 and the monolayer-like film imaged in Chapter 6. Thus far PDMMS appears to self-assemble into a monolayer-like film, with an adsorption profile resembling Langmuir adsorption kinetics when exposed to aluminium oxide in aqueous solvent.

As detailed in section 2.3, the behaviour of SFG $CH_{3(s)}$:$CH_{2(s)}$ signal intensity has been reported for the self-assembly of OTS monolayers, where the extent of order and the number of defects present was found to be directly related to the surface coverage of silane molecules on the surface. At lower surface coverages an increase in the presence of *gauche* defects was detected and the order of molecules within the film directly related to the packing of molecules on the surface[142]. In order to sufficiently determine what the time dependent intensity of the SFG $CH_{3(s)}$:$CH_{2(s)}$ looks like for the formation of a PDMMS film and whether this reflects that of a stable, densely packed, ordered monolayer, a time dependent $CH_{3(s)}$:$CH_{2(s)}$ profile was created for PDMMS.

Defects within the PDMMS propyl chain were measured during the Langmuir-type adsorption mechanism when adsorbed on semi-hemispherical sapphire substrates, created and measured in the controlled environment of the in-situ cell. The IR beam was tuned automatically within the range measured (2800-3800 cm^{-1}) at a step width of 2 cm^{-1}. The time dependent $CH_{3(s)}$:$CH_{2(s)}$ was then directly compared to the XPS adsorption profile with SFG propyl chain order on the primary axis and XPS surface coverage on the secondary axis, to allow a direct comparison to be made. Each time point reported is taken as the average of 3 measurements, and the error quoted as the standard deviation.

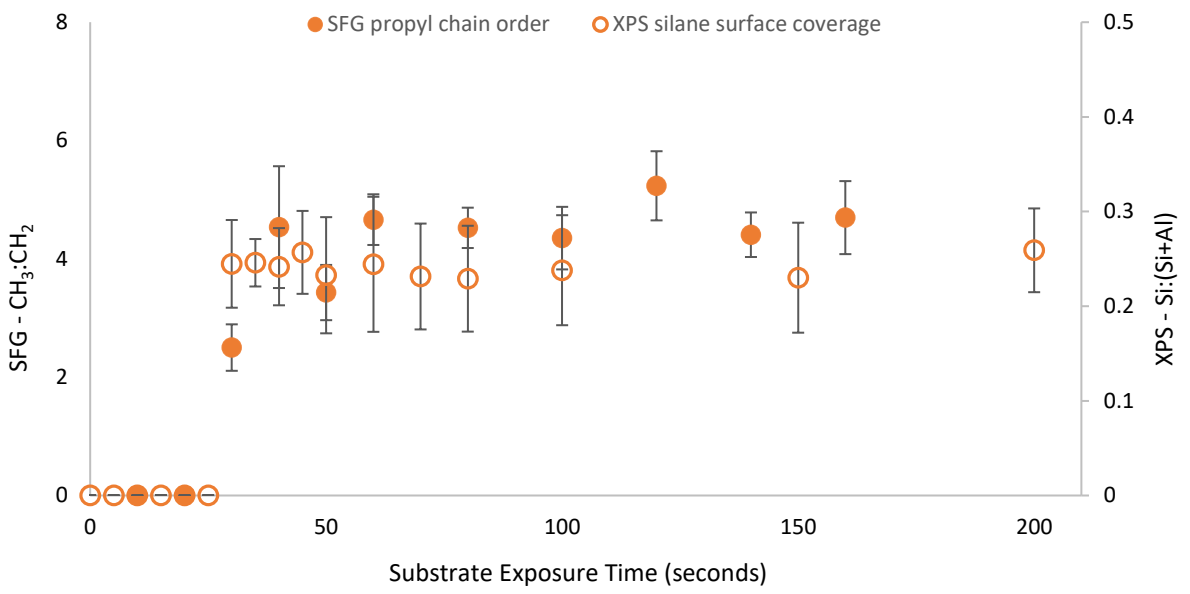

Figure 7.1: Direct comparison of the time dependent $CH_{3(s)}$:$CH_{2(s)}$ SFG signal intensity fit to Equation 2.11 representing propyl chain defects, measured in s-s-p mode (filled circles) and the Si:(Si+Al) silane adsorption measured using XPS (open circles) in the films of 1% v/v PDMMS in aqueous solvent exposed to Al_2O_3.

As predicted PDMMS, which follows a Langmuir type adsorption mechanism displayed SFG propyl chain behaviour reflecting this. Direct comparison to the time dependent surface coverage in Figure 7.1 revealed that as the surface coverage increases to a densely packed film, propyl chains within the film are orientated perpendicular to the substrate with minimal *gauche* defects. Once the formation of a stable monolayer type film has been produced, (evidenced by the presence of a stable PDMMS film post rinse in Chapter 5), the propyl chain order stabilises for this coverage, indicative of a stable monolayer. This decrease in propyl chain defects as surface coverage increases is attributed to molecular packing on the substrate. At low surface coverage the adsorbates take on a random order, blocking adjacent sites and causing patches of free substrate adsorption sites. However, at moderate coverages adsorbates can reorder on the surface, minimising the number of vacant sites, eventually leading to saturation[164].

7.1.2 The order of Propyltrimethoxysilane molecules during oscillatory adsorption

Unlike PDMMS, the multiple hydrolysable groups of PTMS allow it to oligomerise and surface coverage to oscillate however, the self-assembly behaviour of PTMS may not be as different from PDMMS as initially thought. The formation of a stable PTMS monolayer on the surface despite the continued oscillations in surface coverage was first suggested in Chapter 6. AES Si_{KLL} maps of the time dependent

PTMS self-assembly mechanism revealed the presence of 2 different types of film morphology on the surface; large, oligomerised islands surrounded by a monolayer-like film. As the SFG $CH_{3(s)}$:$CH_{2(s)}$ profile has been determined for a PDMMS monolayer with no ability for further oligomerisation, the effect of PTMS oligomerisation was determined through direct comparison to PDMMS.

The order of silane propyl chains within the film during the oscillatory growth mechanism was monitored for PTMS when adsorbed on semi-hemispherical sapphire substrates created and measured in the controlled environment of the in-situ cell. Unlike the SFG spectra of PDMMS which looked remarkably similar despite exposure time, the intensity of the CH_2 symmetric and asymmetric peaks of PTMS films varied greatly during the first 60 seconds of self-assembly. While each spectrum was fitted with Equation 2.11, visually the difference between the spectra of a 5 second and 30 second silane exposure time is striking and shows a clear difference in the $CH_{3(s)}$:$CH_{2(s)}$ ratio.

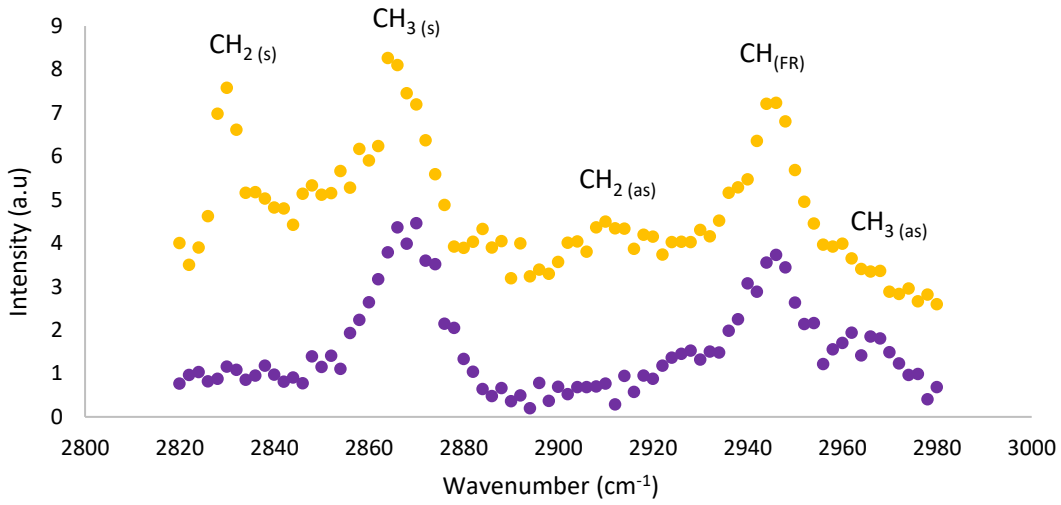

Figure 7.2: The normalised SFG C-H stretching region of PTMS films produced when 1%v/v PTMS in aqueous solvent was exposed to semi-hemispherical sapphire substrates for 5 seconds (purple) and 30 seconds (yellow), measureded using s-s-p polarisation mode. (as) denotes asymmetric stretching, (s) represents symmetric stretching and (FR) Fermi resonance.

After 5 seconds of self-assembly the PTMS film whose C-H stretching region SFG spectra shown in Figure 7.2 appears to be highly ordered, almost free of *gauche defects* and resulted in a $CH_{3(s)}$:$CH_{2(s)}$ value of 5.5. However, the number of *gauche* defects quickly increases and the $CH_{3(s)}$:$CH_{2(s)}$ value decreases to 1.7 after 30 seconds of exposure. The $CH_{3(s)}$:$CH_{2(s)}$ ratio was subsequently measured at increasing exposure time points in *s-s-p* polarisation, compared to the XPS adsorption profile of PTMS and shown in Figure 7.3;

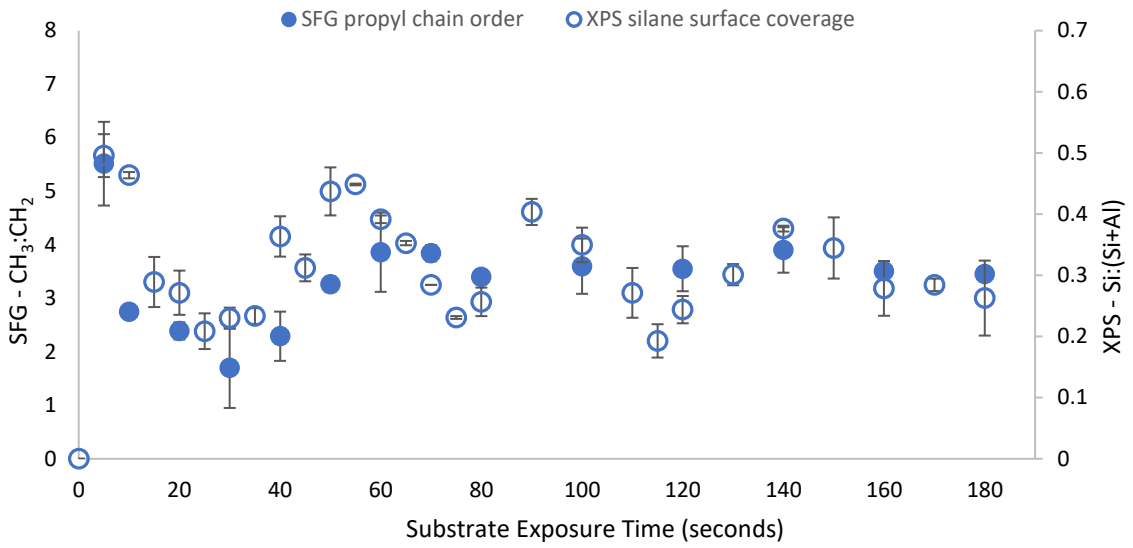

Figure 7.3: Direct comparison of $CH_{3(s)}$:$CH_{2(s)}$ SFG signal intensity fit to Equation 2.11, measured in s-s-p mode (filled circles) and Si:(Si+Al) silane adsorption measured using XPS (open circles) for the films of 1%v/v PTMS in aqueous solvent exposed to Al_2O_3 as a function of exposure time. Each data point represents the average of 3 measurements with the error quoted as the standard deviation.

The presence of a CH_2 peak and hence number of *gauche* defects in the film occurs quickly in conjunction with the oscillatory surface coverage of PTMS. Within the first 5 seconds of film growth while the surface coverage is high, molecules are densely packed on the surface and the presence of defects is low. As desorption of silane molecules occurs and surface coverage decreases the number of defects within the film increases, indicating that in the early stage of PTMS film growth, the number of defects in the film depends on surface coverage and molecular packing much like the PDMMS film shown in Figure 7.1.

Interestingly, the $CH_{3(s)}$:$CH_{2(s)}$ ratio and thus the number of *gauche* defects in the film appears to stabilise around 60 seconds while the surface coverage measured using XPS continues to oscillate. Due to the selectivity rules of SFG explained in detail in section 2.3 a branched, disordered oligomer will not produce a SFG signal and thus, the resulting SFG signal represents ordered monomer units on the surface. The exploitation of SFG as a means of determining oligomerisation has been reported previously by Zhang *et al*.[137], who monitored the CH_3 and CH_2 SFG signals characteristic of these films while increasing the concentration of sodium stearate in solution. Above the critical micelle concentration point, a completely disordered structure is formed and the SFG signal disappeared.

The evolution of PTMS film morphology measured through AES elemental mapping during the oscillatory growth in Chapter 6 confirmed the presence of oligomerised islands while also indicated the formation of a second type of film on the surface in the form of a thin, monolayer-like coverage over the entire substrate. The conclusions presented in Chapter 3 also suggest that the oscillatory

behaviour is due at least initially, to small silane molecules (monomers/dimers/ trimers) indicated by the presence of a measurable oscillation upon the exposure of substrates to solution without a hydrolysis time, before extensive oligomerisation was possible.

Through the direct comparison of the highly selective SFG signal and XPS surface coverage shown in Figure 7.3 it can be said that the first oscillation in surface coverage is contributed to significantly by the condensation of monomer units on the surface. The continued oscillatory behaviour observed with XPS despite stability in the SFG signal indicates that following the first oscillation, oscillatory adsorption behaviour is caused by the subsequent formation of oligomers, weakly bound, easily removed from the surface unable to contribute to the SFG signal. This also helps to explain why the first XPS and SFG peaks following 5 seconds of PTMS self-assembly have both the highest surface coverage and the least number of defects. By the second oscillation fewer monomer units re-adsorb on the substrate, ultimately becoming stable, but resulting in a film with more *gauche* defects than the film created at 5 seconds due to molecular packing of this monolayer film.

7.2 The effect of substrate on self-assembly rate and molecular order

As detailed in Section 2.3.1.4, an SFG signal produced for the quartz/water, quartz/air and quartz/silane interface is stronger and thus easier to optimise than the same interfaces with a sapphire substrate. It is for this reason that films which were not directly compared to the time dependant adsorption curves produced on aluminium foil were created and measured on quartz. The formation of silane films on quartz is well established in the literature, in fact to optimise a SFG signal for the C-H stretching region it is common to use an OTS modified Quartz substrate[142]. While a quartz substrate can be functionalised by silane molecules, the rate constants of silane condensation is highly dependent on the difference between the IEP of the substrate and the pK_a of the adsorbing silanols[42]. The closer the surface IEP is to the pK_a of silanes in solution, the quicker the initial adsorption rate of silane on the surface[42]. The substrate dependant structure of molecules within a film has also been shown previously using SFG[141]. The consequence of this is the rate of silane condensation on quartz substrates will differ to the rate of condensation on sapphire. As a result, all SFG samples not directly compared to the time dependent adsorption profiles of PTMS and PDMMS created on Al oxide were performed on quartz.

As the C-H stretching energy adsorption region of the propyl chain is monitored and unlike in the case of XPS silicon is not being utilised as an elemental marker for the film, the use of a silicon containing substrate is of no consequence. However, as the difference in surface IEP and silane directly impacts the rate of reaction, the time dependent propyl chain order was directly compared for quartz and

sapphire. The $CH_{3(s)}$:$CH_{2(s)}$ ratio as a function of time was measured on a semi-hemispherical quartz substrate and compared to the growth profile on sapphire.

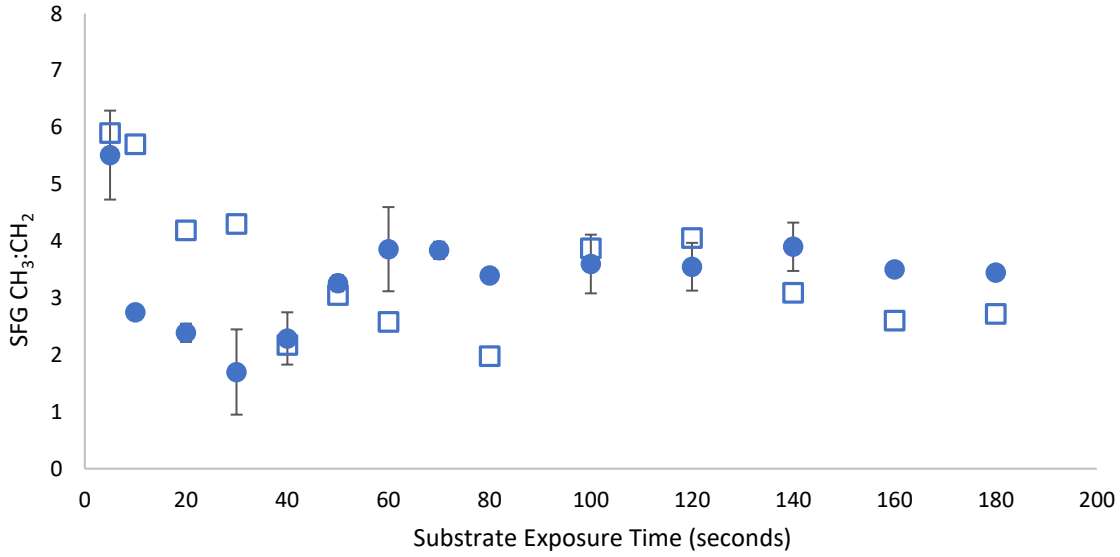

Figure 7.4: The time dependent propyl chain order (from of $CH_{3(s)}$:$CH_{2(s)}$ SFG signal intensity fit to Equation 2.11) of films created when 1%v/v PTMS in aqueous was exposed to quartz (open squares) and sapphire (filled circles) substrates. Measured using s-s-p polarisation mode.

It can be seen clearly in Figure 7.4, the rate of Si-O-substrate condensation differs between quartz and sapphire however, an oscillation is still present for quartz and is simply delayed when compared to that of the sapphire substrate. As the overall behavioural profile is the same for both films this was taken as sufficient evidence for the use of quartz as a substrate when the rate of reaction was deemed irrelevant.

7.3 The Water:Quartz interface during film formation

A key proponent in the proposed mechanism of silane film self-assembly is the role of water molecules which become trapped underneath the film. This entrapped water increases the local water concentration and causes a reversal of the condensation reaction via Le Chatelier's Principle. In order to measure in-situ film growth it is important to measure and understand the substrate-solvent interface, in this case the quartz/water interface. Du *et al.* was the first to report the quartz water interface in 1994[165] and revealed that the structure of water molecules at the quartz-solution interface depends on the pH of solution. Intensity of the hydrogen bonded OH stretching was enhanced in an alkaline solution due to the surface charge of the deprotonated silanol groups on the substrate surface. The structure of water at the quartz-water interface has also been monitored upon

modification of quartz with methyltricholrosilane (H_3C-Si-$(Cl)_3$), changing the hydrophobicity of the quartz surface[148]. The structure of interfacial water-quartz and the effect of a silanol on the structure and dynamics and structure of interfacial water on quartz[166], the structure of water at the interface between a self-assembled monolayer and water[167] and the structure of water at superhydrophobic (silane modified) quartz surfaces[148] have all monitored the structure of water following the modification of the substrate with silane films. Two peaks representing the perfectly hexagonal ice like water stretching (named ice-like) and random asymmetric O-H stretching, a conformation commonly associated with water were identified[168]. In order to determine if the presence of water trapped under the film and hence the conformation of water molecules observed at the quartz-water interface is altered during film formation, the quartz-water interface was monitored before and during PTMS film self-assembly.

Semi-cylindrical quartz substrates were pre-treated and secured in an in-situ cell as detailed in section 2.3.1.2. The O-H stretching region from 3000-3600 cm^{-1} was measured upon the exposure of a clean quartz substrate to solvent. Once the quartz-solvent interface had been measured, 1% v/v PTMS in aqueous solvent was introduced to the cell and the O-H stretching region measured over a period of approximately 20 minutes. The SFG spectra of the resulting PTMS was measured to confirm the presence of a silane film.

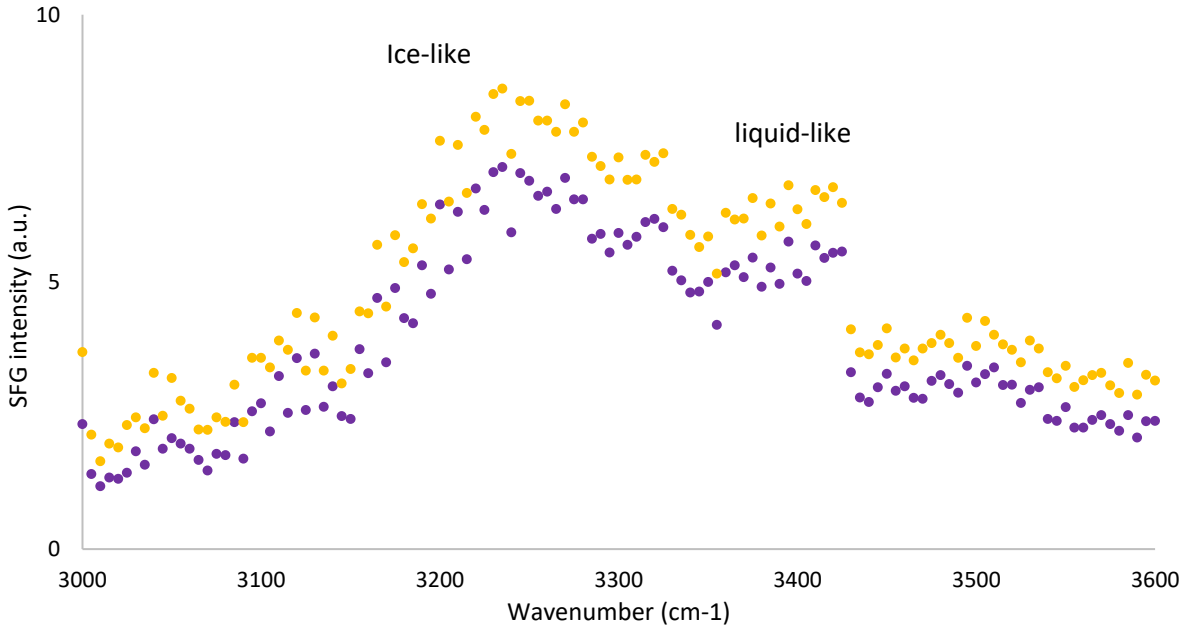

Figure 7.5: The SFG O-H stretching region of the water-quartz interface before (purple) and during (yellow) exposure to 1%v/v PTMS in water. Measureded using s-s-p polarisation mode.

Unfortunately, results do not show a difference between the conformation of water at the interface before and during film formation. This does not mean that there is no water trapped underneath the film during film growth, but that the conformation of this water does not change measurably during the self-assembly of PTMS films. This experiment was then repeated with aqueous solvent in place of Milli-Q water, and the same result observed.

7.4 Film Stability in aqueous environments

As shown in section 2.3.1.4 (Figure 2.11) the addition of water to a silane film increases the presence of CH_2 symmetric and asymmetric stretching in the resulting SFG spectrum. This decrease in $CH_{3(s)}$:$CH_{2(s)}$ may be due to the hydrophobicity of the propyl chain, which in an effort to avoid the aqueous environment alters chain conformation, causing an increase in *gauche* defects. The behaviour of these films upon the removal of water and drying with argon i.e. the recoverability of the propyl chain conformation gives an insight into the stability of these films post-production. While not directly related to the self-assembly mechanism, silane films are commonly used to modify surface hydrophobicity as a form of corrosion protection, hence the stability of these films in aqueous environments is important to consider.

The stability of PTMS films was investigated through repeated and prolonged exposures to water. An ordered film was created by exposing 1%v/v PTMS in aqueous solvent to semi-hemispherical quartz substrates for 5 seconds. The C-H stretching region was measured while the film was exposed to a dry, argon environment. Water was then introduced into the cell and the spectra measured. In order to determine the recoverability of this film, the cell was dried with argon once again and the SFG spectra collected. A comparison of these spectra is shown below;

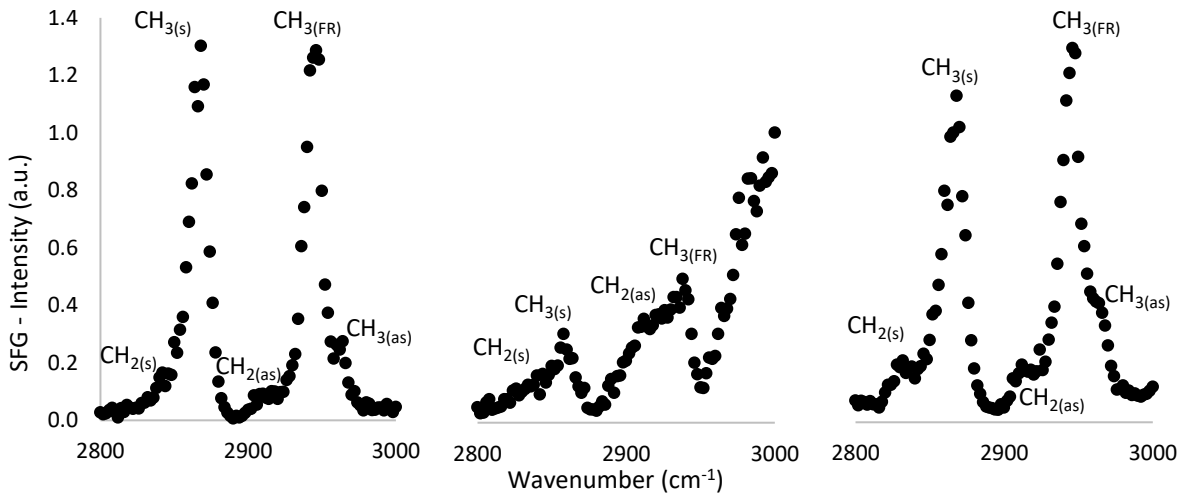

Figure 7.6: The normalised SFG C-H stretching region of a film produced when 1%v/v PTMS in aqueous solvent was exposed to a semi-hemispherical quartz for 5 seconds and dried with argon (left), exposed to water (centre) and after exposure and drying (right), measured in s-s-p polarisation mode. (as) denotes asymmetric stretching, while (s) denotes symmetric stretching and (FR) Fermi resonance.

As described in section 2.3.1.4, the addition of water to the film's environment increases both the gradient of the spectra due to interference from the neighbouring O-H stretching region and the intensity of the CH_2 peaks due to hydrophobicity of the propyl chain. While unfortunately this severe water induced distortion is not conducive to peak fitting, the recovery of these peaks once water was removed from the system and the film dried with argon allowed for films to be fit to Equation 2.11 once again, and the damage acquired during exposure to water quantified.

The recoverability of PTMS films following increasing exposure times and repeated one minute water exposures were measured. Two ordered, 5 second PTMS films were created and the initial $CH_{3(s)}$:$CH_{2(s)}$ measured. The first film was then exposed to water for increasing increments of time, dried with argon and the SFG spectra measured. The second film was repeatedly exposed to water for one minute intervals between which the film was dried with argon and the SFG spectra collected.

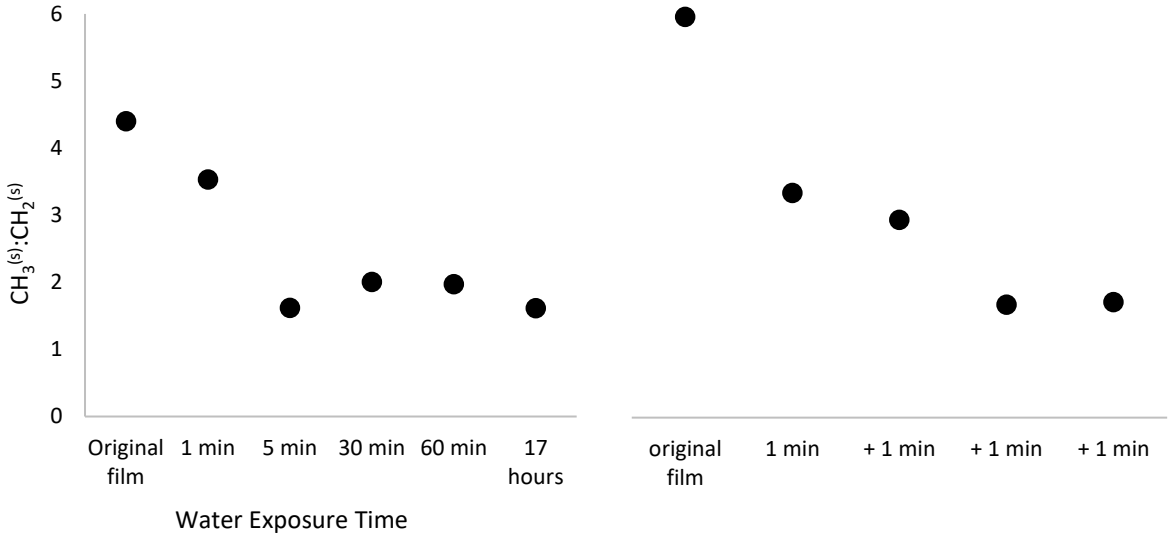

Figure 7.7: The decreasing $CH_{3(s)}:CH_{2(s)}$ of PTMS films as a result of repeated water exposure. Films were created with a 1%v/v PTMS in aqueous solvent on quartz (5 second exposure) and analysed using SFG in s-s-p polarisation mode. Increasing exposure times are shown on the left, while repeated exposures of one minute are shown on the right.

Initially the $CH_{3(s)}:CH_{2(s)}$ of both PTMS films showed a highly ordered film with minimal *gauche* defects however, the films became increasingly disordered with each water exposure. Film stability was not dependent on the length of time it was exposed to water, but rather the number of times the film was exposed and dried. This result has implications in terms of future applications of these molecules, where not only the length of time a film is exposed to water but the number of exposures essential to consider.

The position of peaks during the exposure to aqueous environment was also investigated as peaks within the C-H stretching band of alkyl groups may shift to lower wavenumbers when exposed to water, due to an increase in strain caused by an increase in *gauche* defects.

Table 7.4.1: Peak position and shift of the normalised C-H SFG stretching region upon the exposure to Milli-Q water to a film produced when 1%v/v PTMS in solution was exposed to a semi-hemispherical quartz substrate for 5 seconds, dried with argon (initial film, dry cell), exposure to water (wet cell) and after 1 repetition of exposure and drying (1 exposure repetition, dry cell). Measureded using s-s-p polarisation mode and fit to Equation 2.11.

Initial Film (dry cell)		**Wet Cell**		**1 repetition (dry cell)**	
Peak assignment	**Peak position (cm^{-1})**	**Peak shift (cm^{-1})**	**Peak position (cm^{-1})**	**Peak shift (cm^{-1})**	**Peak position (cm^{-1})**
$CH_{2(s)}$	No peak		2836	+4	2840
$CH_{3(s)}$	2868	-8	2860	+6	2866
$CH_{2(a)}$	2916	-7	2809	+9	2818
$CH_{3(FR)}$	2946	-8	2838	+8	2946
$CH_{3(a)}$	2966		No peak		2966

While a decrease in the wavenumber of the CH_2 peaks was observed, strain due to and increase in the number of *gauche* defects (due to hydrophobicity of the propyl chain) may not be the sole cause. A shift to a lower wavenumber can also indicate hydrogen bonding between the film and water molecules.

In section 7.1.1 the number of *gauche* defects in PTMS and PDMMS films was directly related to surface coverage and silane packing density of a monolayer-like film and it was initially proposed from Figure 7.6 that the increase in CH_2 symmetric and asymmetric stretching was due to the hydrophobicity of the propyl chain, supported by the increase in CH_2 symmetric and asymmetric stretching upon the addition of water to the film. Based on this knowledge it can be said that both hydrophobicity of the propyl chain and molecular packing of silane on the surface have an effect on the number of *gauche* defects measured.

7.5 The orientation and order of Propyltrimethoxysilane molecules during film self-assembly

A significant advantage of SFG over other analytical techniques is its ability to conduct in-situ measurements allowing for real time, in-situ monitoring of silane film formation. As the C-H stretching region of PTMS films cannot be accurately fit in an aqueous environment (as demonstrated in Figure 7.6), along with the measurement of the region of 2800-3000 cm^{-1} requiring a 20-minute acquisition time, the ability to repetitively and quickly measure the entire C-H stretching region is not possible.

However, the intensity of the SFG signal at a chosen wavelength can be measured as a function of time by repetitively pulsing the IR beam at a fixed wavenumber while monitoring the changing intensity of the SFG signal produced, in this case 2870 cm^{-1}. The reason for the use of the $CH_{3(s)}$ peak at 2870 cm^{-1} is 2-fold; firstly, it appears as one of the strongest and consistent peaks in the spectra of ordered (*trans* conformation) PTMS and PDMMS films and secondly, upon the addition of aqueous based solvent to the environment of the film there is little overlap between the OH stretching band beginning at approximately 2900 cm^{-1} and the $CH_{3(s)}$ peak at 2870 cm^{-1}.

An advantage of SFG over other in-situ analytical techniques is that the solvent itself does not contribute to the SFG signal, essential as the aqueous solvent used in to create films in this thesis contain CH_3 groups in the form of acetic acid and ethanol. This is not to say that the use of aqueous solvent does not have an impact on the SFG signal. As detailed in section 2.3.1.4, a change in the optical constants (refractive indices) of aqueous solvent compared to Milli-Q water reduces the intensity of the SFG signal however, there is no contribution by acetic acid or ethanol in the aqueous solvent to peaks in the C-H stretching region. The adsorption of silane onto quartz or sapphire substrates also decreases the intensity of the SFG signal with the difference in the refractive indices of air and silane reported to result in a decrease in the signal intensity by a factor of 3-4 due to the change in the Fresnel coefficients[135]. When conducting in-situ measurements the addition of water-based solvent to the in-situ cell creates a change in the Fresnel factor and decreases the intensity of the SFG signal significantly. To counteract this, quartz substrates which inherently create a stronger SFG signal were used as the rate of reaction is not considered for the in-situ measurements made in this case.

While theoretically suitable, in order to determine if the $CH_{3(s)}$ SFG signal at 2870 cm^{-1} was practically a suitable indicator of the PTMS film the IR signal was fixed and repeatedly pulsed at 2870 cm^{-1} upon the addition of solvent to a clean, dry quartz semi-hemispherical substrate in the flow cell filled with aqueous solvent (Figure 7.8(a)). The absence of a signal at 2870 cm^{-1} confirmed there is no interference in the SFG signal by the aqueous solvent. Aqueous solvent was left in the flow cell and monitoring of the $CH_{3(s)}$ SFG signal began at 0 seconds to gain a baseline. 1%v/v PTMS in aqueous solvent pushed from the syringe into the in-situ flow cell (Figure 7.8(b)).

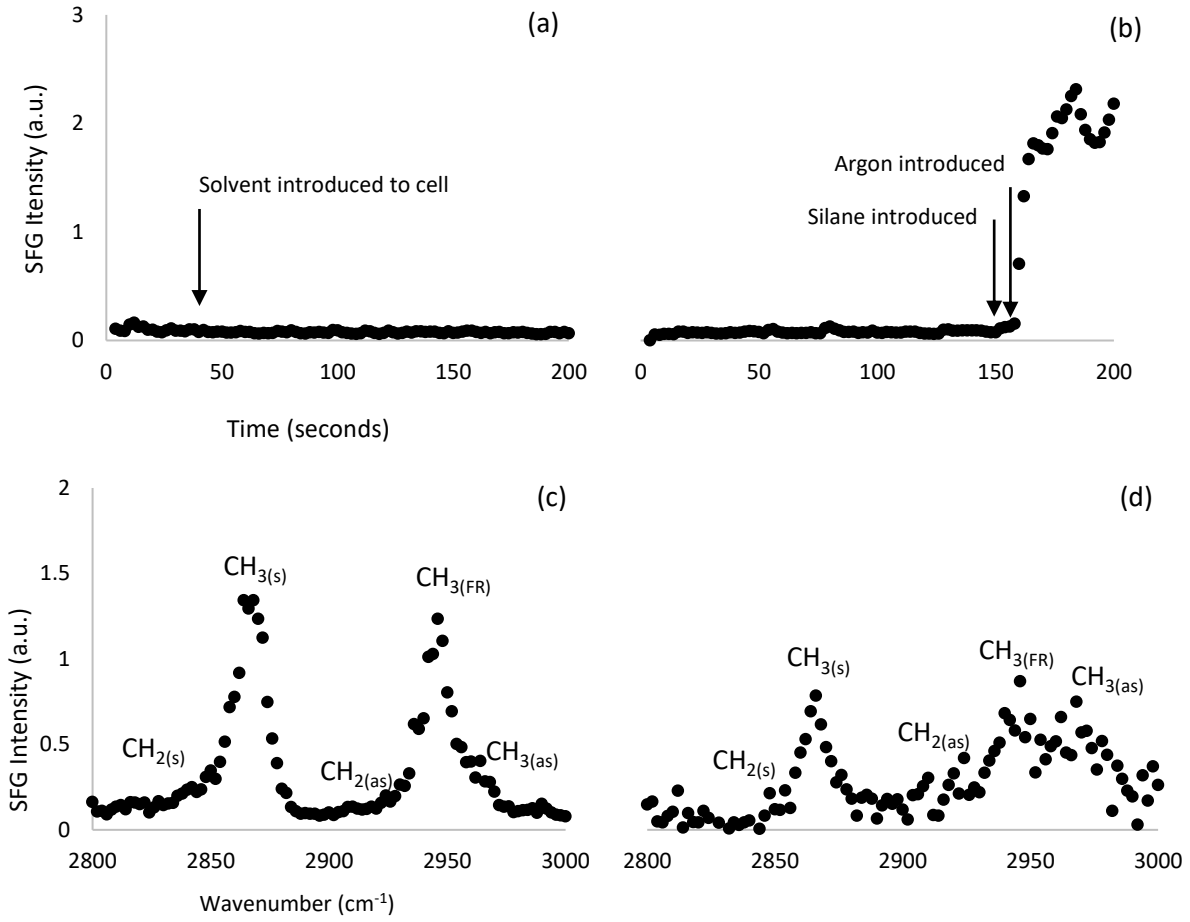

Figure 7.8: Elimination of SFG signal contribution due to the addition of solvent to a semi-hemispherical quartz substrate on the SFG signal produced for IR light repeatedly pulsed at 2870 cm^{-1} (a), the addition of 1%v/v PTMS in aqueous solvent to the cell (b), the subsequent film produced in an argon environment (c) and in the presence of silane free solvent (d).

Unexpectedly, upon the addition of PTMS to the in-situ flow cell, no SFG signal was visible at 2870 cm^{-1}. After 5 seconds argon was flushed through the system, removing the silane solution and drying the cell and the SFG signal then increased indicating that a PTMS film was present but not creating a SFG signal. The SFG spectra from 2800-3000 cm^{-1} was taken under argon and confirmed the presence of a silane film, shown Figure 7.8(c). To determine if the solvent was preventing the creation of an SFG signal, silane free solvent was reintroduced to the cell and the spectra taken once more (Figure 7.8 (d)). The ability to measure an SFG spectrum and a clear $CH_{3(s)}$ peak at 2870 cm^{-1} above any background due to the O-H stretching region in the presence of the aqueous solvent eliminated this as the cause of the SFG signal dampening in Figure 7.8(a). Any change in signal intensity at 2870 cm^{-1} due to a peak shift was eliminated by comparing the peak position upon removal of silane containing solution (Figure 7.8(c)) and in the presence of silane free solvent (Figure 7.8(d)).

The inability to measure an SFG signal when exposed to a solvent containing silane, despite the presence of an ordered film indicates a dampening element in solution during film growth. In order to determine the cause of SFG signal suppression, possible contributors to signal dampening were systematically removed from the system.

While CH groups in ethanol or acetic acid do not contribute to the SFG signal they were eliminated as the cause of signal dampening by repeating the experiment in Milli-Q water. It is important to note that the rate of reaction in Milli-Q water is not directly comparable to that in solvent due to the difference in the pH of solution affecting the rate of silane hyrolysis and condensation.

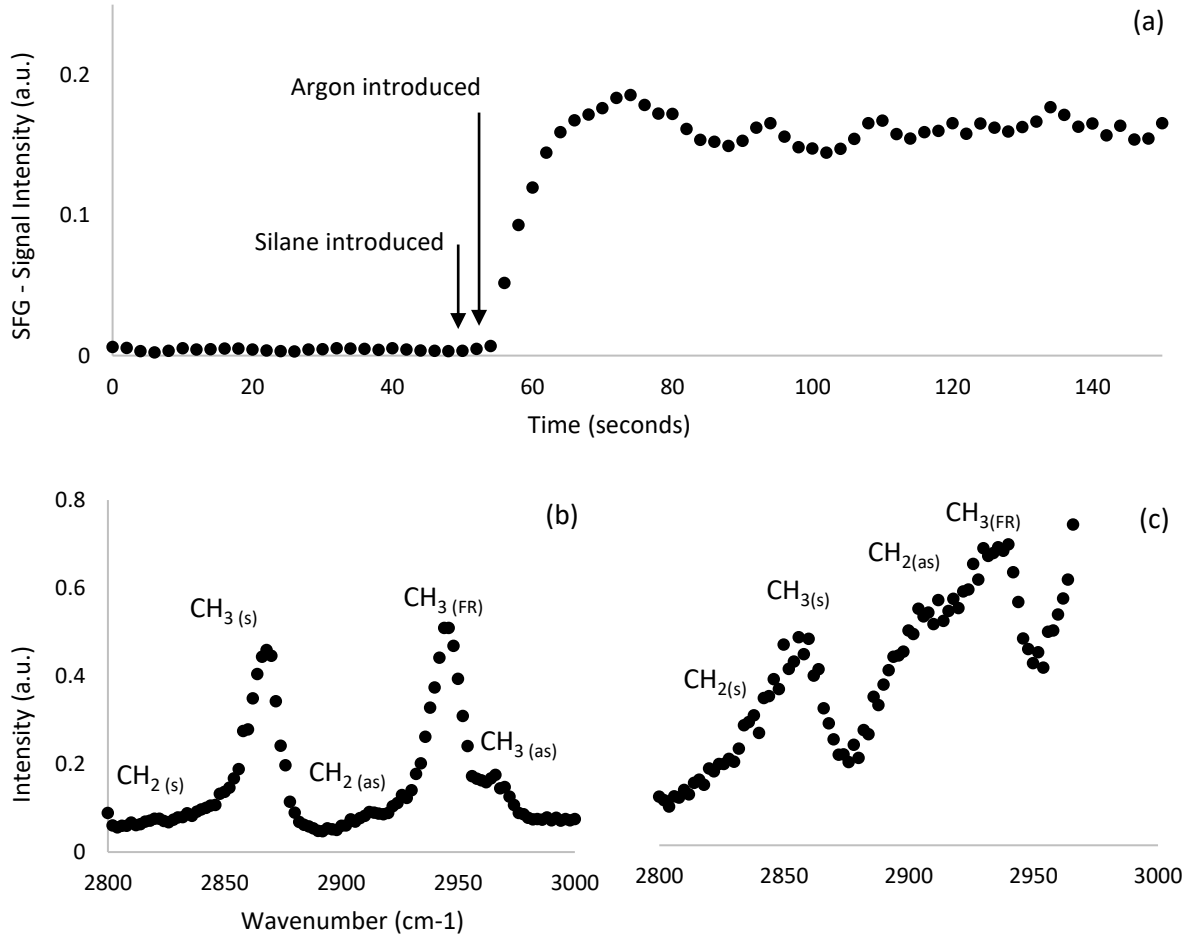

Figure 7.9: The addition of 1%v/v PTMS in Milli-Q water to a semi-hemispherical quartz substrate while monitoring the SFG signal produced for IR light repeatably pulsed at 2870 cm^{-1} (a), the subsequent film produced in an argon environment (b) and an aqueous (Milli-Q water) environment (c).

Once again, while monitoring the $CH_{3(s)}$ SFG signal at 2870 cm^{-1} for PTMS films in Milli-Q water no SFG signal was produced during film formation (Figure 7.9(a)), despite a clear spectrum present when the silane containing solution was removed (Figure 7.9(b)). The SFG signal was also shown to be present in Milli-Q water above any background due to the overlap in the O-H stretching region while being absent in a silane containing solution (Figure 7.9(c)). As the removal of silane from the solvent solution

resulted in the production of an SFG signal for silane molecules on the substrate, it was determined that silane molecules in solution were preventing the SFG being created. Due to SFG selectivity rules if a molecule contains centrosymmetry, the nonlinear susceptibility is not equal to zero and thus the generation of an SFG signal is forbidden[129]. Inversion symmetry must be broken at the interface for an SFG signal to be produced. Therefore, a logical explanation is that silane molecules in solution are orientated such that they create a centre of symmetry with molecules on the surface. This is possible that through the formation of a physisorbed PTMS layer in solution the silane molecule becomes centrosymmetric, rendering it SFG inactive. The presence of physisorbed bilayers resulting in an absence of an SFG signal has been suggested previously for stearic acid at the sodium stearate/quartz interface by Zhang *et al.*[137]. The absence of a CH_3 SFG signal in the presence of a solution containing sodium stearate and the appearance of this peak upon replacement of this solution with argon was taken to suggest the presence of either a physisorbed stearic acid monolayer with very high conformational order in sodium stearate solution or, the presence of a highly disordered film in solution. In the case presented by Zhang, the existence of a bilayer was dismissed by the introduction of deuterated stearic acid molecules to the system and an absence of a signal demonstrating this. The difference between the stearic acid/quartz interface presented by Zhang and the PTMS/quartz interface shown in Figure 7.9 and Figure 7.8 is the presence of an ordered film in both aqueous solvent and water in the absence of silane. The presence of a bilayer preventing the creation of an SFG signal is distinguished from the presence of a disordered film by measuring the SFG signal once this bilayer is removed. If a disordered film was present on the surface an SFG signal would not be created when the silane containing solvent is removed from the flow cell.

As per the thermodynamic model shown in section 1.10, the formation of the covalently bound film occurs first via the formation of a hydrogen bound film. The presence of a second physisorbed layer rendering the film SFG-inactive, along with the surface coverage of rinsed samples showing a removal of species physisorbed to the surface shown in Chapter 5, indicate that film formation occurs via hydrogen bound species and therefore it is highly possible that this occurs by the formation of a physisorbed bilayer. To confirm and further investigate the formation of this bilayer, the stability of the bilayer was tested by monitoring the signal at 2870 cm^{-1} as silane containing solvent was flushed away and replaced with a silane free solution by pushing 10 mL of Milli-Q water through the cell.

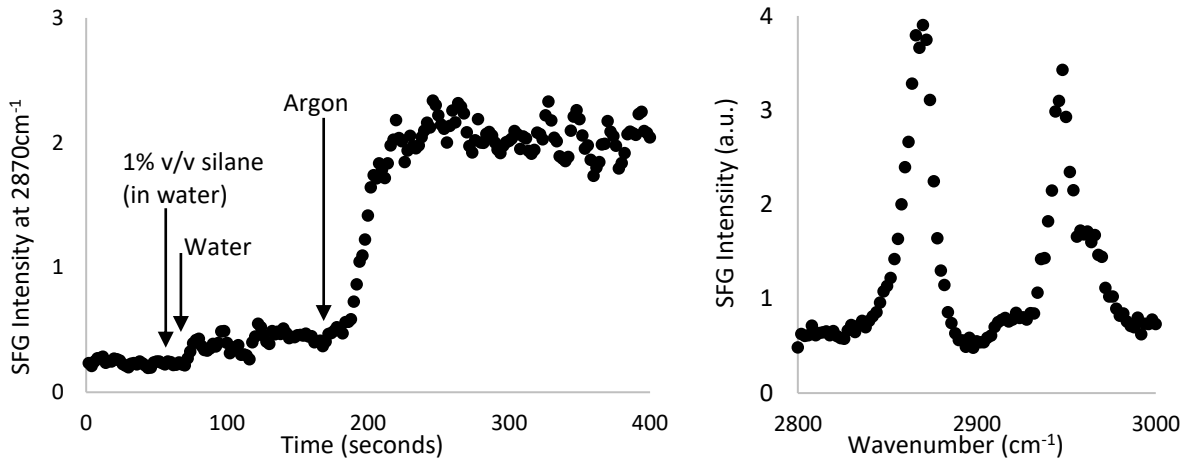

Figure 7.10: The SFG signal contribution due to the removal of Milli-Q water containing silane and replacement with silane free Milli-Q water and subsequent drying of the cell with argon to a semi-hemispherical quartz substrate on the SFG signal produced for IR light repeatedly pulsed at 2870 cm^{-1} (left). The SFG spectrum of the film produced under argon (right).

An increase in the SFG signal representing the symmetric stretching of the terminal methyl group upon removal of the silane containing solution and with it the physiosorbed bilayer, indicates the bilayer formed is very weakly bound to the film which is covalently bound to the substrate below. The conformation of the remaining covalently bound can be seen in the SFG spectra produced immediately after the in-situ measurement. The increase in signal upon removal of water and drying with argon can be attributed to both a change in Fresnel factor and the hydrophobicity of the propyl chain. Unfortunately, this confirmed in-situ measurements of PTMS and PDMMS in solution was not possible, however it provided valuable insight into the mechanism of film formation. As per the previously proposed model, the formation of the covalently bound film occurs via the formation of a hydrogen bound film.

8 Silicon-Aluminium Composite Materials by Means of Silane Functionalised Powders for 3D Printing.

Research in this chapter was made possible through award of the Nicolas Baudin Travel Grant as part of a collaboration between The French Embassy, École Centrale de Nantes, Naval Group and Flinders University under the supervision of Professor Jean-Yves Hascoët, the help of Stéphane Touzé and Dr. Raihan Rumman.

Throughout this thesis a fundamental explanation of silane-substrate condensation has been presented with the goal of developing a greater understanding of the interactions at a molecular level. It is this deeper understanding of silane behaviour which has led to the development of a new, novel application for silane molecules in the form of 3D printed Si-Al composite materials. The following chapter details the functionalisation of aluminium powders with PTMS, aswell as the effect of silane films on the physical characteristics of the powder starting materials and the resulting 3D printed product.

The ability to 3D print metals using a Laser Metal Deposition (LMD) technique has provided opportunities to decrease processing time, create intricate custom structures and reduce the presence of joint failures due to welding defects. Powdered metals are deposited and sintered in layers using a laser and are as such the process is referred to as Additive Manufacturing (a detailed description of the LMD process can be found in section 2.5). While LMD has been shown to allow the successful 3D printing of pure metals along with some alloys, the printing of composite materials has not been extensively explored. The use of metal composite materials in 3D printing is an emerging field and as the market is still currently saturated with alloys and pure metals. As detailed in section 2.5, silicon is commonly found as an impurity in aluminium alloys, however it is often added intentionally to improve the fluidity and castability[76]. It is common for cast alloys to contain anywhere from 5 to 22% silicon as at 12.5%wt Si a eutectic composition is reached[78-80].

8.1 Flowability of Propyltrimethoxysilane functionalised Al powders.

A key physical property of metal powders required for them to be compatible in Laser Metal Deposition (LMD) 3D printing is flowability. As detailed in section 1.11, the typical granulometries of metal powders used for LMD printing sit in the rage of 40-90 µm to ensure adequate melting and fusion[169], making the use of aluminium powders challenging. The flowability of these powders is related to the weight, surface energy and surface roughness of these particles with fine aluminium particles agglomerating naturally due to weak van der Waals forces[89-91,98]. While theoretically, increasing the weight of these particles by increasing their size would increase the flowability, this would have a detrimental impact on the complete melting of particles during the printing process. Altering the surface energy of these particles through coating or functionalising the surface of metal powders has been shown to increase the flowability significantly[92,94].

Despite this knowledge, the flowability of aluminium powders continues to be a challenge in LMD 3D printing. In an attempt to increase the flowability of aluminium powders with the goal of creating printable starting materials, aluminium powders were functionalised with PTMS films. Three unique Al powders were chosen for silane functionalisation based on their potential for LMD 3D-printing and used to determine the impact of powder composition and granulometry on the improved flowability using PTMS films. All three powders were produced using a gas atomisation process containing at least 94% aluminium with granulometries ranging from 23-100 µm. Each powder was given a reference number, for this report the details of which are reproduced from section 2.4.1 for ease of reference and shown below;

Table 8.1.1: Elemental composition and granulometries of powders used for PTMS functionalisation and LMD 3D printing.

Powder Number	Composition	Particle size (µm)
1	$Al_{(94\%)}Cu_{(5\%)}$-$Mg_{(0.33\%)}$	20-63
2	$Al_{(95\%)}$ $Cu_{(5\%)}$	63-80
3	$Al_{(95\%)}$ $Cu_{(5\%)}$	80-100

The composition of powder 1 differs in composition to powders 2 and 3. The presence of copper instead of magnesium may have an impact on the rate of silane condensation however, as the exposure time of powders to the silane containing solution is 1-hour, the difference in rate of reaction is unlikely to have an impact on the amount of silane condensed onto the surface at this scale. Chemical analysis supplied by Aeromet International revealed the presence of Si, Fe, B, Ti and Ag trace elements within the powders, each less than 0.08%, also unlikely to affect the condensation of silane on the surface.

In order to simplify the functionalisation process and move towards a more cost efficient, greener production the entire process was performed in distilled water. All 3 powders underwent the same processing procedure, with the creation of an aluminium powder slurry facilitating PTMS functionalisation (as detailed in section 2.4.1). As the rate of reaction and film growth is not directly compared to other films in this thesis, alterations to solvent composition and experimental procedure in order to optimise the process for this application is of no consequence. The morphology and distribution of these powders was imaged using Scanning Electron Microscopy (SEM) and the presence of silane on the Al powders confirmed using Electron Dispersive X-ray spectroscopy (EDS). An example of EDS spectra for powder 1 with a Si concentration of 7.1% in the area sampled is shown in Figure 8.1. As with XPS and AES, silicon was exploited as an elemental marker in the PTMS film and its presence taken as conformation of successful functionalisation as shown in Figure 8.1.

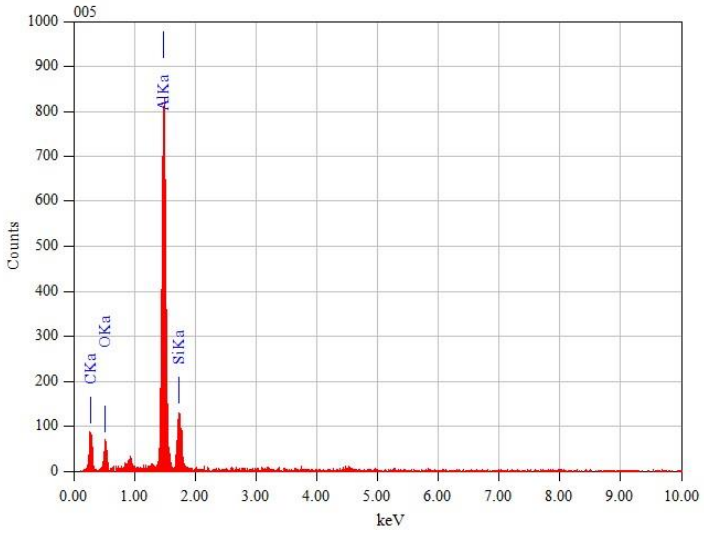

Figure 8.1: EDS spectra of PTMS functionalised Al powder (powder 1) confirming the presence of successful silane functionalisation at 7.1% Si.

The presence of PTMS on the surface of all three Al powder particles was confirmed using SEM-EDS with EDS spectra collected for multiple particles within each powder functionalised. The concentration of silicon ranged between 3% and 12% (Si:(Si+Al) values between 0.11 and 0.31 for comparison to film coverages reported throughout this thesis) in the areas sampled. It is important to note that this concentration of silane is only true for the surface of each particle and does not incorporate silane into the bulk of the particle. It is because of this that concentrations quoted cannot be taken as equivalent to that of an Al-12Si alloy where 12% of the entire particle is silicon. This becomes important when attempting to create materials with eutectic regions created by 12% Si in the matrix.

SEM imaging of powders pre- and post-PTMS functionalisation were used to determine impact of the functionalisation process on the shape or size distribution of individual Al powder particles. A direct comparison between unmodified (left) and PTMS functionalised powders (right) are shown for each powder with a 500 µm Field Of View (FOV) revealing distribution of particles and either a 100 µm or 50 µm FOV revealing surface features of individual particles.

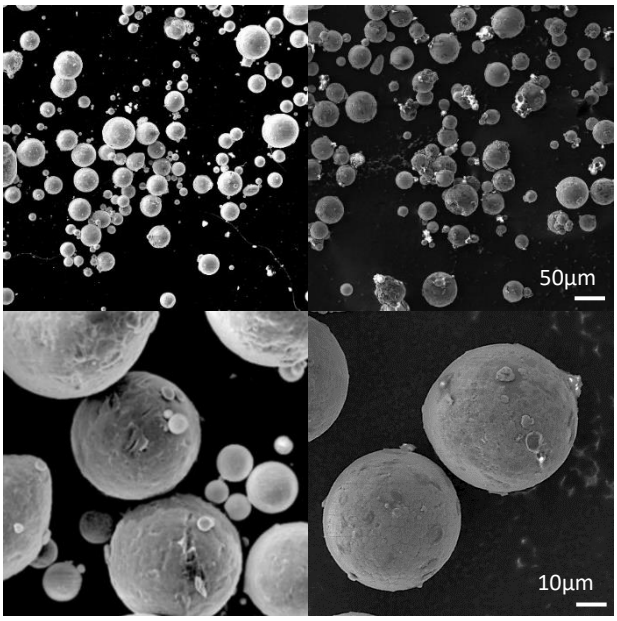

Figure 8.2: SEM images of powder 1, Al-Cu-Mg (20-63 µm). Particles modified with PTMS are shown on the right, while unmodified powders are shown on the left.

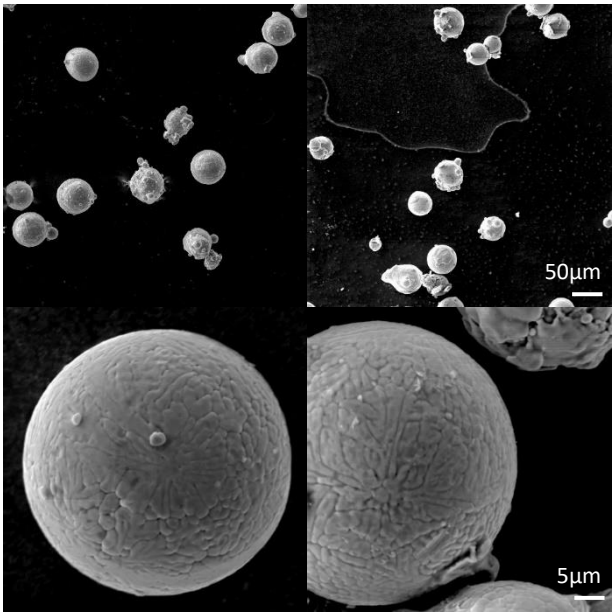

Figure 8.3: SEM images of powder 2, Al-Cu (63-80 µm). Particles modified with PTMS are shown on the right, while unmodified powders are shown on the left.

Comparative SEM images of powders 1 and 2 reveal approximately spherical particles with granulometries within the rage specified for each powder.

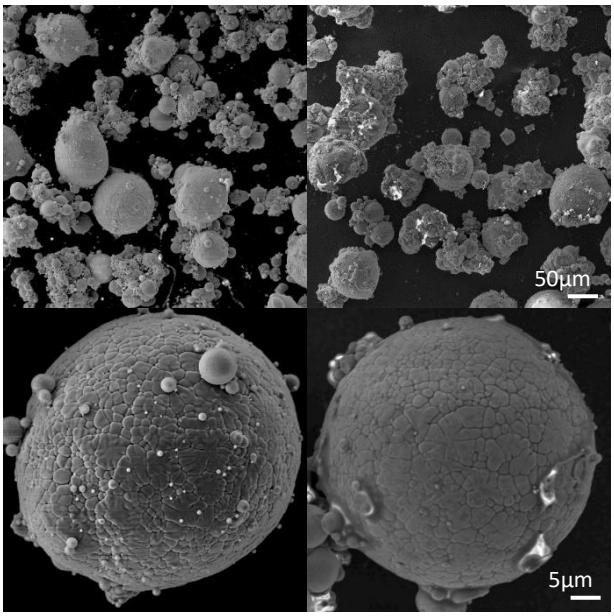

Figure 8.4: SEM images of powder 3, Al-Cu (80-100 µm). Particles modified with PTMS are shown on the right, while unmodified powders are shown on the left.

500µm FOV images for powder 3 shown in Figure 8.4 reveal spherical particles similar to those seen for powders 1 and 2 however, imaging of powder 3 also reveals considerably more satellite shaped particles and agglomeration of smaller particles which may have an effect on the LMD melting and remelting stages. However, SEM imaging of these powders pre- and post-silane functionalisation reveal no change in the shape or granulometries due to the processing required to functionalise the surface. This is crucial as agglomeration of particles will result in a reduction in flowability. Comparative microscopic imaging is also important as it can now be said that any change in physical characteristics such as flowability is due to a change in the surface energy of these particle as a result of PTMS on the surface and not as a result of changes in particle shape or size incurred during the functionalisation process.

In order to determine the impact of PTMS surface functionalisation on the flowability of modified particles, the time taken for 150 g of both modified and unmodified powder to pass through a 5 mm Carney aperture of an LPW PowderFlow standard flowability test kit were compared. The flowability of each powder was measured in triplicate and the average improvement calculated as a percentage of the unmodified powder.

Table 8.1.2: The time taken for both PTMS modified and unmodified Al powders to flow through a 5 mm Carney Flow aperture of a LPW PowderFlow standard flowability test kit. Flow times are the average of 3 replicates with the average improvement calculated as a percentage of the unmodified powder flow rate.

Powder	Modification	Successful Flow	Ave flow time (sec)	% improvement
1	Unmodified	No	-	-
	PTMS	Yes	10.1 ± 0.4	
2	Unmodified	Yes	9.0 ± 0.5	11
	PTMS	Yes	8.0 ± 0.08	
3	Unmodified	Yes	8.0 ± 0.3	43
	PTMS	yes	4.5 ± 0.4	

Unfortunately powder number 1 did not flow through the aperture and although the conversion to a flowable powder through PTMS functionalisation demonstrates a significant improvement in flowability, the % improvement could not be quantified. Following the successful flow through the Carney aperture, powders were passed through the smaller, Hall aperture.

Table 8.1.3: The time taken for both PTMS modified and unmodified Al powders to flow through a 3 mm Hall Flow aperture of a LPW PowderFlow standard flowability test kit. Flow times are the average of 3 replicates with the average improvement calculated as a percentage of the unmodified powder flow rate.

Powder	Modification	Successful Flow	Ave flow time (sec)	% improvement
1	Unmodified	No	-	-
	PTMS	Yes	71.0 ± 1.8	
2	Unmodified	Yes	64.7 ± 2.5	15
	PTMS	Yes	54.3 ± 1.25	
3	Unmodified	No	-	-
	PTMS	yes	24.0 ± 0.05	

As the unmodified powders 1 and 3 did not flow through the Hall Flow aperture, Carney aperture flow rates are used to determine the improvement in flow for these powders. As the average improvement for the Hall and Carney apertures vary slightly for powder 2, the % improvement has been given as a range (11-15%) which represents the average of 3 replicates using each aperture.

Table 8.1.4: Flowability improvement following PTMS functionalisation of aluminium powders measured using a an LPW PowderFlow standard flowability test kit.

Powder	% Improvement in flow, Carney	% Improvement in flow, Hall
1	-	-
2	11	15
3	43	-

The improvement in flow rate recorded for all 3 powders was deemed significant enough to allow for LMD 3D printing.

8.2 LMD 3D Printing of Silane Functionalised Al Powders

While the addition of silane films to the aluminium powders improved flowability such that these powders printable using LMD, it was then thought that the addition of silane to the surface of Al powders may result in the incorporation of silicon into the printed material. As silicon is commonly added to aluminium to improve both castability and wear resistance[76], the addition of silicon to aluminium LMD 3D printed materials has proved cumbersome. Current methods include the addition of silicon carbide[86] powders and the use of Al-Si powders created using a gas atomisation process. The successful incorporation of silicon into the printed aluminium material as well as a method of improving the flowability of these powders using silane films could prove revolutionary in the LMD 3D printing field.

While the flowability of powders is essential for LMD printing, the modification of powders required the re-optimisation of printing parameters including laser power, flow and processing rate. As described in section 2.5, multiple cubes were printed for each powder, labelled A through F with vertical and horizontal wall height optimised for each sample, the details of which are reproduced from section 2.4.1 for ease of reference.

Table 8.2.1: List of 3D-printed PTMS functionalised aluminium samples, their corresponding starting materials and printing wall height parameters.

Printed Sample	Powder	Programmed layer height (mm)
A	1	0.3
B	1	0.2
C	2	0.2
D	2	0.2
E	3	0.2
F	3	0.16

Two samples were printed for each powder with adjustments made to the wall height. Powder 2 was difficult to print with as despite the powder flowing easily through the LMD reservoir, it became stuck in the printing nozzle and began to burn at the nozzle outlet. This will require further optimisation if this powder is to be printed with in the future. Samples were then cross sectioned, mounted in a mixture of conductive copper filled polymer and Bakelite, polished and etched in Keller's reagent as outlined in section 2.5.

The etched surface cross sections of samples A, C and F were investigated for porosity, fusion bands and presence/dispersion of silicon. A 500 µm FOV taken for each surface was used to determine macroscopic details on the surface such as fusion bands between the substrate and 1st layer as well as between subsequently printed layers. The direction of build and porosity were also identified. Smaller areas of each surface (highlighted in the yellow squares in Figure 8.5, Figure 8.7 and Figure 8.9) were mapped using AES to determine the presence and distribution of silicon on the surface. AES maps are created through the accumulation of spectra for each pixel within the map and reveal the relative intensity of either silicon or aluminium on the surface. As in Chapter 6, maps are shown in thermal colour mode with pixels representing the highest relative intensity shown in white, while lowest relative intensities are shown in black. These maps were then directly compared to SEM images of the same area. While other elements are present on the surface of both powdered starting materials and printed materials, aluminium is taken as an elemental marker in the powder starting material while silicon can be exploited as an elemental marker in silane and as such, only Si_{KLL} and Al_{KLL} maps are shown. When printed, the presence of silicon on the surface is of paramount importance as this will confirm the successful incorporation of silicon in to the printed material via PTMS functionalisation and the creation of a new, novel composite material. The morphology of the printed samples was

imaged using SEM and the presence of silicon within the printed bulk material was determined using AES.

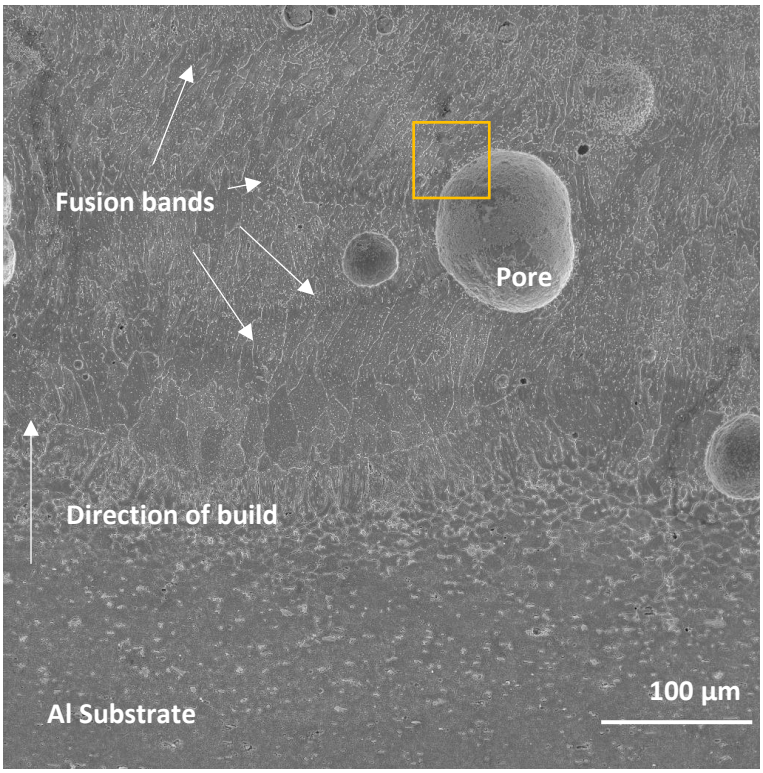

Figure 8.5: SEM image of 3D-printed sample (A) from PTMS functionalised $Al_{(94\%)}Cu_{(5\%)}Mg_{(0.33\%)}$ (20-63 µm) starting powder using a wall height 0.3 mm. FOV 500 µm. The yellow square represents the area imaged and mapped using AES in Figure 8.6.

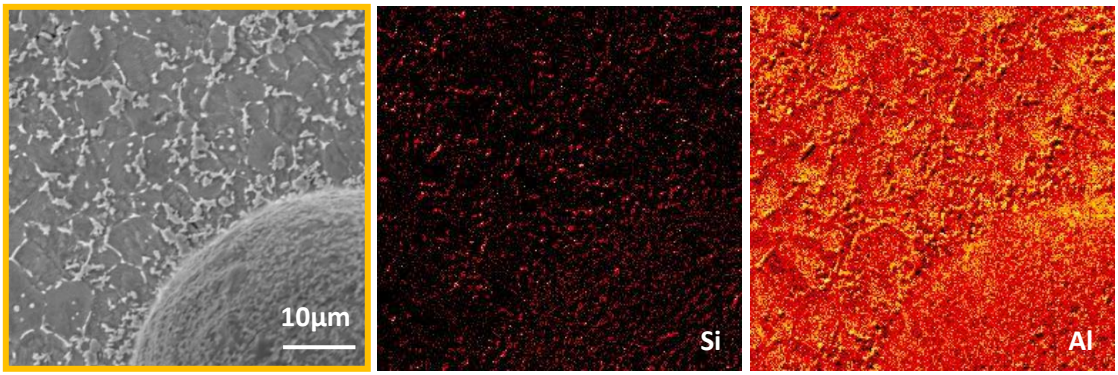

Figure 8.6: SEM image (left) and AES Si_{KLL} (middle), Al_{KLL} (right) relative intensity elemental maps of 3D-printed sample (A) from PTMS functionalised $Al_{(94\%-)}Cu_{(5\%)}$-$Mg_{(0.33\%)}$ (20-63 µm) starting powder using a wall height 0.3 mm. FOV 50 µm.

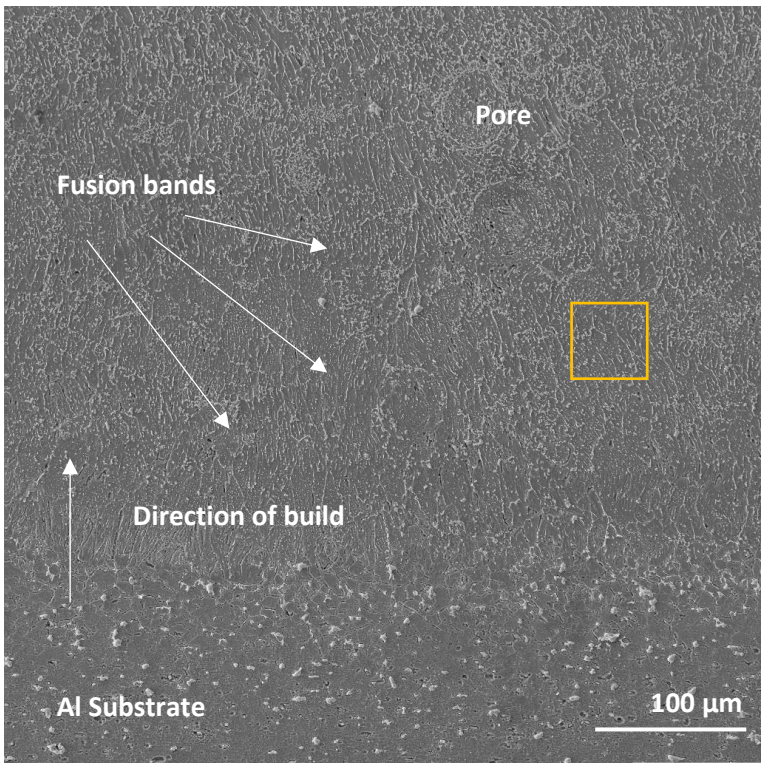

Figure 8.7: SEM image of 3D-printed sample (C) from PTMS functionalised $Al_{(95\%)}$ $Cu_{(5\%)}$ (63-80 µm) starting powder using a wall height 0.2 mm. FOV 500 µm. The yellow square represents the area imaged and mapped using AES in Figure 8.8.

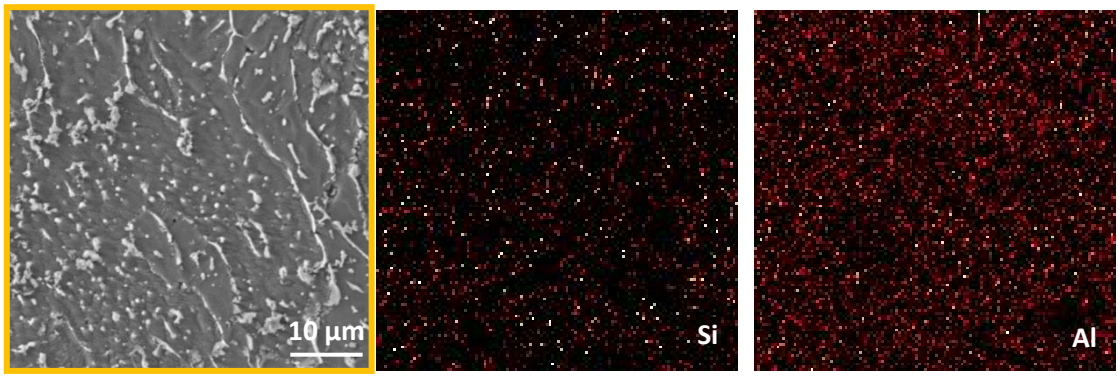

Figure 8.8: SEM image (left) and AES Si_{KLL} (middle), Al_{KLL} (right) relative intensity elemental maps of 3D-printed sample (C) from PTMS functionalised $Al_{(95\%)}$ $Cu_{(5\%)}$ (63-80 µm) starting powder using a wall height 0.2 mm. FOV 50 µm.

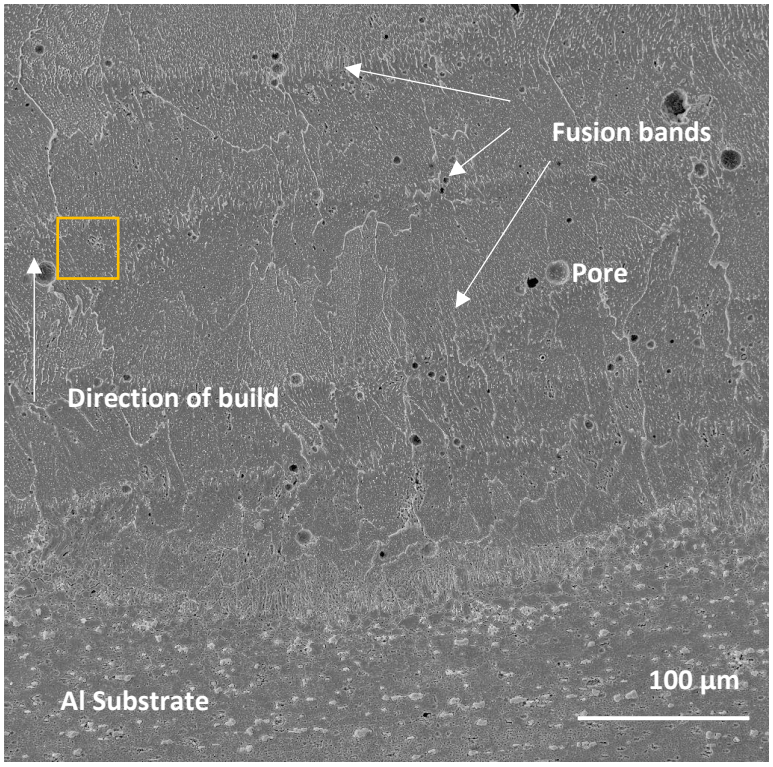

Figure 8.9: SEM image of 3D-printed sample (F) from PTMS functionalised $Al_{(95\%)}$ $Cu_{(5\%)}$ (80-100 µm) starting powder using a wall height 0.16 mm. FOV 500 µm. The yellow square represents the area imaged and mapped using AES in Figure 8.10.

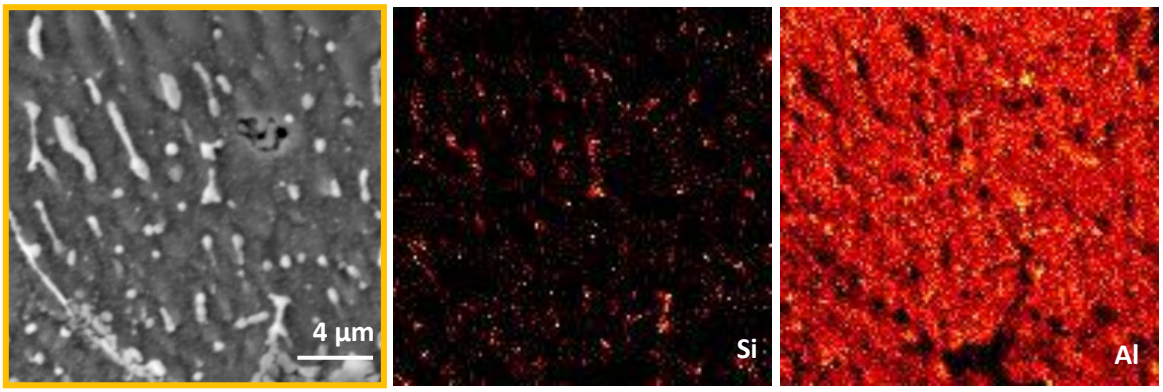

Figure 8.10: SEM image (left) and AES Si_{KLL} (middle), Al_{KLL} (right) relative intensity elemental maps of 3D-printed sample (F) from PTMS functionalised $Al_{(95\%)}$ $Cu_{(5\%)}$ (80-100 µm) starting powder using a wall height 0.16 mm. FOV 20 µm.

SEM imaging and AES elemental surface mapping of all samples created using PTMS functionalised Al powders show not only the successful incorporation of silicon into the printed material but also Al-Si eutectic regions on the surface consistent with eutectic regions observed on the SEM images. Typically identified using SEM imagery alone, AES mapping allows for the confirmation of this assumption but also shows the distribution of silicon on the surface. The successful incorporation of silicon into the printed material confirms a new method achieving Si-Al eutectic regions as well as the creation of a new, novel material 3D printed material. Other macroscopic characteristics of the printed material were then investigated.

Fusion bands present in all three printed samples analysed are caused by the insufficient remelting of the previously deposited layer result in the formation of new grains instead of continuing with the same grain structure as the pervious layer. It is for this reason that fusion bands consist of both course and fine microstructures. These fusion bands are most prominent in sample (F), indicating that samples (A) and (C) have a more cohesive grain structure.

Porosity in the printed products caused by shrinkage of liquid during cooling and solidification is present in all three samples but is especially prominent in Sample (A). Porosity of Sample (A) is considerably greater than the porosity of samples (C) and (F) with large pores ranging in the 50-100 μm region commonly observed. While the porosity of (C) and (F) remain small, sample (F) contains a higher portion of voids in the 10 μm range. Both porosity and voids affect not only the structural integrity of the material but also weight. In order for this to be prevented, the produce must be cooled very slowly as an increase in porosity may indicate a decrease in the rate of solidification. While porosity does decrease some aspects of structural integrity it may also be advantageous to reduce the weight of materials and thus, it is not necessarily important to eliminate porosity, but rather to control it.

The functionalisation of aluminium powders with PTMS has been shown to increase the flowability of these powders and allow for 3D printing using Laser Metal Deposition. This same functionalisation process allowed for the successful incorporation of silicon into the printed material and the creation of Al-Si eutectic regions. While these results are simply preliminary and comprehensive optimisation of the coating process along with the impact of this method on the physical and mechanical properties of the printed materials is required, this method shows great promise and opportunity for expansion in the future.

9 Conclusions.

i stand
on the sacrifices
of a million women before me
thinking
what can I do
to make this mountain taller
so the women after me
can see farther

legacy – rupi kaur

The original contribution to knowledge presented in this thesis has given a greater insight into the mechanism by which organosilane molecules interact with hydroxylated surfaces to condense and form thin films and sheds a light on the self-assembly process on a molecular scale. This has been achieved by presenting a comprehensive picture of silane-substrate interactions through both the ex-situ and in-situ monitoring organosilane films throughout the self-assembly process. The impact of this research has been demonstrated through the functionalisation of aluminium powders enabling for LMD 3D printing of these powders as well as the creation of a new, novel 3D printed composite material.

Based on the initial results presented in this thesis it was proposed that it is a combination of the equilibrium condensation reaction required for silane film growth and the ability of silane molecules to oligomerise which enables the desorption of films from the surface. And as such, an increase in the local water concentration caused by entrapment of water following condensation of silane islands in PTMS and PMDMS films and the hydrophilicity of a hydroxylated substrate, can cause a shift in equilibrium, reversal of the condensation reaction and result in the oscillatory behaviour observed using XPS. This coincided with the absence of such behaviour for the monomethoxy silane, PDMMS. These results led to an extensive investigation into the mechanisms of organosilane film self-assembly and the following conclusions drawn;

In terms of the mechanisms involved in the film growth of all three silanes, there are a few noteworthy factors to consider;

Firstly, the formation of oligomers on the surface seems most plausible as large oligomers bound to the substrate by one or a few bonds are more easily removed and would explain the dramatic and measurable oscillations in coverage observed. AES elemental maps confirmed this morphology by monitoring the film at key points along the adsorption curves as a function of substrate exposure time, as well as the differing rates of self-assembly and oligomerisation for PTMS, PMDMS and PDMMS. As silane molecules of PTMS and PMDMS oligomerise, large silane islands begin to form on the surface and it is the continued desorption, growth and re-adsorption of these islands that contributes to the measurable oscillatory growth observed. The formation of a stable thin, homogenous film along with the presence of silane islands, whose numbers vary collectively during the adsorption/desorption mechanism, was also shown to be present on the surface of both PMDMS and PTMS films using AES. The formation of two different types of films on the surface, highly ordered monolayer like film and large oligomer islands along with the behaviour of individual molecules within this monolayer was determined using SFG. Initial oscillations in surface coverage was found to involve the monolayer-type film, but this quickly stabilises, and the continued oscillatory behaviour is then due to the continued adsorption and desorption of large, disordered silane oligomer islands.

The growth mechanism of monomethoxy PDMMS however, differs greatly from PTMS and PMDMS. Due to its inability to simultaneously oligomerise with other PDMMS molecules and condense to the substrate, the morphology of the PDMMS film remains consistent with that of a monolayer. A Langmuir-type adsorption profile was measured using XPS and film morphology resembling a monolayer mapped with AES. Much like PTMS, when hydrolysed PDMMS molecules absorb to the substrate as monomers, the propyl chain order is dependent on molecular packing on the surface which also stabilises as surface coverage stabilises. The consequence of this mechanism is such that the inability to oligomerise results in PDMMS films resembling a Langmuir growth mechanism, while silanes with the ability to oligomerise create a time dependent oscillation in surface coverage. Despite this, PTMS and PMDMS films behave most like a monolayer during the early stages of film growth, prior to silane oligomerisation. Once the highly ordered monolayers of PTMS and PMDMS films become stable and the continued oscillation in surface coverage is due to the adsorption and desorption of silane oligomers.

Similarly, the amount of silane on the surface is directly related to the ability of silane molecules to oligomerise and the extent to which this occurs. Highest surface coverages occur for PTMS films following 1-hour hydrolysis and reduce as oligomerisation is reduced through both hydrolysis time and number of hydrolysable groups. Once again, the impact of these is not equivalent; a reduction in

hydrolysis time does not reduce the amount of silane on the surface as significantly as reducing the number of hydrolysable groups.

The rate of silane condensation on a substrate has been linked to the difference in IEP and silane pK_a. The SFG $CH_{3(S)}$:$CH_{2(S)}$ signal intensity values were compared for the formation of the PTMS films as a function of time. The oscillation is still present for quartz but delayed when compared to that of the sapphire substrate however, the rate of reaction differs greatly between quartz and sapphire. Despite this, the overall behavioural profile is the same for both films. This was taken as sufficient evidence for the use of quartz as a substrate when the rate of reaction was deemed irrelevant.

Secondly, the rate of reaction is driven by different factors as the reaction progresses. The rate of initial surface condensation is driven by the probability of successful interactions between hydrolysed groups, while the rate of oscillation following this initial condensation is driven by the rate of oligomer growth. Initially a large number of hydrolysable groups results in an increased rate of reaction, but this quickly slows as oligomers swell in size and mobility both in solution and on the surface becomes restricted. The rate of silane-substrate condensation is also different from silane-silane condensation, otherwise monotonic growth would occur, and oscillations in surface coverage would not be observed.

Thirdly, removal of physisorbed species from the surface of PDMMS films confirmed the thermodynamically favourable two-step mechanism and the rate of conversion form hydrogen bound to covalently bound species was inferred. Extension of this method to the time dependent oscillatory adsorption of PTMS and PMDMS films revealed the role of both physisorbed and covalently bound species in the self-assembly mechanism. The persistence of an oscillatory behaviour in the absence of physisorbed species and conformed to the proposed mechanism.

And lastly, in-situ SFG measurements revealed the presence of a physisorbed bilayer during film formation. While the presence of this bilayer made measuring the in-situ intensity of the SFG signal impossible, it gave valuable insight into the mechanism of film formation. A physisorbed bilayer, while not being reported previously for PTMS films is supported by the thermodynamically favourable two-step hydrogen bound to covalently bound mechanism and supports the proposed mechanism of film formation. This two-step mechanism was also demonstrated through the fit of the time dependent PDMMS adsorption profile to a 2-component model. The conversion of Hydrogen bound species θ_1 to covalently bound θ_2 fit the Langmuir-type adsorption profile of the monomethoxy PDMMS. Crucially,

the 10-component model created to demonstrate the multiple oscillation observed experimentally for PTMS, was based on the well-known and widely accepted Langmuir adsorption mechanism and is supported by the known mechanism of silane condensation. The model used to describe the multiple oscillations in PTMS and PMDMS film self-assembly require additional components beyond the 3-component model originally designed to fit the single oscillation previously observed[23,41]. For each adsorption and desorption observed experimentally, two additional components are required to model the oscillation mathematically. The kinetics of these interactions were proposed and determined through the creation of this 10-component model, which highlighted the presence of competing silane-substrate and water-substrate interactions and confirmed that for each oscillation there must be two additional components present in solution in the form of a silane species and a non-silicon containing species thought to be water.

The accumulation of knowledge presented in this dissertation and the deeper understanding of silane film self-assembly allowed for the design and implementation of a new application for silane molecules, and as a result, the creation of a novel Si-Al composite material. The functionalisation of aluminium powders with Propyltrimethoxysilane was shown to increase the flowability of these powders by altering surface energy with no distortion to morphology or granulometries. The increase in flowability of all three aluminium powders was significant enough that it allowed for the 3D printing of these powders using LMD where unfunctionalized versions of the same powders were deemed unprintable. This same functionalisation process allowed for the successful incorporation of silicon into the printed material and the creation of Al-Si eutectic regions commonly created using a mixture of silicon carbide and aluminium powder starting materials. While the application of silanes in this manner is in its preliminary stages, it has already shown great promise in improving the physical properties of the starting material and as a new method of incorporating silicon into 3D printed aluminium structures.

An extensive investigation into the mechanisms of organosilane film self-assembly has given a greater insight into the key factors which contribute to the unusual adsorption behaviour observed. This knowledge has led to a new area of silane applications and the advancement of an existing field of additive manufacturing.

9.1 Recommendations for future work

9.1.1 Further investigation in the mechanism of organosilane film formation

While an in-depth investigation into the mechanism of silane film self-assembly has been presented throughout this thesis, there are further inquiries beyond the work shown above which could help to confirm the proposed mechanism; one such area of research involves slowing the rate of reaction. Throughout this thesis the aqueous solvent used to facilitate silane hydrolysis and condensation was reduced to pH 3 in an attempt to reduce the rate of condensation. As the self-assembly of organosilane films requires hydrolysis followed by condensation, which both sit in their own dynamic equilibrium, it is important to consider both processes when attempting to further decrease the rate of self-assembly. Consequently, pH 3 is also where the rate of hydrolysis is at its fastest[1].

While there is no optimum pH where the rate minimum of both hydrolysis and condensation lies, there are other methods available to reduce the rate of reaction and involve reducing the amount of water present in the solvent. The first method requires the creation of silane films in toluene or a similar anhydrous solvent in order to determine if the oscillatory behaviour is caused by an increase in the local water concentration due to water created as a result of the condensation reaction being trapped underneath the film. Preliminary experiments have been conducted by exposing PTMS molecules to toluene to create a 1%v/v silane in solution, a small amount of water is added to the system to initiate the hydrolysis reaction. If the oscillation in surface coverage is still present in the growth mechanism of these silanes, it would once again give weight to the proposed mechanism. Slowing the rate of reaction may also reveal the presence of oscillations aliased in aqueous solvent.

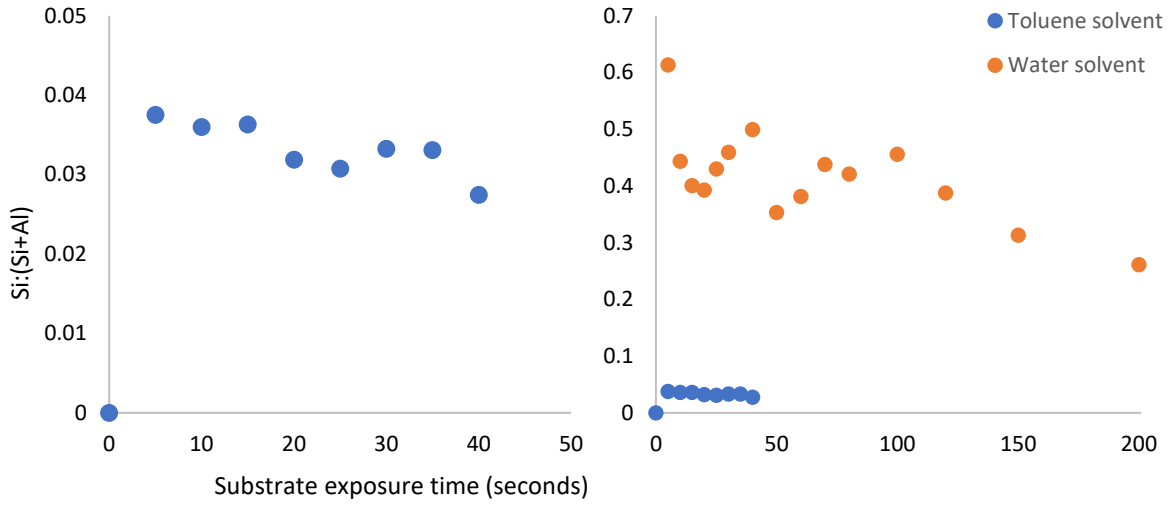

Figure 9.1: The time dependent adsorption profile of 1% v/v PTMS in toluene on diamond polished aluminium foil substrates, without a hydrolysis time (left). Each data point represents a single measurement of a single silane film. The direct comparison of PTMS films created under aqueous solvent presented in section 3.2.2 and toluene is shown on the right.

While confirming that replacing an aqueous solvent with toluene reduces the rate of reaction, the surface coverage of PTMS films is so low that no clear trend can be discerned from the data presented in Figure 9.1. Given the significant reduction in PTMS surface coverage exposure times and sample rate will need to be extended. Auger elemental mapping of these surfaces will also reveal the morphology of these films and support or refute the proposed mechanism of silane film self-assembly.

The second method of reducing the rate of reaction involves reducing the ethanol:water ratio in the aqueous solvent. The effect of reducing the amount of water on the rate of hydrolysis has been reported by Watts *et al.*[32]. The rate of hydrolysis was measured using H^1NMR for different methanol:water ratios in the solvent. By increasing the ratio of methanol:water to 9:1, the rate of hydrolysis began to decrease, while a 100% methanol solvent stopped the reaction completely. While the adsorption profile obtained experimentally for PDMMS was shown to fit a 2-component model in Chapter 4 and molecules are less likely to become trapped under the monolayer film, it is possible for PDMMS molecules to desorb from the surface as an increase in the local water concentration could also be due to the hydrophilicity of the hydroxylated substrate. This would occur if a hydrogen bound PDMMS molecules were to be displaced by a water molecule either before or after conversion to a covalently bound species. As PDMMS molecules are only actively present as monomers in solution allowing a single PDMMS molecule to displace an equivalent monomer on the surface. By reducing the rate of PDMMS-substrate condensation the presence of an oscillation may be confirmed or disproven. Once again, preliminary experiments into the adsorption profile of PDMMS in a 9:1

ethanol:water solvent were conducted using the no hydrolysis method detailed in section 2.2.1 and the results shown below;

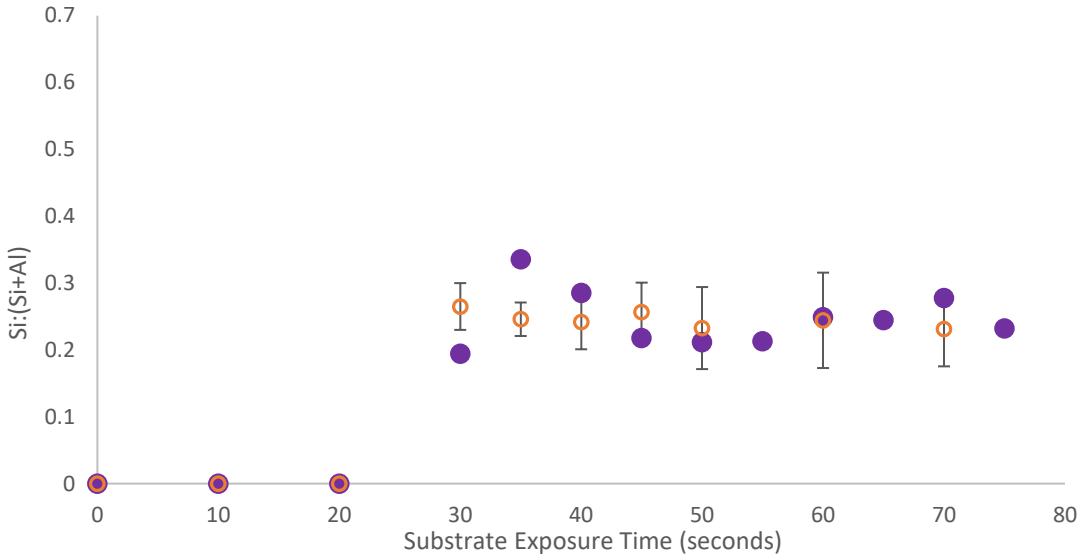

Figure 9.2: The time dependent adsorption profile up the exposure of 1% v/v PDMMS in 9:1 ethanol:water solvent reduced to pH 3 with acetic acid (purple) with no hydrolysis time to diamond polished aluminium foil substrates (purple dots). Each data point represents a single measurement of a single silane film. The time dependent adsorption profile of PDMMS films created under aqueous solvent presented in section 3.4.1 is shown in orange.

Initially it appears as though reducing the rate of reaction does reveal an oscillation in the time dependent surface coverage of PDMMS. However, each data point in Figure 9.2 is based on a single measurement of a PDMMS film. In order to draw further conclusions from data, replicates and extension of the exposure timeline are required. Dependent upon the results of this further investigation, the fit of PDMMS to the 2-component model may need to be revised and additional components required to account for any oscillations observed.

Preliminary investigations into the effect of reducing the rate of reaction for both PTMS and PDMMS films have revealed the need for further investigations into the mechanism of organosilane film formation. it is recommended that these investigations be carried out in order to add to the mechanism of silane film self-assembly presented in this thesis.

In this thesis it has been hypothesised that the change is oscillatory adsorption of PTMS and PMDMS films following a 1-hour hydrolysis time is directly related to the extent of silane oligomerisation prior to exposure to the aluminium oxide substrate. 29Si NMR has been utilised in the analysis of silane derivatives[170]. Analysis of the silane solution by 26Si NMR may give further insight into the extent of

silane oligomerisation in solution. By assessing the changing chemical environments of the central silicon atom.

Similarly, analysis of the silane solution using FTIR may give further insight into the extent of silane condensation prior to exposure to the aluminium substrate and the formation of inert dimers in solution in the case of PDMMS through examining signals at 1079-1088 cm^{-1}, attributed to asymmetric vibrations of Si-O-Si, 952-953 cm^{-1} attributed to asymmetric vibrations of Si-OH, 804-805 cm^{-1} attributed to symmetric stretching vibrations of Si-O-Si and the signals at 459-463 cm^{-1} attributed to the bending vibration of Si-O-Si[171]. It has been reported previously that incomplete condensation of silanes can occur and has been identified using FTIR[172].

9.1.2 Future work of silane functionalised Al powders for LMD 3D printing.

The process of silane powder functionalisation could have a significant impact on the future of Al printing using LMD however, the system requires considerable optimisation and the impact of this method on the structural and mechanical properties must be determined.

Initially, hardness and porosity for the existing samples must be quantified and compared to those of other Al-Si LMD 3D printed and cast eutectic materials. Tensile and deformation behaviour, yield strength, ultimate strength, elastic modulus and elongation to failure tests all need to be conducted in order to make these comparisons.

Following this, optimisation of the system could include both the functionalisation and printing process. Different silane molecules and film coverage may have an impact on both the flowability and the composition of the printed products while optimisation of printing parameters for each modified powder will result in optimum composition of printed materials. Optimisation of silane film coverage to create the desired 12% Si-Al matrix for the creation of eutectic regions and the addition of silicon in concentrations greater than the eutectic composition, known as hypereutectic alloys, is also an area of interest. This is crucial as the size of eutectic Si particles contributes significantly to microhardness, with smaller particles resulting in increased hardness.

This is the direction and focus of our work moving forward.

Reference list

1. Osterholtz FD, Pohl ER. Kinetics of the hydrolysis and condensation of organofunctional alkoxysilanes: a review. *Journal of Adhesion Science and Technology.* 1992;6(1):127-149.
2. Zhao J, Milanova M, Warmoeskerken MMCG, Dutschk V. Surface modification of TiO2 nanoparticles with silane coupling agents. *Colloids and Surfaces A: Physicochemical and Engineering Aspects.* 2012;413(0):273-279.
3. Xie YJ, Hill CAS, Xiao ZF, Militz H, Mai C. Silane coupling agents used for natural fiber/polymer composites: A review. *Compos Pt A-Appl Sci Manuf.* 2010;41(7):806-819.
4. Evonik shows customized invisible protection systems containing Protectosil at BAU 2017 [press release]. December 8 2016.
5. Hooshmand T, Keshvad A, van Noort R. XPS Analysis of Silane Films on the Surface of a Dental Ceramic. *Journal of Adhesion Science and Technology.* 2009;23(7-8):1085-1095.
6. Rachini A, Le Troedec M, Peyratout C, Smith A. Chemical modification of hemp fibers by silane coupling agents. *Journal of Applied Polymer Science.* 2012;123(1):601-610.
7. Zhu DQ, van Ooij WJ. Corrosion protection of metals by water-based silane mixtures of bis-trimethoxysilylpropyl amine and vinyltriacetoxysilane. *Prog Org Coat.* 2004;49(1):42-53.
8. Kregiel D. Advances in biofilm control for food and beverage industry using organo-silane technology: A review. *Food Control.* 2014;40:32-40.
9. Tint World(r) Releases New Nano Ceramic Coatings for Cars. *Plus Company Updates.* 20 October, 2017.
10. Incorporate nanoparticles for antiscratch coating. (Global Developments: Germany). *Advanced Coatings & Surface Technology.* 2003;16(3):9.
11. Larsen KR. The costs of corrosion for Australia's urban water industry. *Materials Performance.* 2015;54(6):19 and 20-21.
12. Wiggins J. Australia's Bridges at Risk. *The Australian Financial Review.* September 7 2018, 2018: 13.
13. Huang M, Zhang H, Yang J. Synthesis of organic silane microcapsules for self-healing corrosion resistant polymer coatings. *Corrosion Science.* 2012;65:561-566.
14. Cho SH, Andersson HM, White SR, Sottos NR, Braun PV. Polydimethylsiloxane-Based Self-Healing Materials. *Adv Mater.* 2006;18(8):997-1000.
15. Cho SH, White SR, Braun PV. Self-Healing Polymer Coatings. *Adv Mater.* 2009;21(6):645-649.
16. Self-healing coatings. In. *Advanced Manufacturing Technology.* Vol 302009:2+.
17. Zwaag Svd. *Self-Healing Materials: An Alternative Approach to 20 Centuries of Materials Science.* Dordrecht : Springer; 2007.
18. Plueddemann EP. *Silane Coupling Agents.* Second Edition. ed. Boston, MA: Springer US; 1991.
19. Ulrich Schubert NH. *Synthesis of Inorganic Materials.* Second ed. Germany: WILEY-VCH; 2005.
20. Britt DW, Hlady V. Protonation, Hydrolysis, and Condensation of Mono- and Trifunctional Silanes at the Air/Water Interface. *Langmuir.* 1999;15(5):1770-1776.
21. Lung CYK, Matinlinna JP. Aspects of silane coupling agents and surface conditioning in dentistry: An overview. *Dental Materials.* 2012;28(5):467-477.
22. Masel RI. *Principles of Adsorption and Reaction on Solid Surfaces.* Toronto, Canada: John Wiley and Sons, Inc.; 1996.
23. Quinton JS, Dastoor PC. Modelling the observed oscillations in the adsorption kinetics of propyltrimethoxysilane on iron and aluminium oxide surfaces. *Surface and Interface Analysis.* 2000;30(1):25-28.
24. Cottrell TL. *The Strengths of Chemical Bonds.* Second ed. London: Butterworths; 1958.
25. Kong G, Lu J, Zhang S, Che C, Wu H. A comparative study of molybdate/silane composite films on galvanized steel with different treatment processes. *Surface and Coatings Technology.* 2010;205(2):545-550.

26. Cho SH, White SR, Braun PV. Room-Temperature Polydimethylsiloxane-Based Self-Healing Polymers. *Chemistry of Materials.* 2012;24(21):4209-4214.
27. Zhao Y, Zhang W, Liao L-p, Wang S-j, Li W-j. Self-healing coatings containing microcapsule. *Applied Surface Science.* 2012;258(6):1915-1918.
28. Bexell U. *Surface Characterisation Using ToF-SIMS, AES and XPS of Silane Films and Organic Coatings Deposited on Metal Substrates* [PhD]: Faculty of Science and Technology, Uppsala University; 2003.
29. Zhu M, Lerum MZ, Chen W. How To Prepare Reproducible, Homogeneous, and Hydrolytically Stable Aminosilane-Derived Layers on Silica. *Langmuir.* 2012;28(1):416-423.
30. Sagiv J. Organized monolayers by adsorption. 1. Formation and structure of oleophobic mixed monolayers on solid surfaces. *Journal of the American Chemical Society.* 1980;102(1):92-98.
31. Bexell U, Olsson M. Characterization of a non-organofunctional silane film deposited on Al, Zn and Al–43.4Zn–1.6Si alloy-coated steel. *Surface and Interface Analysis.* 2001;31(3):223-231.
32. Abel M-L, Joannic R, Fayos M, Lafontaine E, Shaw SJ, Watts JF. Effect of solvent nature on the interaction of -glycidoxy propyl trimethoxy silane on oxidised aluminium surface: A study by solution chemistry and surface analysis. *International Journal of Adhesion and Adhesives.* 2006;26(1–2):16-27.
33. De Graeve I, Tourwé E, Biesemans M, Willem R, Terryn H. Silane solution stability and film morphology of water-based bis-1,2-(triethoxysilyl)ethane for thin-film deposition on aluminium. *Prog Org Coat.* 2008;63(1):38-42.
34. Pan G, Schaefer DW. Morphology and water-barrier properties of silane films on aluminum and silicon. *Thin Solid Films.* 2006;503(1–2):259-267.
35. Cui N-Y, Liu C, Yang W. XPS and AFM characterization of the self-assembled molecular monolayers of a 3-aminopropyltrimethoxysilane on silicon surface, and effects of substrate pretreatment by UV-irradiation. *Surface and Interface Analysis.* 2011;43(7):1082-1088.
36. Iwasa J, Kumazawa K, Aoyama K, et al. In Situ Observation of a Self-Assembled Monolayer Formation of Octadecyltrimethoxysilane on a Silicon Oxide Surface Using a High-Speed Atomic Force Microscope. *The Journal of Physical Chemistry C.* 2016;120(5):2807-2813.
37. Lagutchev AS, Song KJ, Huang JY, Yang PK, Chuang TJ. Self-assembly of alkylsiloxane monolayers on fused silica studied by XPS and sum frequency generation spectroscopy. *Chemical Physics.* 1998;226(3):337-349.
38. Quinton JS. *The Oscillatory Adsorption of Organofunctional Silanes on Metal Oxide Surfaces* [PhD]. New South Wales, Australia: School of Mathematical and Physical Sciences, Universty of Newcastle; 2000.
39. Quinton J, Thomsen L, Dastoor P. Adsorption of organosilanes on iron and aluminium oxide surfaces. *Surface and Interface Analysis.* 1997;25(12):931-936.
40. Quinton JS, Dastoor PC. The effect of experimental conditions on the oscillatory adsorption of propyltrimethoxysilane on aluminium oxide surfaces. *Applied Surface Science.* 1999;152(3–4):131-137.
41. Quinton JS, Dastoor PC. Oscillatory adsorption: a first-principles linear kinetic model. *Surface and Interface Analysis.* 2001;32(1):57-61.
42. Quinton JS, Dastoor PC. Influence of surface electrokinetics on organosilane adsorption. *Surface and Interface Analysis.* 1999;28(1):12-15.
43. Quinton J, Dastoor P, Allison W. PTMS on iron and aluminium oxide surfaces: a study of damped adsorption kinetics. *Surface Science.* 1998;402–404:66-70.
44. Houssiau L, Bertrand P. ToF–SIMS study of organosilane self-assembly on aluminum surfaces. *Applied Surface Science.* 2001;175-176:351-356.
45. Quinton JS, Dastoor PC. Conformational dynamics of γ-APS on the iron oxide surface: an adsorption kinetic study using XPS and ToF-SIMS. *Surface and Interface Analysis.* 2000;30(1):21-24.

46. Mortimer RG. *Physical Chemistry* 2ed. San Diego, California, USA: Elsevier Science & Technology; 2000.
47. Arkles B. Hydrophobicity, Hydrophilicity and Silanes. *Paint & Coatings Industry.* 2006;22(10):114-135.
48. Sims RA, Harmer-Bassell SL, Quinton JS. The oscillatory adsorption of self-assembled organosilane films on aluminium oxide surfaces. *Surface and Interface Analysis.* 2018;50(8):813-818 DOI 10.1016/j.apsusc.2019.01.015.
49. Prutton M. *Surface Physics.* 2nd ed. Oxford, London, UK: Clarendon Press; 1983.
50. 3D Printing Materials 2015-2025: Status, Opportunities, Market Forecasts. *PR Newswire.* 10 December, 2014, 2014.
51. Vasquez M. EMBRACING 3D PRINTING. *Mechanical Engineering.* 2015;137(8):42-45.
52. El Cheikh H, Courant B, Branchu S, Hascoet J, Guillen R. Analysis and prediction of single laser tracks geometrical characteristics in coaxial laser cladding process. *Opt Lasers Eng.* 2012;50(3):413-422.
53. Frazier W. Metal Additive Manufacturing: A Review. *Journal of Materials Engineering and Performance.* 2014;23(6):1917-1928.
54. Kelly S, Kampe S. Microstructural evolution in laser-deposited multilayer Ti-6Al-4V builds: Part I. Microstructural characterization. *Metallurgical and Materials Transactions A.* 2004;35(6):1861-1867.
55. Brandl E, Baufeld B, Leyens C, Gault R. Additive manufactured Ti-6Al-4V using welding wire: comparison of laser and arc beam deposition and evaluation with respect to aerospace material specifications. *Physics Procedia.* 2010;5(2):595-606.
56. Martina F, Mehnen J, Williams SW, Colegrove P, Wang F. Investigation of the benefits of plasma deposition for the additive layer manufacture of Ti–6Al–4V. *Journal of Materials Processing Tech.* 2012;212(6):1377-1386.
57. Williams SW, Martina F, Addison AC, Ding J, Pardal G, Colegrove P. Wire + Arc Additive Manufacturing. *Materials Science and Technology.* 2016;32(7):641-647.
58. Brown CO, Breinan EM, Kear BH, Inventors. Method for Fabricating Articles by Sequential Layer deposition. 1982.
59. Wang XJ, Zhang LC, Fang MH, Sercombe TB. The effect of atmosphere on the structure and properties of a selective laser melted Al–12Si alloy. *Materials Science & Engineering A.* 2014;597(C):370-375.
60. Simchi A. Direct laser sintering of metal powders: Mechanism, kinetics and microstructural features. *Materials Science & Engineering A.* 2006;428(1):148-158.
61. Chou R, Milligan J, Paliwal M, Brochu M. Additive Manufacturing of Al-12Si Alloy Via Pulsed Selective Laser Melting. *The Journal of The Minerals, Metals & Materials Society (TMS).* 2015;67(3):590-596.
62. Borkar T, Gopagoni S, Nag S, Hwang J, Collins P, Banerjee R. In situ nitridation of titanium–molybdenum alloys during laser deposition. *Full Set - Includes `Journal of Materials Science Letters'.* 2012;47(20):7157-7166.
63. Du B, Zou Z, Wang X, Li Q. IN SITU SYNTHESIS OF TiC–TiB2 REINFORCED FeCrSiB COMPOSITE COATING BY LASER CLADDING. *Surface Review and Letters.* 2007;14(2):315-319.
64. Banerjee R, Collins PC, Fraser HL. Laser Deposition of In Situ Ti – TiB Composites. *Advanced Engineering Materials.* 2002;4(11):847-851.
65. Griffith M, Schlienger M, Harwell L, Inventors. Thermal Behaviour in the LENS Process. 1998.
66. Pinkerton AJ, Wang W, Li L. Component repair using laser direct metal deposition. *Proceedings of the Institution of Mechanical Engineers, Part B: Journal of Engineering Manufacture.* 2008;222(7):827-836.
67. Nandy J, Sarangi H, Sahoo S. Microstructure evolution of Al-Si-10Mg in direct metal laser sintering using phase-field modeling. *Advances in Manufacturing.* 2018;6(1):107-117.

68. Mahamood RM, Akinlabi ET. Effect of Laser Power and Powder Flow Rate on the Wear Resistance Behaviour of Laser Metal Deposited TiC/Ti6Al4 V Composites. *Materials Today: Proceedings.* 2015;2(4-5):2679-2686.
69. Hong C, Gu D, Dai D, et al. *Laser metal deposition of TiC/Inconel 718 composites with tailored interfacial microstructures.* Vol 542013.
70. Lalas C, Tsirbas K, Salonitis K, Chryssolouris G. An analytical model of the laser clad geometry. *The International Journal of Advanced Manufacturing Technology.* 2007;32(1):34-41.
71. Muller P, Mognol P, Hascoet J-Y. Modeling and control of a direct laser powder deposition process for Functionally Graded Materials (FGM) parts manufacturing. *Journal of Materials Processing Tech.* 2013;213(5):685-692.
72. Qian T-T, Liu D, Tian X-J, Liu C-M, Wang H-M. Microstructure of TA2/TA15 graded structural material by laser additive manufacturing process. *Transactions of Nonferrous Metals Society of China.* 2014;24(9):2729-2736.
73. Pei X, Wang J, Wan Q, Kang L, Xiao M, Bao H. Functionally graded carbon nanotubes/hydroxyapatite composite coating by laser cladding. *Surface & Coatings Technology.* 2011;205(19):4380-4387.
74. Durejko T, Ziętala M, Polkowski W, Czujko T. Thin wall tubes with Fe3Al/SS316L graded structure obtained by using laser engineered net shaping technology. *Materials and Design.* 2014;63:766-774.
75. De Oliveira U, Ocelik V, De Hosson JTM. Analysis of coaxial laser cladding processing conditions. *Surface & Coatings Technology.* 2005;197(2 3):127.
76. Singh A. *Additive Manufacturing of Al 4047 and Al 7050 Alloys Using Direct Laser Metal Deposition Process*. Detroit MI, USA: Mechanical Engineering, Wayne State University; 2017.
77. Fraenkel W. Metallographische Mitteilungen aus dem Institut für physikalische Chemie der Universität Göttingen. LXIII. Über Silicium-Aluminiumlegierungen. *Zeitschrift für anorganische Chemie.* 1908;58(1):154-158.
78. Pai BC, Rohatgi PK, Venkatesh S. Wear resistance of cast graphitic aluminium alloys. *Wear.* 1974;30(1):117-125.
79. Rohatgi PK, Pai BC. Effect of microstructure and mechanical properties on the seizure resistance of cast aluminium alloys. *Wear.* 1974;28(3):353-367.
80. Yen B. The effect of humidity on friction and wear of an aluminium–silicon eutectic alloy. *J Mater Sci.* 1997;32(3):821-828.
81. Voort GFV, Asensio-Lozano J. The Al-Si Phase Diagram. *Microsc Microanal.* 2009;15(S2):60-61.
82. Abbott T, Parker B. The structures of fully eutectic aluminium-silicon alloy castings. *J Mater Sci.* 1990;25(4):2100-2106.
83. Bayraktar Y, Liang D, Jones H. The effect of growth velocity and temperature gradient on growth characteristics of matrix eutectic in a hypereutectic aluminium-silicon alloy. *J Mater Sci.* 1995;30(23):5939-5943.
84. Mahato A, Verma N, Jayaram V, Biswas SK. Severe wear of a near eutectic aluminium–silicon alloy. *Acta Materialia.* 2011;59(15).
85. John HM, Brennan DY, Jacob MH, Justin AM, Tobias AS, Tresa MP. 3D printing of high-strength aluminium alloys. *Nature.* 2017;549(7672):365.
86. Zhao LZ, Zhao MJ, Song LJ, Mazumder J. Ultra-fine Al–Si hypereutectic alloy fabricated by direct metal deposition. *Materials and Design.* 2014;56:542-548.
87. Biffi CA, Fiocchi J, Bassani P, et al. Microstructure and preliminary fatigue analysis on AlSi10Mg samples manufactured by SLM. *Procedia Structural Integrity.* 2017;7:50-57.
88. Raus AA, Wahab MS, Shayfull Z, Kamarudin K, Ibrahim M. The Influence of Selective Laser Melting Parameters on Density and Mechanical Properties of AlSi10Mg. *MATEC Web of Conferences.* 2016;78:01078.
89. Feng JQ, Hays DA. Relative importance of electrostatic forces on powder particles. *Powder Technology.* 2003;135-136:65-75.

90. Zimon AD. *Adhesion of Dust and Powder.* 2nd ed. Boston, MA, USA: Springer US; 1982.
91. Coelho MC, Harnby N. The effect of humidity on the form of water retention in a powder. *Powder Technology.* 1978;20(2):197-200.
92. Jallo LJ, Schoenitz M, Dreizin EL, Dave RN, Johnson CE. The effect of surface modification of aluminum powder on its flowability, combustion and reactivity. *Powder Technology.* 2010;204(1):63-70.
93. Yang J, Sliva A, Banerjee A, Dave RN, Pfeffer R. Dry particle coating for improving the flowability of cohesive powders. *Powder Technology.* 2005;158(1):21-33.
94. Chen Y, Jallo L, Quintanilla MAS, Dave R. Characterization of particle and bulk level cohesion reduction of surface modified fine aluminum powders. *Colloids and Surfaces A: Physicochemical and Engineering Aspects.* 2010;361(1):66-80.
95. Özel A, Çimenoğlu H. An Overview on Silane Based Metal Pretreatments for Powder Painting. *Diffusion Foundations.* 2016;9:16-29.
96. Crouse C, Pierce CJ, Spowart J. Influencing Solvent Miscibility and Aqueous Stability of Aluminum Nanoparticles through Surface Functionalization with Acrylic Monomers. *ACS Appl Mater Interfaces.* 2010;2(9):2560-2569.
97. Kim HJ, Jung DH, Jung IH, Cifuentes JI, Rhee KY, Hui D. Enhancement of mechanical properties of aluminium/epoxy composites with silane functionalization of aluminium powder. *Composites Part B: Engineering.* 2012;43(4):1743-1748.
98. Stevens N, Tedeschi S, Powers K, Moudgil B, El-Shall H. Controlling unconfined yield strength in a humid environment through surface modification of powders. *Powder Technology.* 2009;191(1):170-175.
99. Hofmann S. *Auger and X-Ray Photoelectron Spectroscopy in Materials Science A User-Orientated Guide.* Dordrecht : Springer; 2012.
100. Chambers RC, Jones WE, Haruvy Y, Webber SE, Fox MA. Influence of steric effects on the kinetics of ethyltrimethoxysilane hydrolysis in a fast sol-gel system. *Chemistry of Materials.* 1993;5(10):1481-1486.
101. Matinlinna JP, Lung CYK, Tsoi JKH. Silane adhesion mechanism in dental applications and surface treatments: A review. *Dental Materials.* 2018;34(1):13-28.
102. Briggs D, Seah MP. *Auger and X-ray Photoelectron Spectroscopy.* Vol 1. 2nd ed: John Wiley and Sons; 1983.
103. Einstein A. Über einen die Erzeugung und Verwandlung des Lichtes betreffenden heuristischen Gesichtspunkt. *Annalen der Physik.* 1905;322(6):132-148.
104. Siegbahn K. Electron spectroscopy for atoms, molecules, and condensed matter. *Science.* 1982;217(4555):111-121.
105. Moulder JF, Stickle WF, Sobol PE, Bomben` KD. *Handbook of X-ray Photoelectron Spectroscopy.* Minnesota, USA.: Perkin-Elmer Corporation Physical Electronics Division; 1992.
106. Barlow AJ. *Plasma Processing Studies With Application To Carbon Nanotube Fluorination* [PhD]: School of Chemical and Physical Sciences, Flinders University; 2011.
107. Kibel MH. X-Ray Photoelectron Spectroscopy. In: O'Connor DJ, Sexton BA, Smart RSC, eds. *Surface Analysis Methods in Materials Science.* Berlin, Heidelberg: Springer Berlin Heidelberg; 1992:165-186.
108. Fairley N. CASA XPS Manual 2.3.15 In: 1.2 ed.: Casa Software Ltd; 2009: http://www.casaxps.com/help_manual/.
109. Seah MP, Dench WA. Quantitative electron spectroscopy of surfaces: A standard data base for electron inelastic mean free paths in solids. *Surface and Interface Analysis.* 1979;1(1):2-11.
110. Cumpson PJ, Seah MP. Elastic Scattering Corrections in AES and XPS. II. Estimating Attenuation Lengths and Conditions Required for their Valid Use in Overlayer/Substrate Experiments. *Surface and Interface Analysis.* 1997;25(6):430-446.
111. Leung Y-L. *XPS Studies of Adhesion at Organosilane-Aluminum Interfaces* [Masters]: Chemistry, University of British Columbia; 1992.

112. Barlow AJ. *Plasma Processing Studies With Application To Carbon Nanotube Fluorination* [PhD]: School Of Chemical and Physical Sciences, Flinders University; 2011.
113. Shirley DA. HIGH-RESOLUTION X-RAY PHOTOEMISSION SPECTRUM OF THE VALENCE BANDS OF GOLD. 1971.
114. Arranz A, Palacio C, García-Fresnadillo D, Orellana G, Navarro A, Muñoz E. Influence of Surface Hydroxylation on 3-Aminopropyltriethoxysilane Growth Mode during Chemical Functionalization of GaN Surfaces: An Angle-Resolved X-ray Photoelectron Spectroscopy Study. *Langmuir.* 2008;24(16):8667-8671.
115. Pleul D, Frenzel R, Eschner M, Simon F. X-ray photoelectron spectroscopy for detection of the different Si–O bonding states of silicon. *Anal Bioanal Chem.* 2003;375(8):1276-1281.
116. Scott P, Wieliczka D, Kruger M. Depth Profiled XPS Analysis of a Polymerized Silicon-Carbon Thin Film. *Plasma Chem Plasma Process.* 2009;29(6):559-566.
117. C.D. Wagner AVN, A. Kraut-Vass, J.W. Allison, C.J. Powell, J.R.Jr. Rumble. NIST Standard Reference Database 20 Version 4.1. 2012.
118. Shimizu KM, Tomoaki. *New Horizons of Applied Scanning Electron Microscopy.* Vol 45: Springer; 2010.
119. Reimer L. *Scanning Electron Microscopy.* Springer; 1998.
120. Persson L. Pierre Auger-A Life in the Service of Science. *Acta Oncologica.* 1996;35(7):785-787.
121. Auger P. Sur l'effet photoélectrique composé. *J Phys Radium.* 1925;6(6):205-208.
122. Sime RL. *Lise Meitner a life in physics.* Berkeley, California, USA: Berkeley : University of California Press; 1997.
123. Childs K, Carlson B, LaVanier L, et al. *Handbook of Auger Electron Spectromicroscopy.* 3rd ed. Minnesota, USA: Physical Electronics, Inc.; 1995.
124. Stojilovic N. Why Can't We See Hydrogen in X-ray Photoelectron Spectroscopy? *Journal of Chemical Education.* 2012;89(10):1331-1332.
125. Savitzky A, Golay MJE. Smoothing and Differentiation of Data by Simplified Least Squares Procedures. *Analytical Chemistry.* 1964;36(8):1627-1639.
126. Scheithauer U. Improved sputter depth resolution in Auger thin film analysis using in situ low angle cross-sections. *Applied Surface Science.* 2001;179(1–4):20-24.
127. Sveen CE, Shi Y. Effect of filament temperature and deposition time on the formation of tungsten silicide with silane. *Thin Solid Films.* 2011;519(14):4447-4450.
128. Franquet A, De Laet J, Schram T, et al. Determination of the thickness of thin silane films on aluminium surfaces by means of spectroscopic ellipsometry. *Thin Solid Films.* 2001;384(1):37-45.
129. Shen YR. Surface properties probed by second-harmonic and sum-frequency generation. *Nature.* 1989;337(6207):519-525.
130. Shen YE SN, Katsuaki Shimazu, Kohei Uosaki. Sum Frequency Generation (SFG) Studies on the Conformational Order of the Self-Assembled Monolayers of Alkanethiols on Silver Surfaces. *Nonlinear Optics.* 2000;24:93-98.
131. Prasad S, Zhu H, Kurian A, Badge I, Dhinojwala A. Interfacial Segregation in Polymer Blends Driven by Acid–Base Interactions. *Langmuir.* 2013;29(51):15727-15731.
132. Himmelhaus M, Eisert F, Buck M, Grunze M. Self-Assembly of n-Alkanethiol Monolayers. A Study by IR−Visible Sum Frequency Spectroscopy (SFG). *The Journal of Physical Chemistry B.* 2000;104(3):576-584.
133. Chen, Wang J, Loch CL, Ahn D, ChenChen Z. Demonstrating the Feasibility of Monitoring the Molecular-Level Structures of Moving Polymer/Silane Interfaces during Silane Diffusion Using SFG. *Journal of the American Chemical Society.* 2004;126(4):1174-1179.
134. Mentore R. *Characterization of ultrathin organic films at the air/silver interface by infrared-visible sum-frequency generation spectroscopy* [Ph.D.]. Ann Arbor, Rensselaer Polytechnic Institute; 1998.

135. Loch CL, Ahn D, Chen Z. Sum Frequency Generation Vibrational Spectroscopic Studies on a Silane Adhesion-Promoting Mixture at a Polymer Interface. *The Journal of Physical Chemistry B.* 2006;110(2):914-918.
136. Loch CL, Ahn D, Chen C, Wang J, Chen Z. Sum Frequency Generation Studies at Poly(ethylene terephthalate)/Silane Interfaces: Hydrogen Bond Formation and Molecular Conformation Determination. *Langmuir.* 2004;20(13):5467-5473.
137. Zhang Y, Noguchi H, Ye S, Uosaki K. Structure of adsorbed molecular layer on fused quartz surface determined sequentially in sodium stearate solution, dry Ar, pure water, and dry Ar by sum frequency generation spectroscopy. *Surface Science.* 2013;607:92-96.
138. Backus EHG, Garcia-Araez N, Bonn M, Bakker HJ. On the Role of Fresnel Factors in Sum-Frequency Generation Spectroscopy of Metal–Water and Metal-Oxide–Water Interfaces. *The Journal of Physical Chemistry C.* 2012;116(44):23351-23361.
139. Loch CL, Ahn D, Chen C, Chen Z. Polymer-Silane Interactions Probed by Sum Frequency Generation Vibrational Spectroscopy. *The Journal of Adhesion.* 2005;81(3-4):319-345.
140. Chen, Loch CL, Wang J, ChenChen Z. Different Molecular Structures at Polymer/Silane Interfaces Detected by SFG. *The Journal of Physical Chemistry B.* 2003;107(38):10440-10445.
141. Ito M, Noguchi H, Ikeda K, Uosaki K. Substrate dependent structure of adsorbed aryl isocyanides studied by sum frequency generation (SFG) spectroscopy. *Physical Chemistry Chemical Physics.* 2010;12(13):3156-3163.
142. Ye S, Nihonyanagi S, Uosaki K. Sum frequency generation (SFG) study of the pH-dependent water structure on a fused quartz surface modified by an octadecyltrichlorosilane (OTS) monolayer. *Physical Chemistry Chemical Physics.* 2001;3(16):3463-3469.
143. Kershner RJ, Bullard JW, Cima MJ. Zeta Potential Orientation Dependence of Sapphire Substrates. *Langmuir.* 2004;20(10):4101-4108.
144. Kelber JA, Niu C, Shepherd K, Jennison DR, Bogicevic A. Copper wetting of α-Al2O3(0001): theory and experiment. *Surface Science.* 2000;446(1–2):76-88.
145. Nelson CE, Elam JW, Cameron MA, Tolbert MA, George SM. Desorption of H2O from a hydroxylated single-crystal α-Al2O3(0001) surface. *Surface Science.* 1998;416(3):341-353.
146. Liu P, Kendelewicz T, Brown Jr GE, Nelson EJ, Chambers SA. Reaction of water vapor with α-Al2O3(0001) and α-Fe2O3(0001) surfaces: synchrotron X-ray photoemission studies and thermodynamic calculations. *Surface Science.* 1998;417(1):53-65.
147. Ge A, Peng Q, Qiao L, et al. Molecular orientation of organic thin films on dielectric solid substrates: a phase-sensitive vibrational SFG study. *Physical Chemistry Chemical Physics.* 2015;17(27):18072-18078.
148. Asanuma H, Noguchi H, Uosaki K, Yu H-Z. Water Structure at Superhydrophobic Quartz/Water Interfaces: A Vibrational Sum Frequency Generation Spectroscopy Study. *The Journal of Physical Chemistry C.* 2009;113(50):21155-21161.
149. Yang S, Noguchi H, Uosaki K. Electronic Structure of the CO/Pt(111) Electrode Interface Probed by Potential-Dependent IR/Visible Double Resonance Sum Frequency Generation Spectroscopy. *The Journal of Physical Chemistry C.* 2015;119(46):26056-26063.
150. Zhu H, Dhinojwala A. Thermal Behavior of Long-Chain Alcohols on Sapphire Substrate. *Langmuir.* 2015;31(23):6306-6313.
151. Liljeblad JFD, Tyrode E. Vibrational Sum Frequency Spectroscopy Studies at Solid/Liquid Interfaces: Influence of the Experimental Geometry in the Spectral Shape and Enhancement. *The Journal of Physical Chemistry C.* 2012;116(43):22893-22903.
152. Nihonyanagi S, Miyamoto D, Idojiri S, Uosaki K. Evidence for Epitaxial Arrangement and High Conformational Order of an Organic Monolayer on Si(111) by Sum Frequency Generation Spectroscopy. *Journal of the American Chemical Society.* 2004;126(22):7034-7040.
153. Myers JN, Chen Z. Polymer molecular behaviors at buried polymer/metal and polymer/polymer interfaces and their relations to adhesion in packaging. *The Journal of Adhesion.* 2016:1-23.

154. Miyamae T, Akiyama H, Yoshida M, Tamaoki N. Characterization of Poly(N-isopropylacrylamide)-Grafted Interfaces with Sum-Frequency Generation Spectroscopy. *Macromolecules.* 2007;40(13):4601-4606.
155. Guyot-Sionnest P, Hunt JH, Shen YR. Sum-frequency vibrational spectroscopy of a Langmuir film: Study of molecular orientation of a two-dimensional system. *Physical Review Letters.* 1987;59(14):1597-1600.
156. Thomsen L, Watts B, Cotton DV, Quinton JS, Dastoor PC. Adsorption and orientation kinetics of self-assembled films of octadecyltrimethoxysilane on aluminium oxide surfaces. *Surface and Interface Analysis.* 2005;37(5):472-477.
157. Shircliff RA, Stradins P, Moutinho H, et al. Angle-Resolved XPS Analysis and Characterization of Monolayer and Multilayer Silane Films for DNA Coupling to Silica. *Langmuir.* 2013;29(12):4057-4067.
158. Zhang F, Sautter K, Larsen AM, et al. Chemical Vapor Deposition of Three Aminosilanes on Silicon Dioxide: Surface Characterization, Stability, Effects of Silane Concentration, and Cyanine Dye Adsorption. *Langmuir.* 2010;26(18):14648-14654.
159. Dietrich PM, Glamsch S, Ehlert C, Lippitz A, Kulak N, Unger WES. Synchrotron-radiation XPS analysis of ultra-thin silane films: Specifying the organic silicon. *Applied Surface Science.* 2016;363:406-411.
160. Waddell TG, Leyden DE, DeBello MT. The nature of organosilane to silica-surface bonding. *Journal of the American Chemical Society.* 1981;103(18):5303-5307.
161. Donohue MD, Aranovich GL. Classification of Gibbs adsorption isotherms. *Advances in Colloid and Interface Science.* 1998;76–77(0):137-152.
162. Sims RA, Harmer SL, Quinton JS. The Role of Physisorption and Chemisorption in the Oscillatory Adsorption of Organosilanes on Aluminium Oxide. *Polymers.* 2019;11(3):410.
163. Sims RA, Harmer-Bassell SL, Quinton JS. The Oscillatory Adsorption of Organosilane Films on Aluminium Oxide: Film Morphology using Auger Electron Spectromicroscopy. *Applied Surface Science.* 2019;475:999-1002.
164. Mansel RI. *Principles of Adsorption and Reaction on Solid Surfaces.* Canada: John Wiley and Sons, Inc.; 1996.
165. Du Q, Freysz E, Shen YR. Vibrational spectra of water molecules at quartz/water interfaces. *Physical Review Letters.* 1994;72(2):238-241.
166. Ishikawa S, Tsuchiya N. Structure of Interfacial Water on Quartz and its Self-diffusion Coefficient Revealed by Molecular Dynamics Simulations. *Procedia Earth and Planetary Science.* 2017;17:853-856.
167. Nomura K, Mikuni S, Nakaji-Hirabayashi T, et al. Water structure at the interfaces between a zwitterionic self-assembled monolayer/liquid water evaluated by sum-frequency generation spectroscopy. *Colloids and Surfaces B: Biointerfaces.* 2015;135:267-273.
168. Dhopatkar N, Defante AP, Dhinojwala A. Ice-like water supports hydration forces and eases sliding friction. *Science Advances.* 2016;2(8):e1600763.
169. Trunov MA, Umbrajkar SM, Schoenitz M, Mang JT, Dreizin EL. Oxidation and melting of aluminum nanopowders. *Journal of Physical Chemistry B.* 2006;110(26):13094-13099.
170. Corminbœuf C, Heine T, Weber J. 29Si NMR chemical shifts of silane derivatives. *Chemical Physics Letters.* 2002;357(1):1-7.
171. Sanaeishoar H, Sabbaghan M, Mohave F. Synthesis and characterization of micro-mesoporous MCM-41 using various ionic liquids as co-templates. *Microporous and Mesoporous Materials.* 2015;217:219-224.
172. Underhill PR, Goring G, DuQuesnay DL. The drying of 3-glycidoxypropyltrimethoxy silane. *Applied Surface Science.* 1998;134(1):247-253.